Université de Montréal

Synthesis of polyelectrolyte brushes on silica-based substrates through surface-initiated polymerization: brush characterization and responsiveness to variation in pH and ionic strength

par

Olga Borozenko

Département de chimie
Faculté des arts et des sciences

Thèse présentée à la Faculté des études supérieures et postdoctorales
en vue de l'obtention du grade de *philosophiæ doctor* (Ph.D.) en chimie

Decembre 2013

Université de Montréal
Faculté des études supérieures et postdoctorales

Cette thèse intitulée:

Synthesis of polyelectrolyte brushes on silica-based substrates through surface-initiated polymerization: brush characterization and responsiveness to variation in pH and ionic strength

Présentée par:
Olga Borozenko

a été évaluée par un jury composé des personnes suivantes:

Prof. Julian X. Zhu, président-rapporteur
Prof. Suzanne Giasson, directrice de recherche
Prof. Will G. Skene, co-directreur de recherche
Prof. Robert E. Prud'homme membre du jury
Prof. Marta Cerruti, examinatrice externe
Prof. François Schiettekatte, représentante du doyen de la Faculté des arts et des sciences

Résumé

Les brosses de polyélectrolytes font l'objet d'une attention particulière pour de nombreuses applications car elles présentent la capacité de changer de conformation et, par conséquent, de propriétés de surface en réponse aux conditions environnementales appliquées. Le contrôle des principaux paramètres de ces brosses telles que l'épaisseur, la composition et l'architecture macromoléculaire, est essentiel pour obtenir des polymères greffés bien définis. Ceci est possible avec la Polymérisation Radicalaire par Transfert d'Atomes - Initiée à partir de la Surface (PRTA-IS), qui permet la synthèse de brosses polymériques de manière contrôlée à partir d'une couche d'amorceurs immobilisés de manière covalente sur une surface. Le premier exemple d'une synthèse directe de brosses de poly(acide acrylique) (PAA) par polymérisation radicalaire dans l'eau a été démontré. Par greffage d'un marqueur fluorescent aux brosses de PAA et via l'utilisation de la microscopie de fluorescence par réflexion totale interne, le dégreffage du PAA en temps réel a pu être investigué. Des conditions environnementales de pH ≥ 9,5 en présence de sel, se sont avérées critiques pour la stabilité de la liaison substrat-amorceur, conduisant au dégreffage du polymère.

Afin de protéger de l'hydrolyse cette liaison substrat-amorceur sensible et prévenir le dégreffage non souhaité du polymère, un espaceur hydrophobique de polystyrène (PS) a été inséré entre l'amorceur et le bloc de PAA stimuli-répondant. Les brosses de PS-PAA obtenues étaient stables pour des conditions extrêmes de pH et de force ionique. La réponse de ces brosses de copolymère bloc a été étudiée *in situ* par ellipsométrie, et le changement réversible de conformation collapsée à étirée, induit par les variations de pH a été démontré. De plus, des différences de conformation provenant des interactions du bloc de PAA avec des ions métalliques de valence variable ont été obtenues. Le copolymère bloc étudié semble donc prometteur pour la conception de matériaux répondant rapidement a divers stimuli.

Par la suite, il a été démontré qu'un acide phosphonique pouvait être employé en tant qu' amorceur PRTA-IS comme alternative aux organosilanes. Cet amorceur

phosphonate a été greffé pour la première fois avec succès sur des substrats de silice et une PRTA-IS en milieux aqueux a permis la synthèse de brosses de PAA et de poly(sulfopropyl méthacrylate). La résistance accrue à l'hydrolyse de la liaison $Si_{substrat}$-O- $P_{amorceur}$ a été confirmée pour une large gamme de pH 7,5 à 10,5 et a permis l'étude des propriétés de friction des brosses de PAA sous différentes conditions expérimentales par mesure de forces de surface. Malgré la stabilité des brosses de PAA à haute charge appliquée, les études des propriétés de friction ne révèlent pas de changement significatif du coefficient de friction en fonction du pH et de la force ionique.

Mots-clé: Brosse de polymère, poly(acide acrylique), Polymérisation Radicalaire par Transfert d'Atomes Initiée à partir de la Surface, conformation brosse, pH- et force ionique, stimuli-répondant, ellipsometrie, dégreffage de brosses et stabilité, propriétés de surface, amorceur siloxane, amorceur phosphonate.

Abstract

Polyelectrolyte (PE) brushes are interesting objects for many advanced applications because they are capable of changing their conformation and, consequently, their surface properties in response to applied environmental conditions. The control over the main brush parameters such as thickness, composition, and macromolecular architecture is essential to get well-defined grafted polymers. This is possible by Surface-Initiated Atom Transfer Radical Polymerization (SI-ATRP) that allows preparing polymer brushes in a well-controlled manner from covalently immobilized initiator layer. The first example of direct synthesis of poly(acrylic acid) (PAA) brushes using water-mediated SI-ATRP from a siloxane-modified mica surface was demonstrated. By attaching a fluorescent tag to PAA and applying Total Internal Reflection Fluorescent microscopy, the monitoring over PAA degrafting in real-time was possible. Environmental conditions of pH≥9.5 with added salt were found to be critical for substrate-initiator linkage stability resulting in polymer detachment.

In order to shield from hydrolysis the sensitive substrate-initiator bond and prevent undesired polymer degrafting, a hydrophobic polystyrene (PS) spacer between initiator and responsive PAA layer was introduced. The obtained PS-*block*-PAA brushes were stable under extreme conditions of pH and ionic strength. The pH responsiveness of obtained block copolymer brushes was studied *in situ* by ellipsometry and the evidence of PAA reversible pH-induced switch from collapsed to extended conformation was provided. Also, the essentially different brush conformations as a result of interaction of PAA block with metal cations of different valency were obtained. Studied block copolymers present a promising responsive material for rapid switching.

Additionally, it was demonstrated that phosphonic acid ATRP initiator could be used as an alternative to organosilanes. The phosphonate initiator was successfully grafted for the first time to silica surface and water-mediated ATRP was applied to synthesize PAA and poly(sulfopropyl methacrylate) brushes. The

confirmed resistivity of $Si_{substrate}$-O-$P_{initiator}$ bond towards hydrolysis in a wide range of pH from 7.5 to 10.5 allowed investigating the friction properties of PAA brushes under different environmental conditions using the Surface Forces Apparatus. Despite PAA brushes stability at high applied load, friction studies revealed non-significant changes in friction coefficient with pH and ionic strength.

Key words: polymer brush, poly(acrylic acid), Surface-Initiated Atom Transfer Radical Polymerization, brush conformation, pH- and ionic strength responsiveness, ellipsometry, brush degrafting and stability, surface properties, siloxane initiator, phosphonate initiator.

Dedicated to my parents, for their teaching and advices that made this achievement possible and to my husband, my closest and strongest supporter and inspirer through this journey.

Disclosure

This thesis consists of three published papers and one submitted paper.

Chapter 2 is a verbatim copy of the paper published in *Macromolecular Symposia* (2010, 297, 1-5). It is co-authored by the research supervisor Prof. Suzanne Giasson and co-supervisor Prof. Will Skene. For this publication, I performed all experiments (prepared the substrate, performed polymer brush synthesis and polymer film imaging), wrote the first draft of the manuscript, and modified it according to comments from my supervisors.

Chapter 3 is a verbatim copy of the full paper published in *Macromolecules* (2011, 44, pp. 8177-8184). It is co-authored by Robert Godin, Kai L. Lau, Wayne Mah, Prof. Gonzalo Cosa, Prof. Suzanne Giasson, and Prof. Will Skene. My contribution to this research is at least 80% of the experimental part (substrate preparation, synthesis of the polymer brushes, polymer film characterization, fluorophore coupling, degrafting studies) and participation in manuscript preparation (manuscript writing and modification, performing final corrections after peer-review). The contribution of co-authors other than my research supervisors is as follows: Robert Godin (PhD student from Prof. G.Cosa's group, McGill) performed fluorescence analysis of PM605 in SDS micelles, designed flow-through chamber and assisted during TIRFM experiments; Kai L. Lau (summer student from Prof. G. Cosa's lab, McGill) performed first successful coupling of fluorophore to acrylic acid and polyacrylic acid in solution; Wayne Mah (MSc student from Prof. G. Cosa's group, McGill) helped with preliminary TIRFM experiments; Prof. G.Cosa (McGill) supervised fluorescent studies and participated in manuscript writing.

Chapter 4 is a verbatim copy of the full paper published in *Polymer Chemistry* (2013, 5, p. 2242-2252). It is co-authored by Charly Ou, Prof. Suzanne Giasson, and Prof. Will Skene. My contribution includes substrate preparation, polymer brushes synthesis and characterization, polymerization kinetic studies, film imaging, brush swelling experiments. Also I prepared the article for publication

(wrote the manuscript, modified it in accordance to feedback from my supervisors). Charly Ou (summer student in Prof. S. Giasson's group) performed salt-dependent swelling studies.

Chapter 5 is a verbatim copy of the full paper submitted to *Polymer Chemistry* (2014). It is co-authored by Vivian Machado, Prof. Suzanne Giasson, and Prof. Will Skene. Here, I performed at least 80% of all experimental studies. This includes substrates preparation, polymer brush synthesis, topographical analysis of initiator- and polymer-covered surfaces, brushes stability studies. Also I prepared the article for publication: wrote the manuscript and modified it in accordance to feedback from my supervisors. Vivian Machado (MSc student from Prof. S. Giasson's group) performed surface forces characterization of polymer-modified substrates and participated in manuscript preparation.

TABLE OF CONTENTS

Chapter 2

Chapter 3

Chapter 4

List of Figures

List of Tables

List of Schemes

List of acronyms, abbreviations and symbols used

α	average degree of ionization
α_B	degree of ionization of free chain in solution
β^I	stability constant of Cu(I) complex
β^{II}	stability constant of Cu(II) complex
Δ	phase difference
Ψ	amplitude ratio
ε_0	vacuum permittivity
ε_T	relative dielectric constant
λ_{GC}	Gouy-Chapman length
v	excluded volume parameter
θ_a	advancing contact angle
θ_{obs}	observed contact angle
ρ	polymer density
σ	brush grafting density
Σ	surface charge density
a	size of monomer
AFM	atomic force microscopy
ATR-FTIR	attenuated total reflection Fourier transform infrared spectroscopy
AOI	area of interest
ATRA	atom transfer radical addition
ATRP	atom transfer radical polymerization
bipy	2,2'-bipyridine
c_{H+}	proton concentration
c_S	salt concentration
d	distance between brush anchoring points
DCM	dichloromethane

DMAP	4-(dimethylamino)pyridine
DP	degree of polymerization
e	elementary charge
EDCl	1-ethyl-3-(3-dimethylaminopropyl)carbodiimide hydrochloride
f	degree of ionization
f_1	fraction of hydrophobic molecules grafted to the surface
f_2	fraction of hydrophilic molecules grafted to the surface
F	polymer chain free energy
F_{el}	elastic free energy
F_{int}	interaction energy
$F_{stretch}$	free energy of stretching
GPC	gel permeation chromatography
h	dry polymer layer thickness
H	swollen polymer layer thickness
HPLC	high-performance liquid chromatography
HR MS	high resolution mass spectrometry
k	extinction coefficient
k_{act}	ATRP activation rate constant
k_B	Boltzmann constant
k_{deact}	dissociation constant
K_{disp}	ATRP deactivation rate constant
K_{disp}^*	Disprosportionation constant
K_D	Conditional disprosportionation constant
K_{eq}	ATRP equillibrium constant
k_p	ATRP propagation constant
k_t	ATRP termination constant
K_X	halidophilicity
l_B	Bjerrum length
L	polymer brush thickness

M_n	number average molecular weight
M_w	mass average molecular weight
MS	mass spectrometry
MSE	mean-squared error
n	refractive index
N	degree of polymerization
N_A	Avogadro's number
NaA	sodium acrylate
NMP	nitroxide mediated polymerization
NMR	nucreal magnetic resonance
p	monomer conversion
PAA	poly(acrylic acid)
PDI	polydispersity index
PE	polyelectrolyte
*pK*a	acid dissociation constant
PM 605	8-Acetoxymethyl-2,6-diethyl-1,3,5,7-tetramethyl pyrromethenefluoroborate
PMAA	poly(methacrylic acid)
PMDETA	*N*,*N*,*N*′,*N*″,*N*″-pentamethyl diethylene triamine
PMOH	8-Hydroxymethyl-2,6-diethyl-1,3,5,7-tetramethylpyrromethene fluoroborate
PPTS	pyridinium-p-toluene-sulfonate
PS	polystyrene
PS-*b*-PAA	polystyrene-*block*-poly(acrylic acid)
PSPMAA	poly(3-sulfopropyl methacrylic acid)
P*t*BA	poly(*tert*-butyl acrylate)
RCE	rotating compensator ellipsometer
Q	brush swelling ratio
R_F	Flory radius
R_g	radius of gyration

R_p	rate of polymerization
r_p	amplitude of *p* orthogonal vector
r_s	amplitude of *s* orthogonal vector
RAFT	reversible addition fragmentation chain transfer polymerization
RMS	root mean square
s	distance between two adjacent grafting points
SDS	sodium dodecyl sulfate
SE	spectroscopic ellipsometry
SFA	surface forces apparatus
SPMA	3-sulfopropyl methacrylate potassuim
T	temperature
T_g	glass-transition temperature
*t*BA	*tert*-butyl acrylate
T-BAG	tethering by aggregation and growth
TFA	trifluoroacetic acid
THF	tetrahydrofurane
TIRFM	total internal reflection fluorescence microscopy
UV-vis	ultraviolet-visible spectroscopy

Acknowledgements

First of all, I would like to thank my supervisors Prof. Suzanne Giasson and Prof. Will Skene for giving me this great opportunity to pursue my PhD studies in their laboratories. I am very grateful for their constant encouragement and guidance throughout my work, the possibility to attend multiple international and local conferences, and detailed reading and correction of this thesis.

I greatly acknowledge Department of Chemistry for providing me a waiver from high tuition fees for international students, as well as granting me the travel scholarship to attend 96th Canadian Chemistry Conference and Exhibition in Quebec City.

I would like to thank Centre for Self-Assembled Chemical Structures (CSACS/CRMAA) for the opportunity to share thoughts and ideas with scientists from different universities working in the same area.

I would like to acknowledge Prof. Antonella Badia, Prof. R.E. Prud'homme, and Prof. Christian Pellerin for granting me an access to their equipment. Also I want to thank our collaborators from McGill University Prof. Gonzalo Cosa and Prof. Peter Grutter as well as students from both groups Robert Godin, Wayne Mah, Matthew Rigby for their guidance and assistance with multiple techniques.

My special thanks to Patricia Moraille and Jacqueline Sanchez for introducing me the magic world of nano imaging. I am extremely grateful for their constant support with ellipsometrical and AFM experiments and, especially, for their inexhaustible humour. All time what I spent in AFM and Ellipso laboratories was a great pleasure to me.

Also I would like to acknowledge Pierre Ménard–Tremblay for his assistance and resourcefulness in GPC analysis. Moreover, I express many thanks to Prof. Christian Pellerin, Marie Richard-Lacroix, and Damien Mauran for helping me with IR experiments, interpreting results, and numerous fruitful discussions.

I am grateful to AIST NT and Andrey Kayev for the high resolution AFM images of phosphonate-modified substrates.

I would like to thank summer intern, Charly Ou, for his diligence and patience in performing ellipsometry kinetics studies.

The past and present members of the Giasson's and Skene's laboratories have been to me the much more than colleagues, through their scientific insights and their emotional support. Béatrice Lego, Andréanne Bolduc, Stéphane Dufresne, Dr. Yanmei Dong, Dr. Satya Barik, Sophie Bishop, Thomas Skalski, Lucie Giraud, Vivian Machado, words cannot describe my gratitude. Especially I would like to thank Andréanne and Sophie for taking care of in-time chemicals and disposables ordering, instruments maintenance and overall lab care. This made my synthetic work pleasant and effective. Also, I would like also to express my sincere thanks to the members of other groups for the good time spending together and helpful advices: Adeline Lafon, Eliza Hutter, Alexandre Moquin, Jean-Richard Bullet, Na Xue, Stéphanie Boissé, Fabien Perineau, Anna Gittsegrad.

I am thankful for the administrative support from André Beauchamp, Christian Reber, Nina Duguay-Hébert, Céline Millette, as well as technical support from Cédric Ginart, Jean-François Myre and Martin Lambert.

Thanks a lot to Maksym Kryuchkov and Iryna Perepichka for their many insightful suggestions in science and everyday life, moral support during early days in Canada and UdeM, and shared wisdom in facing the difficulties of graduate studies.

I would like to thank my dear parents Yurii and Olena Borozenko for giving me courage and determination to pursue my goals. Also I thank my sister Katia who brought me a piece of home when she decided to pursue her graduate studies in UdeM.

Finally, I am evermore grateful to my family: my husband, Vladimir, for his endless love, constant support, and absolute understanding, and to my little treasure, Eva, for giving me a new meaning of life.

Chapter 1

General Introduction

1.1. Polymer brushes. General concept

The term *end-grafted polymers* corresponds to systems where macromolecules are attached by one anchoring point to the surface (interface). During the last decades, such polymer films have served as useful platforms to develop intelligent multifunctional materials for colloidal stabilization against aggregation,[1,2] for numerous biomedical[3-6] and engineering[7-9] applications as well as "smart" substrates having unique properties.[3,10] The large variety of substrates that can be modified with polymer layers includes silica, mica, graphite, metals, carbon, cellulose, etc. The combination of polymer chains with an inorganic material opens new opportunities for contemporary material chemistry in terms of designing hierarchically-ordered structures having well-controlled morphologies and properties.[3]

There are three main conformations of surface end-grafted chains (Figure 1-1): *pancake*, *mushroom*, and *brush*. The *pancake* conformation is characterized by low polymer grafting density with $d>>R_G$, where d is the distance between anchoring points and R_G is the corresponding radius of gyration of polymer chain in solution (Figure 1-1, A). This regime is also characterized by polymer-surface attraction, resulting in spreading of the polymer chains over the substrate. *Mushroom* conformation is observed when the $d \geq 2R_G$ (Figure 1-1, B). With increasing surface coverage, the *brush conformation* is adopted. In this regime d is much smaller than R_G. All chains tend to stretch away from the surface because of strong repulsive segment-segment interactions. (Figure 1-1, C).

The brush conformation exhibits particular properties because of its strong stretching. For example, polymer brushes can be used as ultra-low friction self-lubricating surfaces in artificial implants.[11] "Smart" or stimuli-responsive platforms are also possible with polymer brushes by undergoing conformational changes in response to specific stimuli (pH, ionic strength, light, mechanical stress) and such responsive platforms are extensively used in biology and medicine as nanosensors.[3]

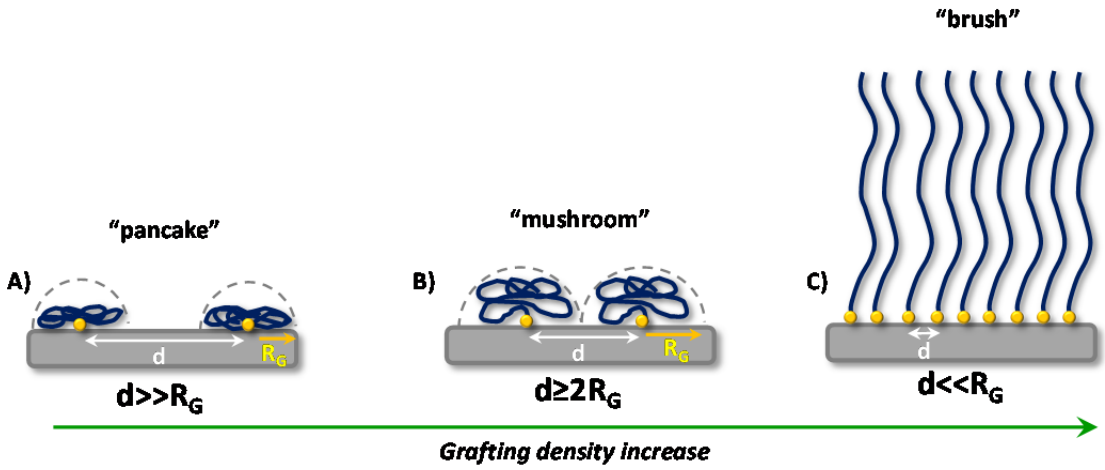

Figure 1-1. Conformations of end-grafted polymer chains A) – "pancake" conformation; B) – "mushroom" conformation; C) – "brush" conformation.

This thesis focuses on the synthesis of polymer brushes and their surface properties at high grafting density. After a brief overview of different grafting methods, the synthesis of polymer brushes using controlled radical polymerization methods will be presented. A general theoretical description of different types of polymer brushes will also be given. The unique surface properties specified by higher-order interactions between adjacent polymer chains will also be reviewed and the current knowledge in the studied field will be provided.

1.2 Polymer grafting methods

Polymer grafting refers to linking (tethering) polymer chains to the substrate. Methods of polymer tethering can be divided into two major groups depending on the type of polymer interaction with the substrate: grafting by physisorption and grafting by chemisorption. Grafting by physisorption relies on physical interactions of the polymer with the substrate. This is straightforward and does not require complicated equipment. However, physisorbed films can be easily detached from the surface, and

their thermal instability leads to poor control over grafting density. Grafting by chemisorption is the covalent bonding of polymers to the substrate. This method is more complicated than physisorption and it requires precise grafting conditions and complex equipment. Chemisorbed polymer layers are more robust than physisorbed films and they show long-lasting stability. This is important for many practical applications.[12-14]

1.2.1 Physisorption of polymers

The physisorption of polymer involves weak interactions (electrostatic, hydrophobic, and hydrogen bonds) between the polymer chain and the substrate. Attaching the polymer to the substrate can be done using coating techniques, absorption from solution, Langmuir-Blodgett, and layer-by-layer deposition (Figure 1-2).[13]

For all *coating techniques* (spin coating, dip coating and spray coating), the molecules are deposited by evaporating the solvent. Spin-coating is a deposition procedure where the polymer is dissolved in a volatile solvent and the solution is spun over the substrate, followed by solvent evaporation (Figure 1-2, I).[15] Dip coating can be separated into several steps: immersion of the substrate into a solution, withdrawal from the coating fluid, and drying (Figure 1-2, II, A-C).[16] Spray coating is done by depositing the polymer solution on a substrate by a sprayer and the film is dried under air (Figure 1-2, III). These techniques can give well-defined polymer thin films when the deposition conditions (solvent, deposition time) are controlled properly. The advantage of dip- and spin-coating is that homogeneous films of the order of few nanometers thick are possible.

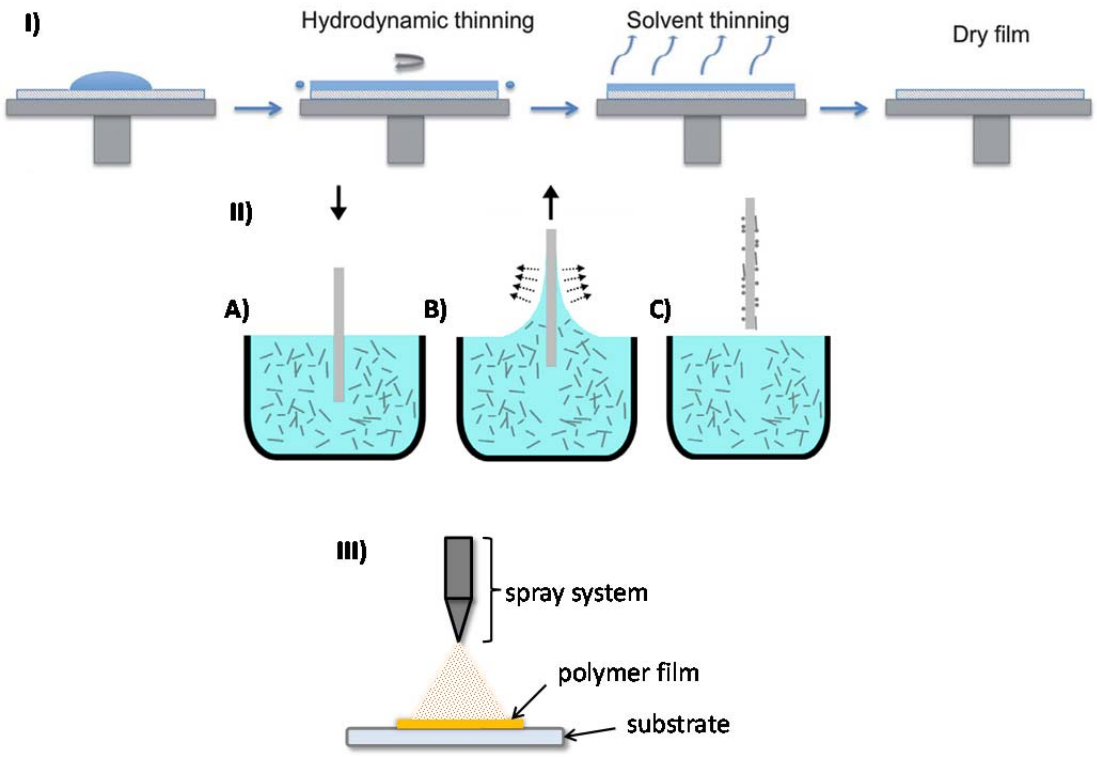

Figure 1- 2. Schematic illustration of different coating processes. I) spin-coating (Reproduced from ref. 15 with the permission of the Royal Society of Chemistry); II) dip coating process includes three steps: immersion of a substrate into the solution (A), withdrawal of the substrate (B), drying (C). (Reproduced from ref. 16 with the permission of Elsevier); and III) spray coating.*

Polymer adsorption from solution. Long polymer chains in solution can adopt numerous conformations because of entropic factors. However, the number of possible polymer conformations of a homopolymer is reduced when absorbed on a substrate. Polymer adsorption occurs when the attractive force between the polymer and the surface is higher than the conformational entropic loss.[17-19] The simplest case is the adsorption of the homopolymer (Figure 1-3, A).

* It is important to mention that all these techniques can be applied for grafting by chemisorption when the used polymer is end-functionalized.

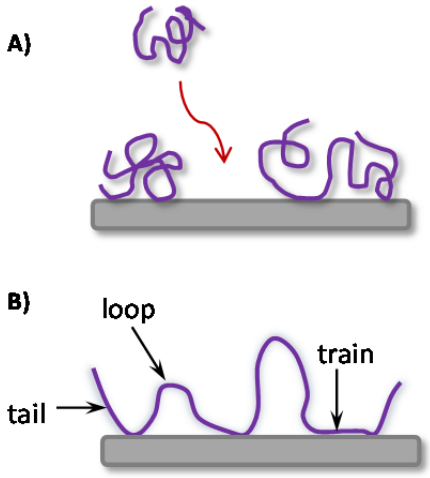

Figure 1-3. A) Schematic representation of homopolymer adsorption on a flat substrate from solution. B) Possible polymer chain conformation.

The possible polymer conformation on the surface was studied experimentally and it was confirmed with computer simulations. Figure 1-3, B shows a typical conformation of a homopolymer chain adsorbed on the substrate. This conformation is represented by a combination of tails, loops, and trains.[20] Tails are the end parts of adsorbed polymer chains that extend far from the surface. Loops are groups of freely spaced adjacent monomers between two surface linked units. In contrast, trains are groups of adjacent units that are bonded to the surface.

In adsorption of diblock copolymers, the poorly-solvated block interacts with the substrate, while, the other block extends away from the surface into solution. The adsorption of diblock copolymers has also attracted much attention, particularly, because such adsorbed macromolecules can be considered as high molecular weight amphiphiles and their morphological characteristics, such as molecular weight and relative length of the blocks, determine macroscopic film properties.[21,22]

Layer-by-Layer (LbL) deposition. This technique is based on stacking of oppositely charged polymers (Figure 1-4). This is done by successively dipping the substrate into solutions containing interacting macromolecules. After each

deposition, the substrate is thoroughly washed to remove the weakly adsorbed molecules and to avoid cross-contamination of the solutions. The driving force for polymer adsorption is the entropic gain from releasing the counter ions. The layers are typically stabilized by electrostatic forces.[23] However, there are some examples where LbL films are stabilized by hydrogen bonding, hydrophobic interactions, DNA hybridization, and covalent bonding.[24]

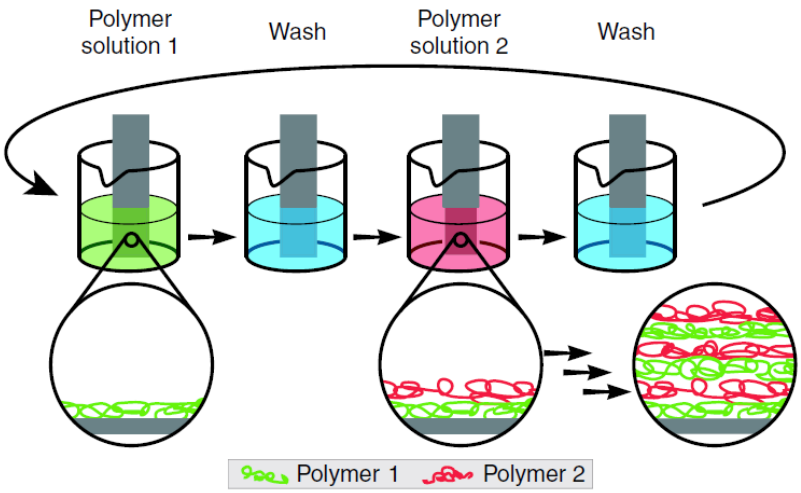

Figure 1-4. Schematic representation of layer-by-layer deposition on a flat surface. (Reproduced from ref. 24 with the permission of Elsevier).

Langmuir-Blodgett (LB) technique. This is an elegant method for fabricating nanostructured films. It was invented by Irving Langmuir and Katherine Blodgett.[25] In this method the insoluble amphiphilic polymer chains form a monolayer at air/water interface. The hydrophilic block usually stays immersed in the aqueous medium while the hydrophobic block tends to be collapsed at the air/liquid interface because of the unfavourable interaction with water. The monolayer can be transferred to a solid support either by touching the monolayer with the substrate horizontally (Langmuir-Schaefer method) or by pulling the substrate vertically out (Langmuir-Blodgett method) (Figure 1-5).[25,26] Once the monolayer is adsorbed, a thin film of accurate thickness and degree of ordering can be formed.[27,28] LB polymer films,

however, suffer from limited mechanical and thermal stability. Particularly, decomposition of LB films often happens at temperature below 100°C.[29] Also LB films can be destroyed under high pressure.

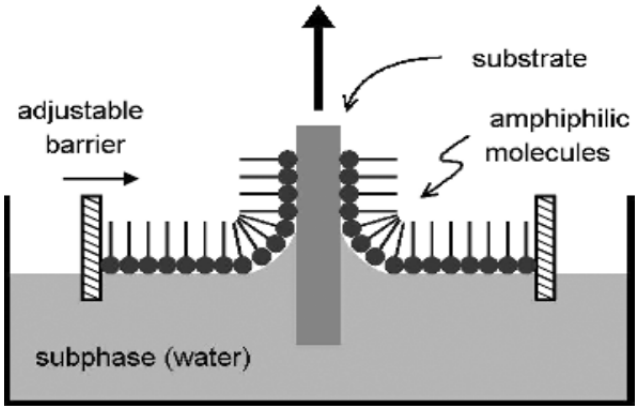

Figure 1-5. Schematic representation of Langmuir-Blodgett deposition.
(Reproduced with permission from ref. 13
Copyright Wiley-VCH Verlag GmbH & Co. KGaA.)

These deposition methods represent simple ways to prepare polymer-coated surfaces. However, the physisorbed polymer films have a limited range of potential applications due to the weak interactions between the substrate and polymers that results in film detachment or displacement. Polymer films can be destroyed by replacing the weakly attached polymers by strongly adsorbed polymers (adsorption-desorption exchange).[30-32]

Also, temperature changes cause many undesired processes with physisorbed polymers. For example, dewetting occurs when a thin polymer film is heated above its glass transition temperature (T_g), resulting in micro- or macroscopic ruptures in the film and to morphology changes.[33-35] Another process is film delamination. This usually occurs at temperature below the T_g, when the film is in a glassy state. Delamination is caused by severe mechanical stress and also results in significant changes in film topography.[24,25]

Chemisorption overcomes most of the above mentioned shortcomings because of the stronger polymer-substrate bond. However, it requires more sophisticated deposition methods and equipment to accurately control the grafting conditions.[1,13]

1.2.2 Chemisorption of polymers

In contrast to physisorbed polymer coatings, chemisorbed layers are more robust because they are linked to the substrate via covalent bond. They can also sustain a larger variety of environmental conditions. There are three methods to get chemically attached polymer layers to the surface: *grafting to* (onto), *grafting through* and *grafting from*.

1.2.2.1 *Grafting to* method

In the *grafting to* method (Figure 1-6), presynthesized polymers are covalently attached to specific sites on the surface through their functional end groups. This results in end-tethered polymer chains.[3] Typical end-groups that react with substrates are silanes,[36-38] hydroxyls,[39] thiols,[40,41] amines[42] and carboxylic acid groups.[43] These chemical bondings are straightforward and are similar to the self-assembly.[13,44] The anchor group is usually polar, and such polar or charged side groups compete with end-grafting. In this case, the attached layer consists of both physisorbed and covalently linked polymers.[45,46] The main advantage of *grafting to* approach is that the polymer can be fully characterized prior to the grafting. This allows the polymers with low molecular weight distribution to be used in grafting, resulting in well-defined polymer brushes.

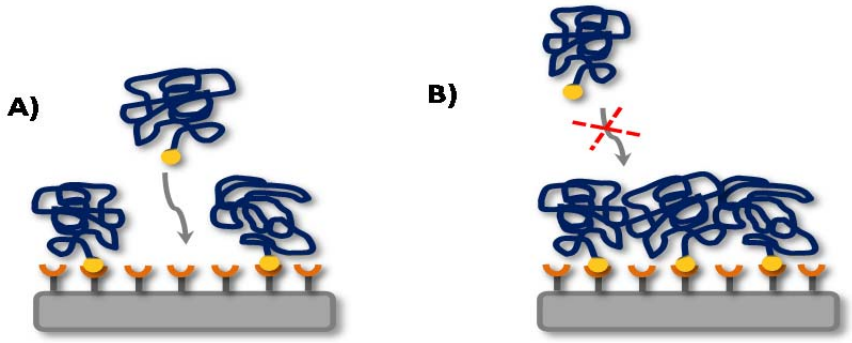

Figure 1-6. A) Schematic illustration of *grafting to*. B) Limitation of grafting to: formation of steric barriers that prevent an additional attachment of polymers.

The main disadvantage of the *grafting to* approach is its grafting density, and consequently, its low polymer film thickness (1-5 nm).[13,37] Large grafting densities are difficult to obtain because the adsorbing chains disfavour further polymer adsorption due to the steric hindrance (or excluded volume) effect (Figure 1-6, B). This effect is more pronounced when increasing the grafting density. However, the grafting density of the brushes prepared with the *graft to* approach can be improved either by grafting the polymer from its melt,[47] or from its concentrated solution,[48] or using a "theta" solvent as the grafting solvent.[49] These approaches usually result in higher polymer grafting density because of the screening of the excluded volume effect.

1.2.2.2 *Grafting through* method

This is a straightforward technique that consists of polymerizing in the presence of a monomer-functionalized substrate.[13] The substrate containing a monomer layer is added to the polymerization mixture. After polymerization, the synthesized polymers remain connected to the substrate.[50,51]

An example of *grafting through* polymerization using reversible addition-fragmentation chain-transfer (RAFT) is shown in Figure 1-7. A crosslinked layer of polycarbazole containing a methacrylate monomer was used for RAFT polymerization of methyl methacrylate and other monomers. The resulting PMMA film was varied from 9 to 22 nm in thickness.[50]

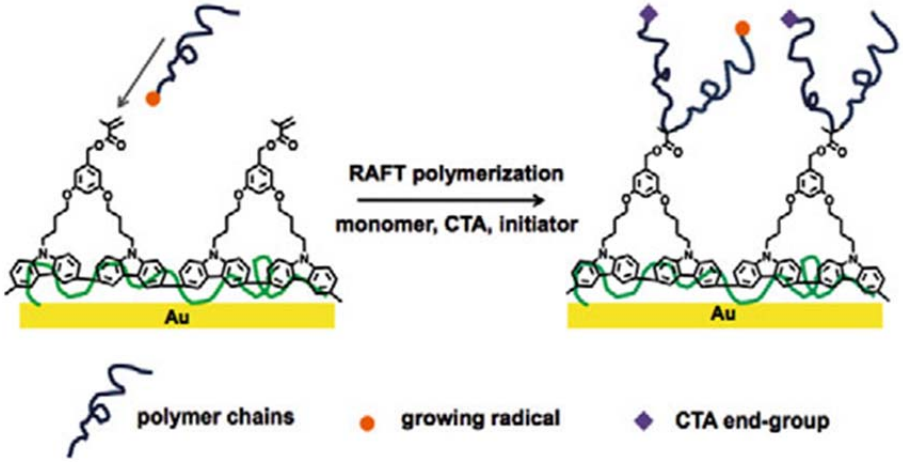

Figure 1-7. Schematic representation of RAFT "grafting through".
CTA refers to chain transfer agent.
(Reproduced from ref. 50 with the permission of Springer).

The *grafting through* has the advantage of being straightforward and utilizes controlled radical polymerizations. It is a good alternative to *grafting to* because it does not require synthesizing end-functionalized polymers. However, it suffers from the same disadvantages as the *grafting to* method, particularly, only limited grafting densities can be obtained.[13]

1.2.2.3 *Grafting from* method

Grafting from is a powerful alternative that involves the *in-situ* polymerization of an initiator-functionalized substrate. For this, the initiating groups are covalently attached to the surface (Figure 1-8).[13,52]

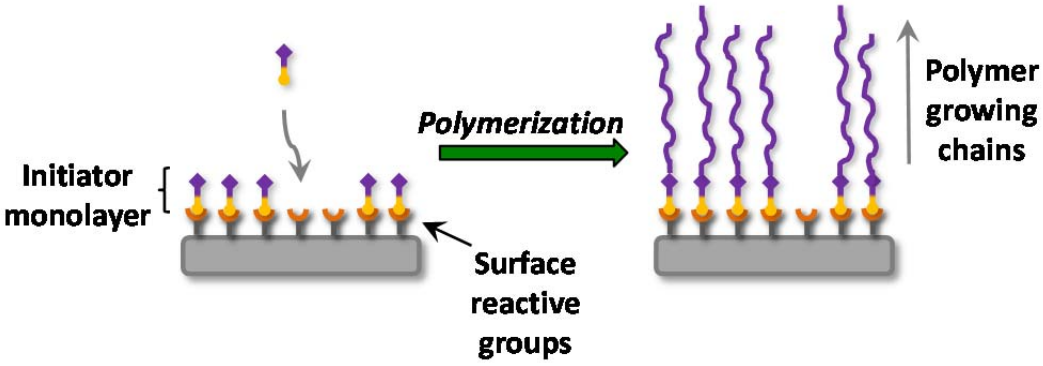

Figure 1-8. Schematic representation of "grafting from" consisting of an initiator covalently immobilized on the surface and polymerization using a controlled polymerization technique.

In contrast to *grafting to*, the *grafting from* method produces well-defined polymer brushes of high grafting density. This is because the grafted layer is swollen by the monomer solution and monomer diffusion towards the growing chains is not limited.[53] It must be noted that the polymer molecular weight distribution of the grafted chains is broader than in the *grafting to* method. This is linked to several aspects, such as polymerization side reactions, low initiator efficiency, and high termination rate between neighbouring propagating radicals.[54]

The *grafting from* method is widely used to synthesize polymer brushes from substrates of different geometries, such as flat, curved, and linear topologies (Figure 1-9).

There are many polymerization techniques that can be used to synthesize polymer brushes, such as anionic,[55,56] cationic,[57,58] ring-opening,[59] ring-opening metathesis,[60] and conventional free radical polymerization.[61,62] However, controlled/"living" radical polymerization (CRP) techniques are particularly attractive to obtain polymer brushes having desired thickness, composition, architecture, and functionality.[37,63,64]

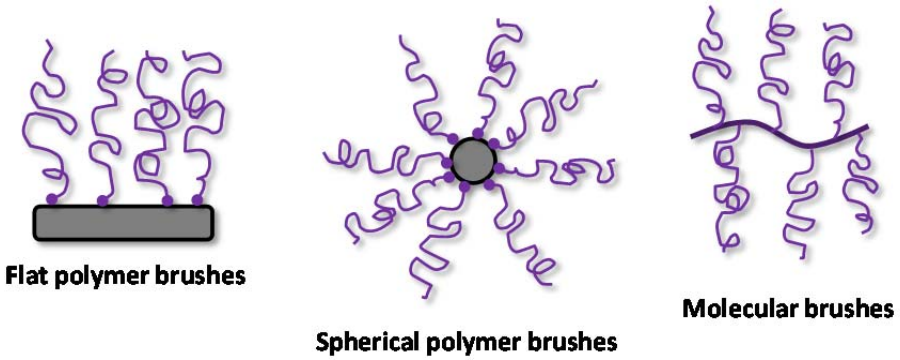

Figure 1-9. Examples of chemically attached brushes on different substrates.

1.3 CRP techniques: General overview

The precise control of polymer molecular weight, composition, and functionality is possible with controlled/ "living" radical polymerization (CRP) methods. There are three main methods of CRP: nitroxide mediated polymerization (NMP), reversible addition-fragmentation chain transfer polymerization (RAFT), and atom transfer radical polymerization (ATRP).

ATRP is the key polymerization technique that we used in the present work. We will therefore provide a brief comparison of CRP to conventional free radical polymerization. A detailed description of ATRP and its use for surface modification will follow.

1.3.1 CRP vs. conventional free radical polymerization

Understanding the principles of conventional free radical polymerization is of importance for investigation the advantages of CRP. Thus, this section focuses on comparing these two radical polymerization methods.

Conventional radical polymerization involves three main steps: initiation, propagation, and termination. The initiation forms the reactive species – radicals,

followed by their addition to the monomer. During the propagation step, the radicals react with the monomer until bimolecular coupling between two radicals occurs. This leads to the formation of a dead polymer and the active sites are irreversibly destroyed (Scheme 1-1).[65]

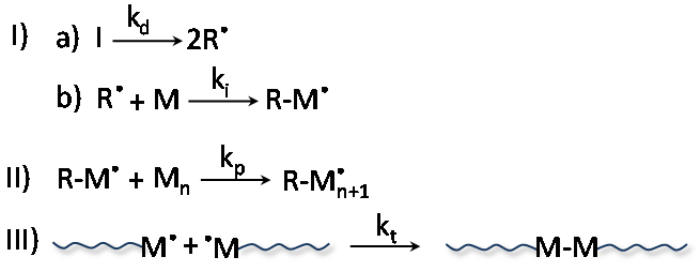

Scheme 1- 1. Schematic illustration of the three main steps of radical polymerization: I) initiation, II) propagation, III) termination, where I is an initiator, R· is a radical, M is a monomer.

The overall kinetics can be expressed by the following equation (1.1):[66]

$$R_p=k_p[M](fk_d[I]_o/k_t)^{1/2} \quad (1.1)$$

where R_p is a rate of polymerization, which is proportional to the initiation efficiency (f), initiator decomposition (k_d), chain propagation (k_p), chain termination (k_t) rate constants, and concentration of monomer ([M]).

The degree of polymerization depends on the termination and transfer rates. When the transfer is close to zero, the polymer average degree of polymerization (DP_n) is proportional to the concentration of initiator ($[I]$) according to eq. 1.2:

$$DP_n=k_p[M](fk_d[I]_ok_t)^{-1/2} \quad (1.2)$$

During free radical polymerization, the radical lifetime is extremely short (less than a second). Such conditions cannot assure proper control over polymer molecular weight and molecular weight distribution. Therefore, well-defined block or

graft copolymers are not readily possible.[46,47] However, this control is possible with "living" polymerization that has a low termination rate.

Radical polymerization having "living" properties is called controlled radical polymerization (CRP). This approach was presented for the first time more than 35 years ago,[67] but it only was employed for controlled radical polymerization. CRP has the advantage of simultaneous initiation and chain growth. A fast exchange between active and dormant species is an absolute requirement for controlled polymerization kinetics. An active species react with just a few monomers within a few milliseconds before it deactivates to the dormant state (Scheme 1-2).

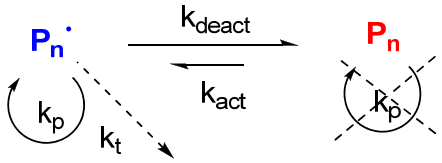

Scheme 1-2. Exchange between active and dormant species in CRP, where P_n is a polymer of length n, $P_n^{\bullet}$ is a polymeric radical of length n.

Some important features between conventional free radical polymerization and CRP are compared in Table 1-1.

There are three main types of CRP: RAFT, NMP and ATRP. RAFT is based on a degenerative transfer mechanism with the presence of a transfer agent, while NMP and ATRP are based on persistent radical effect. This effect relies on the formation of two species, persistent ($Y^{\bullet}$) and transient ($R^{\bullet}$) radicals, during the initiation step (Scheme 1-3, I). Transient radicals can self-terminate (Scheme 1-3, III), while persistent radicals cannot and they disappear only by cross-coupling (Scheme 1-3, II). [70-72] In NMP persistent radicals are free nitroxide species, whereas, in ATRP, it is a metal complex in a higher oxidation state.[65,66,68,69]

Table 1-1. Comparison between free radical polymerization and CRP

Parameter	Free radical polymerization	CRP
1. Initiation	Slow and continuous. Only a small initiator portion is consumed to initiate the reaction.	Fast. Instantaneous initiation and growth of all chains.
2. Growing chain lifetime	Less than a second	Up to several hours
3. Polymerization rate	Fast polymerization	Relatively slow polymerization
4. Portion of dead chains	Almost all chains are dead	The part of dead chains is <10%
5. Steady state	Balance between rates of initiation and termination.	Balance between rates of activation and deactivation
6. Termination	Bimolecular termination and chain transfer (chain-breaking reactions) take place between long chains and generated new chains.	No chain-breaking reactions. Because of the huge number of growing chains, only a small portion of them is terminated (1-10%), the rest of the chains are deactivated, but can be activated back.

*Comparison from information provided by references[13,65,66,68,69]

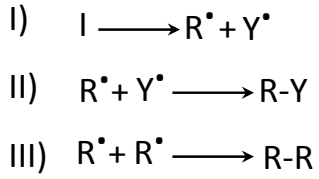

Scheme 1-3. Schematic illustration of formation of persistent Y• and transient R• radicals and their termination.

RAFT is a Radical Addition-Fragmentation chain transfer polymerization assisted by a chain-Transfer (RAFT) agent. The polymerization is started with a conventional free radical initiator (peroxide or AIBN) decomposition that generates

the propagating radicals. The propagating radical adds to the carbon-sulfur double bond of the RAFT agent. This intermediate is further converted to another macroradical and an equilibrium between dormant and active species is established (Scheme 1-4, A).[73,74]

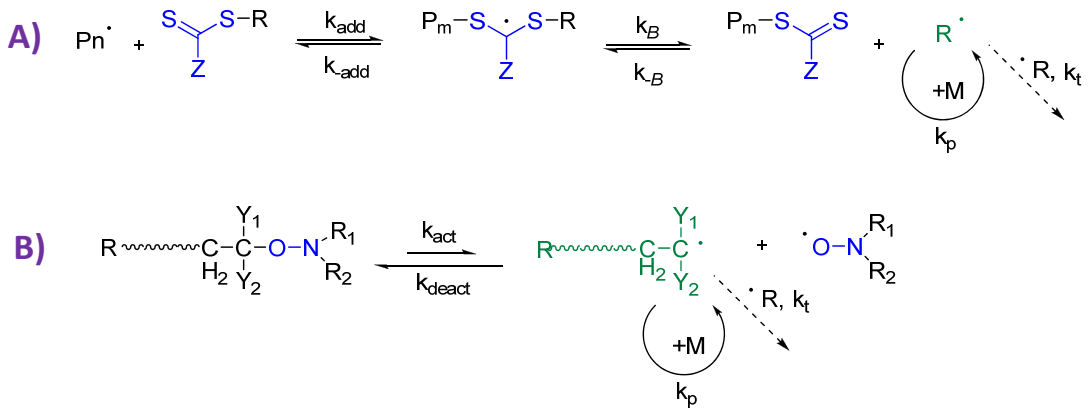

Scheme 1-4. Mechanism of RAFT (A) and NMP (B) polymerizations, where $P_n^{\bullet}$ is a polymeric radical of length n, and k_β is a fragmentation rate coefficient.

The driving force in *NMP* is the thermal homolytic breakage of an alkoxyamine bond followed by monomer addition to the transient radical. The reactive radical can then be capped with a persistent nitroxide to form a dormant species (Scheme 1-4, B).[66,75]

ATRP is discussed more in details in the following sections.

1.3.2. ATRP: General concept

ATRP (Atom Transfer or transition metal catalyzed living Radical Polymerization) was introduced in 1995 by Sawamoto and Matyjaszewski independently.[76,77] This polymerization method is based on atom transfer radical addition (ATRA), a well-known reaction of carbon-carbon bond formation.[78] In turn, ATRA originates from the Kharasch addition reaction that was reported for the first

time in 1940s. ATRA refers to a direct addition of polyhalogeneted alkane to an alkene in the presence of a free radical initiator and involves a free radical mechamism (Scheme 1-5).[79,80]

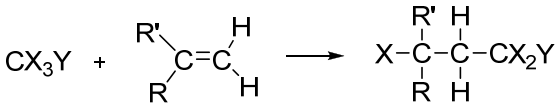

Scheme 1-5. Schematic representation of Kharasch addition.

ATRA is catalyzed by a metal complex. After the initial addition of the monomer to the double bond of an alkene, the obtained product is unstable and reacts with a transition metal complex irreversibly. Consequently, only one addition step occurs.[81,82]

The ATRP mechanism is described in Scheme 1-6. ATRP is based on the reversible oxidation of a transition metal complex (Mt^nL_m) with transport of a halogen atom, (X), from a *dormant species*, (P_n-X). A dynamic equilibrium is established between the halogen-capped polymer chain and the corresponding radical ($P_n^{\bullet}$; *active species*) with a rate constant of activation, (k_{act}), and deactivation, (k_{deact}). Propagating radicals polymerize with a propagation rate constant (k_p) until it is deactivated by the $Mt^{n+1}L_m$ complex. The number of monomer units added during an activation cycle tends to be minimum and the k_{deact} is much larger than k_p.[83] At the end of the polymerization reaction, all the chains are capped with a halogen through reversible halogen exchange reaction. Those can then be used as macroinitiators for further ATRP reactions.

Shifting the equilibrium towards the dormant species and fast switching between the activation-deactivation states assures a low concentration of active species and, consequently, good control over the polymerization. As it has been shown by means of electron paramagnetic resonance (EPR), the concentration of deactivator (that relates to the concentration of active propagating species) does not

exceed 6% for a well-controlled system.[84-86] Adding small portions of deactivator at the beginning of the polymerization can improve the general polymerization control. The role of deactivator in this case shifts the equilibrium towards the dormant species and improves the overall reaction control. Usually about 10% of deactivator is added, corresponding to the deactivator quantity that is generated during polymerization due to irreversible deactivation.[87] Termination reactions can also occur with a rate constant of termination (k_t). However, in well-controlled ATRP, only a few percent (≤5%) of growing polymer chains are subjected to termination.[88] The termination reactions usually occur during the initial step when the concentration of deactivator (as persistent radicals) has not reached yet the optimum.[71,88]

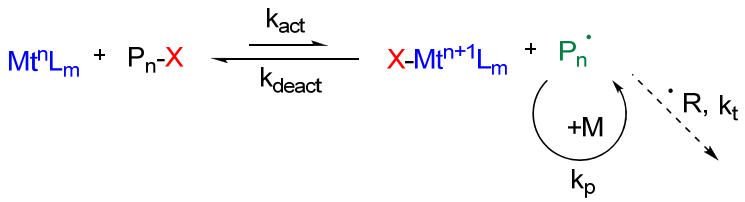

Scheme 1-6. Schematic representation of the ATRP mechanism.

A key component of ATRP is the transition metal complex catalyst.[69,88] The ideal transition metal has two oxidation states that differ by one electron and it must be able to accommodate the halogen atom within the coordination sphere. Suitable metals that satisfy these criteria are iron, ruthenium, nickel, and palladium. However, the most extensively used catalysts for ATRP are copper salts because of their low cost and exceptional versatility. The nitrogen- and phosphorus-based ligands play a vital role in solubilizing the transition metal salt in organic media and they adjust the redox potentials of the transition metal. For copper-mediated reactions, nitrogen-based ligands are the most appropriate. [65,66,68,88] Figure 1-10 shows some examples of generally used ligands and initiators for ATRP.

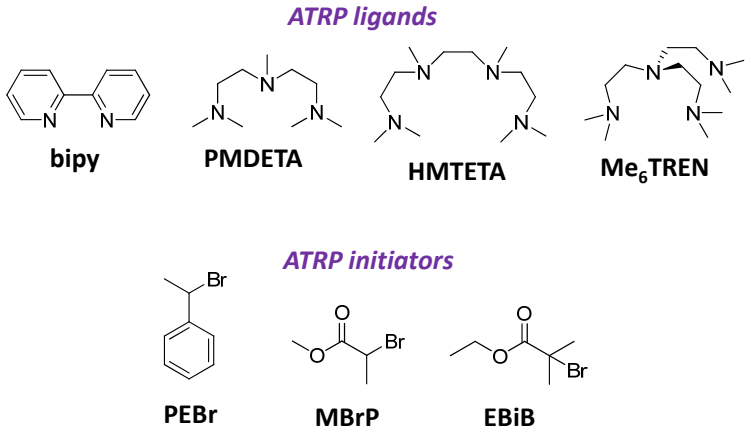

Figure 1-10. Examples of commonly used ligands and initiators in ATRP. Ligands (from left to right): 2,2'-bipyridine (bipy), N,N,N′,N″,N″-pentamethyl diethylenetriamine (PMDETA), 1,1,4,7,10,10-hexamethyl triethylenetetramine (HMTETA), tris[2-(dimethylamino)ethyl]amine (Me_6TREN); Initiators (from left to right): 1-phenyl ethylbromide (PEBr), methyl 2-bromopropionate (MBrP), Ethyl 2-bromo-2-methylpropionate (EBiB)

The role of the initiator is to define the number of propagating polymer chains. The initiator structure determines the activation rate, which should equal the propagation rate for well-controlled reactions. Alkyl halides (R-X) are typically used as initiators in ATRP, where the halide group (X) and alkyl radical (R) are carefully chosen, depending on the catalyst/ligand system. The most active initiator is α-bromophenylacetate because of the active benzyl and ester moieties.[89] Initiators containing multiple halide groups can also be used, resulting in the synthesis of complex architectures.

1.3.2.1. ATRP equilibrium and kinetic aspects

Understanding the impact of kinetic parameters on "living" polymerization is of importance for the synthesis of polymeric materials having defined characteristics. The overall ARTP equilibrium can be separated into four contributing reversible

reactions (Scheme 1-7). ATRP follows first-order kinetics for monomer, initiator and metal complex in its lower oxidation state, and negative first-order kinetics for metal complex in its higher oxidation state. The rate of polymerization, (R_p), is expressed by the following equation (1.3), where k_p is a propagation constant rate, [M] is a concentration of monomer, [P$^{\bullet}$] is a concentration of polymeric radical, [PX] is a concentration of polymer, [$XM_t^{n+1}L_m$] is a concentration of deactivator, [$M_t^nL_m$] is a concentration of activator , and K_{eq} the overall equilibrium constant:

$$R_p = k_p[M][P^{\cdot}] = k_p[M]K_{eq}\frac{[PX][Mt^nL_m]}{[XMt^{n+1}L_m]} \quad (1.3)$$

The overall equilibrium constant, (K_{eq}), is defined by equation 1.4, where k_{act} and k_{deact} are activation and deactivation rate constants, respectively. Both constants, k_{act} and k_{deact}, are strongly influenced by the structure of the ligand, monomer, and environmental conditions. Thus, all these parameters are highly important for polymerization control.[68,82,83]

Contributing reactions for Cu-mediated ATRP

$$Cu^{(I)}Br/L \rightleftharpoons Cu^{(II)}Br/L + e^{\ominus}$$
$$Br^{\bullet} + e^{\ominus} \rightleftharpoons Br^{\ominus}$$
$$R\text{-}Br \rightleftharpoons R^{\bullet} + Br^{\bullet}$$
$$Br^{\ominus} + Cu^{(II)}Br/L \rightleftharpoons Br\text{-}Cu^{(II)}Br/L$$

Scheme 1-7. Schematic representation of the contributing reactions of Cu-mediated ATRP.

$$K_{eq} = \frac{k_{act}}{k_{deact}} = \frac{[P\cdot][Mt^{n+1}L_m]}{[Mt^nL_m][PX]} \quad (1.4)$$

The synthesis of polymers having controlled architectures requires controlling the degree of polymerization (DP) and polydispersity index (PDI). The degree of

polymerization is determined by the initial concentration of initiator, ([*I*]), and conversion, (*p*) according to eq. 1.5:

$$DP = \frac{[M]_0}{[I]_0} \times p \tag{1.5}$$

The molecular weight distribution in well-controlled systems typically is less than 1.1.[88] Equation 1.6 shows how the PDI is affected by concentration of the deactivator [$XM_t^{n+1}L_m$], monomer conversion and k_p/k_{deact} ratio.[90]

$$PDI = \frac{M_w}{M_n} = 1 + \left(\frac{2}{p} - 1\right)\left(\frac{[P_nX]k_p}{k_{deact}[XM_t{}^{n+1}L_m]}\right) \tag{1.6}$$

It can be concluded that the presence of the catalyst, which deactivates the growing chain faster, will result in a smaller k_p and k_{deact} ratio and, consequently, a polymer with a narrow PDI will be obtained.[88] Also, the PDI can be easily decreased by increasing the deactivator concentration or by pushing the polymerization to high conversions. Equation 1.6 shows the ideal situation where no chain termination and transport occur. However, in reality, the termination and transfer occur. They can be limited by lowering the degree of polymerization.[89,90] Accomplishing these requirements results in well-defined polymers having narrow molecular weight distribution.

1.4. Surface-Initiated ATRP (SI-ATRP)

In general, ATRP is the most versatile and robust polymerization technique for modifying surfaces. The first example of polymer brush synthesis via SI-ATRP was reported in 1997 by Huang and Wirth, where they successfully polymerized acrylamide from the benzyl chloride monolayer on silica particles.[91]

The key to SI-ATRP is the polymerization of a surface-attached initiator monolayer. This results in an end-tethered polymer layer. SI polymerization is based

on the same kinetic principles and rules as solution polymerization. Scheme 1-8 shows a typical ATRP from an initiator-functionalized flat surface.[92]

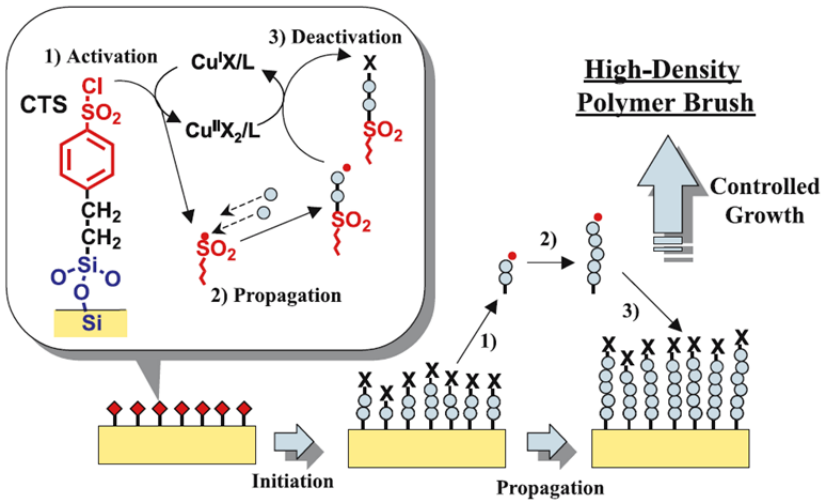

Scheme 1-8. Schematic representation of SI-ATRP using Cu-based catalyst. (Reproduced from ref. 64 with the permission of Springer).

The first step is the attachment of the initiator (2-(4-chlorosulfonylphenyl) ethyltriethoxysilane, (CTS), to silica via a covalent Si_{surf}-O-Si_{init} bond. The Cu(I)X/L complex is transformed into a higher oxidation state (Cu(II)X_2/L) by a halogen transition (*activation*). This results in a free radical at the end of the polymer chain, which reacts with monomers (*propagation*) until it is capped with the halogen (*deactivation*). The activation-deactivation occurs repeatedly and results in the simultaneous growth of surface-attached chains.

1.4.1. SI-ATRP characteristics

In spite of identical mechanism and general kinetic similarities between SI and solution ATRP, there are specific features of SI-ATRP that must be reviewed.

1. The properties of the polymer film can be tuned by the initiator grafting density. This requires proper control over the initiator grafting process.

There are several ways to do this. The most common way is varying the concentration of deposited initiator molecules and/or the coupling time.[93] It can also be done by grafting a mixture of active and inactive ("dummy") initiators in different ratios.[94] Alternatively, a portion of grafted initiator can be destroyed under radiation exposure (post-grafting treatment).[95] These approaches assure the proper number of initiator molecules to be attached to the substrate that, in turn, results in desired polymer brush characteristics (thickness, molecular weight, architecture).

2. Low concentration of surface-attached initiator on flat surfaces causes slow generation of deactivating species. This results in extremely low deactivator concentration and, consequently, high probability of termination reactions. To overcome this, a deactivator or sacrificial initiator has to be added to the polymerization solution (see section 1.4.2 for details).
3. SI-ATRP is characterized by a limited rate of propagation due to the unavoidable hindered monomer and catalyst diffusion to the growing chain ends.[96] This affects the polymerization kinetics and results in lower molecular weight of grafts compared to free chains. However, the opposite trend of larger M_n of grafts than free chains was also reported (see section 1.2.3 for details).
4. Termination. As it was shown by Gao et al. for flat surfaces, the radical centers are distributed quite sparsely over the attached chains, even at high grafting density. The bimolecular termination is impossible when two radicals are separated by more than 1000 nm. However, termination takes place when the chain is activated in close proximity to the existing radical. Two radicals come together via activation-deactivation exchange with the catalyst in solution. This mechanism is called "migration-termination"[97] or "radical migration" (Scheme 1-9).[98]

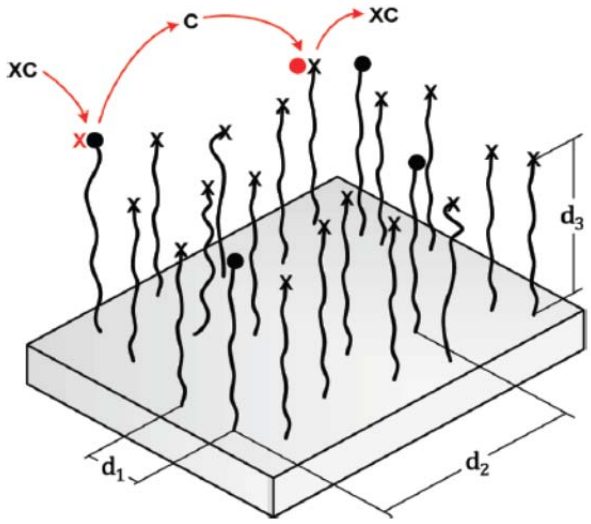

Scheme 1-9. Schematic representation of the "radical migration" mechanism. (X) represents dormant chain end, while (•) corresponds to active radicals. (Reprinted with permission from ref. 98 Copyright 2012 American Chemical Society.)

"Migration" mechanism was first described for surface-initiated RAFT polymerization. It was then called "rolling migration" because chain-end radicals interact with adjacent dormant chains, so active sites migrate from one chain to another and never leave the surface[99] resulting in high radical termination. In contrast to SI-RAFT, radical "migration" in SI-ATRP occurs through solution phase, and the term "hopping migration" is applied.[98] SI-ATRP radical "migration" is assured by diffusion of the catalyst molecules from solution. So, the termination rate is directly proportional to the concentration of activator, and higher catalyst concentration results in more terminations to occur.[97,98]

5. Self-initiation side reaction can be present during SI-ATRP. A recent report showed the presence of thermal self-initiation in solution during the SI polystyrene polymerization.[100] The analyzed free chains had lower molecular weight and larger PDI comparing to graft chains because they are formed continuously. Meanwhile the attached chains are initiated simultaneously and grow homogeneously.

1.4.2. Addition of deactivator or free initiator

The formation of highly homogeneous and smooth polymer layers requires a high degree of control over the polymerization process. One of the most important parameters affecting the polymerization kinetics is the deactivator concentration. Surface-initiated polymerization can be controlled only poorly because the concentration of dormant species attached to the surface is low.[92] There are two approaches that address this shortcoming. The first approach adds Cu(II) deactivator to the polymerization medium to assure sufficient concentration of deactivator and, consequently, good control over polymerization. This approach was shown for the first time by Matyjaszewski, where a linear increase in polymer film thickness over time was observed. The linear correlation suggests a living character of the grafting reaction.[96]

Adding free (sacrificial) initiator is an alternate way to control the surface-initiated polymerization. In this case, the initiator plays the same role as the deactivator (Cu(II)). Additionally, free polymer formed in solution can be used to measure the molecular weight of grafted chains, assuming the polymerization occurs at the same rate in solution as on the surface. This is particularly essential for flat substrates, where the amount of polymer generated on the surface is insufficient for analysis with conventional techniques such as GPC and NMR.[92,101] However, as reported recently, there is much uncertainty concerning the equivalence between M_n of free and grafted chains (see following section for details).

1.4.3. M_n of grafted chains vs. free polymer

Many reports claim that the M_n of free polymers differs from the M_n of grafted chains.[102-105] In general, the grafted propagating chains have fewer conformational degrees of freedom than in solution and confinement effects during surface-initiated polymerization are expected. The substrate curvature is also an

essential parameter that defines the accessible volume for catalyst and monomers to diffuse to the growing chains.[54] Figure 1-11 shows the accessible volume decrease (highlighted in purple) for substrates of different geometries where polymer brushes of identical grafting density and thickness are grafted.

For convex substrates, the M_n of grafted and free chains was shown to be similar. In contrast, for flat or concave surfaces, higher M_n of free polymer was measured compared to the M_n of grafts.[102,104,106] There are a few examples where the M_n of free chains was lower than the M_n of grafted ones on flat substrates.[103,107] The authors explained this result in terms of elevated local viscosity and increased local concentration of Cu(I) species.

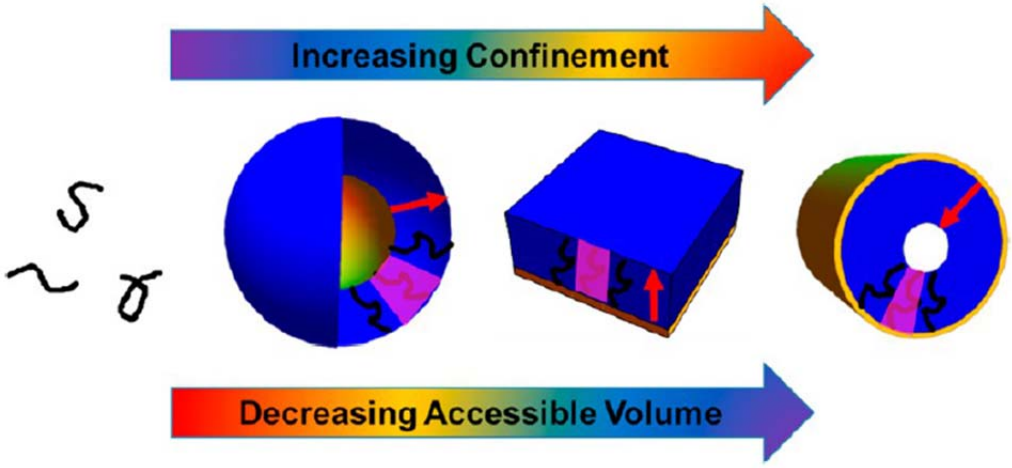

Figure 1-11. Schematic illustration of the confinement effect in SI-ATRP. Accessible volume decreases from convex to flat and to concave substrate. (Reprinted with permission from ref. 54 Copyright 2013 American Chemical Society.)

High grafting density results in high concentration of growing chains near the surface. This, in turn, results in increased local viscosity that limits the mobility of attached molecules and decreases the probability of the termination reaction compared to the bulk. The grafted chain ends are situated within the "viscous front" that corresponds to a region close to the surface but is separated from the bulk. The

diffusion of Cu(I) is higher in comparison to Cu(II), because of the Cu(I) smaller size. Thus, the increased concentration of the Cu(I) shifts the equilibrium to the side of active species.[107]

1.5. ATRP in aqueous medium

Water-mediated ATRP is of significant interest for two main reasons. Firstly, water is environmentally friendly, ready accessible and it is a cheap solvent. Secondly, the development of new materials requires the synthesis of well-defined polyelectrolytes, ionomers, and polymers with hydrophilic functional groups.[108-110] Therefore, the direct synthesis of hydrophilic polymers will result in significant reduction of processing costs since a deprotection step of an hydrophobic polymer is not required. There are numerous reports of successful water-mediated ATRP in heterogeneous systems, such as miniemulsions, emulsions, and microemulsions.[111-116] However, some applications that involve, for example, the preparation of substrate-attached polymer films require a water-assisted homogeneous system.

The first report in 1998 of water-mediated ATRP described the polymerization of 2-hydroxyethyl acrylate with CuBr/bipy.[117] The resulted polymer showed narrow PDI at high conversions (more than 80 %) demonstrating that ATRP can be easily performed in water. Since then, many water-mediated ATRP studies have been published, with different catalysts such as CuBr/HMTETA,[118] CuBr/TPMA (Tris[(2-pyridyl) methyl]amine),[119] and CuBr/Me_6TREN.[120] In general, ATRP in water is much faster than in organic media and it can be done at room temperature. However, the presence of side reactions that do not occur with organic-mediated ATRP makes water-assisted ATRP challenging.[121-123]

1.5.1. Side reactions in water-mediated ATRP

Scheme 1-10 demonstrates the overall process of water-mediated ATRP and its side reactions (highlighted in blue).

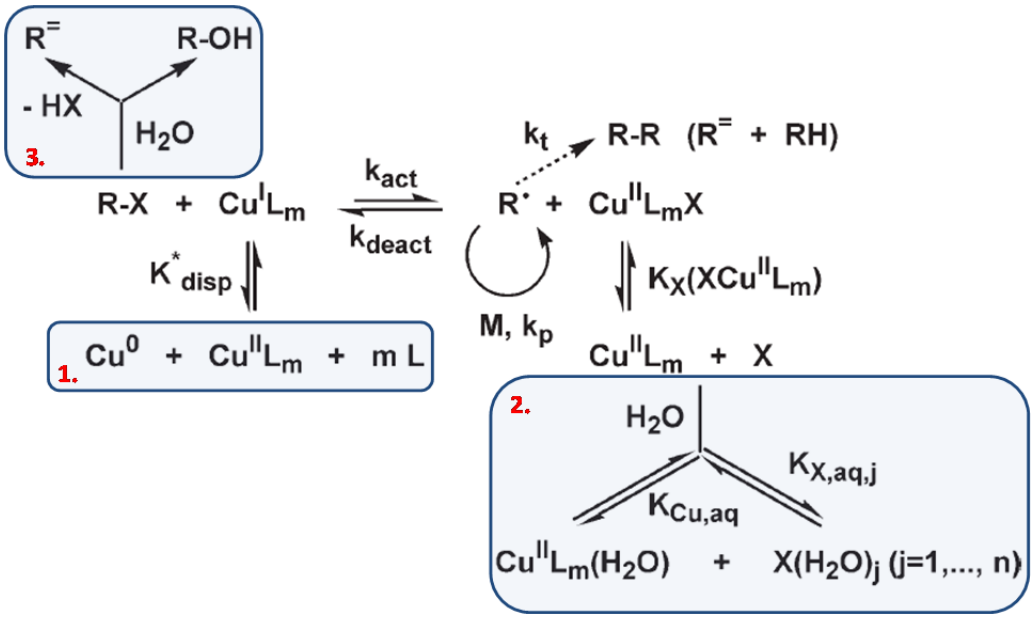

Scheme 1-10. Schematic representation of ATRP in water.
Side reactions are highlited in blue.
(Adopted with permission from ref. 121. John Wiley and Sons)

Side reactions of water mediated ATRP include:

1. *Disproportionation reaction of Cu(I) metal complex*. The Cu(I) catalyst is not stable in water and it disproportionates. The Cu(I) converts into a species with two different oxidation states (Cu(II) and Cu(0)) (eq. 1.7).[124-126] K_{disp} of the noncomplexed Cu(I) is 10^6.[127] This value is much lower in organic solvents. For example, in DMF $\log K_{disp}$= 4.26[128] and $\log K_{disp}$ = 0.56 in ethanol.[129]

$$Cu^{I} + Cu^{I} \underset{}{\overset{K_{disp}}{\rightleftharpoons}} Cu^{II} + Cu^{0} \qquad K_{disp} = \frac{[Cu^{II}]}{[Cu^{I}]^2} \tag{1.7}$$

Disproportionation facilitates the polymerization, because of the superior activity of the Cu(0) species. Alkyl halide initiators can be exceptionally activated by the presence of Cu(0) through outer-sphere electron transfer (OSET) mechanism. Cu(0) species is able to generate a propagating radical and Cu(I).[130] As was reported in literature, OSET is negligible compared to inner-sphere electron transfer (regular atom transfer) mechanism, however for controlled radical polymerization, the disproportionation has to be reduced in an optimum way.[131,132] Disproportionation can be significantly reduced by adding less polar solvents, such as methanol, ethanol, or acetone to the polymerization medium. K_{disp} is also affected by the ligand addition. When the ligand (L) is added, it forms complexes with Cu(I) and Cu(II), and the equilibrium constant K_{disp} changes to the conditional disproportionation constant, K^*_{disp}.[121] K^*_{disp} is described by the relative stabilization of the two oxidation states (eq.1.8)

$$K^*_{disp} = \frac{[Cu^{II}]_{tot}}{[Cu^{I}]_{tot}^{\,2}} = \frac{1 + \sum_{j=1}^{m} \beta_j{}^{II} [L]^j}{(1 + \sum_{j=1}^{m} \beta_j{}^{I} [L]^j)^2} K_{disp} \tag{1.8}$$

where K_{disp} is the disproportionation constant in the absence of ligand, β^I and β^{II} are stability constants of Cu(I) and Cu(II) complexes.

The main parameter that determines the ligand choice is a low $([\beta^I]/([\beta^{II}])^2$ ratio. There are several ligands that satisfy this condition and can form active complexes in water: HMTETA, TPMA, bipy.[121,122]

2. *Loss of halide of Cu(II) deactivator*. Copper-based deactivator complexes ($X\text{-}Cu^{II}L_m$) are unstable in water and they likely dissociate to form $Cu^{II}L_m$ species that cannot be reactivated.[123] The concentration of deactivator (X-

$Cu^{II}L_m$) depends on the total concentration of Cu(II), concentration of halide species (X), and Cu(II) halidophilicity, K_X (eq. 1.9, 1.10):

$$[XCu^{II}L_m] = \frac{F - \sqrt{F^2 - 4K_X{}^2[Cu^{II}]_{tot}[X]_{tot}}}{2K_X} \quad (1.9)$$

where F is described by eq. 1.10

$$F \equiv 1 + K_X[Cu^{II}]_{tot} + K_X[X]_{tot} \quad (1.10)$$

Halido- or halogenophilicity measures the affinity of the halogen atom to the transition metal in its higher oxidation state. It cannot be directly measured but it can be calculated from overall ATRP kinetic. K_X value depends on the ligand type and nature of the metal center, and it is larger for more active catalyst and for chlorine compared to bromine. In the presence of protic solvent, halidophilicity significantly decreases.[133]

The low concentration of X-$Cu^{II}L_m$ deactivator that arises from the inactive $Cu^{II}L_m$ species results in PDI broadening, according to eq. 1.6. There are a few methods that can be used to prevent PDI broadening and improve the polymerization control. Firstly, an ATRP catalyst with high halidophilicity can be selected.[122,123,134] Secondly, increasing deactivator amount (up to 80 mol%) of the total catalyst amount is sufficient for good polymerization control.[123] Thirdly, adding extra halide salt (either Cu(I) or Cu(II)) will also improve the overall reaction control by forming additional deactivator species.[122]

3. *Other side reactions*. Other side reactions related to the initiator stability and monomer coordination usually accompany water-mediated ATRP. The hydrolysis of the alkyl halide initiator and dormant chain ends can occur. These phenomena result in the polydispersity broadening and reducing the amount of end halides.[121,134] The monomer can also be coordinated with Cu(I) by interacting with the double bond. This was

investigated for styrene, octene, methyacrylate, and methyl methacrylate. From the measured Cu(I)-monomer binding constants, it was concluded that methyl acrylate binds twice as strong to Cu(I) than methyl methacrylate and the monomer affinity to Cu(I) decreases in the order: methyl acrylate > styrene > 1-octene > methyl methacrylate. Moreover, the coordination is more pronounced at room temperature compared to elevated temperatures.[135] The monomer coordination with the ATRP metal catalyst is relatively weak. However, monomer functional groups, such as amines, amides, and carboxylic acids, can displace the ligand from both Cu(I) and Cu(II) complexes and result in the catalyst deactivation. In order to prevent these undesired processes, a ligand that form a very stable complex must be chosen.[135,136]

From the above discussion, it can be concluded that ATRP in water is an attractive and promising area of polymer synthesis. It overcomes many disadvantages of polymerization in organic solvents, such as high temperatures, long polymerization times, and addition of free initiator.[137-140] However, the initiator, ligand, metal catalyst, and monomer have to be selected with care to minimize the side reactions and to obtain well-defined polymers of desired architectures and functionality.

1.5.2. Direct synthesis of polyelectrolyte brushes using water ATRP

The regular way of synthesis of surface-attached polyelectrolytes involves two stages: polymerization of their esters, and subsequent deprotection. For example, the synthesis of polyacrylic acid brushes starts with the polymerization of methyl-, ethyl-, or *tert*-butyl acrylate followed by hydrolysis or pyrolysis of side protective groups. The deprotection reaction usually involves treatment with strong acids that can result in partial polymer chain detachment from the surface.[141] Clearly, direct synthesis of polyelectrolyte brushes is beneficial. First of all, this approach eliminates

deprotection step. It also involves less synthetic steps and, consequently, it reduces processing costs and time. For direct polymerization water-based medium as a solvent is usually used. Such media are compatible with a wide range of substrates. For example, pre-assembled sample for surface forces measurements includes a layer of the glue that can be easily dissolved in acetone or toluene under heating or in the presence of chlorinated solvents. Usually the regular functionalization of substrates with polyelectrolytes involves the utilization of organic solvents, which are undesired in terms of stability of such samples. The direct approach is a good alternative that prevents sample exposure to organic solvents. Another advantage of direct polymerizations is the fast kinetics. In water, polymer layers of larger thicknesses can be grown within shorter time compared to regular synthetic approach. For example, a 40 nm thick P*t*BA layer can be obtained after 15 h of polymerization of *t*BA, resulting in 14 nm thick PAA brushes.[142] In contrast, with water-based ATRP of sodium acrylate, more than 100 nm thick PAA layer can be synthesized within 1h (Chapter 5).[†]

ATRP in water can be applied to a large variety of monomers. However, as it was shown for acrylic and methacrylic acids, their direct polymerization is impossible because of their fast coordination with metal complexes and formation of inactive ATRP catalyst.[143] Acid monomer in its salt form can be used instead, as shown for the first time by Ashford et al.[144] They used a CuBr/bipy system to polymerize sodium methacrylate in water at 90^0. Good control over molecular weight and a PDI of less than 1.3 was achieved. Sankhe et al. proposed a mechanism of $[Cu(II)L]^+$ complexation with polymethacrylic acid during its synthesis from sodium methacrylate on the gold surface (Scheme 1-11).[145]

[†] The initiator grafting density is identical for both examples.

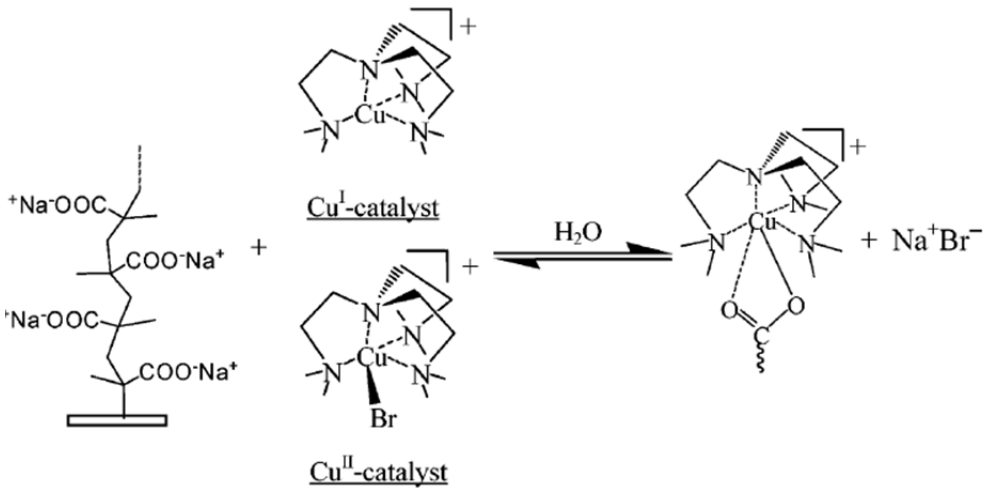

Scheme 1-11. Schematic representation of possible coordination of deprotonated PMAA with $[Cu(II)L]^+$ complex.
(Reprinted with permission from ref. 145
Copyright 2006 American Chemical Society.)

Here, carboxylate ions show higher affinity to copper ions in comparison with sodium ions. This results in ion exchange. The interaction of growing polyacid chain with $[Cu(II)L]^+$ complex leads to the displacement of halogen from the $[Cu(II)L]^+$ catalyst complex and the formation of a halogen-sodium ion pair. The resulting carboxylate complexes are weak deactivators and they cannot be reduced to an active catalyst.[143] This affects the polymerization control and accelerates the termination.

The choice of pH is critical for water ATRP because amino-based ligands are susceptible to protonation.[146,147] Particularly, bipyridine becomes protonated at pH 6 and below.[144] The protonated ligand cannot coordinate Cu(I) and Cu(I) precipitates. At high pH, the rate of propagation is reduced because of the high charge density along the polymer chain. This was shown for free radical polymerization of methacrylic acid.[148] A balance between ligand protonation and reduced propagation is possible with $8<pH<9$.[144]

As was discussed above, many side reactions occur in pure water, leading to uncontrolled polymerization and broad polydispersity. For well-defined polymers the control over polymerization process is required. Reducing of the water content by adding an aprotic solvent can help to restore the control. Methanol, for example, stabilizes catalyst complexes and improves overall polymerization control. [121,123] As it was demonstrated for solution polymerization of sodium 4-styrene sulfonate, the polymerization is poorly controlled in water, but the control is restored after adding methanol as co-solvent.[149] For surface-initiated polymerization, it was shown by Santonicola et al. thar PMAA brushes grow faster when polymerized using 1:1 water-methanol mixture compared to pure water.[150]

In spite of the extreme popularity of polyacrylic and poly(methacrylic acids) for the fundamental investigations and practical applications, the number of experimental studies reporting their direct synthesis is limited.[10] There are some examples of surface-initiated polymerizations of methacrylate and acrylate sodium salts using water-mediated ATRP. Poly(methacrylic acid) chains from chitosan microspheres were synthesized with CuBr/PMDETA at 30^{o}C.[151] Dong et al. demonstrated the synthesis of 30 nm thick PAA film from silica. They utilized CuBr/bipy catalyst and performed the reaction at 30^{o}C during 2 h.[152] The medical degreased cotton was functionalized with a PNaA layer using CuBr/PMDETA catalyst.[153] Sodium methacrylate was successfully polymerized by Tugulu et al. with CuBr/bipy for 2.5 h at 25^{o}C. The obtained thickness varied depending on the monomer concentration, pH, and polymerization time.[154] In the present work, the direct synthesis of polyacrylic acid brushes from silica surface was done using water ATRP in the presence of a CuBr/bipy catalyst (Chapter 2, 5). CuBr/bipy catalyst was selected because it stays active and stabile in water. It also shows high halidophilicity and low $[\beta^{I}]/([\beta^{II}]$ ratio that result in low Cu(I) complex disproportionation.[121,122] pH between 8 and 9 was adjusted in order to prevent bipyridine protonation. Water-methanol (5:1) mixture was used to reduce side reaction and keep polymerization control.

1.6. End-grafted polymer architectures and applications

Besides controlling the molecular weight and brush thickness, control over brush architecture is also possible by SI-CRP methods. SI-CRP methods have been widely used to prepare homopolymer brushes, block- and random copolymer brushes as well as highly branched and cross-linked polymer brushes.[10] Figure 1-12 shows examples of different brush architectures that can be obtained via SI-CRP. Some of them are discussed below in details.

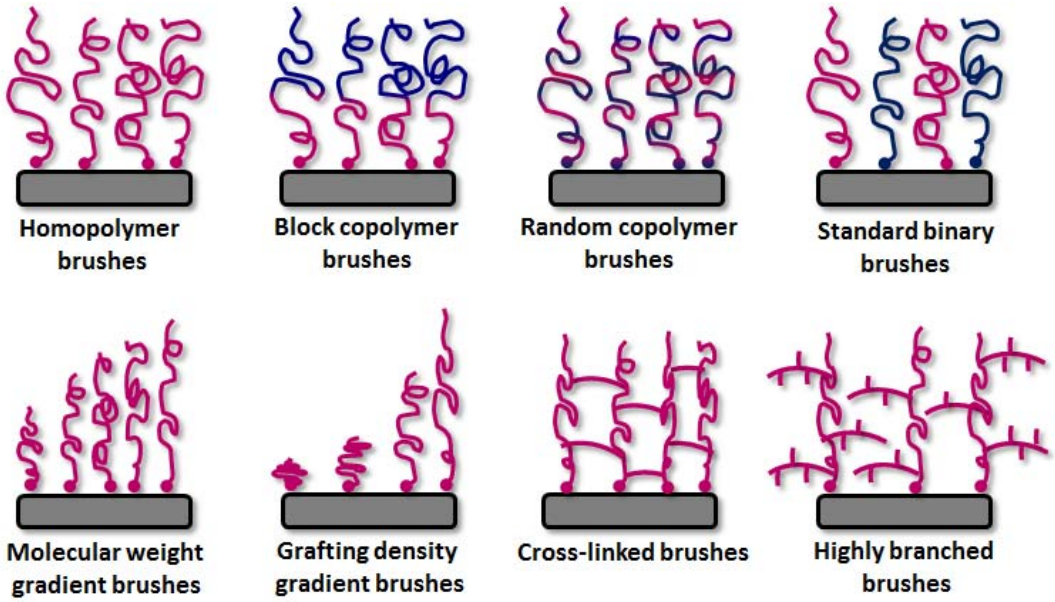

Figure 1-12. Schematic illustration of different polymer brush architectures obtained via SI-CPR.

Homopolymer brushes correspond to one type of end-attached polymer chains. Most of them can be easily obtained in one-step synthesis. The range of their applications is extremely broad and covers many developing technological fields (organic electronic devices, nanosensors, transport systems, microreactors, etc).[10,58] For example, poly(triphenylamine acrylate) brushes can be advantageously used in

electronic devices because of their improved charge mobility in comparison to spin-coated film of the same polymer.[155] Poly(N-isopropylacrylamide) brushes grafted from mesoporous silica particles are utilized in delivery system, where the controlled release of trapped analyte is performed by changing the temperature.[156] Poly(glycidyl methacrylate) brushes grafted to the inner wall of microreactor and modified with organic catalyst, can be used in catalytical applications, where the amount of generated catalyst can be tuned by varying the brush thickness the.[157]

Block copolymer brushes consists of two or more chemically different polymer blocks. They gained exceptional attention because of their ability to undergo vertical phase separation due to the immiscibility of different blocks. This type of architecture exhibits more complex response towards the external stimuli than homopolymer brushes. This was proved by many theoretical investigations and computer simulations. Zhulina et al. showed a variety of possible nanostructures depending on the grafting density, polymer molecular weight, ratio between blocks, and the interaction energies between blocks and between blocks and solvent.[158,159] There are many examples of the reversible rearrangement of tethered block copolymers. For example, rearrangement of polystyrene-*block*-poly(N, N'-dimethyl acrylamide) and poly(N, N'-dimethyl acrylamide)-*block*-poly(methyl methacrylate) brushes was studied by Baum and Brittain.[160] They used the contact angle technique to detect brush rearrangements after brush treatment with selective solvents. Boyes at al. investigated poly(methyl methacrylate)-*block*-polystyrene brushes using AFM.[141] They observed interesting morphologies upon brush exposure to dichloromethane and cyclohexane. Also, Xu et al. demonstrated solvent responsiveness for gradual poly(n-butyl methacrylate)-*block*-poly(2-(N, N'-dimethylamino)ethyl methacrylate brushes depending on the relative length of the blocks.[161] Thus, the surface properties of block copolymer brushes can be switched by "activation" of one or other block, leading to nano-structured films. This behaviour is now employed in many applications such as stimuli responsive platforms, separation membranes, nanoactuators.[10,162,163]

Mixed polymer brushes are composed of two different polymers attached to the substrate randomly. They can be subjected either to dynamic vertical segregation in a selective solvent or segregation in a lateral direction with a non-selective solvent. The important distinctive feature of mixed polymer brushes is their ability to alter their surface composition upon an external trigger. This characteristic is mainly determined by the grafting density and film thickness, and it can be used to tune the polymer film surface properties such as adhesion, friction, wettability, etc. [164-166] For example, Minko et al. employed mixed poly(2-vinyl-pyridine)-*block*-poly(ethylene oxide) and poly(2-vinyl-pyridine)-*block*-polystyrene brushes to modify silica nanoparticles to create responsive colloidal systems.[167]

Cross-linked polymer brushes can be prepared either by SI polymerization of bifunctional monomers or by post-modification of presynthesized polymer brushes.[10] Cross-linking has a significant influence on polymer mechanical stability, permeability, and swelling properties. Kim et al. observed smaller size of hybrid nanoparticles, consisting of gold nanoparticles and crosslinked end-grafted poly(N-isopropyl acrylamide) chains, in comparison to the non crosslinked hybrids.[168] They associated this with the presence of cross-links that prevent formation of hydrogen bonds between amine groups and water molecules. Li et al. showed a significant increase of friction coefficient of poly(acrylamide) brushes with increasing the crosslinker content.[169] They explained this behaviour by reducing the portion of lubricious brush structures after cross-linking and reduced water content inside the brush.

1.7. Polymer brushes. Theoretical description

End-grafted polymer layers usually refer to assemblies of macromolecules, tethered by one end to the solid substrate. The polymer conformation is inherently determined by the way in which the polymer is attached to the surface, the polymer's degree of ionization (α), grafting density (σ), and the thickness of the polymer layer

(L). However, the conformation of an end-grafted polymers is extremely sensitive to conditions such as temperature, pressure, solvent, ionic strength, and pH, to name but a few. The brush behaviour is the focus of many theoretical models. Some of these are presented in the current section

1.7.1. Neutral brushes

The first scaling model of neutral end-grafted polymers at the interface was proposed by Alexander[17] and de Gennes[170]. Depending on the grafting density of attached chains, two regimes have been studied: overlapping coils and separate coils.

For large grafting density, when the distance between two anchoring points, d, is much smaller than R_F, Flory radius of polymer chain in a good solvent ($R_F=aN^{3/5}$), polymer chains are strongly overlapped (*overlapping coils regime)*. Figure 1-13 is a schematic representation of Alexander's model for overlapping coils. In this regime, $\sigma<N^{-6/5}$ and $d=a\sigma^{-1/2}$, where N is a degree of polymerization, and a is a length of each repeating unit.[17]

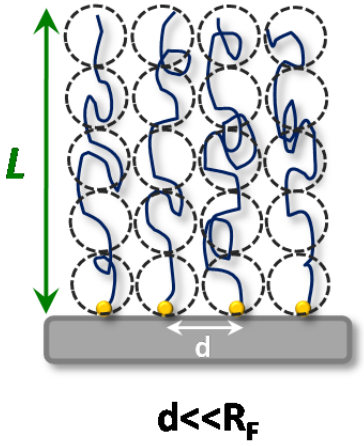

Figure 1-13. Alexander's model of neutral stretched brushes in a good solvent. Each circle schematically represents a chain segment which behaves as a random coil.

For high grafting density, neutral polymer chains tend to stretch away from the surface and adopt a brush-like conformation. The stretching is a result of segment-segment interactions, which is balanced by free elastic energy. The polymer chains' free energy, F, can be expressed as a sum of two contributions, the elastic free energy F_{el}, and the segment-segment interaction energy, F_{int} (eq. 1.11, 1.12).[13]

$$F = F_{el} + F_{int} \tag{1.11}$$

$$\frac{F}{kT} \sim \frac{L^2}{2a^2N} + \frac{\nu N^2 \sigma}{2La^2} \tag{1.12}$$

v is an excluded volume parameter and L is a film thickness.

Free elastic energy or stretching energy can expressed by the following equation (eq.1.13)[170]:

$$\frac{F_{el}}{kT} = \frac{L^2}{a^2N} \tag{1.13}$$

where k is the Boltzmann constant and T the temperature. The free energy per volume (interaction energy), in terms of excluded volume interaction is expressed as (eq. 1.14)[170]:

$$\frac{F_{int}}{kT} = \frac{1}{2}\nu\frac{\varphi^2}{a^6}kT \tag{1.14}$$

where φ is a crossover value, which is equal to v/a^3.

In good solvent the monomer-solvent interactions are dominated over monomer-monomer interactions. The film thickness (L) in this case is proportional to the polymer molecular weight of grafted chains:[170]

$$L \sim N(\nu\sigma)^{1/3} \tag{1.15}$$

For a poor solvent, the interaction between monomers is attractive, leading to collapse of the polymer chain. The equation shows a slightly different exponent for the grafting density (eq. 1.16)[13,171]:

$$L \sim N\sigma^{1/2} \tag{1.16}$$

The *separate coils* regime occurs at low grafting density, when d is much larger than R_F (Figure 1-14). [170] In a good solvent, the polymer chains hardly interact with each other and the grafting density satisfies the following condition: $\sigma > N^{-6/5}$.

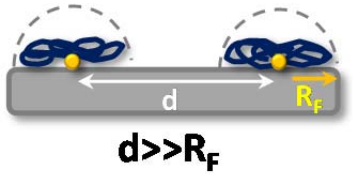

Figure 1-14. Schematic representation of the separate coils model. Distance between two anchoring sites (d) is much larger than Flory radius (R_F).

1.7.2. Polyelectrolyte brushes

For polymer brushes formed from polyelectrolyte chains, additional considerations need to be addressed that take into account the electrostatic interactions within the brush layer. Great interest has been attracted by charged end-grafted polymers because they offer one additional parameter that can be used to tune their conformation, i.e. the ionic strength of the medium. Polyelectrolyte brushes can be separated into two groups: strongly and weakly charged brushes. Polyelectrolytes from both groups can undergo conformational changes upon changes in pH (weakly charged brushes) and ionic strength (weakly and highly charged brushes).[1,172-175]There are several theoretical approaches based on scaling laws, molecular dynamics, self-consistent mean-field theory or strong-stretching theory that describe polyelectrolyte brushes.[176-179]

1.7.2.1. Strongly charged polyelectrolyte brushes

Strongly charged (or *quenched*) brushes can be characterized by fixed degrees of dissociation that do not vary with the pH and ionic strength. The swelling

behaviour of strongly charged polyelectrolyte brushes, described by Pincus using a simple scaling model, assumes the presence of a fixed fraction of dissociated units (*f*) neutralized by counterions, which are localized either inside or outside the brush. [177] The Pincus model only takes into account the osmotic pressure and it disregards excluded volume of repeating units. There are two main regimes for highly charged brushes: *osmotic* and *Pincus* regimes.

The main parameter characterizing the highly charged brush regime is the Gouy-Chapman length, λ_{GC}, which is a height of the effectively bound counter ionic layer. It can be expressed in terms of surface charge density Σ:

$$\lambda_{GC} = (2\pi l_B \Sigma)^{-1} \tag{1.17}$$

where l_B is the Bjerrum length‡ and Σ is a product of elementary charge *e*, degree of ionization *f* , degree of polymerization *N* and grafting density ρ_a (eq.1.18):

$$\Sigma = efN\rho_a \tag{1.18}$$

In case, when all counterions are confined inside the brush in order to compensate the immobilized charges of the grafted chains, brush enters the *osmotic regime*. The polymer layer thickness is then determined by a balance between the osmotic pressure of the counter-ions inside the brush and the stretching entropy. The Gouy-Chapman length, in this case, is smaller than the brush thickness *L* (Figure 1-15, A). The brush height in this case can be defined as follows (eq.1.19): [13,172]

$$L_{OsB} \propto Naf^{1/2} \tag{1.19}$$

In contrast, when the counterion distribution extends into the bulk far beyond the brush, the osmotic pressure is relatively week compared to the large

‡ $l_B = \frac{e^2}{4\pi\varepsilon_0\varepsilon_T k_B T}$

where ε_0 is the vacuum permittivity, ε_T the relative dielectric constant of the medium, k_B the Boltzmann constant, and *T* the temperature in Kelvin.

uncompensated electrostatic segment-segment repulsion. This is the *Pincus regime* (Figure 1-15, B). Thickness in this regime is much smaller than λ_{GC} and it depends on the grafting density (ρ_a): [1,177]

$$L_{PB} \propto N^3 N a f^2 l_B \rho_a \tag{1.20}$$

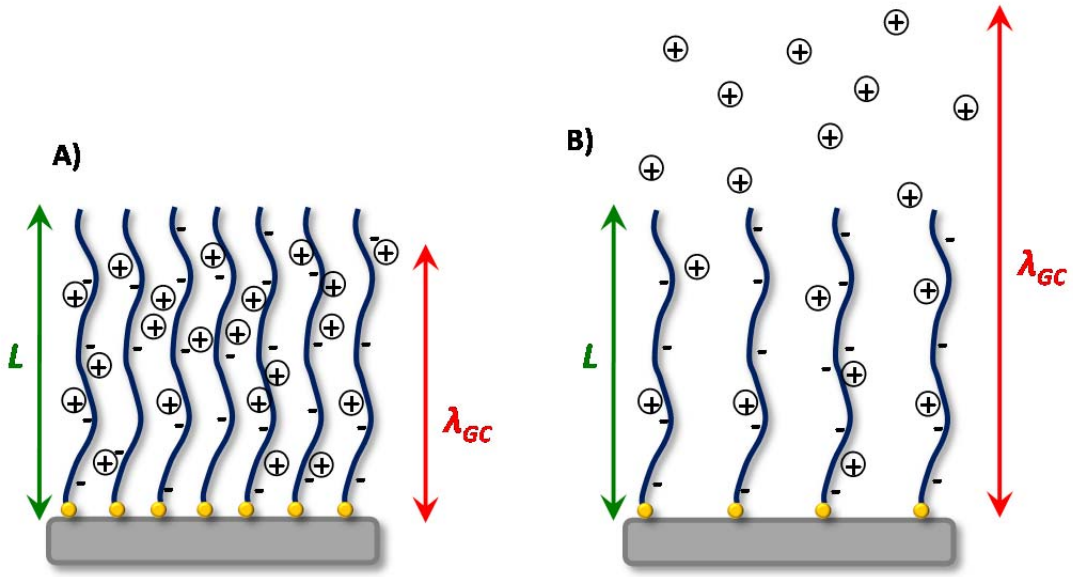

Figure 1-15. Polyacid brushes in the osmotic (A) and Pincus (B) regimes.

The presence of salt ions has a significant influence on the polymer brush conformation as it can screen the electrostatic interactions within the brush. Pincus model predicts different behaviors of polyelectrolytes brushes depending on salt concentration (Figure 1-16).

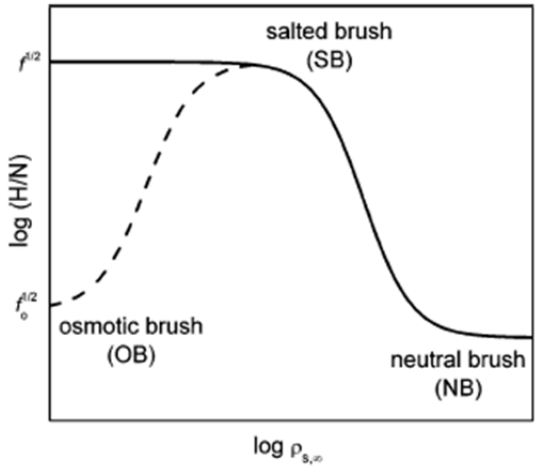

Figure 1-16. Illustration of different brush regimes for strong (solid line) and weak (dashed line) polyelectrolytes. The Y-axis represents polymer brush thickness and the X-axis corresponds to the external salt concentration. (Reprinted with permission from ref.175 Copyright 2007 American Chemical Society.)

For highly charged polyelectrolyte brushes, low added salt concentration does not affect the brush thickness as the salt ions screen the superficial polymer layer only.[180] When the added salt concentration increases, there is an important difference between concentration of the free counter ions inside and outside the brush (*salted brush regime)*. In this regime, the addition of salt significantly screens the electrostatic interactions within the brush and the brush height becomes dependent on the salt concentration according to (eq. 1.21):[1,13,173]

$$L_{SB} \propto Nac_S^{-1/3}\alpha^{1/3} \tag{1.21}$$

At significantly high salt concentration, when the electrostatic interactions are highly screened and the osmotic pressure within the brush is significantly reduced, polyelectrolytes behave as a *neutral brush* and the thickness scales as described by eq. 1.15 Thus, the thickness of such polyelectrolyte brushes is insensitive to further increase in external salt concentration.[173].

1.7.2.2. Weak polyelectrolyte brushes

In contrast to highly charged brushes, where the degree of dissociation is fixed, for weakly charged (or *annealed*) brushes, the degree of dissociation can be tuned with pH and ionic strength. This allows a large variety of polymer conformations to be obtained. Weak polybasic brushes extend upon decreasing pH, while weak polyacid brushes extend with increasing pH. The first theoretical description of the properties of weak polyelectrolyte brushes was proposed by Zhulina and coworkers.[174] They used the mean-field theory to predict conformational changes of weakly charged polyelectrolyte brushes upon changes in the ionic strength of the aqueous medium. They considered a polyacid brush where the charge density is a result of dissociation of a neutral polymer unit HA to a negatively charged polymer unit A^- and a proton H^+:

$$[HA] = [H^+][A^-] \tag{1.22}$$

for which the dissociation constant can be written as follows:

$$K_D = \frac{[H^+][A^-]}{[HA]} \tag{1.23}$$

The average degree of dissociation, α is:

$$\alpha = \frac{[A^-]}{[A^-][AH]} \tag{1.24}$$

and it is related to the K_D:

$$\frac{\alpha}{1-\alpha} = \frac{K_D}{c_{H^+}} \tag{1.25}$$

where C_{H^+} is the concentration of protons inside the brush.

Similarly to quenched brushes, two main regimes are defined for weakly charged brushes depending on the external salt concentration. At low ionic strength,

the counter-ions from polymer chains are localized inside the brush and the brush is globally neutral. When the ionic strength increases, there is an increase in the effective electrostatic potential at polymer/water interface, which is defined as the ratio between counter-ion concentrations inside and outside the brush. For weakly charged brushes at low salt concentration, such a regime is called the *annealed osmotic brush regime*. The degree of dissociation α in this regime is:

$$\alpha \cong \left[\frac{\alpha_B}{1-\alpha_B}\alpha\sigma(C_{H^*}+C_S)\right]^{2/3} \tag{1.26}$$

where C_s is the concentration of the salt ions, and α_B is the degree of dissociation of the polymer chains in solution. The thickness in this regime depends on the grafting density and the salt concentration according to equation 1.27:[174]

$$H_{AOsB} \propto N\alpha^{4/3}\sigma^{1/3}\left(\frac{\alpha_B}{1-\alpha_B}(C_H+C_S)\right)^{1/3} \tag{1.27}$$

For quenched brushes, where the number of charges is fixed, this regime is not expected to exist . The two last equations show that the degree of ionization of the brush can be smaller than that of the free polymer chains in solution for a given pH and ionic strength ($\alpha<\alpha_B$) and the brush height can increase upon increasing salt concentrarion (Figure 1-16). Moreover, Zhulina's model predicts a maximum brush height for a critical salt concentration (C_S^{max}) which corresponds to the transition between the osmotic and salted brush regimes and depends on the grafting density and degree of dissociation of the free chains:[181]

$$C_S^{max} \sim \sigma(\alpha_B)^{1/2} \tag{1.28}$$

At high salt concentration, the electrostatic potential which is the ratio between counter-ion concentrations inside and outside the brush becomes negligible and $\alpha \approx \alpha_B$. This results in the same equation as for the quenched brushes and it is called the salted brush regime (eq.1.21).[182]

1.8. Polymer brushes responsiveness

Given their sensitivity to environmental conditions, end-tethered polymers can be used to modify surface properties in a controlled and reversible manner via changes in their conformation upon changes in the properties of the surrounding medium. Depending on the brush chemical structure and brush conformation, brush properties can be tuned upon many different external stimuli such as temperature, solvent, light, electric field, pH.[10] The conformation of weakly charged polymers can be easily tuned with pH and/or ionic strength.

1.8.1. Responsiveness of weakly charged polymer brushes

Weakly charged brushes can be characterized by a non-fixed number of charges along the polymer chain, i.e. they can change their degree of ionization in response to pH and ionic strength. Weakly charged brushes are very interesting for many applications because they can adopt a wide range of conformations. For example, pH sensitive PS-*b*-PMAA brushes are used as a carrier in controlled delivery systems, where pH-induced switching between collapsed and swollen conformations assures the release of trapped dye molecules.[183] Another example is pH-responsive nanoporous platforms, where nanovalves are possible by functionalization of porous silicon nitride films with PMAA brush (Figure 1-17, A).[184] In this system, pH changes induce changes in PMAA brush conformation and, consequently, ion permeation control through the pores can be achieved. Additionally, PAA-functionalized materials are used as pH-sensitive platforms for antibody or protein immobilization.[185,186] Moreover, pH-responsive polymers can be used as pH-active nanoactuators.[8,187] Particularly, reversible mechanical actuation was shown by Zhou at al. for the first time (Figure 1-17, B).[187] They used poly(methacryloyl ethylene phosphate) brushes to functionalize cantilevers.

Conformational brush changes with variation of pH and ionic strength induce cantilever bending in a controlled manner.

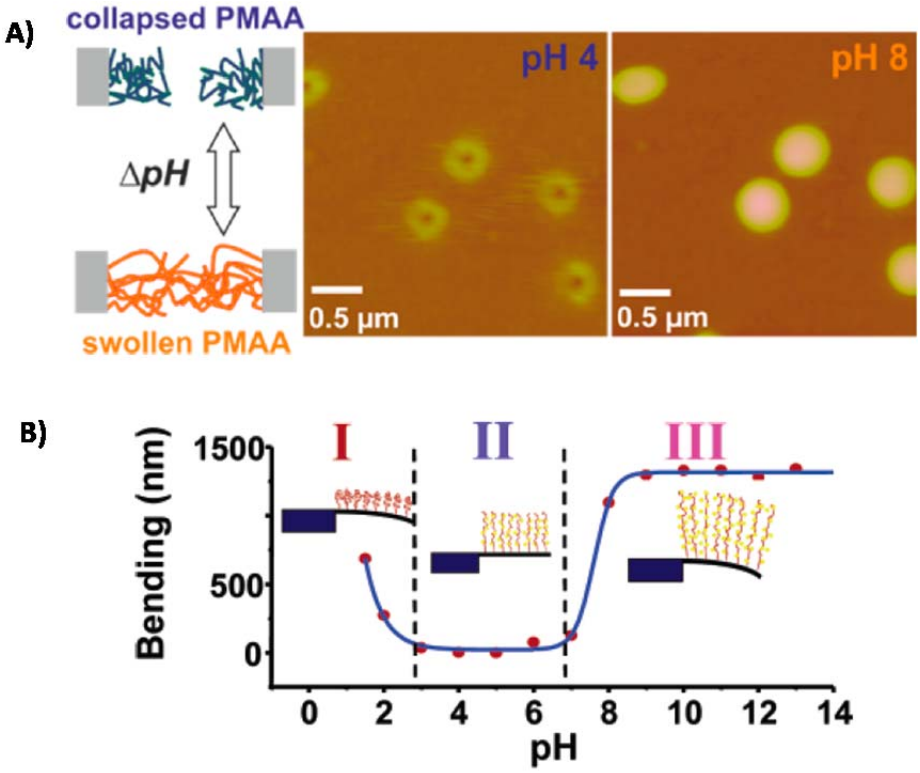

Figure 1-17. Practical applications of weakly charged polymer brushes. A) Nanoporous platforms functionalized with PMAA brushes (Reprinted with permission from ref. 184 Copyright 2013 American Chemical Society.) B) Controlled bending of a cantillever modified using polymethacryloyl ethylene phosphate brushes (Reprinted with permission from ref. 187 Copyright 2006 American Chemical Society.)

1.8.1.1. Swelling behaviour

The brush swelling/collapsing results in a change in polymer layer thickness because of the internal structural reorganizations upon external stimuli. For weak polyanionic brushes, such reorganizations are caused by changes in pH and ionic strength as described in section 1.7.2.2. There are some examples of swelling

behavior of weakly negatively charged polymer brushes upon changes in pH and ionic strength. Biesalski et al. performed PMAA brush swelling studies using multiple-angle null-ellipsometry.[172] The authors investigated PMAA brush responsiveness to pH increase from 2 to 10. PMAA thickness was pH independent at pH<3. Within the pH range from 3.5 to pH 4.5, PMAA thickness increased almost 3 times. At pH 10, the thickness reached the maximum, resulting in a 4 times increase from the initial value. This relates to an increase in the degree of dissociation that, in turn, results in an increase in osmotic pressure within the brush and polymer layer swelling. Also, authors studied the influence of salt concentration from 1 to 10^{-4} mol/L on brush thickness.[172] The maximum swollen thickness was measured at intermediate salt concentration (0.001 mol/L) that is in agreement with theoretical predictions.

The responsiveness of PAA layer to the change in ionic strength at different grafting densities was investigated by Curie et al. using multiscope ellipsometer.[188] They found non-monotonic brush thickness change with salt concentration at a fixed pH and grafting density. At pH 3, the brush height was independent on the ionic strength while, at higher pH (4.0 and 5.8), it increased with increasing salt concentration. The thickness reached its maximum value at salt concentration of 0.1M and, then, it decreased with further increase in salt concentration as expected from the model presented by Figure 1-16. Santonicola et al. investigated the PMAA brush pH-induced switching behavior between pH 4 and 8 using multiscope null ellipsometry.[150] They found that the swelling factor, which is the ratio between maximum and minimum thickness values, is stable over 4 repetitive pH cycles and that no degrafting occurrs during these cycles. Interestingly, the PMAA brushes reach the equilibrium with surrounding medium in 1 min and brushes thickness remains stable within the following 30 min, before pH is changed. Unfortunately, no explanations was provided for obtained results.

Liu et al. investigated PAA-conformational switching upon pH changes from 3.2 to 6.6 using a quartz crystal microbalance with dissipation (QCM-D). The changes in frequency and dissipation confirmed the periodic brush swelling and collapsing. Additionally, they studied changes in shear viscosity and elastic shear modulus that also have a periodic character and correlate well with changes in brush thickness. Shear viscosity increases with increasing pH because of PAA chain hydration. Moreover, the increase in pH causes an increase in electrostatic repulsions and results in an increase in the elastic shear modulus.

Aulich et al. studied pH-dependent PAA switching using infrared spectroscopic ellipsometry (IRSE).[189] This technique allows monitoring changes in adsorption and changes in polymer film optical properties simultaneously. Particularly, they observed intensity changes of COO^- vs COOH vibrational bands with pH increase from 2 to 10. The pH was tuned by adding potassium hydroxide or hydrochloric acid directly to the liquid cell. The COOH vibrational band decreases with increasing pH, while the intensitiy of COO^- asymmetric and symmetric stretching bands rises. These results indicate that the increases of the number of deprotonated carboxylic acid groups with pH leads to brush swelling. Besides, a hysteresis-like swelling behavior was observed during pH increase and decrease. This behavior was explained by a complex mechanism related to the concentrations of K^+ and Cl^- within the brush. During pH increase at low Cl^- concentrations, only the uppermost polymer layer dissociates. At pH higher than 6, the concentration of chloride is sufficient to penetrate through the brush and dissociate most of the carboxylic acid groups. Decrease in pH leads to minor structural changes until pH 8 is reached. From pH 8 to 7, only the uppermost layer is re-protonated. The deep region of the brush still contains high concentration of potassium ions that cannot be neutralized by low concentration of chloride ions. The brush is in a strongly negatively charged state. At pH from 7 to 6, when the concentration of chloride ions is sufficient, the reprotonation occurs and brush deepest region collapses.

Titration experiments using FTIR spectroscopy were done by Dong[190] and Santonicola[150] for PMAA brushes. In both studies the degree of dissociation of PMAA layer vs pH was determined by integrating the area under the characteristic band of carboxylic acid group. The obtained titration curves were fitted using a sigmoidal function to determine the effective pK_a of brush. The obtained pK_a of brush from both studies (pK_a=6.5±0.1[150] and pK_a=6.9±0.03[190]) are larger than the pK_a of the free polymer in solution. This can be explained by brush high segment density and small free volume within the brush in terms of Alexander and de Gennes scaling model presented before.

1.8.1.2. Wettability

Wettability, or degree of wetting, of a surface by a liquid is the ability of that liquid to cover the surface. This depends on the relative values of the surface tension between each pair of the three existing phases (surface, liquid and air). Each surface tension acts upon its respective interface, and define the contact angle θ at which the liquid contacts the surface (Figure 1-18). The smaller is the angle, the better the liquid will spread or wet the surface. Equilibrium considerations allow the wetting or contact angle to be predicted from the surface tensions. This is known as the Young's equation (1.29)[191]:

$$\gamma_{SG} = \gamma_{SL} + \gamma_{LG} cos\theta_C \quad (1.29)$$

where γ_{SG}, $\gamma_{SL,}$ and γ_{LG} correspond to surface tensions between solid and gas, solid and liquid, and liquid and gas, respectively (Figure 1-18).

The most commonly method used to measure the contact angle is the sessile drop method. In this method, the drop of liquid is placed on the surface using a syringe and the angle between the liquid and surface is measured using a goniometer.

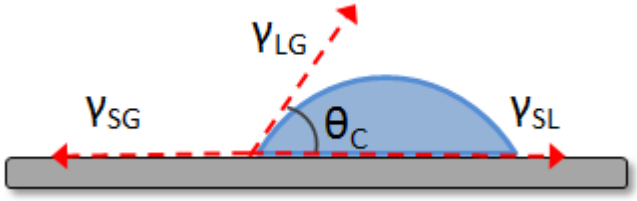

Figure 1-18. Schematic representation of contact angle (θ) of a droplet of liquid on solid surface.

The geometry of droplets of liquid on the surface determines either material's surface is hydrophobic or hydrophilic. The surface is hydrophilic if the droplet spreads over a large surface area, and measured contact angle is less than 90^{o} (Figure 1-19, A). In contrast, if the droplet forms a sphere on the surface, and contact angle is more than 90^{o}, the surface is considered hydrophobic (Figure 1-19, B). Hydrophilicity is characterized by high surface energy, while hydrophobicity is indicated by low surface energy.[192]

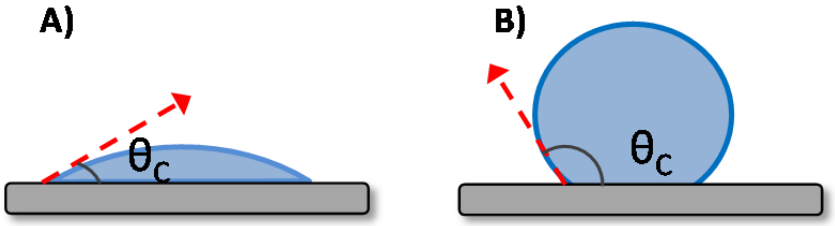

Figure 1-19. Schematic representation of contact angle for hydrophilic (A) and hydrophobic (B) surfaces.

The surfaces with different degrees of ionization show different contact angles.[193,194] For example, for a weak polyanionic brush, the surface was found to be hydrophobic at low pH, but hydrophilic at high pH.[189,190,195] pKa of the top polymer film layer (pK_a^{surf}) can be estimated from the variation in the contact angle as a function of pH. This method was described by Creager et al.[196] The pK_a^{surf} is estimated as an inflection point from the curve where the degree of dissociation is

plotted vs. pH. In turn, the degree of dissociation at certain pH can be found from cos theta value using the following equation:[196]

$$cos\theta = cos\theta_{low\,pH} - \frac{RT\,\Gamma_{acid}}{\gamma_{lv}} \ln[1-\alpha] \tag{1.30}$$

where α is the degree of dissociation, Γ_{acid} the absolute surface coverage of acid groups, γ_{lv} the surface energy at liquid/vapour interface, and $cos\theta_{low\,pH}$ corresponds to the contact angle at certain pH, which resulted in protonation of all acidic groups. Dong et al. showed that the pK_a^{surf} of PMAA and PAA brushes are almost 2 units smaller than the pKa of the corresponding polymer, pK_a^{bulk}.[190] They suggested that carboxylic acid groups located closer to the polymer surface are easier to be dissociated than groups buried near the substrate.

The water contact angle analysis was also used to estimate the stability of the polymer film. PAA layer was subjected to repetitive pH switch from 3 to 10.[195] A reproducible change in water contact angle with pH over 4 cycles was observed. This suggests that the PAA carboxylic acid groups can be protonated/deprotonated several times without decreasing the brush stability at the interface.

1.8.1.3. Adhesion and friction between polymer-bearing surfaces

Polymer-functionalized substrates are intensively used to produce surfaces with high and low adhesion or friction. Such substrates are utilized in engineering and biomedical fields. In general, adhesion is the interatomic interaction at the interface of two surfaces.[197] The adhesive force can be expressed as the force required to separate two adhesive surfaces apart and, for polymer surfaces, it strongly depends on the way and the velocity at which the surfaces are separated as well as on the time the surfaces remain into adhesive contact.[198,199] Among the variety of adhesion mechanisms, three of them are generally used to explain the experimental data: mechanical coupling, molecular bounding and thermodynamic adhesion.[197] When two polymer-bearing surfaces are sliding against each other, shear and

frictional forces arise between them. The friction coefficient is a relative measure of friction, and it is expressed as a ratio between friction force and applied external force. The value of friction coefficient can vary from near zero to more than one. For polymer-polymer interaction, the typical range for friction coefficient is 0.05-1.0;[200] however, recent experimental studies extend this typical range from 0.0006[201] to 1.06.[202]

The adhesion and tribological properties of polymer layers can be investigated using Atomic Force Microscopy (AFM), Surface Forces Apparatus (SFA), microtribometer, and pin-on-disc macrotribometer. Microtribometer and pin-on-disc macrotribometer work at micro- and macroscales respectively, while AFM and SFA use nano- and milli-scales of applied load. Microtribometer was developed to measure the tribological properties between two solid bodies. The usual pair of sample is a flat substrate and ceramic or metallic ball. The spherical probe is loaded with precise weight, and control station provides linear motion of the ball over the flat surface. Thus, the friction force between the probe and the sample is measured. Additionally, obtained scar images are recorded and analyzed in order to provide information about the wear. Pin-on-disc consists of a rotating disc and a fixed "pin" that is the analyzed sample. The load of 1-10 N (up to 60 N) can be applied and a friction force up to 10 N can be measured. This is a powerful technique that allows simple test of friction and wear for many sample geometries (ball, cylinder, cub).

While the investigation of tribological responses on macroscale is important for practical studies, the techniques that use nanoscale (AFM and SFA) allow to investigate the mechanisms of effective lubrication. In AFM, the sharp tip of the cantilever is approached close to the surface, and the cantilever is deflected. Cantilever deflection is used to determined the interaction force between the tip and the surface via Hooke's law. Deflection of the cantilever in vertical direction as a function of tip-surface distance can be presented as a force vs. distance curve. This curve contains information about adhesive and repulsive forces between the tip and

the surface. To measure the friction force, the lateral cantilever bending has to be monitored.[198]

For SFA, the two samples are two crossed cylinders. The forces can be estimated from the deflection of the spring that supports one of the cylinders. The main advantage of SFA in comparison to AFM is that the absolute separation distance between the two surfaces can be measured using multiple beam interference fringes of equal chromatic order (FECO) (Figure 1-20).[198] In SFA experiments, the surface pressure is controlled by controlling applied load.

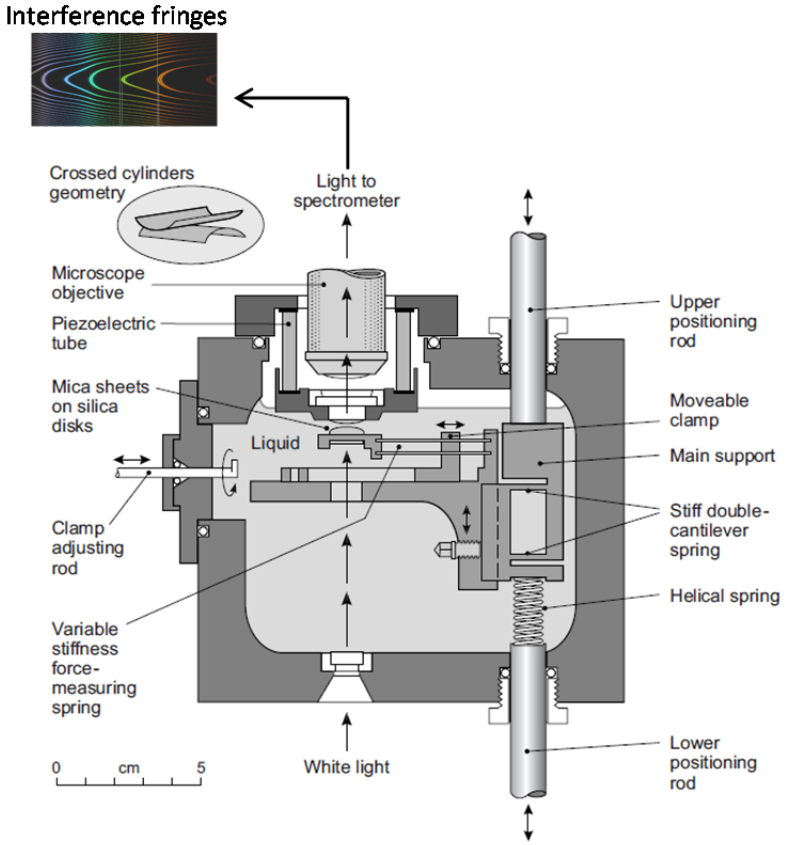

Figure 1-20. Schematic representation of Surface Forces Apparatus. (Reproduced from ref. 198 with the permission of Elsevier)

The surface interactions and properties of grafted polymers are strongly dependent on polymer chain conformation. Many studies aiming to correlate the surface interactions between polymer bearing surfaces (adhesion, friction) with the polymer properties (degree of ionization, conformation, molecular weight), and the environmental conditions (pH, ionic strength, temperature, solvent quality) have been reported.[203-207] Sudre et al. studied the adhesion between poly(N,Ndimethylacrylamide) and polyacrylamide as model gels and PAA brushes. They found the adhesion decreases when pH increases, which was explained by the formation of hydrogen bonds at the interface.[208]

Landherr et al. studied the friction between polymer brushes (polydimethylsiloxane, polystyrene or poly(propylene glycol)-poly(ethylene glycol) block copolymer brushes) and non-functionalized surfaces.[209] They correlated the surface coverage (σ) and the fraction of the friction force arising from the adhesion (ε). The experimental data showed a very close agreement to $\varepsilon \sim \sigma^{4/3}$ scaling prediction regardless of the polymer nature, which confirmed negligible contribution of adhesion to friction. Also in their previous work, they reported, that ε ranges from 0.003 to 0.008 for thick polydimethylsiloxane network.[210]

Chen et al. correlated the molecular weight of grafted chains with adhesion.[211] For polystyrene and poly(vinylbenzyl chloride) layers, both friction and adhesion decrease with increasing of MW. Moreover, cross-linking leads to low adhesion while bond-breaking to high adhesion. This was attributed to the increase in the number of chains "ends" at the interface.

Ramakrishna et al. aimed to understand the adhesion between poly(L-lysine)-poly(ethylene glycol) (PLL-g-PEG) copolymers grafted to rough and flat surfaces, and polyethylene colloidal probe. Upon adsorption of PLL-g-PEG to the rough surface, adhesion decreases, but the lowest friction is achieved when a smooth surface is modified with the same brushes. This was related to the smaller contact area for a brush-functionalized flat surface compared to a rough surface. Decrease in

the contact area led to a decrease of adhesion and, consequently, to a decrease of friction.[212]

Many theoretical and simulation studies tried to elucidate the lubricating mechanism of polyelectrolyte interaction.[213-216] It was shown that friction coefficient correlates with the number of shearing polymer segments within the interpenetration region regardless of ionic strength and polymer degree of polymerization.[217] However, the role of polymer conformation as well as many other parameters (salt concentration, nature of the polyelectrolyte brush, presence of counter-ions) in effective lubrication is not clear yet. In general, polyelectrolyte brushes in aqueous environment reveal extremely low friction coefficient: it has been shown that the frictional forces between two opposing charged polymer brushes can be reduced to extremely low values ($\mu \approx 0.0006–0.001$ at pressure of several atmospheres).[201] The authors explained this behavior by the superior resistance towards brush interpenetration, as well as by the presence of mobile counter-ions, resulting in increased osmotic pressure. In contrast, Liberelle et al. reported much higher friction coefficients ($\mu \approx 0.1$-0.3) depending on the applied pressure for end-grafted PAA brushes.[218] They associated this with an increased mutual interpenetration upon compression, similar to the neutral brushes. Interestingly, no surface damage or polymer removal occurred even at high applied load (ca. 40 atm) confirming the superior robustness of these charged polymer brushes. Other studies for poly(2-(dimethylamino)ethyl methacrylate) brushes grafted from gold surface were performed using AFM.[202] The authors aimed to determine the role of the degree of dissociation on brush frictional properties. The results obtained contradict the results obtained for PAA brushes by Liberelle et al. The enhanced lubrication was revealed at low pH and explained by the formation of highly charged hydrated layers. Friction coefficient decreases from ca 1 to ca 0.1 when the pH decreases from 11 to 3 at 24^{o}C. At high pH, when brushes collapse completely, the friction is low compared to partially collapsed chains, and that was explained by an increased surface roughness.

Additionally, most of the tribological studies were performed using physisorbed polymers that can detach in the presence of small ions. These ions screen the electrostatic interactions with the surface and compete with the polyelectrolytes to the available adsorption sites. Therefore, the covalent attachment of polymer chains is prefered for surface properties studies. The ideal polymer system should be able to sustain high loads and extreme environmental conditions, and be wear resistant. Such system should also still be responsive and show reversible behavior upon changes in environmental conditions.

1.9. Ellipsometry. Basic principle

Ellipsometry is an optical technique that is widely used for investigating thin film dielectric properties. It measures the changes in light polarization after reflection from a planar surface. The name "ellipsometry" is attributed to this technique due to the fact that elliptical polarization is used.[219-222]

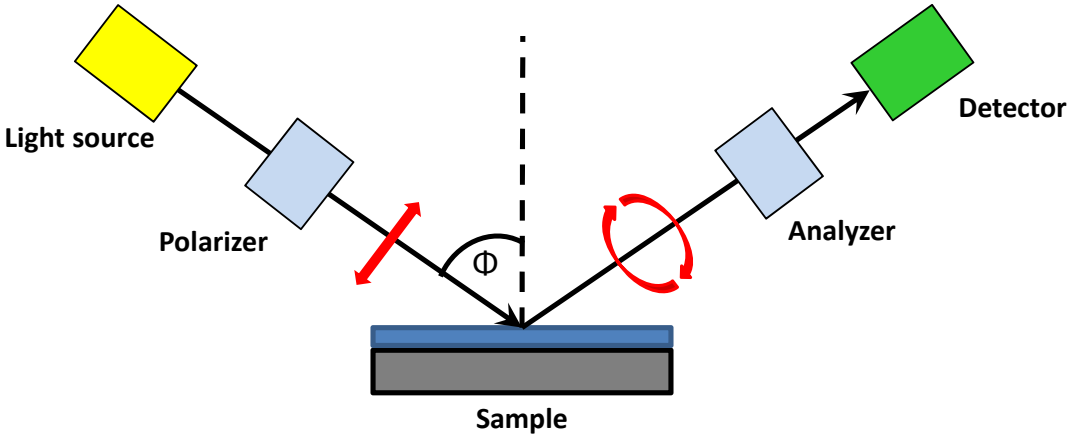

Figure 1-21. Schematic representation of set up for ellipsometry measurements.

A typical ellipsometry set up consists of a light source, polarizer, analyzer and detector (Figure 1-21). The type of light source determines the type of the instrument. A single-wavelength ellipsometer uses a specific wavelength laser as the light source,

usually helium-neon lasers. A spectroscopic ellipsometer uses a broad spectral range (in ultraviolet, visible or infrared region) light source. For example, ellipsometer M-2000 VASE employs a white light source ranging from 370 to 1000 nm. The polarizer converts the unpolarized light into linearly polarized light. After reflection from the substrate, elliptically polarized light enters the analyser and, then, the detector, which converts the light into an electronic signal.[219,220,222]

It is usual to describe the state of polarization using two orthogonal vectors *s* and *p* (Figure 1-22, A). One of them is parallel to the plane on incidence (*p*) and another is perpendicular to the plane of incidence (*s*) (Figure 1-22, B).

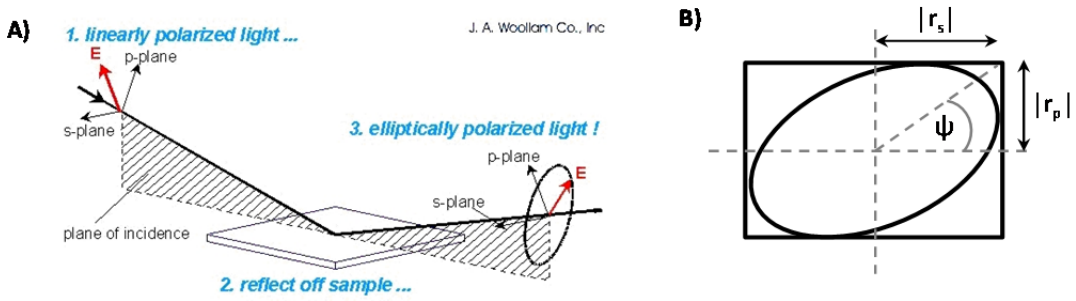

Figure 1-22. A) Typical geometry of an ellipsometric measurement. B) Schematic representation of *p* and *s* vector orientation in an elliptically polarized light. Reproduced with permission from J.A. Woollam Co., Inc.

Both components change their amplitudes differently after interacting with the surface. This change can be expressed by a complex reflectance ratio ρ (eq. 1-31):[220,222]

$$\rho = \frac{r_p}{r_s} = \left|\frac{r_p}{r_s}\right| \exp(i\Delta) = \tan\psi \exp(i\Delta) \tag{1.31}$$

where r_p and r_s are amplitudes of p and s components, respectively (Fresnel coefficients), tan ψ is the amplitude ratio, and Δ is the phase difference after reflection.

There are several advantages of the ellipsometric technique: 1) it is nonconductive and non-destructive; 2) it is an absolute measurement (no references needed); 3) it is of high precision and fast; 4) it is suitable for in situ experiments.[220,223] However, ellipsometry uses an indirect data analysis requiring a model.

The experimental ψ and Δ values cannot be directly converted into optical constants n (refractive index) and k (extinction coefficient). Thus, a suitable and representive model must be used. The constructed model should include information about the substrate, layers, their quantity and approximate thicknesses. Once the appropriate model is built, the measured ψ and Δ values are compared to the ψ and Δ values provided by the model (fitting process). Using the Levenberg-Marquardt fitting algorithm, the model parameters are varied until the best correlation with the experimental values is obtained. After the fitting process, the optical (n and k) and structural (film thickness, porosity, crystallinity, anisotropy, uniformity) parameters of the analysed layer can be obtained.[220,222] The mean squared error (MSE) parameter is typically used to estimate the difference between the experimental and calculated values (eq. 1.32).[224]

$$MSE = \frac{1}{2N - M}\sum_{i=1}^{N}\left[\left(\frac{\psi_i{}^{mod} - \psi_i{}^{exp}}{\sigma_{\psi,i}{}^{exp}}\right)^2 + \left(\frac{\Delta_i{}^{mod} - \Delta_i{}^{exp}}{\sigma_{\Delta,i}{}^{exp}}\right)^2\right] \tag{1.32}$$

where N is the number of measured ψ and Δ pairs, M is the number of fitting parameters, $\sigma_{\Delta,i}{}^{exp}$ and $\sigma_{\psi,i}{}^{exp}$ are the experimental standard deviations for Δ and ψ of ith data points, obtained from the error bars of calibration parameters.

When experimental data match perfectly the built model, MSE value should be equal to 0. But in real measurements this is impossible to achieve. And the

theoretical model is considered to describe well the experimental data when MSE value tends to zero.[225]

In the optical model, each layer should include information about its wavelength dependent optical parameters (*n* and *k*). This dependence is available as a tabulated list and integrated into the analyzing software. However, for some layers, tabulated values do not describe the material properly. In this case, the dispersion model is the way to model the optical properties. For homogeneous layers, the Cauchy normal dispersion model can be used (eq. 1.33). It correlates the refractive index with the wavelength and it can be applied to any transparent material in the visible region (*k=0*):[220,222]

$$n(\lambda) = A_n + \frac{B_n}{\lambda^2} + \frac{C_n}{\lambda^4} \tag{1.33}$$

λ is the wavelength, *A, B, C* are Cauchy coefficients, which describe wavelength dependent refractive index changes. For absorbing materials, the area of absorption is modeled using Lorentz, Harmonic, and Gaussian oscillator-based models.[222]

1.9.1. Ellipsometry for characterizing polymer films

Ellipsometry is an attractive technique to study the macroscopic parameters of polymer films. It provides information about the film thickness, porosity, composition, and the surface and interface roughness, without damaging the film.[220]

1. Film thickness. When light interacts with the film, a portion of it is reflected from the film surface. Another portion travels through the film and it is reflected back from the substrate. The interference between reflected and transmitted light includes amplitude and phase information that is used to estimate the thickness. For polymer-coated surfaces, this is the most popular method since it is non-destructive, does not require

special sample pre-treatment, and it is technically easy and fast to perform.[221,222]

2. Porosity. Information about porosity percentage as well as the pore distribution within the layer can also be obtained using this technique. It requires an accurate model for determining the porosity percentage at the interface and in bulk. The model involves the effective medium approximation (EMA), where two or more materials (void and polymer in porous material) are mixed together.[226] This is the physical model where macroscopic parameters are estimated based upon fractions of the optical properties of its components. [227,228]

3. Composition, surface/interface roughness. For heterogeneous systems consisting of two or more materials, the ratio between components can also be established using the EMA model. Rough surfaces are also considered as heterogeneous systems, where one of the components is ambient.[227,229,230]

1.9.2. Liquid ellipsometry for studying polymer dynamics

The optical properties of polymer films in situ can be studied by ellipsometry. The structural changes within the film can be monitored through changes in optical constants. Structural changes of polymer chains usually lead to changes in the film dimensions caused by swelling and collapsing. By monitoring the variation in optical properties, it is possible to obtain information about polymer conformational changes on the surface. There are several examples where swelling process as a function of time, temperature, changes in pH, and applied voltage was observed by ellipsometry. Zudans et al. monitored the swelling dynamics of poly(dimethyl diallyl ammonium chloride)-silica composite with time.[231] Hydration caused significant changes within the film, and the transformation from dry to early hydrated and then to fully hydrated

film was observed by a combination of ellipsometry and electrochemistry. Temperature induced swelling studies of neutral poly(N-isopropyl acrylamide) (PNIPAM) brushes were done by Kostruba et. al.[232] They monitored the thickness variation of PNIPAM brushes with the temperature of the surrounded solution. The authors found the temperature-dependent behaviour is determined by a phase transition. Changes in refractive index indicate that only the outer parts of the PNIPAM brushes are subjected to structural changes. Another example of temperature-driven structural conformations of PNIPAM brushes was presented by Rauch.[233] They monitored the swelling dynamics and the measured water content inside the brush using the EMA Bruggerman approximation.[233] Ramos et al. studied brush hydration and estimated the polymer water content by two techniques: Quartz Crystal Microbalance (QCM) and spectroscopic ellipsometry.[234,235] Spectroscopic ellipsometry determined the optical mass, while QCM measured the acoustic mass, being composed of the polymer and the solvent masses. The water content was calculated from the difference between the acoustic and optical masses. The voltage-induced swelling of poly-(2-(dimethylamino)ethyl methacrylate) brushes was studied by Weir et al. using optical ellipsometry.[236] The authors concluded that voltage-induced swelling resulted in a wider range of possible brush conformations in comparison to pH-induced conformational changes. Finally, multiple other examples of pH responsiveness studied by ellipsometry for homopolymer,[172,233,237] mixed,[238] and block copolymer brushes[188] have been reported. All these examples demonstrate that ellipsometry is a useful tool for quantitatively probing thin films and surfaces in the presence of fluids.

1.9.3. Experimental data analysis and modeling

This section describes the rational behind the model choice for evaluation of polystyrene-*block*-poly(acrylic acid) (PS-*b*-PAA) brushes thickness under different environmental conditions (pH and salt concentration). For in situ experiments, the

cell filled with liquid is used. The Horizontal Liquid Cell™ (J. A. Woollam Co) is described in Chapter 4. The studied polymer film should demonstrate sufficient optical contrast, i.e. *n* and *k* values, that are distinct from the medium (water).[231] Prior to in situ measurements, the dry film thickness and corresponding optical constants must be determined. The refractive index of each block in PS-*b*-PAA brushes is bigger than the refractive index of water (n_{water}=1.3330). The refractive index of 1.5893 is measured for a 10 nm thick PS layer. This value is close to the reported value at 589.3 nm ($n_{PS(bulk)}$=1.590-1.592) for PS in bulk.[239] A refractive index of 1.4788 is measured for a 12 nm PAA film, which is slightly different from the value reported in the literature ($n_{PAA(bulk)}$=1.527).[239] This discrepancy between measured and values reported in the literature values can be explained by a fraction of voids (air) between the grafted chains that decreases the overall refractive index of the layer.

The generic optical model consisting of five layers, as described in Figure 1-23, A was used to analyse the experimental data obtained in air. The dry thickness of each layer is measured prior to grafting the next layer. To determine the thickness of the top layer, thicknesses of all underlying layers have to be known and to remain fixed. **L#0** is a silica substrate and its thickness is fixed as 1 mm. **L#1** represents a silicon oxide layer. The thickness of this layer can vary from wafer to wafer. Usually, the silicon oxide thickness is stated by the manufacture. However, the exact SiO_2 thickness has to be determined prior to the substrate modification. Silicon wafers from University Wafer Co (100-mm diameter, boron-doped, (100) orientation, one side polished) with an average silicon oxide thickness of 2 nm is used. **L#2** represents the initiator layer, and its thickness is measured prior to polymerization. The initiator layer thickness is 0.2±0.03 nm and it is modeled using Cauchy equation with fixed Cauchy coefficients (A_n=1.45, B_n=0.01 and C_n=0) resulting in MSE of 2.0-2.3. PS layer (**L#3**) is modeled using "polystyrene_g.mat" layer from the WVASE library. MSE for this layer thickness does not exceed 2.5. The top PAA layer (**L#4**) is also

modeled using the Cauchy equation with fixed A_n, B_n, and C_n coefficients and a MSE of less than 5 is usually obtained.

The top "H_2O" layer is added to the above described model for experiments done in liquid environment (water or buffer) as shown in Figure 1-23, B. The same top model layer ("$H_2O\_22^o$") is used for all experiments in water and in buffer because the refractive index of 0.1 M Tris buffer (n_b=1.3344) is similar to the refractive index of pure water. The swollen PAA layer is modeled usingx the Cauchy equation with non-fixed A_n and B_n coefficients. This means that the software finds the best correlation between experimental and modeled values not only by varying the thickness but also by changing A_n and B_n coefficients. This approach results in minimum MSE values.

Figure 1-23 shows Ψ and Δ values for PS-*b*-PAA layer in air (A') and in water (B'). The dashed green line is an experimental Ψ values, and the dashed blue line represents experimental Δ values. The red line corresponds to the generated data from the model.

The spectrum of PS-*b*-PAA brushes in water is different than in air. This indicates reorganization within the brush. Since the PS layer is hydrophobic and does not undergo any structural change in presence of water, these spectrum changes can be associated with solvation of hydrophilic PAA layer. A good overlap between the experimental and generated data confirms that the selected models for both dry and wet measurements represent the film composition correctly.

The structural changes within the PAA layer induced by pH and ionic strength can be precisely monitored in-situ with ellipsometry by measuring the thickness and refractive index of the layer. The thickness of PAA layer increases with pH (Table 1-2). This is expected due to the increase of the number of dissociated carboxylic acid groups with pH leading to electrostatic repulsion between the chains, and, therefore, to brush extending.

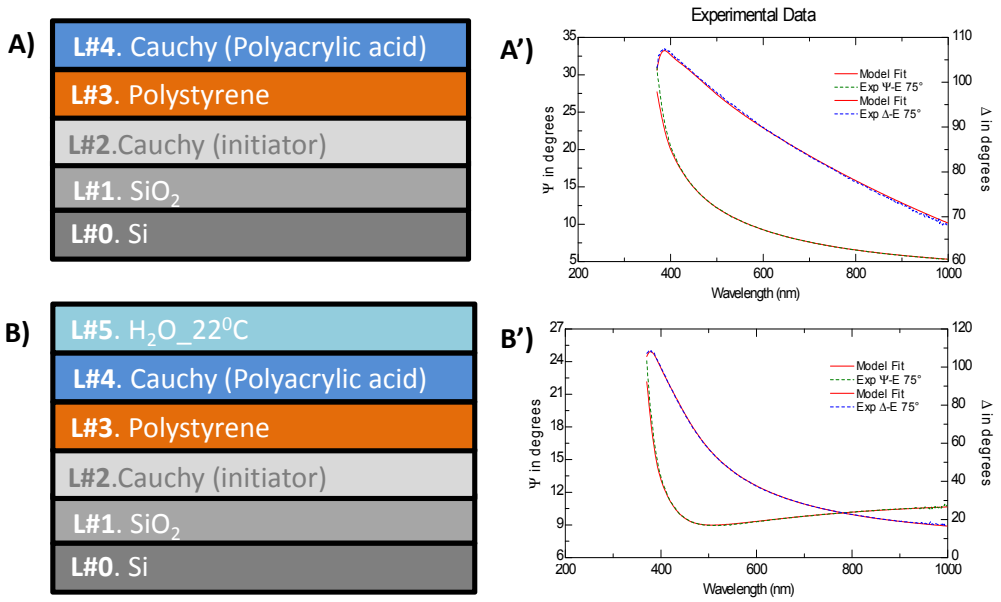

Figure 1-23. Optical model for the PS-*b*-PAA brushes in air (A) and MilliQ water (B) and the corresponding experimental data of Ψ and Δ obtained in air (A') and liquid (B'). Thickness of the PS layer is 3.1 nm (in air) and PAA is 12.2 nm in dry state and 28.1 nm in water.

Table 1-2. Refractive indices obtained by ellipsometry at 589.3 nm and corresponding PAA layer thickness at different conditions. Refractive index and thickness were estimated using the Cauchy model

PAA layer	Refractive index	Thickness, nm
air	1.4788±0.0002	12.2±0.01
water	1.4235±0.0011	28.1±0.2
pH 6.5	1.4106±0.0143	47.6±11.7
pH 7.5	1.3975±0.0075	54.1±8.2
pH 8.5	1.3874±0.0061	78.3±0.7
pH 9.5	1.3765±0.0032	117.4±0.3
pH 10.5	1.3616±0.0002	137.0±1.5

The error is a standard deviation from three different measurements.

The swollen polymer layer is a mixed phase of polymer chains and analyte. The refractive index of the polymer film immersed in the medium depends on the portion of the analyte trapped within the layer. Thus, in case of PAA layer immersed into water-based buffer solution, the overall refractive index of the swollen PAA layer decreases with increasing the portion of water trapped within the brush. Table 1-2 shows that the refractive index of the PAA layer decreases while pH and the thickness increase. This can be explained by conformational changes within the PAA. Particularly, a pH increase leads to the deprotonation of PAA carboxylic acid groups. The presence of negative charges along the polymer chains results in strong chains repulsions and in a brush extension. Moreover, with increasing the degree of dissociation, PAA layer becomes more hydrophilic and attracts more water inside the brush. The increase in water content results in a decrease in the PAA layer refractive index. So, the refractive index value is a good indicator of structural changes within the polymer brushes.

1.10. Total Internal Reflection Fluorescence Microscopy (TIRFM)

The total internal reflection fluorescence microscopy is a sensitive spectroscopic technique having a high signal-to-noise ratio. The main advantage of TIRF over other fluorescence microscopies as conventional fluorescence or confocal is its selective excitation such that only a thin layer of the fluorophore close to the substrate is examined. This is contrast to other fluorescence methods that examine the bulk properties in solution. Selective excitation with TIRF provides a high contrast.[240-243]

TIRF microscopy is based on the total internal reflection (TIR) phenomenon.[241, 242] This occurs when the incident light travels through a medium having a high and low refractive index at an angle greater than the critical angle. In

general, the refraction angle (θ_2) is always greater than the angle of incidence (θ_1) (Figure 1-24, A). When $\theta_2=90^o$, θ_1 is the critical angle (Figure 1-24, B). The light is completed reflected when θ_1>the critical angle. The resulting *total* reflection is called *internal* because the energy from the incident wave is confined within the original medium.

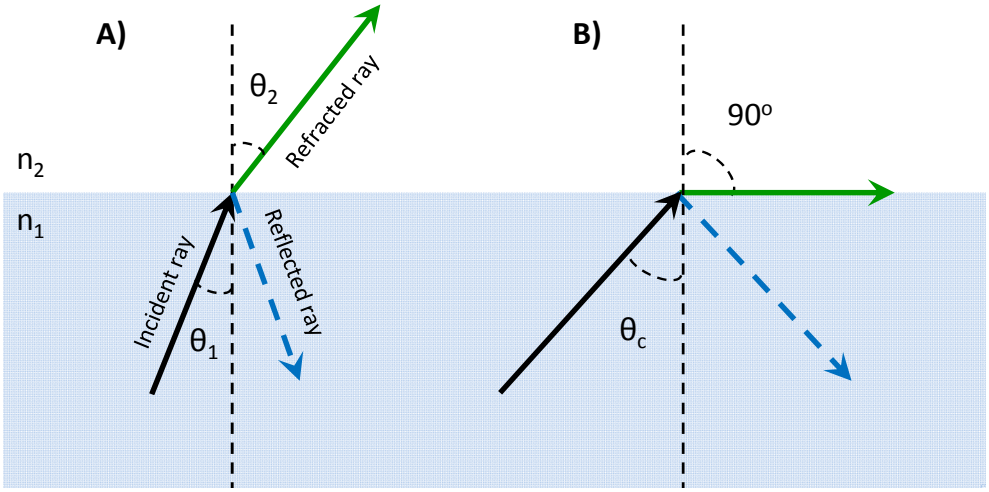

Figure 1-24. TIR principle. A) Typical geometry incident, refrected and reflected light at the medium boundary. B) Critical angle, above which total internal reflection occurs.

When the incident wave passes the critical angle, the evanescent wave with the same frequency as an incident light, is generated. The evanescent wave creates a very thin electromagnetic field (evanescent field) that penetrates the second medium. It propagates parallel to the surface and excites the fluorophores that are within 100 nm and exponentially decreases with increasing the distance from the surface.[241, 242] Thus, only fluorophores that are located close to the surface emit. In TIRF microscopy, a monochromatic laser is aligned within the objective. Two types of optical arrangement are used to direct the light: prism and numerical aperture.

TIRF microscopy is widely used to visualize biological samples such as living cells, because of it slow phototoxic effects. Additionally, TIRF microscopy has multiple applications in biochemistry and biology, such as selective visualization of the cell/substrate contrast, visualization of single fluorescent molecules, micromorphological structures, and dynamics of living cells.[240,241] Additionally TIRF microscopy is also used to investigate the electrofluorochromic properties of metal-organic compounds.[243]

1.11. Objective and structure of the thesis

The objective of the present work was to prepare well-defined weakly charged polymer brushes from silica-based surfaces, and to investigate their responsiveness to changes in pH and ionic strength, as well as their stability under different environmental conditions. Then, we aim to correlate physical and chemical properties of the end-grafted polymers (thickness of the polymer layer, grafting density, degree of ionization of the polymer), environmental conditions (ionic strength, pH, compression, and shear) and interactions (friction, adhesion and distance dependent forces) between opposing functionalized polymer-coated surfaces. This knowledge will allow identifying the key parameters which are effective in controlling adhesion and friction between polymer-bearing surfaces.

The thesis includes six chapters:

Chapter 1 represents a general introduction to polymer brushes. It describes methods of brush preparation, characterization and overview of recent achivements in the polymer brush field.

Chapter 2 is a verbatim copy of the paper published in *Macromolecular Symposia* (**2010**, *297*, 1-5). It presents a first report of direct synthesis of poly(acrylic acid) brushes from initiator-functionalized mica surface using water-assisted ATRP.

Chapter 3 is a verbatim copy of the full paper published in *Macromolecules* (**2011**, *44*, 8177-8184). Here, we confirm that hydrolysis of substrate-initiator bond results in polymer brush cleavage, and we determine the conditions under which hydrolysis occurs. We used fluorescence polymers for the direct spectroscopic monitoring of polymer degrafting from silica via Total Internal Reflection Fluorescence Microscope.

Chapter 4 is a verbatim copy of the full paper published in *Polymer Chemistry* (**2014**, *5*, 2242-2252). We prepared polystyrene-*block*-poly(acrylic acid) brushes using SI-ATRP and studied their responsiveness to variation of pH and ionic strength using spectroscopic ellipsometry. We showed that the hydrophobic polystyrene block of the copolymer protects the substrate-initiator bond against hydrolysis.

Chapter 5 is a verbatim copy of the full paper submitted to *Polymer Chemistry*, where we present a first report of covalent attachment of organophosphonic acid ATRP initiator to silica surface. Obtained organophosphonate layer was used to initiate polymerization, and prepared polyelectrolyte brushes were characterized by AFM, ATR-FTIR, and contact angle. Friction properties of PAA brushes as a function of pH and ionic strength were studied.

Chapter 6 includes the main conclusions and future perspectives. In this chapter our significant contribution to the field is specified, and ideas for future work are proposed.

1.12. References

(1) Currie, E. P. K.; Norde, W.; Stuart, M. A. C. *Adv. Colloid. Interface Sci.* **2003**, *100*, 205

(2) Milner, S. T.; Witten, T. A.; Cates, M. E. *Macromolecules* **1988**, *21*, 2610.

(3) Azzaroni, O. *J. Polym. Sci. Pol. Chem.* **2012**, *50*, 3225.

(4) Schon, P.; Kutnyanszky, E.; Ten Donkelaar, B.; Santonicola, M. G.; Tecim, T.; Aldred, N.; Clare, A. S.; Vancso, G. J. *Colloids Surf., B* **2013**, *102*, 923.

(5) Zhu, B.; Eurell, T.; Gunawan, R.; Leckband, D. *J. Biomed. Mater. Res.* **2001** *56*, 406.

(6) Welch, M.; Rastogi, A.; Ober, C. *Soft Matter* **2011**, *7*, 297.

(7) Chen, T.; Chang, D. P.; Zhang, J. M.; Jordan, R.; Zauscher, S. *Adv. Funct. Mater.* **2012**, *22*, 429.

(8) Comrie, J. E.; Huck, W. T. S. *Macromol. Rapid Commun.* **2008**, *29*, 539.

(9) Howse, J. R.; Topham, P.; Crook, C. J.; Gleeson, A. J.; Bras, W.; Jones, R. A. L.; Ryan, A. J. *Nano Lett.* **2006**, *6*, 73.

(10) Barbey, R.; Lavanant, L.; Paripovic, D.; Schuwer, N.; Sugnaux, C.; Tugulu, S.; Klok, H. A. *Chem. Rev.* **2009**, *109*, 5437.

(11) Moro, T.; Takatori, Y.; Ishihara, K.; Konno, T.; Takigawa, Y.; Matsushita, T.; Chung, U. I.; Nakamura, K.; Kawaguchi, H. *Nat. Mater.* **2004**, *3*, 829.

(12) G. Decher, J. B. S. *Multilayer Thin Films*; Wiley-VCH Verlag GmbH & Co. KGaA, 2003.

(13) Advincula, R. C. R., Jürgen; Caster, Kenneth C.; Brittain, William J.; *Polymer Brushes: Synthesis, Characterization, Applications*; 1st ed.; Wiley, John & Sons, 2004.

(14) Richard A.L. Jones, R. W. R. *Polymers at surfaces and interfaces*; Cambridge University Press, 1999.

(15) Toolan, D. T. W.; Howse, J. R. *J. Mater. Chem. C* **2013**, *1*, 603.

(16) Sachse, C.; Muller-Meskamp, L.; Bormann, L.; Kim, Y. H.; Lehnert, F.; Philipp, A.; Beyer, B.; Leo, K. *Org. Electron.* **2013**, *14*, 143.

(17) Alexander, S. *J. De Phys.* **1977**, *38*, 983.

(18) Fleer, G. J. L., J. *Adsorption From Solution at the Solid/Liquid Interface*; Academic Press: New York, 1983.

(19) Halperin, A.; Tirrell, M.; Lodge, T. P. *Adv. Polym. Sci.* **1992**, *100*, 31.

(20) Chakraborty, A. K.; Golumbfskie, A. J. *Annu. Rev. Phys. Chem.* **2001**, *52*, 537.

(21) Tassin, J. F.; Siemens, R. L.; Tang, W. T.; Hadziioannou, G.; Swalen, J. D.; Smith, B. A. *J. Phys. Chem.* **1989**, *93*, 2106.

(22) Moghaddam, M. S.; Chan, H. S. *J. Chem. Phys* **2006**, *125*.

(23) Wohl, B. M.; Engbersen, J. F. J. *J. Control. Release* **2012**, *158*, 2.

(24) Quinn, J. F.; Johnston, A. P. R.; Such, G. K.; Zelikin, A. N.; Caruso, F. *Chem. Soc. Rev.* **2007**, *36*, 707.

(25) Levine, M. J.; Schwarz, J. A. *J. Chem. Educ.* **1988**, *65*, 638.

(26) Degennes, P. G. *Colloid. Polym. Sci.* **1986**, *264*, 463.

(27) Roberts, G. G. *Contemp. Phys.* **1984**, *25*, 109.

(28) Yang, P. D.; Kim, F. *ChemPhysChem* **2002**, *3*, 503.

(29) Embs, F.; Funhoff, D.; Laschewsky, A.; Licht, U.; Ohst, H.; Prass, W.; Ringsdorf, H.; Wegner, G.; Wehrmann, R. *Adv. Mater.* **1991**, *3*, 25.

(30) Frantz, P.; Granick, S. *Phys. Rev. Lett.* **1991**, *66*, 899.

(31) Johnson, H. E.; Douglas, J. F.; Granick, S. *Phys. Rev. Lett.* **1993**, *70*, 3267.

(32) Krabi, A.; Stuart, M. A. C. *Macromolecules* **1998**, *31*, 1285.

(33) Reiter, G. *Phys. Rev. Lett.* **1992**, *68*, 75.

(34) Reiter, G. *Langmuir* **1993**, *9*, 1344.

(35) Sharma, A.; Reiter, G. *J. Colloid Interface Sci.* **1996**, *178*, 383.

(36) Liberelle, B.; Giasson, S. *Langmuir* **2007**, *23*, 9263.

(37) Pyun, J.; Jia, S. J.; Kowalewski, T.; Matyjaszewski, K. *Macromol. Chem. Phys.* **2004**, *205*, 411.

(38) Reiter, G.; Auroy, P.; Auvray, L. *Macromolecules* **1996**, *29*, 2150.

(39) Tate, R. S.; Fryer, D. S.; Pasqualini, S.; Montague, M. F.; Pablo, J. J. d.; Nealey, P. F. *J. Chem. Phys* **2001**, *115*, 9982.

(40) Taylor, W.; Jones, R. A. L. *Langmuir* **2010**, *26*, 13954.

(41) Corbierre, M. K.; Cameron, N. S.; Lennox, R. B. *Langmuir* **2004**, *20*, 2867.

(42) Lee, S. H.; Park, J. S.; Koo, C. M.; Lim, B. K.; Kim, S. O. *Macromol. Res.* **2008**, *16*, 261.

(43) Stafford, C. M.; Fadeev, A. Y.; Russell, T. P.; McCarthy, T. J. *Langmuir* **2001**, *17*, 6547.

(44) Zdyrko, B.; Luzinov, I. *Macromol. Rapid Commun.* **2011**, *32*, 859.

(45) Ishida, H.; Chiang, C. H.; Koenig, J. L. *Polymer* **1982**, *23*, 251.

(46) Naviroj, S.; Koenig, J. L.; Ishida, H. *J. Macromol. Sci., Phys.* **1983**, *B22*, 291.

(47) Iyer, K. S.; Luzinov, I. *Macromolecules* **2004**, *37*, 9538.

(48) Zdyrko, B.; Hoy, O.; Kinnan, M. K.; Chumanov, G.; Luzinov, I. *Soft Matter* **2008**, *4*, 2213.

(49) Karim, A.; Tsukruk, V. V.; Douglas, J. F.; Satija, S. K.; Fetters, L. J.; Reneker, D. H.; Foster, M. D. *J. Phys. II* **1995**, *5*, 1441.

(50) Grande, C. D.; Tria, M. C.; Felipe, M. J.; Zuluaga, F.; Advincula, R. *Eur. Phys. J. E* **2011**, *34*, 1.

(51) Hashimoto, K.; Fujisawa, T.; Kobayashi, M.; Yosomiya, R. *J. Macromol. Sci., Chem.* **1982**, *A18*, 173.

(52) Barbey, R.; Lavanant, L.; Paripovic, D.; Schuwer, N.; Sugnaux, C.; Tugulu, S.; Klok, H. A. *Chem. Rev.* **2009**, *109*, 5437.

(53) Brittain, W. J.; Minko, S. *J. Polym. Sci. Pol. Chem.* **2007**, *45*, 3505.

(54) Hui, C. M.; Pietrasik, J.; Schmitt, M.; Mahoney, C.; Choi, J.; Bockstaller, M. R.; Matyjaszewski, K. *Chem. Mater.* **2013**.

(55) Sakellariou, G.; Park, M.; Advincula, R.; Mays, J. W.; Hadjichristidis, N. *J. Polym. Sci. Pol. Chem.* **2006**, *44*, 769.

(56) Advincula, R.; Zhou, Q. G.; Park, M.; Wang, S. G.; Mays, J.; Sakellariou, G.; Pispas, S.; Hadjichristidis, N. *Langmuir* **2002**, *18*, 8672.

(57) Jordan, R.; Ulman, A. *J. Am. Chem. Soc.* **1998**, *120*, 243.

(58) Advincula, R. In *Adv. Polym. Sci*. Jordan, R., Ed. 2006; Vol. 197, p 107.

(59) Schneider, M.; Fetsch, C.; Amin, I.; Jordan, R.; Luxenhofer, R. *Langmuir* **2013**, *29*, 6983.

(60) Haque, H. A.; Kakehi, S.; Hara, M.; Nagano, S.; Seki, T. *Langmuir* **2013**, *29*, 7571.

(61) Prucker, O.; Rühe, J. *Langmuir* **1998**, *14*, 6893.

(62) Prucker, O.; Rühe, J. *Macromolecules* **1998**, *31*, 592.

(63) Pyun, J.; Kowalewski, T.; Matyjaszewski, K. *Macromol. Rapid Commun.* **2003**, *24*, 1043.

(64) Tsujii, Y.; Ohno, K.; Yamamoto, S.; Goto, A.; Fukuda, T. *Adv. Polym. Sci.* **2006**, *197*, 1.

(65) Odian, G. *Principles of polymerization*; 4th ed.; A. John Wiley & Sons, Inc.: Hoboken, New Jersey, United States, 2004.

(66) Braunecker, W. A.; Matyjaszewski, K. *Prog. Polym. Sci.* **2007**, *32*, 93.

(67) Matyjaszewski, K.; Kubisa, P.; Penczek, S. *J. Polym. Sci. Pol. Chem.* **1974**, *12*, 1333.

(68) Matyjaszewski, K. *Prog. Polym. Sci.* **2005**, *30*, 858.

(69) Matyjaszewski, K.; Spanswick, J. *Mater. Today* **2005**, *8*, 26.

(70) Fischer, H. *Macromolecules* **1997**, *30*, 5666.

(71) Fischer, H. *J. Polym. Sci. Pol. Chem.* **1999**, *37*, 1885.

(72) Fischer, H. *Chem. Rev.* **2001**, *101*, 3581.

(73) Keddie, D. J.; Moad, G.; Rizzardo, E.; Thang, S. H. *Macromolecules* **2012**, *45*, 5321.

(74) Smith, A. E.; Xu, X. W.; Mccormick, C. L. *Prog. Polym. Sci.* **2010**, *35*, 45.

(75) Brinks, M. K.; Studer, A. *Macromol. Rapid Comm.* **2009**, *30*, 1043.

(76) Kato, M.; Kamigaito, M.; Sawamoto, M.; Higashimura, T. *Macromolecules* **1995**, *28*, 1721.

(77) (77) Wang, J.-S.; Matyjaszewski, K. *J. Am. Chem. Soc.* **1995**, *117*, 5614.

(78) Minisci, F. *Acc. Chem. Res.* **1975**, *8*, 165.

(79) Kharasch, M. S.; Jensen, E. V.; Urry, W. H. *Science* **1945**, *102*, 128.

(80) vandeKuil, L. A.; Grove, D. M.; Gossage, R. A.; Zwikker, J. W.; Jenneskens, L. W.; Drenth, W.; vanKoten, G. *Organometallics* **1997**, *16*, 4985.

(81) Pintauer, T.; Matyjaszewski, K. *Chem. Soc. Rev.* **2008**, *37*, 1087.

(82) Matyjaszewski, K. *Curr. Org. Chem.* **2002**, *6*, 67.

(83) Matyjaszewski, K. *Macromolecules* **1998**, *31*, 4710.

(84) Kajiwara, A.; Matyjaszewski, K. *Macromol. Rapid Commun.* **1998**, *19*, 319.

(85) Kajiwara, A.; Matyjaszewski, K.; Kamachi, M. *Macromolecules* **1998**, *31*, 5695.

(86) Matyjaszewski, K.; Kajiwara, A. *Macromolecules* **1998**, *31*, 548.

(87) Jeyaprakash, J. D.; Samuel, S.; Dhamodharan, R.; Rühe, J. *Macromol. Rapid Commun.* **2002**, *23*, 277.

(88) Matyjaszewski, K.; Xia, J. H. *Chem. Rev.* **2001**, *101*, 2921.

(89) Matyjaszewski, K. *Macromolecules* **2012**, *45*, 4015.

(90) Patten, T. E.; Matyjaszewski, K. *Acc. Chem. Res.* **1999**, *32*, 895.

(91) Huang, X.; Wirth, M. J. *Anal. Chem.* **1997**, *69*, 4577.

(92) Tsujii, Y.; Ohno, K.; Yamamoto, S.; Goto, A.; Fukuda, T. *Adv. Polym. Sci.* **2006**, *197*, 1.

(93) Lego, B.; François, M.; Skene, W. G.; Giasson, S. *Langmuir* **2009**, *25*, 5313.

(94) Tugulu, S.; Klok, H.-A. *Biomacromolecules* **2008**, *9*, 906.

(95) Yamamoto, S.; Ejaz, M.; Tsujii, Y.; Fukuda, T. *Macromolecules* **2000**, *33*, 5608.

(96) Matyjaszewski, K.; Miller, P. J.; Shukla, N.; Immaraporn, B.; Gelman, A.; Luokala, B. B.; Siclovan, T. M.; Kickelbick, G.; Vallant, T.; Hoffmann, H.; Pakula, T. *Macromolecules* **1999**, *32*, 8716.

(97) Gao, X.; Feng, W.; Zhu, S.; Sheardown, H.; Brash, J. L. *Macromol. React. Eng.* **2010**, *4*, 235.

(98) Zhou, D.; Gao, X.; Wang, W.-j.; Zhu, S. *Macromolecules* **2012**, *45*, 1198.

(99) Tsujii, Y.; Ejaz, M.; Sato, K.; Goto, A.; Fukuda, T. *Macromolecules* **2001**, *34*, 8872.

(100) Tchoul, M. N.; Dalton, M.; Tan, L.-S.; Dong, H.; Hui, C. M.; Matyjaszewski, K.; Vaia, R. A. *Polymer* **2012**, *53*, 79.

(101) Edmondson, S.; Osborne, V. L.; Huck, W. T. S. *Chem. Soc. Rev.* **2004**, *33*,

(102) Gorman, C. B.; Petrie, R. J.; Genzer, J. *Macromolecules* **2008**, *41*, 4856.

(103) Koylu, D.; Carter, K. R. *Macromolecules* **2009**, *42*, 8655.

(104) Pasetto, P.; Blas, H.; Audouin, F.; Boissiere, C.; Sanchez, C.; Save, M.; Charleux, B. *Macromolecules* **2009**, *42*, 5983.

(105) Ohno, K.; Morinaga, T.; Koh, K.; Tsujii, Y.; Fukuda, T. *Macromolecules* **2005**, *38*, 2137.

(106) Huang, C. L.; Tassone, T.; Woodberry, K.; Sunday, D.; Green, D. L. *Langmuir* **2009**, *25*, 13351.

(107) Behling, R. E.; Williams, B. A.; Staade, B. L.; Wolf, L. M.; Cochran, E. W. *Macromolecules* **2009**, *42*, 1867.

(108) Lowe, A. B.; McCormick, C. L. *Chem. Rev.* **2002**, *102*, 4177.

(109) Macknight, W. J.; Earnest, T. R. *Macromol. Rev.* **1981**, *16*, 41.

(110) Finch, C. A. *Brit. Polym. J.* **1984**, *16*, 157.

(111) Li, M.; Min, K.; Matyjaszewski, K. *Macromolecules* **2004**, *37*, 2106.

(112) Min, K.; Gao, H.; Matyjaszewski, K. *J. Am. Chem. Soc.* **2005**, *127*, 3825.

(113) Min, K.; Gao, H. F.; Matyjaszewski, K. *J. Am. Chem. Soc.* **2006**, *128*, 10521.

(114) Min, K.; Oh, J. K.; Matyjaszewski, K. *J. Polym. Sci. Pol. Chem.* **2007**, *45*, 1413.

(115) Oh, J. K.; Perineau, F.; Matyjaszewski, K. *Macromolecules* **2006**, *39*, 8003.

(116) Oh, J. K.; Tang, C.; Gao, H.; Tsarevsky, N. V.; Matyjaszewski, K. *J. Am. Chem. Soc.* **2006**, *128*, 5578.

(117) Coca, S.; Jasieczek, C. B.; Beers, K. L.; Matyjaszewski, K. *J. Polym. Sci. Pol. Chem.* **1998**, *36*, 1417.

(118) Wang, X. S.; Armes, S. P. *Macromolecules* **2000**, *33*, 6640.

(119) Oh, J. K.; Perineau, F.; Charleux, B.; Matyjaszewski, K. *J. Polym. Sci. Pol. Chem.* **2009**, *47*, 1771.

(120) Zhang, Q.; Wilson, P.; Li, Z.; McHale, R.; Godfrey, J.; Anastasaki, A.; Waldron, C.; Haddleton, D. M. *J. Am. Chem. Soc.* **2013**, *135*, 7355.

(121) Tsarevsky, N. V.; Matyjaszewski, K. *J. Polym. Sci. Pol. Chem.* **2006**, *44*, 5098.

(122) Tsarevsky, N. V.; Matyjaszewski, K. *Chem. Rev.* **2007**, *107*, 2270.

(123) Tsarevsky, N. V.; Pintauer, T.; Matyjaszewski, K. *Macromolecules* **2004**, *37*, 9768.

(124) Bortolamei, N.; Isse, A. A.; Di Marco, V. B.; Gennaro, A.; Matyjaszewski, K. *Macromolecules* **2010**, *43*, 9257.

(125) Braunecker, W. A.; Tsarevsky, N. V.; Gennaro, A.; Matyjaszewski, K. *Macromolecules* **2009**, *42*, 6348.

(126) Matyjaszewski, K.; Nakagawa, Y.; Jasieczek, C. B. *Macromolecules* **1998**, *31*, 1535.

(127) Ciavatta, L.; Ferri, D.; Palombari, R. *J. Inorg. Nucl. Chem.* **1980**, *42*, 593.

(128) Malyszko, J.; Scendo, M. *J. Electroanal. Chem.* **1989**, *269*, 113.

(129) Randles, J. E. B. *J. Chem. Soc.* **1941**, 802.

(130) Percec, V.; Guliashvili, T.; Ladislaw, J. S.; Wistrand, A.; Stjerndahl, A.; Sienkowska, M. J.; Monteiro, M. J.; Sahoo, S. *J. Am. Chem. Soc.* **2006**, *128*, 14156.

(131) Matyjaszewski, K.; Tsarevsky, N. V.; Braunecker, W. A.; Dong, H.; Huang, J.; Jakubowski, W.; Kwak, Y.; Nicolay, R.; Tang, W.; Yoon, J. A. *Macromolecules* **2007**, *40*, 7795.

(132) Zhang, Y. Z.; Wang, Y.; Peng, C. H.; Zhong, M. J.; Zhu, W. P.; Konkolewicz, D.; Matyjaszewski, K. *Macromolecules* **2012**, *45*, 78.

(133) Tsarevsky, N. V.; Braunecker, W. A.; Brooks, S. J.; Matyjaszewski, K. *Macromolecules* **2006**, *39*, 6817.

(134) Tsarevsky, N. V.; Braunecker, W. A.; Vacca, A.; Gans, P.; Matyjaszewski, K. *Macromol. Symp.* **2007**, *248*, 60.

(135) Braunecker, W. A.; Tsarevsky, N. V.; Pintauer, T.; Gil, R. R.; Matyjaszewski, K. *Macromolecules* **2005**, *38*, 4081.

(136) Braunecker, W. A.; Pintauer, T.; Tsarevsky, N. V.; Kickelbick, G.; Matyjaszewski, K. *J. Organomet. Chem.* **2005**, *690*, 916.

(137) Jones, D. M.; Brown, A. A.; Huck, W. T. S. *Langmuir* **2002**, *18*, 1265.

(138) Jones, D. M.; Huck, W. T. S. *Adv. Mater.* **2001**, *13*, 1256.

(139) Kizhakkedathu, J. N.; Norris-Jones, R.; Brooks, D. E. *Macromolecules* **2004**, *37*, 734.

(140) Perruchot, C.; Khan, M. A.; Kamitsi, A.; Armes, S. P.; von Werne, T.; Patten, T. E. *Langmuir* **2001**, *17*, 4479.

(141) Boyes, S. G.; Akgun, B.; Brittain, W. J.; Foster, M. D. *Macromolecules* **2003**, *36*, 9539.

(142) Borozenko, O.; Godin, R.; Lau, K. L.; Mah, W.; Cosa, G.; Skene, W. G.; Giasson, S. *Macromolecules* **2011**, *44*, 8177.

(143) Patten, T. E.; Matyjaszewski, K. *Adv. Mater.* **1998**, *10*, 901.

(144) Ashford, E. J.; Naldi, V.; O'Dell, R.; Billingham, N. C.; Armes, S. P. *Chem. Commun.* **1999**, 1285.

(145) Sankhe, A. Y.; Husson, S. M.; Kilbey, S. M. *Macromolecules* **2006**, *39*, 1376.

(146) Coessens, V.; Pintauer, T.; Matyjaszewski, K. *Prog. Polym. Sci.* **2001**, *26*, 337.

(147) Mincheva, R.; Paneva, D.; Mespouille, L.; Manolova, N.; Rashkov, I.; Dubois, P. *J. Polym. Sci. Pol. Chem.* **2009**, *47*, 1108.

(148) Blauer, G. *J. Polym. Sci.* **1953**, *11*, 189.

(149) Iddon, P. D.; Robinson, K. L.; Armes, S. P. *Polymer* **2004**, *45*, 759.

(150) Santonicola, M. G.; de Groot, G. W.; Memesa, M.; Meszynska, A.; Vancso, G. J. *Langmuir* **2010**, *26*, 17513.

(151) Huang, L.; Yuan, S.; Lv, L.; Tan, G.; Liang, B.; Pehkonen, S. O. *J. Colloid Interface Sci.* **2013**, *405*, 171.

(152) Dong, R.; Krishnan, S.; Baird, B. A.; Lindau, M.; Ober, C. K. *Biomacromolecules* **2007**, *8*, 3082.

(153) Zheng, Y. Q.; Deng, S. B.; Niu, L.; Xu, F. J.; Chai, M. Y.; Yu, G. *J. Hazard. Mater.* **2011**, *192*, 1401.

(154) Tugulu, S.; Barbey, R.; Harms, M.; Fricke, M.; Volkmer, D.; Rossi, A.; Klok, H.-A. *Macromolecules* **2006**, *40 (2)*, 168.

(155) Whiting, G. L.; Snaith, H. J.; Khodabakhsh, S.; Andreasen, J. W.; Breiby, D.; Nielsen, M. M.; Greenham, N. C.; Friend, P. H.; Huck, W. T. S. *Nano Lett.* **2006**, *6*, 573.

(156) Fu, Q.; Rao, G. V. R.; Ista, L. K.; Wu, Y.; Andrzejewski, B. P.; Sklar, L. A.; Ward, T. L.; Lopez, G. P. *Adv. Mater.* **2003**, *15*, 1262.

(157) Costantini, F.; Bula, W. P.; Salvio, R.; Huskens, J.; Gardeniers, H.; Reinhoudt, D. N.; Verboom, W. *J. Am. Chem. Soc.* **2009**, *131*, 1650.

(158) Zhulina, E. B.; Singh, C.; Balazs, A. C. *Macromolecules* **1996**, *29*, 8254.

(159) Zhulina, E. B.; Singh, C.; Balazs, A. C. *Macromolecules* **1996**, *29*, 6338.

(160) Baum, M.; Brittain, W. J. *Macromolecules* **2002**, *35*, 610.

(161) Xu, C.; Wu, T.; Drain, C. M.; Batteas, J. D.; Fasolka, M. J.; Beers, K. L. *Macromolecules* **2006**, *39*, 3359.

(162) Xu, C.; Wu, T.; Mei, Y.; Drain, C. M.; Batteas, J. D.; Beers, K. L. *Langmuir* **2005**, *21*, 11136.

(163) Yu, K.; Wang, H.; Xue, L.; Han, Y. *Langmuir* **2006**, *23*, 1443.

(164) Hur, S.-M.; Frischknecht, A. L.; Huber, D. L.; Fredrickson, G. H. *Soft Matter.* **2013**, *9*, 5341.

(165) Ionov, L.; Minko, S. *Acs Appl. Mater. Inter.* **2012**, *4*, 483.

(166) Usov, D.; Gruzdev, V.; Nitschke, M.; Stamm, M.; Hoy, O.; Luzinov, I.; Tokarev, I.; Minko, S. *Macromolecules* **2007**, *40*, 8774.

(167) (167) Motornov, M.; Sheparovych, R.; Lupitskyy, R.; MacWilliams, E.; Hoy, O.; Luzinov, I.; Minko, S. *Adv. Funct. Mater.* **2007**, *17*, 2307.

(168) Kim, D. J.; Kang, S. M.; Kong, B.; Kim, W. J.; Paik, H. J.; Choi, H.; Choi, I. S. *Macromol. Chem. Phys.* **2005**, *206*, 1941.

(169) Li, A.; Benetti, E. M.; Tranchida, D.; Clasohm, J. N.; Schönherr, H.; Spencer, N. D. *Macromolecules* **2011**, *44*, 5344.

(170) Degennes, P. G. *Macromolecules* **1980**, *13*, 1069.

(171) Toomey, R.; Tirrell, M. *Annu. Rev. Phys. Chem.* **2008**, *59*, 493.

(172) Biesalski, M.; Johannsmann, D.; Ruhe, J. *J. Chem. Phys.* **2002**, *117*, 4988.

(173) Minko, S. *Polym. Rev.* **2006**, *46*, 397.

(174) Zhulina, E. B.; Birshtein, T. M.; Borisov, O. V. *Macromolecules* **1995**, *28*, 1491.

(175) Wu, T.; Gong, P.; Szleifer, I.; Vlcek, P.; Subr, V.; Genzer, J. *Macromolecules* **2007**, *40*, 8756.

(176) Matsen, M. W. *J. Chem. Phys.* **2002**, *117*, 2351.

(177) Pincus, P. *Macromolecules* **1991**, *24*, 2912.

(178) Zhulina, E. B.; Wolterink, J. K.; Borisov, O. V. *Macromolecules* **2000**, *33*, 4945.

(179) Murat, M.; Grest, G. S. *Macromolecules* **1989**, *22*, 4054.

(180) Rühe, J.; Ballauff, M.; Biesalski, M.; Dziezok, P.; Gröhn, F.; Johannsmann, D.; Houbenov, N.; Hugenberg, N.; Konradi, R.; Minko, S.; Motornov, M.; Netz, R.; Schmidt, M.; Seidel, C.; Stamm, M.; Stephan, T.; Usov, D.; Zhang, H. In *Polyelectrolytes with Defined Molecular Architecture I*; Schmidt, M., Ed.; Springer Berlin Heidelberg: 2004; Vol. 165, p 79.

(181) Israels, R.; Leermakers, F. A. M.; Fleer, G. J. *Macromolecules* **1994**, *27*, 3087.

(182) Ruhe, J.; Ballauff, M.; Biesalski, M.; Dziezok, P.; Grohn, F.; Johannsmann, D.; Houbenov, N.; Hugenberg, N.; Konradi, R.; Minko, S.; Motornov, M.; Netz, R. R.; Schmidt, M.; Seidel, C.; Stamm, M.; Stephan, T.; Usov, D.; Zhang, H. N. *Polyelectrolytes with Defined Molecular Architecture I* **2004**, *165*, 79.

(183) Kumar, S.; Dory, Y. L.; Lepage, M.; Zhao, Y. *Macromolecules* **2011**, *44*, 7385.

(184) de Groot, G. W.; Santonicola, M. G.; Sugihara, K.; Zambelli, T.; Reimhult, E.; Voros, J.; Vancso, G. J. *ACS Appl. Mater. Interfaces* **2013**, *5*, 1400.

(185) Kurosawa, S.; Aizawa, H.; Talib, Z. A.; Atthoff, B.; Hilborn, J. *Biosens. Bioelectron.* **2004**, *20*, 1165.

(186) Bittrich, E.; Rodenhausen, K.; Eichhorn, K.-J.; Hofmann, T.; Schubert, M.; Stamm, M.; Uhlmann, P. *Biointerphases* **2010**, *5*, 159.

(187) Zhou, F.; Shu, W. M.; Welland, M. E.; Huck, W. T. S. *J. Am. Chem. Soc.* **2006**, *128*, 5326.

(188) Currie, E. P. K.; Sieval, A. B.; Fleer, G. J.; Stuart, M. A. C. *Langmuir* **2000**, *16*, 8324.

(189) Aulich, D.; Hoy, O.; Luzinov, I.; Brucher, M.; Hergenroder, R.; Bittrich, E.; Eichhorn, K. J.; Uhlmann, P.; Stamm, M.; Esser, N.; Hinrichs, K. *Langmuir* **2010**, *26*, 12926.

(190) Dong, R.; Lindau, M.; Ober, C. K. *Langmuir* **2009**, *25*, 4774.

(191) Chow, T. S. *J. Phys.: Condens. Mat*. **1998**, *10*, L445.

(192) Adamson, A. W. *Physical chemistry of surfaces*; Wiley, 1990.

(193) Holmesfarley, S. R.; Reamey, R. H.; McCarthy, T. J.; Deutch, J.; Whitesides, G. M. *Langmuir* **1985**, *1*, 725.

(194) Houbenov, N.; Minko, S.; Stamm, M. *Macromolecules* **2003**, *36*, 5897.

(195) Bousquet, A.; Ibarboure, E.; Teran, F. J.; Ruiz, L.; Garay, M. T.; Laza, J. M.; Vilas, J. L.; Papon, E.; Rodriguez-Hernandez, J. *J. Polym. Sci. Pol. Chem.* **2010**, *48*, 2982.

(196) Creager, S. E.; Clarke, J. *Langmuir* **1994**, *10*, 3675.

(197) Awaja, F.; Gilbert, M.; Kelly, G.; Fox, B.; Pigram, P. J. *Prog. Polym. Sci.* **2009**, *34*, 948.

(198) Israelachvili, J. N. *Intermolecular and Surface Forces*; Elsevier Science, 2010.

(199) Luengo, G.; Campbell, S. E.; Srdanov, V. I.; Wudl, F.; Israelachvili, J. N. *Chem. Mater.* **1997**, *9*, 1166.

(200) Ashby, F.; Jones, D. R. H. *Engineering materials: an introduction to their properties and applications*; Pergamon Press, 1980.

(201) Raviv, U.; Giasson, S.; Kampf, N.; Gohy, J.-F.; Jérôme, R.; Klein, J. *Nature* **2003**, *425*, 163.

(202) Nordgren, N.; Rutland, M. W. *Nano Lett.* **2009**, *9*, 2984.

(203) Kampf, N.; Raviv, U.; Klein, J. *Macromolecules* **2004**, *37*, 1134.

(204) Klein, J.; Kamiyama, Y.; Yoshizawa, H.; Israelachvili, J. N.; Fredrickson, G. H.; Pincus, P.; Fetters, L. J. *Macromolecules* **1993**, *26*, 5552.

(205) Müller, M. T.; Yan, X.; Lee, S.; Perry, S. S.; Spencer, N. D. *Macromolecules* **2005**, *38*, 5706.

(206) Raviv, U.; Giasson, S.; Kampf, N.; Gohy, J. F.; Jerome, R.; Klein, J. *Langmuir* **2008**, *24*, 8678.

(207) Müller, M. T.; Yan, X.; Lee, S.; Perry, S. S.; Spencer, N. D. *Macromolecules* **2005**, *38*, 3861.

(208) Sudre, G.; Olanier, L.; Tran, Y.; Hourdet, D.; Creton, C. *Soft Matter* **2012**, *8*, 8184.

(209) Landherr, L. J. T.; Cohen, C.; Agarwal, P.; Archer, L. A. *Langmuir* **2011**, *27*, 9387.

(210) Landherr, L. J. T.; Cohen, C.; Archer, L. A. *Langmuir* **2011**, *27*, 5944.

(211) Chen, N.; Maeda, N.; Tirrell, M.; Israelachvili, J. *Macromolecules* **2005**, *38*, 3491.

(212) Ramakrishna, S. N.; Nalam, P. C.; Clasohm, L. Y.; Spencer, N. D. *Langmuir* **2013**, *29*, 175.

(213) Kumar, N. A.; Seidel, C. *Macromolecules* **2005**, *38*, 9341.

(214) Seidel, C. *Macromolecules* **2003**, *36*, 2536.

(215) Sokoloff, J. B. *J. Chem. Phys.* **2008**, *129*.

(216) Matsen, M. W. *Eur. Phys. J. E* **2012**, *35*.

(217) Sirchabesan, M.; Giasson, S. *Langmuir* **2007**, *23*, 9713.

(218) Liberelle, B.; Giasson, S. *Langmuir* **2008**, *24*, 1550.

(219) Azzam, R. M. A.; Bashara, N. M. *Ellipsometry and polarized light*; North-Holland Pub. Co., 1977.

(220) Fujiwara, H. *Spectroscopic Ellipsometry: Principles and Applications*; Wiley, 2007.

(221) N. Hilfiker, J.; Bungay, C. L.; Synowicki, R. A.; Tiwald, T. E.; Herzinger, C. M.; Johs, B.; Pribil, G. K.; Woollam, J. A. *J. Vac. Sci. Technol., A* **2003**, *21*, 1103.

(222) Tompkins, H. G.; Irene, E. A. *Handbook of Ellipsometry*; William Andrew Pub., 2005.

(223) Hilfiker, J. N.; Bungay, C. L.; Synowicki, R. A.; Tiwald, T. E.; Herzinger, C. M.; Johs, B.; Pribil, G. K.; Woollam, J. A. *J. Vac. Sci. Technol. A* **2003**, *21*, 1103.

(224) Johs, B.; Herzinger, C. M. In *Phys. Status Solidi C*; Arwin, H., Beck, U., Schubert, M., Eds. 2008; Vol. 5, p 1031.

(225) Oates, T. W. H.; Ryves, L.; Bilek, M. M. M. *Opt. Express* **2008**, *16*, 2302.

(226) Aspnes, D. E. *Thin Solid Films* **1982**, *89*, 249.

(227) Nagy, N.; Deak, A.; Horvolgyi, Z.; Fried, M.; Agod, A.; Barsony, I. *Langmuir* **2006**, *22*, 8416.

(228) Othman, M. T.; Lubguban, J. A.; Lubguban, A. A.; Gangopadhyay, S.; Miller, R. D.; Volksen, W.; Kim, H. C. *J. Appl. Phys.* **2006**, *99*.

(229) Madsen, M. V.; Sylvester-Hvid, K. O.; Dastmalchi, B.; Hingerl, K.; Norrman, K.; Tromholt, T.; Manceau, M.; Angmo, D.; Krebs, F. C. *J. Phys. Chem. C* **2011**, *115*, 10817.

(230) Ng, A.; Li, C. H.; Fung, M. K.; Djurisic, A. B.; Zapien, J. A.; Chan, W. K.; Cheung, K. Y.; Wong, W. Y. *J. Phys. Chem. C* **2010**, *114*, 15094.

(231) Zudans, I.; Heineman, W. R.; Seliskar, C. J. *Chem. Mater.* **2004**, *16*, 3339.

(232) Kostruba, A.; Ohar, M.; Kulyk, B.; Zolobko, O.; Stetsyshyn, Y. *Appl. Surf. Sci.* **2013**, *276*, 340.

(233) Rauch, S.; Eichhorn, K. J.; Oertel, U.; Stamm, M.; Kuckling, D.; Uhlmann, P. *Soft Matter* **2012**, *8*, 10260.

(234) Ramos, J. I.; Moya, S. E. *Macromol. Chem. Phys.* **2012**, *213*, 549.

(235) Ramos, J. J. I.; Moya, S. E. *Macromol. Rapid Commun.* **2011**, *32*, 1972.

(236) Weir, M. P.; Heriot, S. Y.; Martin, S. J.; Parnell, A. J.; Holt, S. A.; Webster, J. R. P.; Jones, R. A. L. *Langmuir* **2011**, *27*, 11000.

(237) Rauch, S.; Uhlmann, P.; Eichhorn, K.-J. *Anal. Bioanal. Chem.* **2013**, 1.

(238) Hinrichs, K.; Aulich, D.; Ionov, L.; Esser, N.; Eichhorn, K.-J.; Motornov, M.; Stamm, M.; Minko, S. *Langmuir* **2009**, *25*, 10987.

(239) Brandrup, J., Immergut, E. H., Grulke, E. A., Abe, Akihiro, Bloch, Daniel R, Eds *Polymer Handbook, 4th ed*; Wiley: New York, 1999.

(240) Axelrod, D. *Method Enzymol* **2003**, *361*, 1.

(241) Axelrod, D. *Traffic* **2001**, *2*, 764.

(242) Mattheyses, A. L.; Simon, S. M.; Rappoport, J. Z. *J. of Cell Sci.* **2010**, *123*, 3621.

(243) Miomandre, F.; Pansu, R. B.; Audibert, J. F.; Guerlin, A.; Mayer, C. R. *Electrochem. Commun.* **2012**, *20*, 83

Chapter 2

Direct Polymerization of Polyacrylic Acid on Mica Substrates using ATRP – A Preliminary Study[§]

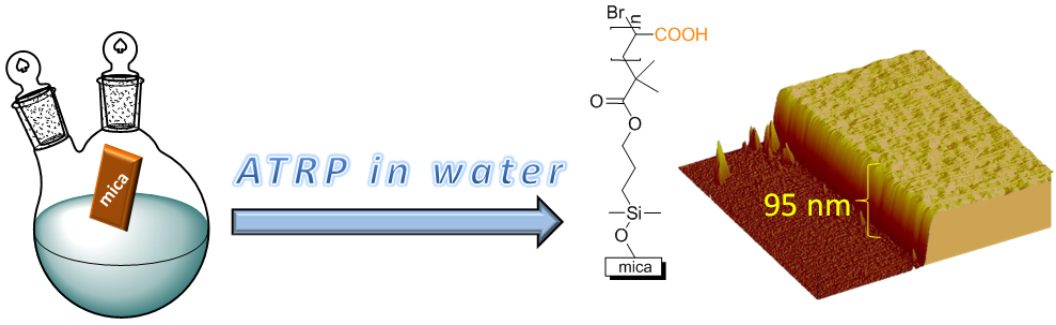

[§] This chapter is a verbatim copy of the paper published in *Macromolecular Symposia* 2010, 297, pp. 1-5. It is co-authored by W.G. Skene and Suzanne Giasson.

2.1 Summary

Unprecedented direct polymerization of sodium acrylate (NaA) on mica and silica substrates was undertaken using standard ATRP polymerization conditions at room temperature. The resulting thickness of the poly(sodium acrylate) (PNaA) grafted layer was determined using ellipsometry and AFM.

2.2 Introduction

Polymers brushes covalently attached to surfaces provide the means to modify surface properties of substrates to develop responsive surfaces such as anti-fouling surfaces[1-3] selective permeation membranes[4,5] and self-biolubricating surfaces.[6,7] Polyelectrolytes (PE) brushes represent responsive layers because their degree of ionization can be reversibly varied via pH and ionic strength which results in conformational changes. Therefore, controlled conformational responses to variations in the surrounding environmental conditions result in tuneable interfacial surface properties.[8,9]

The most precise and reliable means for measuring surface interactions between brushes is the Surface Forces Apparatus (SFA). The transparency and atomically smooth surface of cleaved mica make it an ideal substrate for SFA measurements. Direct polymerization of polymer brushes from mica is desired because it affords the means to modulate molecular weight, which in turns influences the brush height and conformation. We recently demonstrated that poly-*tert*-butyl acrylate could be prepared on mica by controlled polymerization using ATRP.[10] Although poly-*tert*-butyl acrylate can be converted into polyacrylic acid by hydrolyzing the *tert*-butyl group,[11] direct polymerization of acrylic acid involves fewer synthetic steps, and more particularly, the hydrolysis with strong acids is eliminated. This reduces the possibility of unwanted polymer cleavage from the

substrate. Unfortunately, ATRP of acrylic acid is not possible as a result of reduced catalyst reactivity with the carboxylic acid.[12] Conversely, sodium acrylate (NaA) can be polymerized by ATRP.[13] Although NaA is possible to polymerize on silica substrates, its direct polymerization affording poly (sodium acrylic acid) (PNaA) on mica has not been demonstrated. Successful polymerization of NaA on mica is important for investigating the changes in surface properties and surface forces induced by changes in ionic strength and pH. Herein, we present our preliminary results for the polymerization of NaA on mica as a proof of concept for NaA polymerization on mica in addition to demonstrating that absolute brush height measurements by AFM is possible.

2.3 Results and Discussion

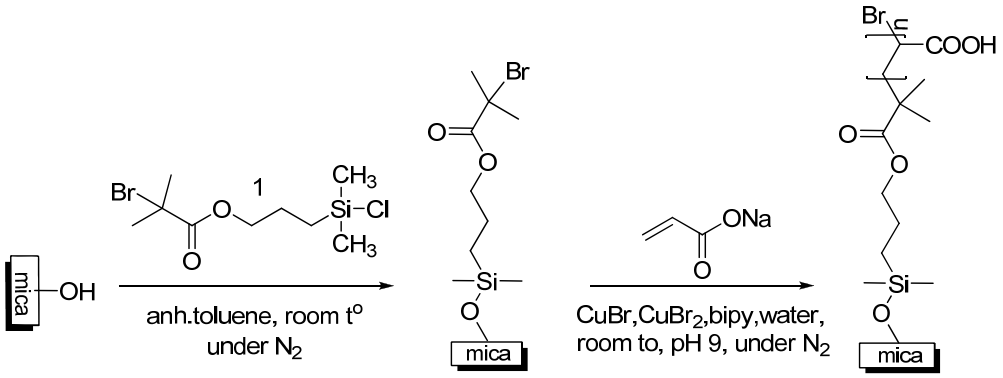

Scheme 2-1. Schematic of immobilization of **1** and direct polymerization of NaA on mica.

Polymerization of NaA was done using a previously reported ATRP initiator (**1**) that was immobilized on mica, as illustrated in Scheme 2-1, with a controlled surface density as previously reported.[14] Mica sheets were first cleaved. A mica strip was then laid across a portion of the freshly cleaved mica to form a mask. The

exposed mica was subsequently activated by H_2O/argon plasma using a Plasma Prep II from SPI Supplies to create hydroxyl groups.[15] The initiator was chemically attached to these OH groups using self-adsorption from solution.[14]

The polymerization of PNaA was done in the following manner: NaA was added to a fixed volume of water and then left to stir at room temperature until it was completely dissolved. The pH of the monomer solution was adjusted to that previously reported.[16] Bipyridine, CuBr and $CuBr_2$ were mixed in a round-bottomed flask and then deoxygenated under vacuum and backfilled with argon three times. The monomer solution was also deoxygenated under argon for 30 minutes after which it was transferred to the flask containing the copper-ligand mixture followed by stirring for 3 hours, until the solution was homogeneous. A clean initiator-functionalized mica substrate was placed in a flame-dried Schlenk flask under a stream of argon followed by deoxygenation under vacuum and then backfilled with argon three times. The above-described polymerization solution was transferred into the Schlenk flask at room temperature under a stream of argon followed by stirring. After 70 minutes, the surfaces were removed, rinsed with water, absolute ethanol, extracted and then washed three times for two hours with Milli Q, rinsed again with absolute ethanol and Milli Q water and then dried under nitrogen. A typical polymerization was done with the following: water (5 mL, 280 mmol), NaA (2.79 g, 30 mmol), bipy (155 mg, 0.99 mmol, CuBr (57 mg, 0,40 mmol), and $CuBr_2$ (18 mg, 0.08 mmol). AFM imaging and polymer film thickness measurements were carried out as previously reported.[10]

We initially investigated the smoothness of the immobilized **1** on mica. As seen in Figure 2-1, the root mean square (rms) value measured by AFM confirms that a homogeneous surface coverage on mica is possible. A smooth and homogenous initiator layer on the substrate is desired because the roughness of this layer can ultimately affect the polymer layer smoothness. A smooth initiator layer will ensure a smooth polymer layer (*vide infra*).

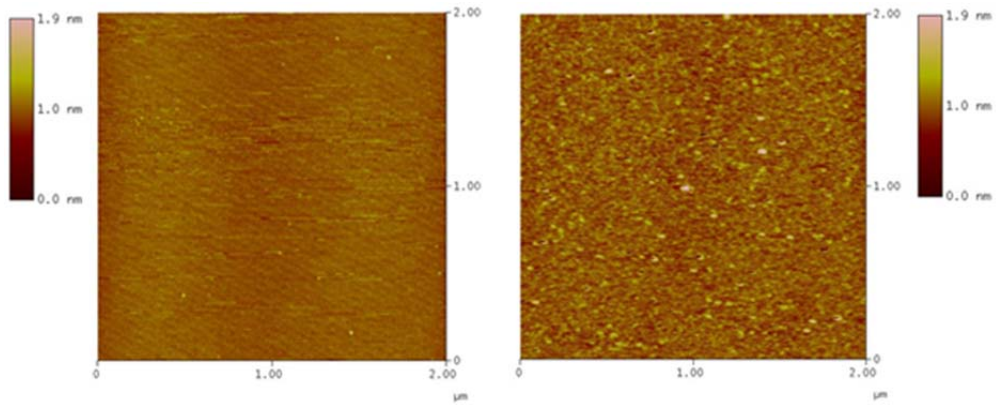

Figure 2-1. AFM images of freshly cleaved mica and mica covered with initiator layer.

The polymerization of NaA was done on mica with **1** in order to confirm that ATRP using this monomer was possible. The topology of the resulting polymer layer on mica was studied with AFM and compared to that of virgin mica as illustrated in Figure 2-2. From this figure, the smoothness of the polymer layer is evident. Moreover, the smooth polymer layer makes for easy determination of the absolute polymer thickness by comparing the step-height difference between the virgin mica and the polymer regions. The calculated thickness of the pNaA layer using the step-height method was 94.5 nm.

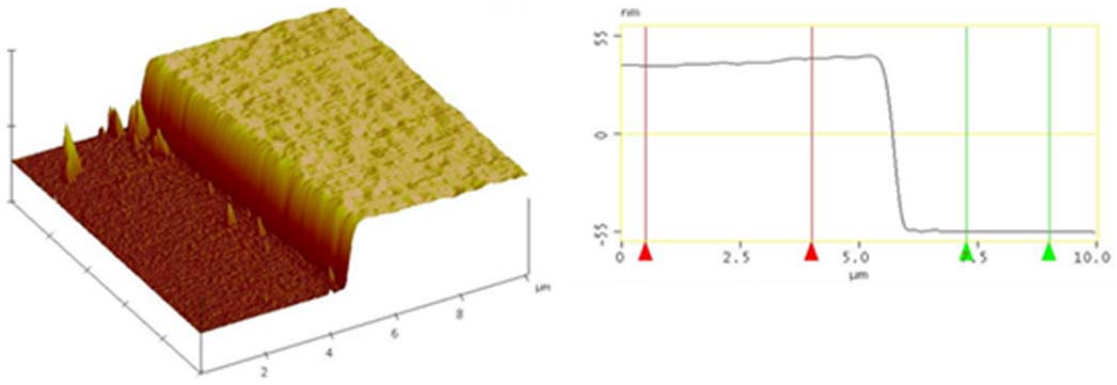

Figure 2-2. AFM image showing the step-height difference between the polymer layer of PNaA and the pristine mica.

The direct polymerization of NaA on a silica substrate was also investigated using similar polymerization conditions as with mica. This was done as a control test for comparing with NaA polymerized directly from mica. Comparisons of the resulting grafted polymer layers between mica and silica were done using an AFM step-height method and ellipsometry correspondingly. Ellipsometry was selected as a non-destructive technique to measure a thickness of the polymer layer. However, the multilayer mica structure results in a complex phase and amplitude signal, which is difficult to resolve. Thus, AFM was used as an alternative method for mica samples.

The silicon wafer on which PNaA was obtained was investigated by ellipsometry. The resulting polymer layer grafted from the initiator-modified silica shows a thickness of 57.3 nm, which is different from that obtained from functionalized mica. (Figure 2-3, Table 2-1).

Although comparable thickness were obtained for both poly(butyl acrylate) (PBA) and PNaA (Table 2-1), the direct polymerization of the latter is advantageous because the polymerization is much faster and can be done at room temperature. Unwanted polymer degrafting possible by thermal cleavage is therefore minimized with the polymerization of NaA. The direct polymerization using NaA is advantageous because the polymerization can be done at room temperature. Moreover, by eliminating the hydrolysis step required with poly-*tert*-butyl acrylate,[11] for instance, there is no risk of degrafting the polymer from the substrate. Nonetheless, the step-height measurements confirm that directly polymerization at room temperature of NaA on mica is possible.

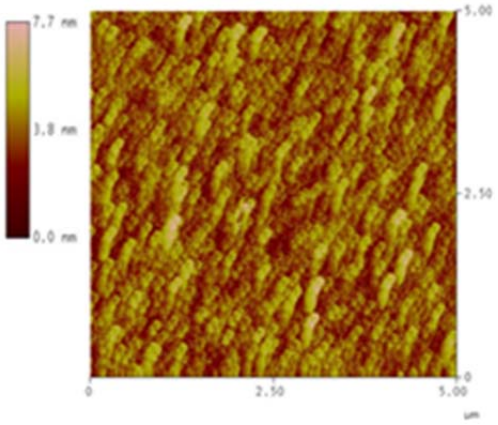

Roughness (5x5µm) obtained by AFM	0.1 nm
Thickness measured by ellipsometry	57.3 nm

Figure 2-3. AFM topographical micrograph of PNaA polymerized on a silicon wafer.

To confirm that the thickness of the polymer layer measured by step-height for mica was not an isolated phenomenon, we repeated the polymerization several times. Polymer layers on the order of 90 nm in thickness were consistently obtained and varied only as a function of polymerization time, consistent with controlled polymerization kinetics.

Table 2-1. Comparison of polymer layer thickness of PNaA polymerized via ATRP under similar polymerization conditions on mica and silica wafers.

Substrate	**Film thickness, nm**	**Measurement Technique**
Mica	94.5	AFM Step-height
Silicon wafer	57.3	Ellipsometry

In conclusion, we demonstrated that NaA can be directly polymerized on activated mica using an ATRP initiator covalently linked to the substrate. The polymerization of NaA on mica resulted in thick PNaA films within 70 minutes of 95 nm in thickness. The absolute thickness of the polymer layer was measured by AFM using the step-height method. Under similar conditions, the ARTP polymerization of NaA on mica gave consistently thicker films than on silicon wafers. Direct polymerization of NaA on mica provides the means to prepare polymers with tailored degrees of polymerization and for eventual surface-properties studies using SFA.

2.4 Acknowledgement

The authors acknowledge financial support from le Fonds de Recherche sur la Nature et les Technologies and the Natural Sciences and Engineering Research Council Canada. O.B. thanks the Université de Montréal for a graduate scholarship. Prof. R. E. Prud'homme and Mrs. B. Lego are also acknowledged for granting access to their AFM and for preliminary work, respectively.

2.5 References

(1) Giglio, E.; Cometa, S.; Cioffi, N.; Torsi, L.; Sabbatini, L. *Anal. Bioanal. Chem.* **2007**, 389, 2055.

(2) Zdyrko, B.; Hoy, O.; Luzinov, I. *Biointerphases* **2009**, 4, Fa17.

(3) Hollmann, O.; Gutberlet, T.; Czeslik, C. *Langmuir* **2007**, 23, 1347.

(4) Ito, Y.; Ochiai, Y.; Park, Y. S.; Imanishi, Y. *J. Am. Chem. Soc.* **1997**, 119, 1619.

(5) Park, Y. S.; Ito, Y.; Imanishi, Y. *Chem. Mater.* **1997**, 9, 2755.

(6) Briscoe, W. H.; Klein, J. J. *Adhesion* **2007**, 83, 705.

(7) Raviv, U.; Giasson, S.; Kampf, N.; Gohy, J. F.; Jerome, R.; Klein, J. *Langmuir* **2008**, 24, 8678.

(8) Ballauff, M.; Borisov, O. Curr. Opin. *Colloid Interface Sci.* **2006**, 11, 316.

(9) Rühe, J.; Ballauff, M.; Biesalski, M.; Dziezok, P.; Gröhn, F.; Johannsmann, D.; Houbenov, N.; Hugenberg, N.; Konradi, R.; Minko, S.; Motornov, M.; Netz, R.; Schmidt, M.; Seidel, C.; Stamm, M.; Stephan, T.; Usov, D.; Zhang, H. In *Polyelectrolytes with Defined Molecular Architecture* I; Schmidt, M., Ed.; Springer Berlin Heidelberg: **2004**; Vol. 165, p 79.

(10) Lego, B.; François, M.; Skene, W. G.; Giasson, S. *Langmuir* **2009**, 25, 5313.

(11) Liu, T.; Casado-Portilla, R.; Belmont, J.; Matyjaszewski, K. *J. Polym. Sci. Pol. Chem.* **2005**, 43, 4695.

(12) Patten, T. E.; Matyjaszewski, K. *Adv. Mater.* **1998**, 10, 901.

(13) Dong, R.; Krishnan, S.; Baird, B. A.; Lindau, M.; Ober, C. K. *Biomacromolecules* **2007**, 8, 3082.

(14) Lego, B.; Skene, W. G.; Giasson, S. *Langmuir* **2008**, 24, 379.

(15) Liberelle, B.; Giasson, S. *Langmuir* **2007**, 23, 9263.

(16) Tugulu, S.; Barbey, R.; Harms, M.; Fricke, M.; Volkmer, D.; Rossi, A.; Klok, H.-A. *Macromolecules*, **2006**, 40 (2), 168.

Chapter 3

Monitoring in Real-Time the Degrafting of Covalently Attached Fluorescent Polymer Brushes Grafted to Silica Substrates– Effects of pH and Salt**

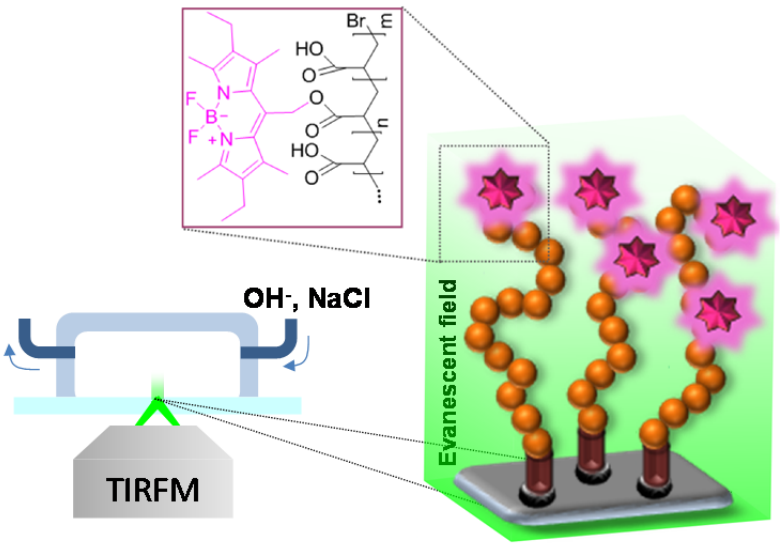

** This chapter is a verbatim copy of the paper published in *Macromolecules* 2011, 44 (20), pp. 8177-8184. It is co-authored by Robert Godin, Kai Lin Lau, Wayne Mah, Gonzalo Cosa, W. G. Skene and Suzanne Giasson.

3.1 Abstract

Poly(acrylic acid) (PAA) covalently immobilized on glass substrates was made fluorescent by grafting a BODIPY derivative (PMOH) via an ester linkage. Although only ng/cm^2 of polymer are understood to be immobilized onto the SiO_2 substrate, the fluorophore-tagged polymer was readily visible to the naked eye and its fluorescence was easily detected. The characteristic BODIPY emission, centered at 550 nm, was used to follow the degrafting of PAA from the glass substrates in aqueous solution in real-time using Total Internal Reflection Fluorescence (TIRF) microscopy. The substrate-initiator bond hydrolysis and the conditions at which the PAA degrafting occurred were unequivocally confirmed in real-time by TIRF microscopy. No cleavage of the polymer occurred between pH 6.5 and 10.5 in the absence of NaCl. In contrast, polymer degrafting from the substrate occurred at pH ≥ 9.5 when 10 mM NaCl was added to the buffer solution.

3.2 Introduction

Polymer bearing surfaces are of interest because of their thermal and solvent response,[1,2] their prospective use as protein and cell adhesive platforms,[3-5] or as self-biolubricating substrates, among others.[6] Surface-tethered polymer chains provide the means to tailor the surface properties by undergoing externally stimulated conformational changes. This is particularly true for polyelectrolyte polymers such as poly(acrylic acid) (PAA) whose degree of ionization is highly influenced by pH, ionic strength, and the presence of multivalent species.[7,8] Various polymer conformations including pancake and brushes are possible with end-tethered polyelectrolytes by varying surface density and the media.[9] The control of conformational properties have allowed for advances in areas such as surface friction

modulation, switchable wettability, autophobicity,[10-12] antifouling[13-16] and lubricity,[6,17-21] to name but a few.

Surface-bound polymers of well-defined discrete degrees of polymerization and high surface homogeneity are desired for ensuring control of surface properties and reversible surface response with external stimuli such as temperature, pH and ionic strength. These polymers can be obtained by controlled polymerization with an ATRP initiator chemically linked to the substrate. For silica substrates, the substrate–initiator linkage ($Si_{substrate}$-O-$Si_{initiator}$ bond) is generally robust enough for both sustaining the reaction conditions required for ATRP and subsequent polymer brush formation and characterization. We recently showed that PAA brushes built on mica by anchoring polystyrene-polyacrylic acid (PS-b-PAA) diblock copolymers in a polystyrene monolayer covalently attached to OH-activated mica surfaces resist to cleavage at pH 5.5 with added salt for several days.[22] However, there is still uncertainty regarding the robustness of the substrate-polymer bond and whether it is resistant to the extreme pH and ionic strengths that are required for conformational analyses of polyelectrolyte brushes. It is unknown whether these extreme conditions hydrolyze the Si-O-Si bond and cleave the polymer from the substrate leading to undesired decrease in polymer grafting density, similar to what was reported for poly(methacrylic acid) brushes and PAA brushes grafted from mica.[23-25]

Knowing the conditions under which undesired polymer cleavage occurs is pivotal for accurate surface-property studies. They are also important for controlling reversible polymer conformational changes, while preventing polymer degrafting. Although we previously provided indirect evidence for polymer cleavage from mica at high pH and salt concentrations,[26] determining the exact conditions under which PAA cleavage occurred was not possible. Also, unequivocal evidence for polymer degrafting from silica substrates has not yet been demonstrated. Therefore, direct evidence for polymer degrafting and the conditions under which it occurs on glass substrates is of importance for accurate structure-property studies.

Motivated by the need to unequivocally confirm polymer cleavage from silica substrates and to determine the exact pH and ionic conditions at which the undesired cleavage occurs, we explored a number of techniques to follow this process, including AFM and ellipsometry. On the one hand, AFM is a sensitive method for accurate step-height measurements for micron-sized areas, the low scan rate and limited sample area however preclude the analyses of multiple samples for accurately assessing the degrafting conditions in solution. It is also a static analytical tool requiring the samples to be equilibrated in the given solution prior to analyses. Therefore, detecting the real-time degrafting in solution is not possible. On the other hand, rapid surface analyses over larger areas are possible by ellipsometry. However, direct quantitative measurements in solution under various conditions are problematic owing to local variations in refractive indices with changes in pH and salt concentration.

Total Internal Reflection Fluorescence (TIRF) microscopy is an ideal method for studying the degrafting of covalently linked polymer brushes from silica surfaces and it is a suitable alternative to AFM and ellipsometry. The evanescent field achieved in total internal reflection enables selective excitation of the region in close proximity (tens to hundreds of nanometers) to the surface resulting in strong signals with low background emission.[27, 28] Labeling of the otherwise non-emissive PAA would make it compatible with TIRF microscopy usage while providing the sensitivity required for detecting the sub-ng polymer quantities grafted on the substrate. An additional advantage of TIRF microscopy is that multiple samples of various medium conditions can be tested on a single silica substrate, therefore minimizing the variability in grafting density, surface roughness, and other inherent inconsistencies between different substrates. By far, the main advantage of this technique is that solutions of desired pH and salt concentration can be flowed directly over the substrate during the fluorescence measurements (Figure 3-1). Therefore, the pH and ionic strengths required for polymer degrafting can be directly obtained in

real-time by monitoring the fluorescence decrease as a function of the media being flowed over the substrate.

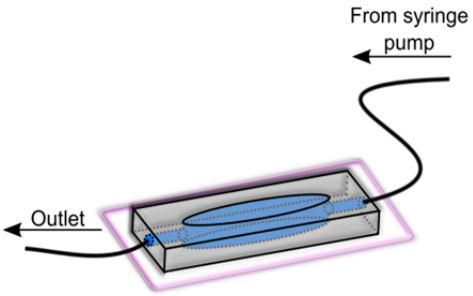

Figure 3-1. Flow-through chamber of a silicon elastomer mounted on the glass coverslip bearing the PMOH-PAA.

Although, TIRF microscopy is well suited for studying the degrafting of PAA from silica substrates in real-time and is advantageous relative to other techniques, the polymer must be fluorescent. As a result, we herein report the preparation of a fluorescently tagged PAA and the use of TIRF microscopy for unequivocally confirming polymer degrafting from glass substrates. The pH and salt conditions required to promote polymer cleavage from the substrate are presented.

3.3 Experimental section

3.3.1 Materials

Chemicals were used as received from Aldrich unless otherwise stated. Copper bromide (CuBr) was purified as previously reported.[29] *Tert*-butyl acrylate (*t*BA) and styrene were purified by passing through a column of basic alumina, followed by vacuum distillation immediately prior to use. 8-Acetoxymethyl-2,6-diethyl-1,3,5,7-tetramethyl pyrromethenefluoroborate (PM 605) was purchased from Exciton, Inc (Dayton, OH). MilliQ water was taken from a Millipore grade A 10 purification system. Silicon wafers were obtained from University Wafer Co. All

glassware was oven-dried at 120^{o} C overnight. Glass coverslips (Fisherbrand No. 1) for TIRF microscopy experiments were purchased from Fisher Scientific.

8-Hydroxymethyl-2,6-diethyl-1,3,5,7-tetramethylpyrromethene fluoroborate (PMOH). PMOH was prepared from its commercially available ester (PM 605) following previously reported methods.[30-33]

3.3.2 Substrate preparation and initiator immobilization

Glass slides (22 x 22 mm^2) were cut in half using a diamond pencil. The glass substrates were treated with a Piranha solution (H_2SO_4/H_2O_2 70:30 v/v) for 15 min for removing organic residues and for silanol activation. The activated surfaces were then rinsed with water and ethanol and dried under a gentle stream of nitrogen. The initiator, 3-(chlorodimethylsilyl)propyl-2-bromoisobutyrate synthesized according to known means,[29] was dissolved in anhydrous toluene (1 mM).[29] Functionalization of one side of the substrate was done by covering the top side of the slide with a drop of the initiator solution. The solution was allowed to react for 15 minutes at room temperature after which the slides were sequentially washed with toluene, absolute ethanol, and MilliQ water. They were dried with nitrogen and used immediately for surface-initiated polymerization.

Silicon wafers were cut to 12 x 22 mm^2 pieces and treated with Piranha solution for 15 min. The substrates were then washed thoroughly with MilliQ water and absolute ethanol, dried under nitrogen and placed in a compartmentalized reactor containing the initiator (1 mM) that was dissolved in anhydrous toluene.[29] After 17 h, the substrates were removed from the reactor, rinsed with toluene, absolute ethanol, MilliQ water, and then dried under nitrogen. The substrates were stored in a vacuum dessicator until used.

3.3.3 Surface-initiated polymerization of *tert*-butyl acrylate (*t*BA) with added free initiator

Polymerization of the *t*BA on the initiator-functionalized glass substrates was carried out as previously reported.[34] Residual physisorbed polymers on the glass slides were removed by Soxhlet extraction with THF for 8 h. The slides were stored in a dessicator until used. The resulting polymerization solution was diluted with acetone and passed through a column of neutral alumina for removing the copper salts. The polymer solution was then concentrated in vacuo, and the molecular weight was determined by GPC with the appropriate concentration in THF.

3.3.4 Surface-initiated polymerization of styrene with added free initiator

Freshly distilled styrene and acetone were deoxygenated under argon for 1 h. CuBr (30 mg, $2x10^{-4}$ mol) was placed into a 50 mL double-necked round bottomed flask. The flask was degassed under vacuum at room temperature and backfilled with argon three times. Deoxygenated styrene (9.2 mL, $8x10^{-2}$ mol), deoxygenated acetone (4.6 mL), and hexamethyltriethylenetetramine (HMTETA) (100 μL, $4x10^{-4}$ mol) were added to CuBr, and the mixture was stirred at room temperature under argon until a homogeneous green solution was obtained. A clean initiator functionalized glass slide was placed in a flame-dried Schlenk flask, which was deoxygenated under vacuum and backfilled with argon three times. The above-described polymerization solution was transferred into the reaction flask followed by injection of ethyl-2-bromoisobutyrate as the free initiator (30 μL, $2x10^{-4}$ mol). The flask was heated at 65 ^{0}C for 48 h with stirring. The Schlenk flask was then placed in a cold bath and the solution was diluted with acetone. The surface was removed and cleaned thoroughly with THF, acetone and absolute ethanol and dried under stream

of nitrogen. A Soxhlet extraction in THF was used for 8 h for removing any physisorbed polymer. The bulk reaction mixture was passed through a column of neutral alumina to remove the catalyst. The solvent was then evaporated and the polymer molecular weight was determined by GPC.

3.3.5 Hydrolysis of surface grafted poly(*tert*-butyl acrylate) (P*t*BA) to PAA

tert-Butyl ester cleavage was done by treating the P*t*BA–grafted glass slides with trifluoroacetic acid (dichloromethane/TFA 10:1 v/v) at room temperature with stirring overnight. The glass substrates were then washed repeatedly with absolute ethanol and MilliQ water, and then dried under a nitrogen stream.

3.3.6 Coupling of PMOH to PAA

PMOH (20 mg), 1-ethyl-3-(3-dimethylaminopropyl)carbodiimide hydrochloride (EDCI; 60 mg) and 4-(dimethylamino)pyridine (DMAP; 60 mg) were dissolved in anhydrous dichloromethane (20 ml) in a 100 mL double neck round-bottom flask. PAA-functionalized glass substrates were placed in a compartmentalized reactor equipped with stir bar. The above-prepared solution was transferred to the reactor by cannula and the mixture was then stirred at room temperature for 4 h under argon. The slides were removed from the reaction mixture, washed sequentially with dichloromethane, acetone, absolute ethanol, MilliQ water and then dried under a nitrogen stream. The physisorbed PMOH was removed by Soxhlet extraction with dichloromethane for 8 h. The fluorophore containing slides were analyzed by UV-Vis absorption and fluorescence.

3.3.7 Degrafting of PAA

Trizma base buffer solution (0.1 M) was prepared with MilliQ water and the pH was adjusted to 6.5, 7.5, 8.5, 9.5 and 10.5 with different volumes of HCl (0.1 M). The pH was measured with a Symphony SB20 pH meter with Ag/AgCl electrode. The ionic strength was varied by adding NaCl (10 mM) to the Trizma buffer solution. The buffer solution of the given pH was flowed over the polymer-substrates during imaging.

3.3.8 Surface characterization

Contact angle measurements

Measurements were carried out using an FTA200 dynamic contact angle analyzer (First Ten Angstrom) in the equilibrium static mode, using MilliQ water as the probe liquid. Data analyses were performed using Fta32 Video software and three separate measurements were done for each glass substrate. The average contact angle value was determined within an experimental precision of ± 3°. The empirical Cassie-Baxter equation and modified related equations[35,35] were used to evaluate the relative surface density (or surface coverage) of grafted molecules on the glass surface. These equations correlate the equilibrium contact angle (θ_{obs}) of a chemically heterogeneous surface to the surface coverage of the different molecules on the surface and predict an increase in water contact angle with an increase in surface coverage of small hydrophobic molecules:

$$\left[1+\cos\left(\theta_{obs}\right)\right]^2 = f_1\left[1+\cos\left(\theta_1\right)\right]^2 + f_2\left[1+\cos\left(\theta_2\right)\right]^2$$

$$f_1 + f_2 = 1 \qquad (3.1)$$

The water contact angle of a surface covered with a maximum number of hydrophobic molecules, $f_1 = 1$, is presumed to be $\theta_1 = 90$, and the water contact angle of uncovered glass surface, $f_2 = 1$, is $\theta_2 = 0$.

AFM measurements

The dry thickness of all samples was measured before and after TIRF measurements at room temperature (Figure 3-S4). The samples were left in MilliQ water at least 2 h, rinsed with absolute ethanol, dried with nitrogen and the step-height measured by AFM film. The AFM was equipped with a NanoScopeV extended controller and a MultiMode microscope (Digital Instruments, Santa Barbara, CA). All AFM images were collected in the tapping mode using an Arrow-NCR silicon probe with a spring constant of 42 N/m and a resonance frequency of 300 KHz (Nanoworld). Data analyses were performed using the NanoScope 7.30 software. A scalpel was used to scratch and expose the bare slide and step-height between the native glass and the PAA layer was measured in the dry state by an AFM cross sectional height image. The thickness of each sample was measured at three different regions.

Ellipsometry measurements

Experiments were conducted using an Ellipsometer M-2000V from J.A. Woollam Co. in air at an incident angle of 75° and a wavelength range of 370–1000 nm. Four independent measurements at different areas were done for each sample.

Ensemble characterization

The absorption measurements were done on a Cary-500 spectrometer and the fluorescence studies were performed on an Edinburgh Instruments FLS-920 fluorimeter by exciting at 520 nm. Fluorescence experiments in micelles were performed on a PTI Quantamaster 40 equipped with a Quantum Northwest TC 425 temperature controller (at 20°C) by exciting at 500 nm.

TIRF microscopy

The PMOH-functionalized surface-grafted polymers were imaged using a wide-field objective-based total internal reflection (TIRF) microscopy set-up consisting of an inverted microscope (IX71, Olympus) equipped with a laser-based TIRF illumination module (IX2-RFAEVA-2, Olympus).[36,37] Laser excitation was provided by a 25 mW, 532 nm output, diode-pumped cw laser (CL532-025-S, CrystaLaser), attenuated with metallic ND filters and providing 2 – 7 μW output at the objective. The excitation beam was directed to the sample by reflection on a dichroic beamsplitter (z532rdc) and focused on the back focal plane of a high numerical aperture (N.A. = 1.45) oil-immersion objective (Olympus PLAN APO 60X). Images were additionally magnified two-fold via an internal lens and a relay lens system and then captured on a back illuminated electron multiplying charge-coupled device (EMCCD) camera (Cascade II:512B, Roper Scientific) using gains between 3700 and 4095 and frame exposure times of 0.6 s to 1.5 s. Laser and camera settings were adjusted for each sample in order to obtain initial fluorescence intensities of ca. 120 A.U., while minimizing laser-induced photobleaching. The original 66 x 66 μm^2 TIRF images were cropped to half of the size, corresponding to the reflected channel from a 640dcxr dichroic mirror (< 640 nm) in a two color emission setup. To further minimize photobleaching in areas of interest (AOI), images were focused on a subsection of the sample area (round dark regions near

middle of images) using an iris positioned in the excitation laser beampath. Image acquisition was started with this iris closed, which was then fully opened during the acquisition. Each image was acquired after repositioning the sample in a new, non illuminated region to minimize photobleaching of the AOI.

TIRF image analysis

From the captured movies, the first complete frame in which the iris is fully opened was selected from the others and then further analysed with the Image Pro 5.1 software. The image analyses consisted of first selecting an AOI to ignore the photobleached focus point as well as consistently darker edges. A histogram of individual pixel intensities was constructed for all of the pixels contained in the AOI (ca. 70 000 pixels, corresponding to a sample area of ca. 1200 μm^2). The histograms were then fitted to a Gaussian function in order to extract the center of the fluorescence intensity distribution. When multiple images were taken within 5 minutes of each other, only the averaged center of the distribution was reported and the errors bars corresponding to the standard deviation were added.

TIRF sample chamber

Polymer-functionalized glass coverslips were typically washed with dichloromethane and ethanol prior to use. Flow chambers were assembled by depositing a homemade silicone gasket on the glass substrate. These gaskets were designed to have a narrow chamber with an inlet and an outlet holes for inserting the flow tubing. Chambers were fabricated using SYLGARD® 184 Silicone Elastomer Kit (Dow Corning Corporation). The undersized glass substrates (ca. 12 mm x 22 mm) were then affixed to flat metal plates, which served as the sample holder. The chambers were closed by pressing a clean, blank coverslip on top of the gasket. The sample chambers had internal volumes of ~ 50 µL. Solutions of known pH and NaCl concentration were continuously flowed at a rate of 1 μL/min over the substrate using

a syringe pump system for periods of 2 h or more. One freshly prepared PAA-PMOH covered glass slide for each buffer solution at a given pH and ionic strength was analyzed.

3.4 Results and discussion

3.4.1 Fluorescent Monomer Synthesis

PMOH (Scheme 3-1) was prepared according to known means.[32] This was the chosen fluorophore because its spectroscopic properties are well known and its alcohol derivative could be coupled to the immobilized PAA density of P*t*BA according to standard coupling protocols. This would provide the required fluorescent polymer for TIFR measurements.[23,38] The advantage of PMOH over other dyes is that it has a strong absorption extinction coefficient, narrow fluorescence emission, high emission quantum yield, and photochemical stability.[23,39-41] These properties make it possible to detect the sub-ng quantities of the polymer immobilized on the glass substrates (Figure 3-S1 and 3-S2).

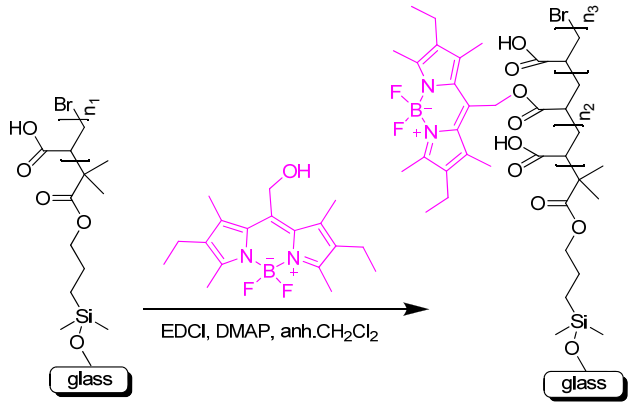

Scheme 3-1. Schematic representation of PMOH coupling to immobilized PAA to provide the fluorescent polymer, PAA-PMOH.

3.4.2 Fluorescent Polymer Synthesis

Immobilization of a uniform initiator layer was carried out on only one side of the spectroscopically transparent silica surface, specifically the one in contact with the aqueous solutions. This is necessary to avoid background fluorescence from the layer not in contact with the flow solution. Contact angle measurements were done for confirming initiator grafting to the substrate. The measured contact angle of θ_{water}= 72^o (Table 3-1) is in agreement with our previous results[29,34] and confirms that the initiator is coupled to the substrate in comparison to Piranha-solution treated native glass slides whose contact angle is 0^o. The equilibrium contact angle of a chemically heterogeneous surface can be related to the fraction of the initiator groups in terms of the phenomenological modified Cassie-Baxter equation (Eq. 3-1). According to this equation, a contact angle of 72^o corresponds to a surface coverage value of 76% (Table 1). The surface density of end-grafted polymers synthesized using the *graft from* method inherently depends on the initiator grafting density.

Controlled surface polymerization was subsequently done with the failsafe ATRP of *t*BA using ethyl-2-bromoisobutyrate as free initiator. Following polymerization at 60^{o}C for 15 hours, the water contact angle measured was 83^o (Table 3-1). Controlled polymerization was confirmed by the linear increase of both the polymer layer thickness and the average molecular weight of free-polymer in solution. The trend provides indirect evidence that polymer degrafting does not occur under the polymerization conditions, otherwise both variable film thickness and variable molecular weight of the free-polymer in solution would be observed. The molecular weight of the free polymer, relative to polystyrene standards, was determined by GPC. The grafting density σ of the P*t*BA layer was calculated from the dry polymer thickness d ($\sigma = d\rho N_A/M_n$ where ρ is the density of P*t*BA (1.047 g.cm^{-3})), N_A is the Avogadro's number and M_n is the number average molecular weight of the grafted polymer chains which is assumed to be similar to that of the free polymer in solution (60 326 g/mol). We use this assumption because it was not

possible to determine the molecular weight of the very small amount of generated grafted chains. It has been shown that the molecular weight of the grafted polymer grown by ATRP can be similar to or slightly smaller than the molecular weight of free polymer in solution.[42,43] High grafting density of 0.41 chain/nm^2 was found (Table 1). The distance between two adjacent grafted end-groups can be estimated as $s = 1/\sigma^{1/2}$ = 1.56 nm and compared to the characteristic size of the chains in order to evaluate the conformation of the chains. As the polymer layer is in a dry state, we assumed that the grafted chains adopt a collapsed state with a characteristic dimension R = 1.95 nm ($R \approx aN^{0.33}$, where a is a characteristic dimension of repeating unit, 0.25 nm)[44] and N is the average number of repeating units of the P*t*BA chains which is assumed to be the same as that of the free polymer chains in solution, i.e., 471. Pancake and mushroom conformations are specific to polymer chains tethered at low grafting density (or $s > R$) while the brush conformation prevails at high grafting density (or $s << R$).[45] Our results (R is slightly larger than s) suggest that the grafted chains adopt a conformation at the frontier between the brush and mushroom conformations.

Table 3- 1. Surface properties of initiator-functionalized and PAA-functionalized silica substrates

Initiator layer		Polymer layer					
		P*t*BA				PAA	
θ_{water} (±2°)	f_1	θ_{water} (±2°)	dry thickness (±2nm)*	Mn (g·mol^{-1})	σ** (chain/nm^2)	θ_{water} (±2°)	dry thickness (±4nm)*
72	76	80	40	60 326	0.41	35	14

*The thickness was measured by AFM step height method

** $\sigma = (d\rho N_A)/M_n$ where d is the dry layer thickness, ρ is the density of P*t*BA (1.047 g/cm^{-3}), N_A is the Avogadro's number, and Mn is the number average molecular weight of the grafted polymer chains and it is similar to the Mn of the free polymer.

An underestimation of molecular weight for the attached polymer chains would result in a smaller polymer grafting density σ for a given polymer layer thickness *d*, or a larger distance between grafted chains *s*, and therefore, the chains would adopt a mushroom conformation. However, in a good solvent or when ionized, the collapsed grafted chains are expected to stretch into a brush conformation for a given grafting density and chain length.[45,46]

Removal of the *tert*-butyl deprotecting group was carried out by refluxing the polymer-immobilized glass substrates in trifluoroacetic acid/dichloromethane,[47] resulting in a decrease in the water contact angle to θ_{water}=35°. PMOH was subsequently coupled to PAA with EDCI to afford the fluorescent polymer, PAA-PMOH (Scheme 3-1). Covalent coupling of PMOH to the immobilized PAA was spectroscopically confirmed by the characteristic absorbance and fluorescence of the PMOH ester, which peaked at 550 and 564 nm, respectively (Figure 3-2). The surfaces were then washed via Soxhlet extraction in dichloromethane for 8 hours in order to remove any potentially physisorbed PMOH. Neither the absorbance nor fluorescence intensity changed after Soxhlet extraction, confirming covalent attachment of the PMOH to the polymer and covalent attachment of the polymer to the silica substrate.

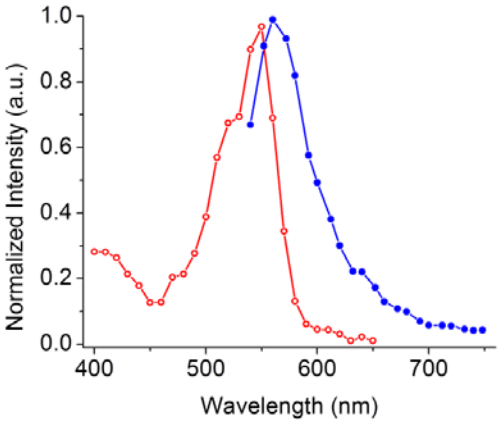

Figure 3-2. Normalized absorption (○) and emission (●) spectra (λ_{ex}=520 nm) of immobilized PAA-PMOH on silica slides.

PMOH was grafted to the immobilized PAA layer in low amounts in order to ensure fluorimetric visualization of the polymer layer while minimizing polymer insensitivity towards both variations in pH and salt concentration arising from fluorophore tagging on every repeat unit. Also of note is the direct polymerization of AA-PMOH by ATRP on initiator-covered silica substrate that was attempted according to standard methods.[48] Unfortunately, no polymer could be detected either in solution or on the surface. Subsequently, direct polymerization of AA (acrylic acid) using modified ATRP protocols was pursued. Although AA could be polymerized from the surface in water, the control of film thickness is relatively difficult to obtain because of fast polymerization kinetics[49] and hydrolytic side reactions occurring in aqueous media.[24] Indeed, the variable polymer thickness (between 10 and 120 nm), despite consistent polymerization conditions, confirms that the surface polymerization of AA is not controlled and that PAA is most likely cleaved from the substrate under the ATRP polymerization conditions of high pH (pH > 8) and salt concentration required for AA (vide infra).

3.4.3 TIRF Microscopy Degrafting Studies

Fluorescence from the PMOH-PAA immobilized on glass substrates was observed when immersing the substrates in aqueous solutions of increasing pH when excited with the TIRF system. The laser power transmitted through the objective was attenuated to 2-7 μW for minimizing any PMOH photobleaching during the experiments. The top surface, to which was grafted the PMOH-PAA, was adapted with a ca. 50 μL volume flow chamber for both exposing the polymer layer to a constant flow of desired solution and washing away any degrafted polymer (Figure 3-1).

Figure 3-3 displays typical fluorescence images of a 66 x 33 μm^2 region obtained at close to neutral pH (pH = 6.5, top left panel A) and high pH (pH =10.5,

top right panel B). The images were obtained shortly after initial exposure and following long exposure to the NaCl-free buffer solution. Images with smooth intensity profiles were observed, confirming the homogeneous distribution of the PMOH-PAA layer across the slide. Intensity variations of ca. 10% were observed for a given sample as a result of different regions being monitored (see for example Figure 3-3E, pH 6.5 or 7.5) and variations in the laser power. The intensity of a sub-region (delimited by the rectangle and square in Figure 3-3 A and B) was further analyzed to indirectly quantify surface density of the immobilized polymer over time. The histogram of the intensity per pixel was obtained for a given pH with increasing exposure times to the solution (Figure 3-3 C and D). New regions in the same substrate were then imaged at each time delay for minimizing PMOH photobleaching followed by plotting the intensity/pixel value at the center of the Gaussian-fitted histogram vs. time (bottom panel E, Figure 3-3). It is obvious from the statistically analyzed data graphically summarized in Figure 3-3E that no polymer degrafting occurs regardless of pH at low ionic strength.

Polymer degrafting at a high ionic strength was next investigated as a function of time and pH (Figure 3-4) with a NaCl concentration of 10 mM. Although the monovalent salt was not expected to directly promote polymer cleavage,[25,50] it however can increase the degree of dissociation of PAA leading to polymer backbone extension with increasing density of negative charges.[51,51] The expected extended conformation in turn exposes the substrate–initiator bond to hydroxyl ions, which potentially promotes degrafting. However, the exact location (within the initiator) where bond rupture occurs is unknown because the C-O, Si-O, Si-C bonds are all potentially labile and susceptible to hydrolysis. Our results further suggest that the substrate–initiator bond is protected against hydrolysis at low ionic strength most probably because of the collapsed conformation of polymer segments close to the surface. However, at extreme pH with added salt, the end-grafted chains are ionized resulting in an extended brush conformation that exposes the substrate–initiator bond making it more susceptible to hydrolysis by hydroxyl ions.

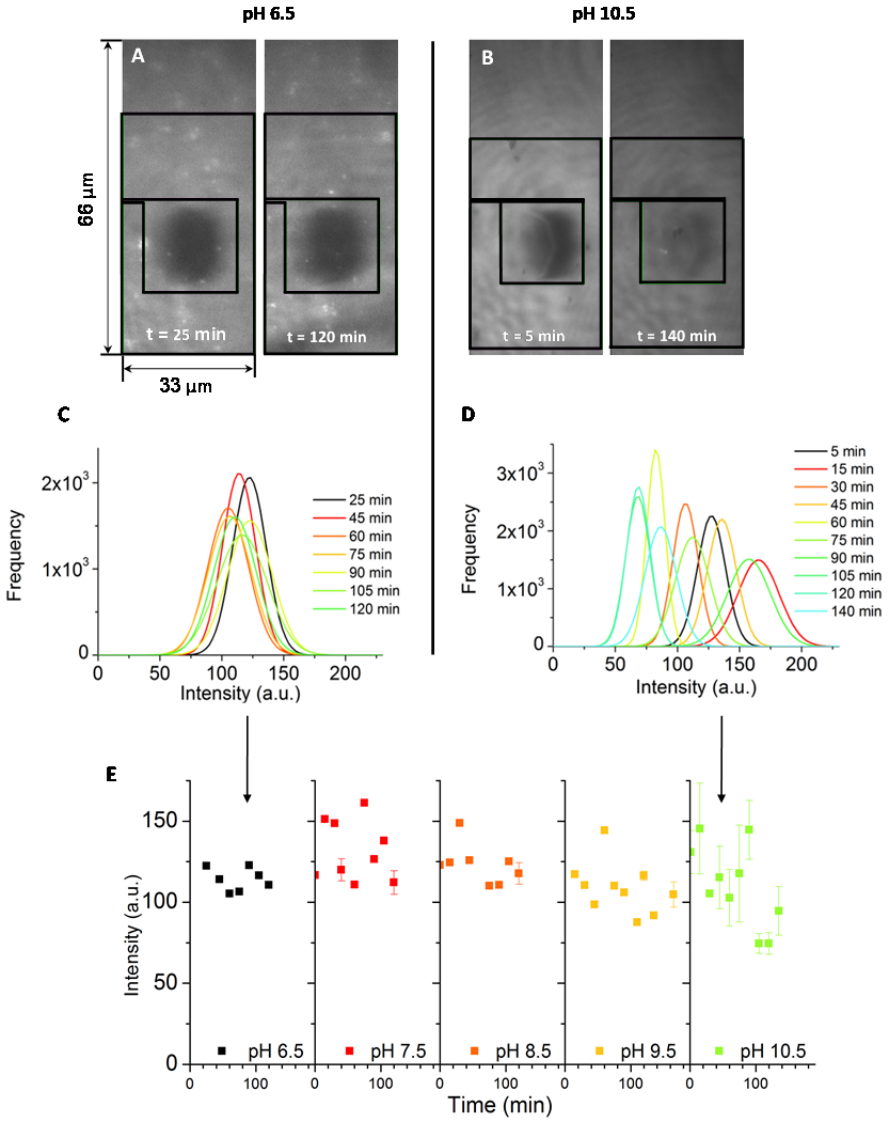

Figure 3-3. Time-dependent PMOH-PAA fluorescence as a function of pH with no added NaCl. **A** and **B**: TIRF images of substrates after flowing at low (**A**) and high pH (**B**) NaCl-free solutions for increasing amounts of time. **C** and **D**: Time evolution of Gaussian-fitted individual pixel fluorescence intensity distributions when flowing at low (**C**) and high pH (**D**) NaCl-free solutions. **E**: Center of Gaussian-fitted pixel fluorescence intensity distributions versus time for all the salt-free solutions studied. The analyzed area is delimited by the square and rectangle on the corresponding picture.

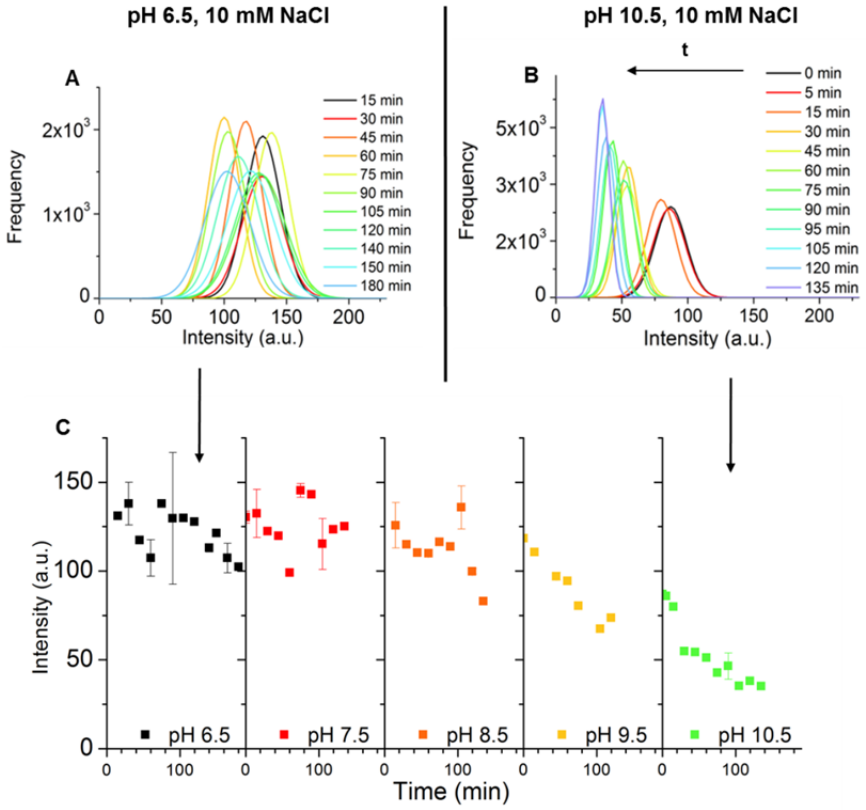

Figure 3-4. Time and pH dependence of PMOH-PAA degrafting at 10 mM NaCl. **A** and **B**: Time evolution of Gaussian-fitted individual pixel fluorescence intensity distributions when flowing at low (**A**) and high pH (**B**) with 10 mM NaCl. **C**: Center of Gaussian-fitted pixel fluorescence-intensity distributions versus time for all solutions studied at 10 mM NaCl.

AFM step-height cross-sectional measurements (Figures 3-5 and 3-S4) were done before and after the TIRF measurements to ensure that the disappearance of the fluorescence signal was due to polymer cleavage and not from either fluorophore cleavage from the polymer or fluorophore quenching processes. The step-height analysis revealed a drastic change in polymer film thickness for the substrates exposed to 10 mM NaCl at pH 10.5 (Figure 3-5 C and D). This is in contrast to the polymer thickness that remained unchanged before and after exposing to pH 10.5

without added salt (Figure 3-5 A and B). The height difference between the bare substrate and the polymer layer can quantitatively be determined from the AFM step-height measurements.

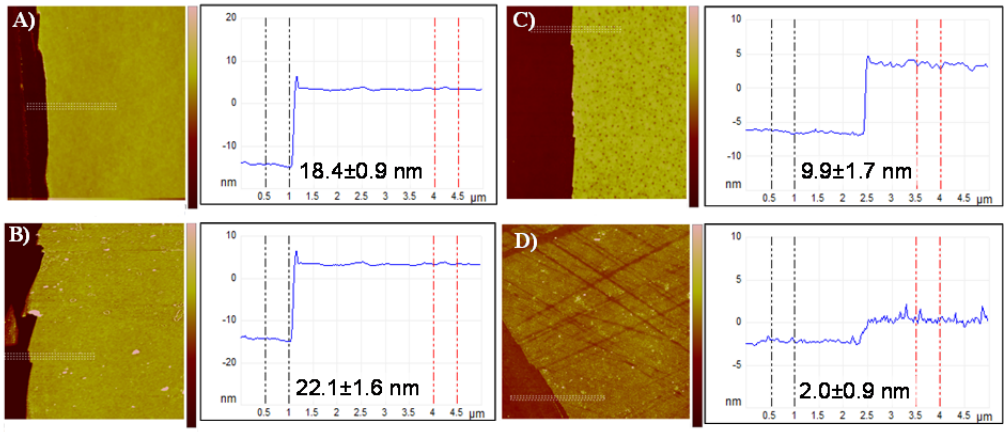

Figure 3-5. AFM images (10x10 µm) in the dry state showing the step-height difference between the bare glass and the polymer layer: A) before and B) after exposing the substrate to buffer solution at pH 10.5 and C) before and D) after exposing the substrate to buffer solution at pH 10.5 with added salt. The dashed rectangles (0.3 x 5 µm) refer to the step-height analyzed areas.

The degrafting ratio, defined as the ratio between the polymer layer thickness after and before exposure to buffer solution, is ca. 0.2 for the substrate exposed to pH 10.5 with added salt. This suggests that more than 80% of the polymer is cleaved from the substrate. Similarly, 40% of the polymer is degrafted from the substrate exposed to pH 9.5 with added salt (Figure 3-6). Conversely, no polymer degrafting was observed by AFM for the substrate exposed to pH 9.5 without salt. The AFM results corroborate the TIRF measurements in that polymer degrafting occurs only in the presence of salt at pH ≥9.5.

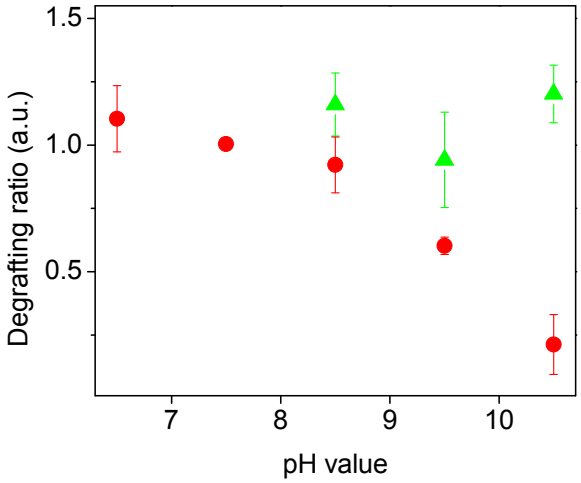

Figure 3-6. The average PMOH-PAA polymer degrafting ratio taken as the ratio between the polymer layer thickness after and before exposing the substrates to different pH without (▲) and with (●) added salt. Three different ratios were obtained for each substrate and the standard deviation was used as the error bar.

Further confirmation that the observed change in fluorescence intensity arises from polymer degrafting rather than hydrolysis of the PMOH-PAA bond was obtained by studying the fluorescence of a PMOH-PAA model system, PM605, in micelles. The hydrolysis of PM605 to PMOH (inset top Figure 3-7) would give rise to a hypsochromic shift in the fluorescence emission (right panel Figure 3-7).[30-32,39,52,53]. No change in either the emission spectrum shape or intensity was observed upon incubating PM605 for extended periods of time in solutions of pH and ionic strength similar to those used for the TIRF microscopy studies. Only a slight fluorescence increase was observed at 564 nm at the onset of the measurement because of PM605 diffusing into the micelles. In contrast, hydrolysis of PM605 would result in a decrease in intensity at 564 nm. The steady-state emission intensity vs. time analyses of PM605 in SDS micelles confirm that ester hydrolysis or bleaching of the dye do not occur. The results further confirm that the fluorescence

decrease observed in TIRF microscopy is a result of PAA degrafting from the substrate and not from PMOH hydrolysis.

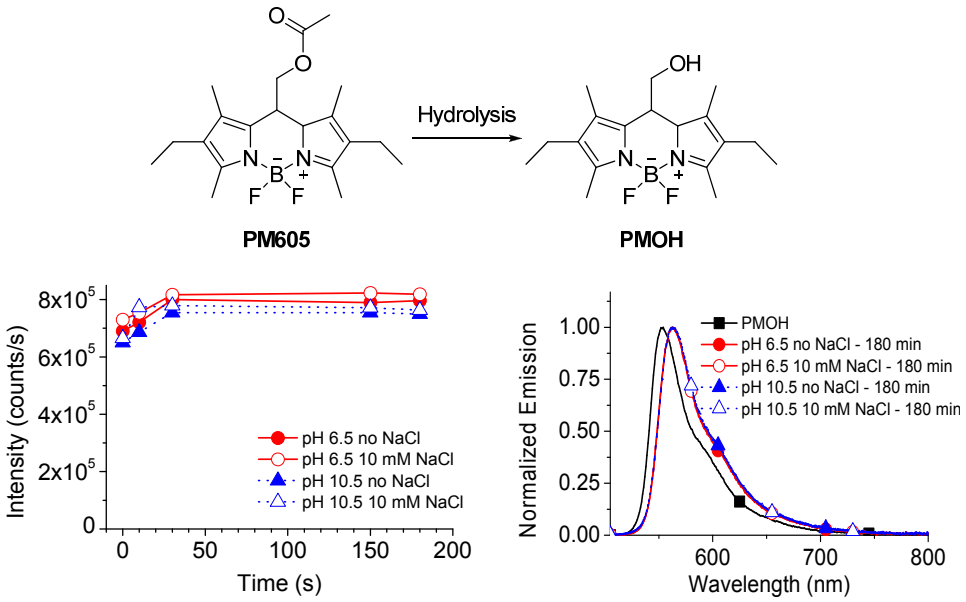

Figure 3-7. Fluorescence emission spectra of PM605 and PMOH in sodium dodecyl sulfate (SDS, 10 mM) micelles and Trisma (0.1 M) buffer solution. Left: Fluorescence intensity acquired at the emission maximum of PM605 following various incubation periods in aerated solutions at pH 6.5, at 0 and 10 mM NaCl (red, closed and open circles, respectively), and pH 10.5 at 0 and 10 mM NaCl (blue, closed and open triangles, respectively). Right: Normalized steady-state fluorescence spectra at various pH and NaCl concentrations after incubation for 180 minutes. The spectra of PMOH, (which is blue-shifted with respect to PM605), is shown for comparison illustrating that no ester hydrolysis and formation of PMOH occurs during this time period. Excitation was performed at 500 nm in all experiments.

A rough estimate of the degrafting rate can be estimated from the time-dependent fluorescence change in Figure 3-4E. The degrafting rate for pH 9.5 and 10.5 with added NaCl is approximately the same. The lack of sensitivity of the degrafting rate to [OH^-] and the sudden onset of degrafting can be interpreted by a change in polymer conformation when the pH is increased close to 9.5 at high ionic

strengths. Although, the [OH^-] is expected to be sufficient to induce polymer degrafting at pH < 9.5, the polymer conformation is tightly collapsed at low ionic strength and protects the labile substrate-initiator bond. A combination of high pH and high ionic strength are thus needed to induce the conformation change of grafted PAA. These results are in good agreement with our previous study showing conformation change of PAA brushes with pH and salt.[23]

In order to protect the labile substrate-initiator bond at the polymer/substrate interface from undesired hydrolysis, a hydrophobic layer can be inserted between the substrate and the PAA as similarly done with a PS-b-PAA copolymer grafted to mica.[22] The presence of the innermost hydrophobic layer directly bond to mica is expected to act as a protective layer against hydrolysis of the substrate-initiator bond by preventing water and hydrated ions from reaching the substrate. Therefore, we have grafted a polystyrene layer directly from the glass substrate using the immobilized ATRP initiator. The thickness of the grafted polystyrene layer measured by ellipsometry was 10 nm. The substrate was then exposed to pH 10.5 solution for 2.5 hours and then cleaned. No change in the polymer film thickness was observed by ellipsometry regardless of ionic strength, confirming that the polystyrene layer can provide a robust layer or spacer protecting the labile substrate-initiator bond against hydrolysis. As the PS chains contain a terminal bromine, they allow for subsequent polymerization of AA by ATRP block copolymerization. This is actively being pursued.

3.5 Conclusion

Degrafting of covalently immobilized fluorescent PAA from glass substrates was unequivocally confirmed in solution via TIRF microscopy. The real-time fluorescence measurements confirm that the substrate–initiator bond is labile and can be cleaved. Cleavage of the covalently bound polymer only occurred at pH ≥ 9.5 in

the presence of salt. The combination of high pH and added salt most probably induces a conformational change of the polymer layer, allowing hydrolysis of the substrate-initiator bond at the polymer/glass interface. Although the exact salt and pH induced conformation change is unknown, the hydroxyl ions nonetheless penetrate through the PAA layer to the substrate and hydrolyze the glass–initiator bond. The absence of polymer degrafting with 10 mM NaCl at pH < 9.5 suggests that the polymer adopts a compact conformation close to the surface and protects the glass–initiator bond against hydrolysis. Regardless of conformation, we provided unprecedented real-time evidence for the degrafting of PAA from glass substrates. The stability of the covalently attached hydrophobic-hydrophilic copolymer layer is currently being investigated.

3.6 Acknowledgements

This work was supported by le Fonds de recherches sur la nature et les technologies and the Natural Sciences and Engineering Research Council (NSERC) Canada. WGS thanks both the Alexander von Humboldt Foundation and the RSC for a JWT Jones Travelling Fellowship, allowing this manuscript to be completed. RG thanks NSERC for a postgraduate scholarship; KLL thanks both the Faculty of Science at McGill University and the Centre of Self-Assembled and Chemical Structures for undergraduate scholarships. The authors thank Prof. R. E. Prud'homme for access to AFM.

3.7 Supporting information

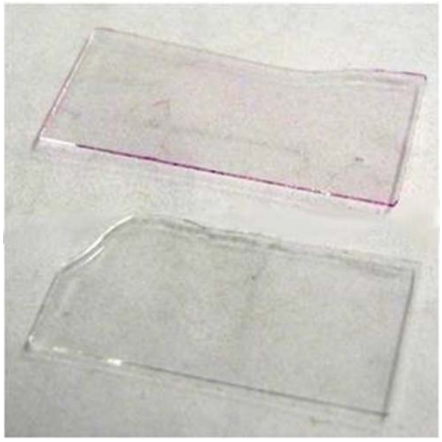

Figure 3-S1. PAA-PMOH covered glass slide (top) and blank silica (bottom) under ambient light.

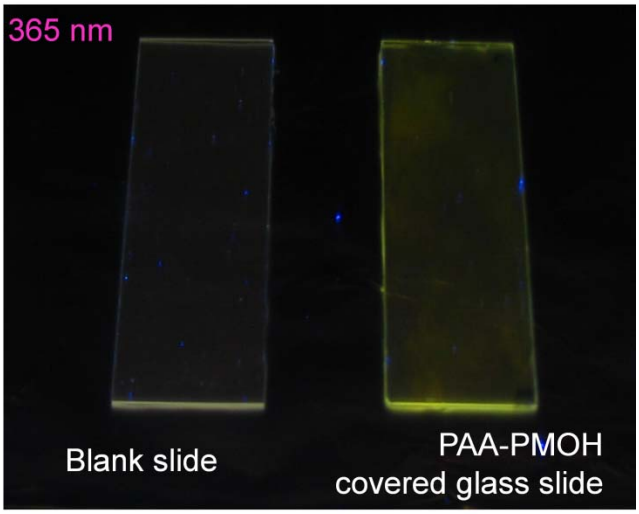

Figure 3-S2. PAA-PMOH covered glass slide (a) and blank silica (b) under UV lamp (λ=365 nm)

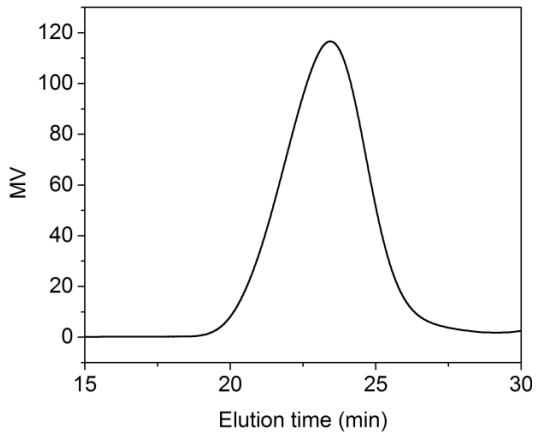

Figure 3-S3. Gel permeation chromatogram of poly(*tert*-butyl acrylate). M_n=60 326 g/mol.

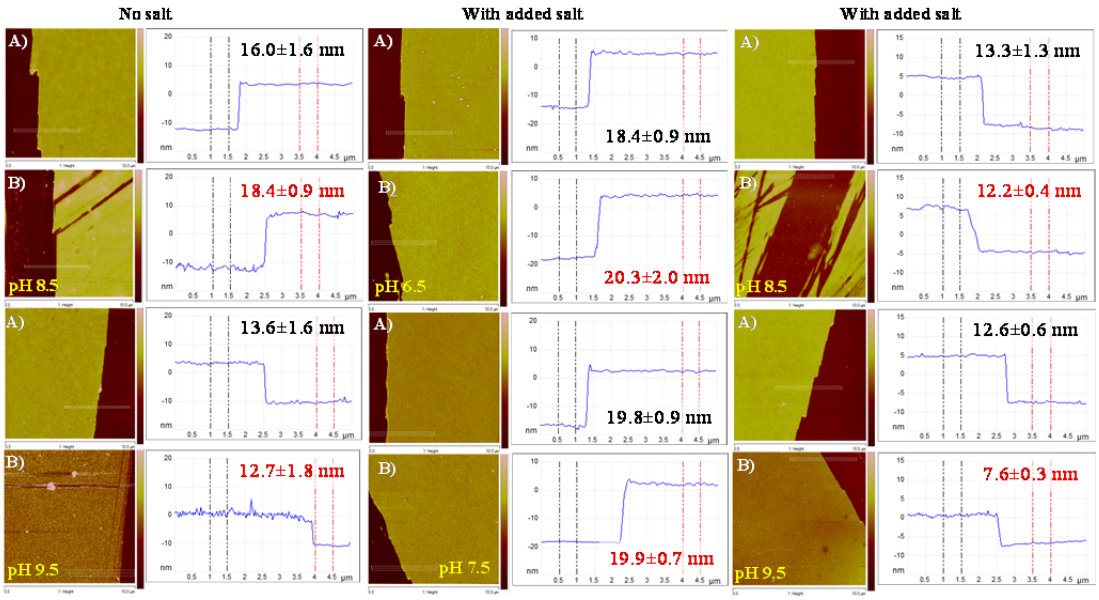

Figure 3-S4. AFM images in the dry state showing the step-height difference between the native glass and the polymer functionalized surface: A) before and B) after exposing the substrate to buffer solution at different pH.

3.8 References

(1) Jonas, A. M.; Glinel, K.; Oren, R.; Nysten, B.; Huck, W. T. S. *Macromolecules* **2007**, *40*, 4403.

(2) Aoki, H.; Kitamura, M.; Ito, S. *Macromolecules* **2008**, *41*, 285.

(3) Harris, B. P.; Kutty, J. K.; Fritz, E. W.; Webb, C. K.; Burg, K. a. J. L.; Metters, A. T. *Langmuir* **2006**, *22*, 4467.

(4) Jain, P.; Baker, G. L.; Bruening, M. L. *Annu. Rev. Anal. Chem.* **2009**, *2*, 387.

(5) Wischerhoff, E.; Uhlig, K.; Lankenau, A.; Borner, H. G.; Laschewsky, A.; Duschl, C.; Lutz, J.-F. *Angew. Chem. Int. Ed* **2008**, *47*, 5666.

(6) Raviv, U.; Giasson, S.; Kampf, N.; Gohy, J.-F.; Jérôme, R.; Klein, J. *Nature* **2003**, *425*, 163.

(7) Gong, P.; Wu, T.; Genzer, J.; Szleifer, I. *Macromolecules* **2007**, *40*, 8765.

(8) Wu, T.; Gong, P.; Szleifer, I.; Vlcek, P.; Subr, V.; Genzer, J. *Macromolecules* **2007**, *40*, 8756.

(9) Liu, G.; Yan, L.; Chen, X.; Zhang, G. *Polymer* **2006**, *47*, 3157.

(10) Reiter, G.; Auroy, P.; Auvray, L. *Macromolecules* **1996**, *29*, 2150.

(11) Reiter, G.; Khanna, R. *Langmuir* **2000**, *16*, 6351.

(12) Epps, T. H.; DeLongchamp, D. M.; Fasolka, M. J.; Fischer, D. A.; Jablonski, E. L. *Langmuir* **2007**, *23*, 3355.

(13) Zdyrko, B.; Klep, V.; Li, X. W.; Kang, Q.; Minko, S.; Wen, X. J.; Luzinov, I. *Mater. Sci. Eng. C-Biomimetic Supramol. Syst.* **2009**, *29*, 680.

(14) De Giglio, E.; Cometa, S.; Cioffi, N.; Torsi, L.; Sabbatini, L. *Anal. Bioanal. Chem* **2007**, *389*, 2055.

(15) Hollmann, O.; Gutberlet, T.; Czeslik, C. *Langmuir* **2007**, *23*, 1347.

(16) Xu, F. J.; Neoh, K. G.; Kang, E. T. *Prog. Polym. Sci.* **2009**, *34*, 719.

(17) Dunlop, I. E.; Briscoe, W. H.; Titmuss, S.; Jacobs, R. M. J.; Osborne, V. L.; Edmondson, S.; Huck, W. T. S.; Klein, J. *J. Phys. Chem. B* **2009**, *113*, 3947.

(18) Zeng, H. B.; Tian, Y.; Zhao, B. X.; Tirrell, M.; Israelachvili, J. *Langmuir* **2009**, *25*, 4954.

(19) Vyas, M. K.; Nandan, B.; Schneider, K.; Stamm, M. *J. Colloid Interf. Sci.* **2008**, *328*, 58.

(20) Kobayashi, M.; Kaido, M.; Suzuki, A.; Ishihara, K.; Takahara, A. *J. Jpn. Soc. Tribol.* **2008**, *53*, 357.

(21) Drummond, C.; Rodriguez-Hernandez, J.; Lecommandoux, S.; Richetti, P. *J. Chem. Phys.* **2007**, *126*, 184906/1.

(22) Liberelle, B.; Banquy, X.; Giasson, S. *Langmuir* **2008**, *24*, 3280.

(23) Loudet, A.; Burgess, K. *Chem. Rev.* **2007**, *107*, 4891.

(24) Tugulu, S.; Barbey, R.; Harms, M.; Fricke, M.; Volkmer, D.; Rossi, A.; Klok, H.-A. *Macromolecules,* **2006**, *40*, 168.

(25) Witte, K. N.; Kim, S.; Won, Y.-Y. *J. Phys. Chem. B* **2009**, *113*, 11076.

(26) Lego, B.; Skene, W. G.; Giasson, S. *Macromolecules* **2010**, *43*, 4384.

(27) Axelrod, D. *Traffic* **2001**, *2*, 764.

(28) Axelrod, D. In *Methods in Enzymology*; Gerard, M., Ian, P., Eds.; Academic Press: 2003; Vol. 361, p 1.

(29) Lego, B.; Skene, W. G.; Giasson, S. *Langmuir* **2008**, *24*, 379.

(30) Khatchadourian, A.; Krumova, K.; Boridy, S.; Ngo, A. T.; Maysinger, D.; Cosa, G. *Biochemistry* **2009**, *48*, 5658.

(31) Krumova, K.; Oleynik, P.; Karam, P.; Cosa, G. *J. Org. Chem.* **2009**, *74*, 3641.

(32) Oleynik, P.; Ishihara, Y.; Cosa, G. *J. Am. Chem. Soc.* **2007**, *129*, 1842.

(33) Amat-Guerri, F.; Liras, M.; Carrascoso, M. L.; Sastre, R. *Photochem. Photobiol.* **2003**, *77*, 577.

(34) Lego, B.; François, M.; Skene, W. G.; Giasson, S. *Langmuir* **2009**, *25*, 5313.

(35) Israelachvili, J. N.; Gee, M. L. *Langmuir* **1989**, *5*, 288.

(36) Lo, P. K.; Karam, P.; Aldaye, F. A.; McLaughlin, C. K.; Hamblin, G. D.; Cosa, G.; Sleiman, H. F. *Nat. Chem.* **2010**, *2*, 319.

(37) Ngo, A. T.; Lau, K. L.; Quesnel, J. S.; Aboukhalil, R.; Cosa, G. *Can. J. Chem.* **2011**, *89*, 385.

(38) Pecher, J.; Guenoun, P.; Chevallard, C. *Cryst. Growth Des.* **2009**, *9*, 1306.

(39) Lopez Arbeloa, F.; Banuelos, J.; Martinez, V.; Arbeloa, T.; Lopez Arbeloa, I. *Int. Rev. Phys. Chem.* **2005**, *24*, 339.

(40) Wood, T. E.; Thompson, A. *Chem. Rev.* **2007**, *107*, 1831.

(41) Haugland, R. P. *Handbook of Fluorescent Probes and Research Products*; 10 ed.; Molecular Probes, Inc.: Eugene, OR, 2005.

(42) Ohno, K.; Morinaga, T.; Koh, K.; Tsujii, Y.; Fukuda, T. *Macromolecules* **2005**, *38*, 2137.

(43) Behling, R. E.; Williams, B. A.; Staade, B. L.; Wolf, L. M.; Cochran, E. W. *Macromolecules* **2009**, *42*, 1867.

(44) Mori, H.; Boker, A.; Krausch, G.; Muller, A. H. E. *Macromolecules* **2001**, *34*, 6871.

(45) Pincus, P. *Macromolecules* **1991**, *24*, 2912.

(46) Degennes, P. G. *Macromolecules* **1980**, *13*, 1069.

(47) Kurosawa, S.; Aizawa, H.; Talib, Z. A.; Atthoff, B.; Hilborn, J. *Biosens. Bioelectron.* **2004**, *20*, 1165.

(48) Dong, R.; Krishnan, S.; Baird, B. A.; Lindau, M.; Ober, C. K. *Biomacromolecules* **2007**, *8*, 3082.

(49) Tsarevsky, N. V.; Pintauer, T.; Matyjaszewski, K. *Macromolecules* **2004**, *37*, 9768.

(50) Zhulina, E. B.; Birshtein, T. M.; Borisov, O. V. *Macromolecules* **1995**, *28*, 1491.

(51) Konradi, R.; Ruhe, J. *Macromolecules* **2005**, *38*, 4345.

(52) Arbeloa, F. L.; Prieto, J. B.; Martínez, V. M.; López, T. A.; Arbeloa, I. L. *ChemPhysChem* **2004**, *5*, 1762.

(53) Krumova, K.; Cosa, G. *J. Am. Chem. Soc.* **2010**, *132*, 17560.

Chapter 4

Polystyrene-block-poly(acrylic acid) brushes grafted from silica surfaces: pH- and salt-dependent switching studies††

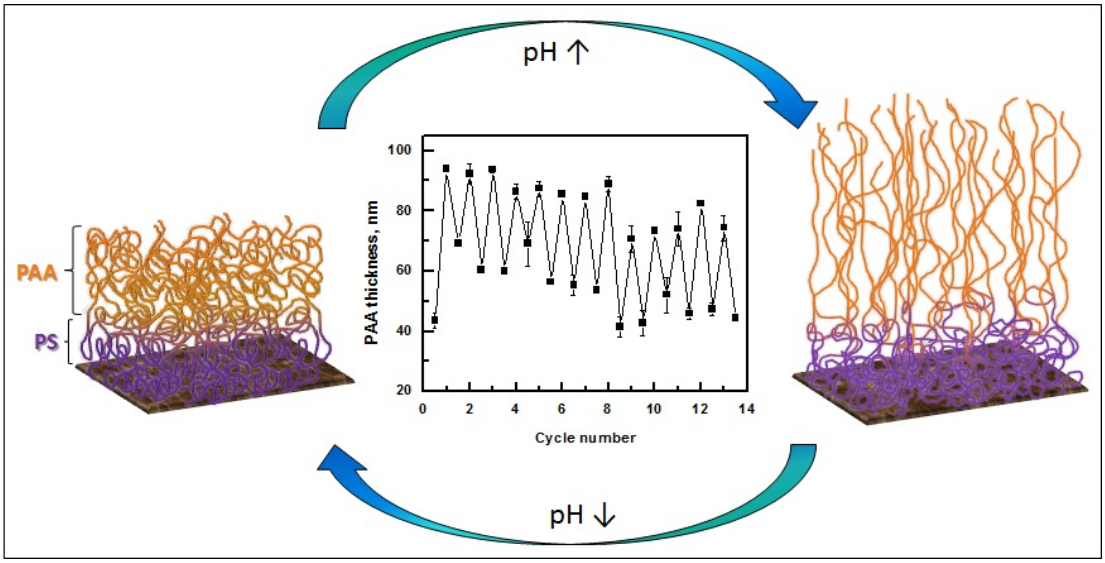

†† †† This chapter is a verbatim copy of the paper published in *Polymer Chemistry* (**2014**, *5*, 2242-2252). It is co-authored by Charly Ou, W. G. Skene and Suzanne Giasson.

4.1. Abstract

We report the preparation, characterization and responsive behavior of polystyrene-*block*-poly(acrylic acid) (PS-*b*-PAA) copolymer brushes grafted from silica substrates using Surface-Initiated Atom Transfer Radical Polymerization (SI-ATRP). pH-dependent swelling behavior was investigated *in situ* by ellipsometry and it confirmed that PAA chains can be reversibly switched from collapsed to extended conformations. It also confirmed that the grafted copolymer brushes were stable under extreme alkaline conditions of pH and with added salt. We showed that the hydrophobic polystyrene block of the copolymer protects the substrate-initiator bond against hydrolysis that would otherwise cause undesired polymer degrafting from the substrate. Also, we provide evidence of fundamentally different brush conformations with metal cations of increasing valency. Monovalent sodium and cesium ions caused brush stretching while only collapsed brushes were observed with divalent calcium ions.

4.2. Introduction

Polymer brushes generally consist of a monolayer of chains that are attached at one end to a substrate, while the free-end is exposed to the surrounding medium. Over the past few decades, polymer brushes have shown to be extremely useful for many applications, such as antifouling, cell adhesion substrates,[1-4] biosensors,[5-7] nanocomposites,[8] stationary phases in high performance chromatography,[9-11] microreactors[12-14] or microactuators.[15,16] Particular properties of charged polymer or polyelectrolyte brushes have attracted the greatest attention as their degree of dissociation, conformation, and brush height that can be reversibly tuned by pH and ionic strength.[17] These variable properties are understood to govern the swelling and collapse of the polyelectrolyte brushes contingent on the type of electrolyte, their

concentration, and pH. Systems based on these responsive brushes have showed promise as smart materials, pH-gated hybrid membranes,[18] nanoporous polymer-functionalized platforms,[19] and pH-sensitive nanosensors.[20]

Linking polymer brushes to substrates is done either by "grafting to" or "grafting from".[21] "Grafting to" involves the pre-synthesis of end-functionalized polymers and their subsequent attachment to a surface. Limited grafting density is possible with this approach because of unfavorable steric interactions between grafted polymer chains at high grafting density. In contrast, a wide range of grafting densities is possible when polymerizing directly on initiator-coated substrates in the "grafting from" approach. The polymer layer thickness, composition and conformation of the resulting polymer-coated substrate can be controlled when employing controlled radical polymerization methods.

A strong and irreversible polymer/substrate bond is required for accurate structure-property studies under various and extreme environmental conditions. This is particularly important since the chain conformation is a key parameter that determines the surface properties of polymer films.[22] The swelling-collapsing of covalently attached polymer layers is also of importance because there is a lack of accurate swelling studies that cover a full range of pH and salt effects, especially pH $\geq$ 10, on smooth and well characterized dense polyelectrolyte brushes. This is in part owing to physisorbed copolymers that were weakly attached to the substrate in previous structure-properties investigations.[23-25] However, covalently bonded polymers to the surface can also detach under particular conditions.[26,27] This is the case for "grafting from" polyacrylic acid (PAA) brushes that cleaves from the surface at pH$\geq$9.5 in the presence of added salt (10 mM NaCl).[28] The extended polymer conformation adopted under such conditions favors water penetration throughout the brush layer to the substrate where it can hydrolyze the exposed $Si_{substrate}$-O-$Si_{initiator}$ bond, resulting in polymer detachment. In contrast, a collapsed compact polymer conformation adopted at low pH prevents water and salt from reaching the surface and protects the substrate-initiator bond against cleavage.[28] The operating window for

assessing environmental structural effects is therefore limited with labile grafted polymers because of the potential polymer detachment from the substrate under certain conditions. Knowing the conditions that induce substrate–polymer bond cleavage, polymers that protect the labile bond against unwanted substrate-bond breaking can be designed and prepared. A PS-*b*-PAA copolymer covalently tethered to the substrate at the polystyrene end would be an ideal stimuli-responsive copolymer for hydrophilic surface-property studies. The hydrophobic polystyrene block would be consistently collapsed on the surface and it would prevent water from reaching the polymer-substrate interface. This would act as a hydrophobic barrier and protect the fragile surface-polymer bond against cleavage even under extreme pH and ionic strength. Meanwhile, the hydrophilic PAA brush would remain stimuli-responsive with different polymer conformations being controlled by environmental changes, similar to previously investigated PAA brushes.[24,25,29]

We therefore prepared a PS-*b*-PAA diblock copolymer via Surface-Initiated Atom Transfer Radical Polymerization (SI-ATRP) on silica wafers. The robustness of the covalent PS–substrate bond and the capacity of the copolymer to undergo conformational changes under extreme pH were evaluated. AFM and ellipsometry were used to investigate swelling-collapse cycles of the copolymer layer as a function of pH and presence of different types of salt. An extended window to examine the environmental conditions for swelling and conformation changes of charged polymer brushes is therefore possible with this copolymer that does not cleave from the surface. The knowledge gained from this study provides new insight into brush swelling mechanisms and support theoretical models.

4.3. Experimental section

4.3.1. Materials and chemicals

Silicon wafers were obtained from University Wafer Co (100-mm diameter, boron-doped, (100) orientation, one side polished). All chemicals were used as received from Aldrich unless specified. Copper bromide (CuBr) was purified according to previous methods.[30] *Tert*-butyl acrylate (*t*BA) and styrene were purified to remove the inhibitor by passing through a column of basic alumina, followed by vacuum distillation immediately prior to use. MilliQ water was obtained from Millipore A10 purification system with a resistivity of 18.2 MΩ·cm at 25° C. All glassware was oven-dried at 120 ^{o}C overnight.

4.3.2. Substrate preparation and initiator immobilization

Silicon wafers were cut into 1x2 cm^2 pieces using a diamond pencil, rinsed with acetone and dried under nitrogen. The substrates were immersed into a Piranha solution (H_2SO_4 concentrated /H_2O_2 70:30 v/v) for 20 min to remove the organic residues and activate the silica surface. (*Caution: Piranha solution is highly corrosive and should be used with extreme carefulness!*) Then, the substrates were washed multiple times with MilliQ water, absolute ethanol, followed by drying thoroughly under nitrogen.

The ATRP initiator, 3-(chlorodimethylsilyl)propyl-2-bromoisobutyrate was synthesized using the previously reported procedure.[30] The clean silicon substrates were immersed into 1 mM initiator solution in toluene and allowed to react with the initiator overnight at room temperature under nitrogen.[30] The substrates were then washed with toluene, absolute ethanol and dried under a steam of nitrogen. The freshly prepared initiator-modified substrates were either used for surface-initiated polymerization or stored in a desiccator until used.

4.3.3. Surface-initiated ATRP of styrene with added free initiator

CuBr (30 mg, $2x10^{-4}$ mol) was placed in a 50 mL double-necked round-bottomed flask. The flask was degassed under vacuum at room temperature and backfilled with argon three times. Freshly distilled styrene was purged with argon for 1 h. Deoxygenated styrene (14 ml, $4x10^{-2}$ mol), and *N*,*N*,*N*′,*N*″,*N*″-pentamethyldiethylenetriamine (PMDETA) (150 μL, $7.5x10^{-4}$ mol) were added to CuBr, and the mixture was stirred at room temperature under argon until a homogeneous light green solution was obtained. A clean initiator functionalized silicon wafer was placed in an oven-dried Schlenk flask, which was deoxygenated under vacuum and backfilled with argon three times. Ethyl-2-bromoisobutyrate as the free initiator (30 μL, $2x10^{-4}$ mol) was added to the mixture and the polymerization solution was transferred into the reaction flask. The flask was immersed in an oil bath heated at 90 ^{0}C for a given period of time with stirring. Opening the Schlenk flask and exposing the catalyst to air stopped the reaction. The surface was removed and cleaned thoroughly with THF, acetone and then dried under stream of nitrogen. The free polymer in solution was precipitated in methanol and dried under vacuum. The white polymer powder was solubilized in THF and analyzed by GPC.

4.3.4. Surface-initiated polymerization of *tert*-butyl acrylate (*t*BA) with added free initiator

A typical synthesis of *t*BA brushes from PS-modified silicon wafer was done as previously reported.[31] After polymerization, the substrate was cleaned by Soxhlet extraction with THF for 8 hrs in order to remove the physisorbed polymer, dried under nitrogen and stored in a desiccator until used. The resulting polymerized solution was concentrated under vacuo, diluted with THF, and the molecular weight of the free polymer was analyzed by GPC.

4.3.5. Hydrolysis of surface grafted poly(*tert*-butyl acrylate) (P*t*BA) to PAA

The hydrolysis of covalently attached P*t*BA brushes to PAA was done as previously reported.[28] Afterwards, the substrates were washed repeatedly with absolute ethanol and MilliQ water, then dried under a nitrogen stream, and stored in desiccator until used.

4.3.6 Swelling studies of PAA

Trizma base buffer solution (0.1 M) was prepared with MilliQ water and the pH was adjusted to 6.5, 7.5, 8.5, 9.5 and 10.5 with different volumes of HCl (0.1 M). The pH was measured with a Symphony SB20 pH meter with Ag/AgCl electrode. The ionic strength was controlled by adding NaCl aqueous solution (10 mM) to the Trizma buffer solution.

4.3.7. Molecular weight determination

The number- and weight-average molecular weights (M_n and M_w, respectively) of the prepared polymers were measured by GPC. The GPC system consisted of Waters 717 plus autosampler, three columns (Phenomenex Phenogel 500A, $10e^4$ and $10e^5$), a Waters 1525 binary HPLC pump, and a Waters 2414 refractive index detector. The eluent was THF at a flow rate of 1 mL min^{-1}, and the column and detector temperature was 35 °C. The polymer molecular weights were determined relatively to polystyrene standards (Shodex).

4.3.8 Surface characterization

Contact angle measurements

Measurements were carried out using an FTA200 dynamic contact angle analyzer (First Ten Angstrom) in the equilibrium static mode, using MilliQ water as the probe liquid. Data analyses were performed using Fta32 Video software and three separate measurements were done for each silica substrate.

AFM measurements

Dry state topographical AFM studies were done using a MultiMode microscope equipped with a NanoScope V extended controller (Digital Instruments, Santa Barbara, CA) at room temperature. The surfaces were imaged in the tapping-mode using a silicon cantilevered tip from Nanoworld with resonance frequency of ~285 kHz and a spring constant of 42 N/m. At least three different areas were analyzed on each sample.

Liquid AFM images were recorded using a Dimension 3100 MultiMode Scanning Probe Microscope equipped with Veeco NanoScope V extended controller (Digital Instruments, Santa Barbara, CA) by using MLCT silicon nitride probes (triangular E tip) with a resonance frequency of ~38 kHz and a spring constant of 0.1 N/m**.** A sample was placed in a custom-made Teflon liquid cell filled with buffer solution and left to equilibrate for at least 1 hr before imaging**.** All images were recorded in the tapping mode at 1 kHz scan rate; 512 x 512 pixels image resolution and weak oscillation damping (10-15%). Data analyses were performed using the NanoScope 7.30 software. A scalpel was used to make a scratch on the polymer layer and the vertical distance, or step, between the outer layer of the polymer and the scratched area was used as a reference for the thickness of the dry polymer layer. This thickness was measured at three different regions on each sample.

Spectroscopic ellipsometry

Ellipsometric measurements on the PS-*b*-PAA brushes both in dry and wet states were performed using M-2000V ellipsometer (J. A. Woollam Co). This is a Rotating Compensator Ellipsometer (RCE) equipped with a CCD array spanning the wavelength range from 370 to 1000 nm and mounted on a manual angle base with a fixed angle of incidence of 75°. Ψ and Δ values were acquired by averaging ellipsometric measurements for at least 50 cycles of the RCE and all measurements were performed at ambient temperature (22 °C).

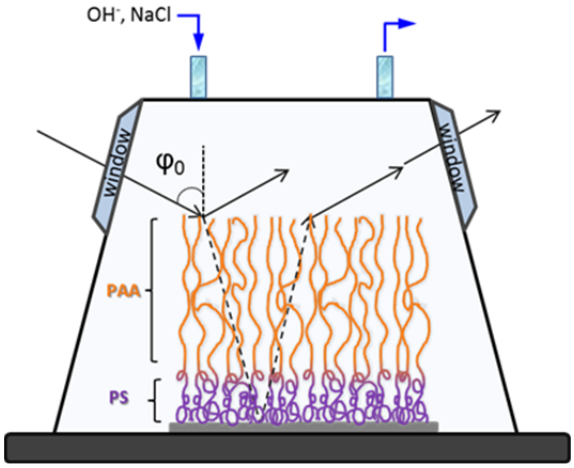

Figure 4-1. Schematic representation of liquid cell used for ellipsometry measurements.

For ellipsometric measurements in liquid, the 5 mL Horizontal Liquid Cell™ (J. A. Woollam Co) equipped with two fused silica windows was used (Figure 4-1). The sample was positioned over a custom-made 7.0 x 3.8 cm PTFE sample holder and then the cell cover was placed over the sample and fastened to the mounting plate with 4 screws. Light passed through one of the windows at 75° and then it was reflected from the silicon surface and exited at the opposite window. The liquid cell had two independent ports for solution input and output. The liquid entering the cell flowed over the sample and then it exited the chamber from the outport on top of the

cell. The total cell volume was 5 ml. The solution of study was manually pumped into the chamber with a syringe and the sample was equilibrated for one hour (unless otherwise stated). Switching between buffer solutions of different pH and salt concentration was done by purging the cell with MilliQ water (200 mL) to remove traces of the buffer solution. The cell was then filled with the buffer solution of desired pH (200 mL). Afterwards, the substrate was equilibrated for one hour with the new buffer solution before measuring.

Modeling and data fitting were carried out using the WVASE32 software (J. A. Woollam Co, version 3.768). The WVASE32 software fitted the ellipsometric angles Ψ and Δ calculated from an optical model to the experimentally measured values of Ψ and Δ. The Levenberg-Marquardt multivariate regression algorithm[33] was used to determine the layer thickness and the optical constants. The mean-squared error (MSE) was used to quantify the difference between experimental and calculated data, and it was minimized during the fitting process.[32]

The angle of incidence was fitted at each step of the fitting process in order to correct for slight sample misalignment. The Cauchy equation was used to model the dispersion of the materials for which the refractive index was not included in the software library:

$$n(\lambda) = A + \frac{B}{\lambda^2} + \frac{C}{\lambda^4} \qquad \text{(Equation 4-1)}$$

where n is the refractive index, A, B and C are parameters, and λ is the wavelength.

In order to evaluate n, the dry thickness h, and the thickness of swollen layer H, an optical model consisting of five consecutive layers as illustrated in Figure 4-2 was constructed. The bottom layer (L#0) models the silicon substrate and the top layer (L#5) represents the surrounding aqueous medium, i.e. the different buffer solutions. As the refractive index of the buffer solutions measured by refractometry had refractive indexes similar to pure water (n_b=1.3344), layer #5 was assumed to be

pure water. A 2 nm (±0.03 nm) thick silicon oxide layer (L#1) was measured prior to surface modifications and it was kept constant in the subsequent steps of the process. The initiator layer (L#2) was modeled as a Cauchy layer and its thickness was evaluated as 0.2±0.03 nm and MSE=2.13 prior to polymer brush growth. The thickness of the polystyrene film (L#3) was measured using "polystyrene_g.mat" layer from WVASE library. The polyelectrolyte brush layer (PAA) was considered as a single Cauchy layer (L#4) and assumed to be transparent and homogeneous.

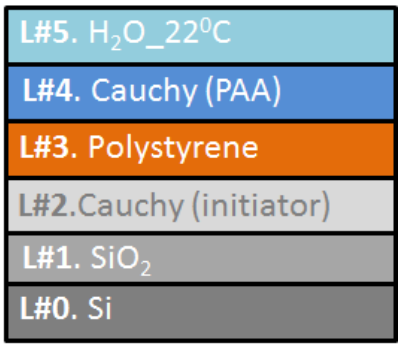

Figure 4-2. Optical model used to calculate the thickness of swollen PAA brushes by ellipsometry.

The Cauchy approximation was used (Equation 1) for all thickness measurements done with the liquid cell. For the dry polymer films with a thickness less than 10 nm, fixed Cauchy parameters A=1.45, B=0.01 and C=0 were used, as generally reported for transparent films.[34] The film thickness in the dry state was measured using the same model as Figure 4-2, but without water as a top layer. The MSE of less than 5 was obtained for all measurements.

4.4 Results and discussion

4.4.1 Synthesis of Polystyrene-*block*-poly(acrylic acid) brushes

Scheme 4-1 shows the synthetic route for preparing the tethered polystyrene-b-poly(acrylic acid) diblock copolymer brushes using a free initiator. We chose the monofunctional chlorosilane because it is well-known to form uniform monolayers.[30] This is in contrast to multifunctional chlorosilanes that result in disordered multilayers when assembled from solution.[35, 36] The first step was grafting the initiator to the activated silica surface. This involved reacting the monochlorosilane initiator with the silicon wafer, resulting in a Si-O-Si bond. The reaction was done in anhydrous toluene and lead to a covalently attached initiator monolayer. Grafting the initiator to the surface was confirmed by water contact angle measurements and ellipsometry.[30,31] The measured contact angle of 78°±2 and thickness of 0.2 nm are in good agreement with previously reported values for a densely grafted initiator monolayer.[28] The initiator surface coverage was estimated using the Cassie-Baxter equation[37] and was relatively high (ca 85 ± 1%) for all samples.

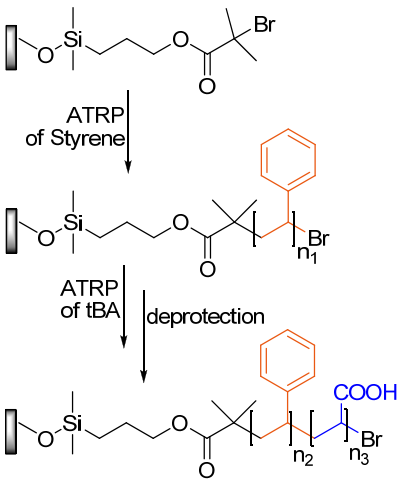

Scheme 4-1. Synthetic route for the synthesis of PS-*b*-PAA brushes grafted from silica wafer.

The targeted PS-*b*-PAA block-copolymer brushes were prepared in three steps: 1) SI-ATRP of styrene with the initiator covalently attached to the substrate, 2) subsequent SI-ATRP of *t*BA by exploiting the dormant halogen end on the polystyrene brush, and 3) P*t*BA deprotection via acid hydrolysis. Styrene polymerization was done in two ways: 1) from the initiator-functionalized silica and 2) in solution by adding a sacrificial initiator of identical concentration for all the polymerizations. The sacrificial initiator plays a significant role in controlling the surface-initiated ATRP and the preparation of well-defined polymers. In the absence of sacrificial initiator, the polymerization reaction is less controlled. This results in inhomogeneous and rough polymer films. Homogeneous surface polymerization and hence controlled polymerization can be improved by adding free initiator to the solution.[38] The additional advantage of adding free initiator to the reaction is the molecular weight of the free polymer from solution can be measured by standard solution polymer molecular weight characterization methods. This is important because the amount of polymer cleaved from the flat substrate is on the order of sub-micrograms, which is insufficient for analysis by conventional polymer characterization methods. Therefore, the molecular weights of the polymers in solution were used as an indicator of molecular weight of the grafted chains.[38, 39] However, it is important to note that the molecular weight of tethered polymers and those free in solution are not consistently similar. The substrate curvature can account for some molecular weight discrepancies between surface tethered and free polymers owing to surface moderated catalyst and monomer diffusion differences.[40] For convex surfaces, grafted and free polymers have similar molecular weights. In contrast, the molecular weight of free polymers is usually higher than polymers tethered to flat and concave surfaces.[41-44] However, there are limited examples of free polymers having lower molecular weight than polymers grafted on flat surfaces.[45, 46] This was explained by high local viscosity and limited mobility of attached molecules on the surface favour Cu(I) diffusion to the growing front while decreasing terminations between growing chains.[45]

In our previous study, we examined whether a PS block could successfully protect the substrate-initiator bond against cleavage under extreme pH and salt concentration. A 10 nm PS block thickness was arbitrary chosen and it was found to protect the substrate-initiator bond, regardless of pH and salt concentration.[28] In the present work we prepared the set of PS of varying thickness ranging from 1.7 to 10.1 nm with the objective of finding the minimum PS thickness required to protect the substrate-initiator bond against environmental cleavage. Targeted degree of polymerization of 200 resulted in a polymer molecular weight of 22.8 kg/mol at 100 % conversion for styrene. The linear variation of free polymer molecular weight with time up to ca. 19 h (Figure 4-3 A) and the relatively high molecular weight of free polymer (21 kg/mol) confirm controlled polymerization under the given reaction conditions within this time frame. Moreover, the molecular weight distribution remained low (maximum PDI is 1.1) throughout the polymerization, typical for a living polymerization reaction (Figure 4-3 B). The thickness of the polystyrene layer constantly increased with both molecular weight of the free polymer and polymerization time (Figure 4-3 C) up to a maximum of 13.1 nm at ca. 19 h. This trend implies there is sufficient deactivator in solution to provide controlled growth of the polymer film.[38] After 19 h, the decrease in polymer thickness as well as in polymer molecular weight was observed indicating possible polymerization control loss. This was also reported by Jeyaprakash[47] and Liu.[48] A potential explanation for the loss of controlled surface polymerization of styrene is the decrease in active chain ends[47] caused by the increase in chain-transfer and other side reactions.[38, 49] Regardless, the topography of the polystyrene layer measured by AFM was smooth and uniform with a rms of 0.2 nm (Figure 4-3 D). Grafting of PS to the silica wafer was additionally confirmed by ATR-FTIR (Figure 4-S1). Measurements were done after Soxhlet purification to remove any physisorbed polymers. The characteristic signals around 3030 cm^{-1} and 1440 cm^{-1} are attributed to the aromatic C-H and C=C stretching, respectively, confirming the covalently grafted polystyrene on the substrate.[50-53]

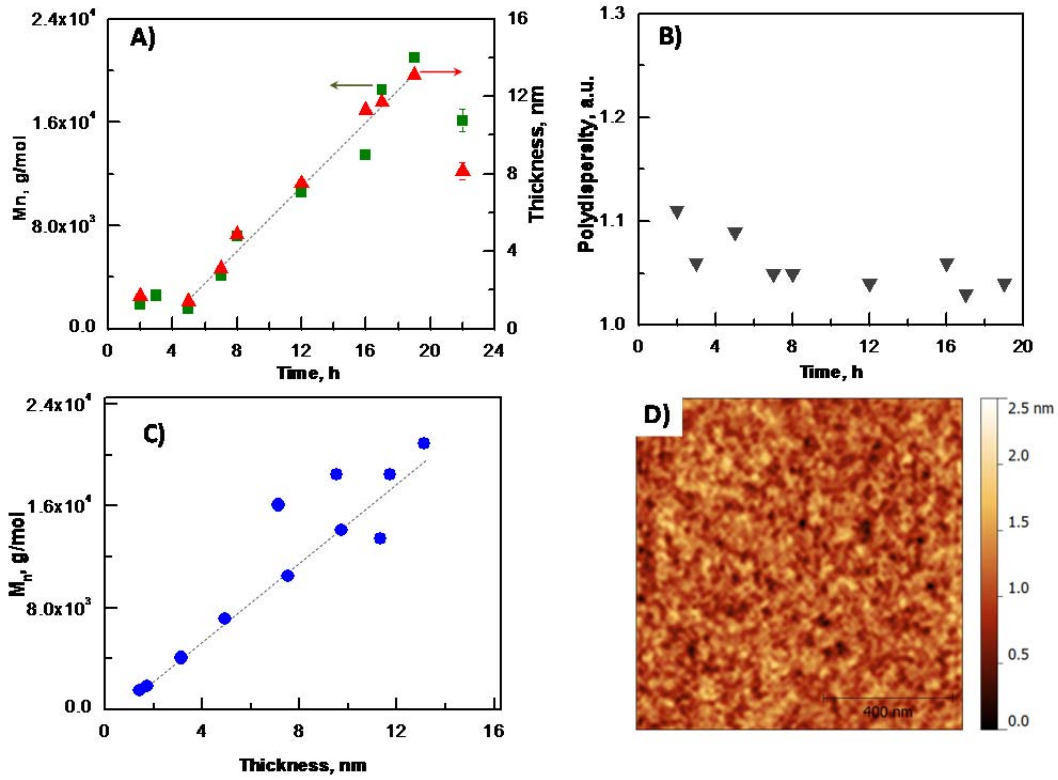

Figure 4-3. A) M_n of free polystyrene (squares) and PS thickness (triangles) as a function of time. Styrene/initiator/CuBr/PMDETA=200:1:1:3.75. The dashed line is a guide for the eye. Each square represents separate, but identical polymerization reactions. A standard deviation of 0.1 nm was obtained for all thickness values. **B)** Evaluation of the free polymer PDI as a function of polymerization time. **C)** Polystyrene film thickness vs. molecular weight (M_n) of the free polymer in solution. The dashed line is used only as a guide for the eye. **D)** Typical surface morphology of polystyrene brushes grafted from silica substrate. The thickness of the displayed sample is 10 nm.

The P*t*BA block was synthesized by ATRP (see Scheme 4-1) from the end bromide groups of the grafted polystyrene chains. The polymerization was initiated from polystyrene layers having thickness ranging from 2 to 10 nm by adding CuBr, PMDETA and free initiator as previously reported.[31] The P*t*BA blocks were

hydrolyzed to the desired acrylic acid by immersing the substrates in 10% TFA solution in dichloromethane for ca. 15 h. The thickness of the resulting PS-*b*-PAA brushes decreased by more than 50 % (Table 4-S1) and the water contact angle decreased from 80^0-82^0 (PS-b-P*t*BA film) to 25^0-37^0 (PS-*b*-PAA brushes). The topography of the PS-b-P*t*BA appeared to be smooth with a rms of 0.6 nm (Figure 4-4 A1, B1). The deprotection step, resulting in PAA brushes led to a slight decrease in the surface roughness (rms of 0.3 nm) (Figure 4-4 A2, B2). This could be attributed to an increase in the chain flexibility caused by the loss of the *tert*-butyl groups.[54] However, after immersing the polymer brush in water for ca. 12 h, rinsing with ethanol, drying under nitrogen, the PAA layer appeared less homogeneous with a surface roughness of 0.9 nm (Figure 4-4 A3, B3). This can be explained by a reorganization of the PAA film with washing. Indeed, the PAA layer is expected to be neutral and relatively hydrophobic right after hydrolysis.[26] The resulting surface appears smooth because the hydrophobic chains minimize their contact with the solvent and the effect of polydispersity on the surface roughness in the collapsed state is expected to be negligible.[26,31] However when immersed in water at pH ≈ 5.5, the PAA chains are slightly charged and can extend into well-defined nanodomains.

Accurate structure-properties studies require knowing the polymer grafting density since the polymer conformation is inseparably linked to it. The grafting density of each block was therefore calculated using Equation 4-2:

$$\sigma = \frac{d\rho N_A}{Mn} \qquad \text{(Equation 4-2)}$$

where d is the dry thickness of the polymer layer, ρ represents polymer density (1.05 g/cm^3 for PS[55] and 1.047 g/cm^3 for P*t*BA[55]), M_n is the number average molecular weight of free polymer in solution and N_A is Avogadro's number.

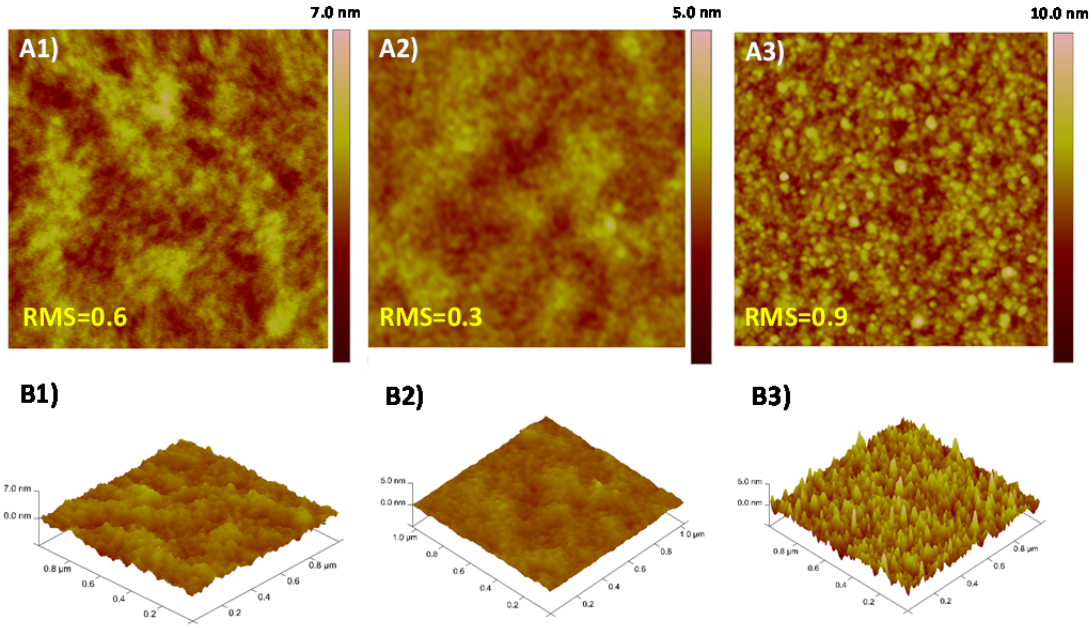

Figure 4-4. Top-view (A1) and 3D (B1) AFM images of 1x1 µm scan size PS-b-P*t*BA brushes: PS layer = 1.7 nm and P*t*BA layer=41 nm. A2) and B2) PS-*b*-PAA brushes immediately after deprotection. A3) and B3) PS-*b*-PAA brushes after exposure to water (MilliQ) and drying under nitrogen, PAA=18.1 nm.

The grafting densities ranged from 0.6 to 0.3 chains/nm^2 for the PS block and from 0.2 to 0.4 chains/nm^2 for the P*t*BA block. The conformation of the attached polymer chains can be determined by comparing the distance between two adjacent grafting points s, ($s = 1/\sigma^{1/2}$) with the size of the polymer chains. As the polymer layer thickness was measured in air (Table 4-1), we used the radius of gyration R_G of a collapsed polymer coil as the reference size for the grafted chains, i.e. $R_G \approx aN^{0.33}$ where a refers to the length of each repeating unit (0.25 nm for PS and P*t*BA, and corresponds to vinyl chain length[56, 57]), and N is the degree of polymerization.[58] If the distance between adjacent grafting sites is significantly smaller than the size of the chains, $s << R_G$, the polymer chains are forced to extend from the surface and form a brush conformation.[58, 59] For both PS and P*t*BA, s is similar or slightly larger than R_G (Table 4-1), indicating that the grafted copolymer chains adopt an intermediate

mushroom-brush conformation. However, in good solvent or when ionized, a stretched brush conformation is expected.[58]

Table 4-1. Composition of PS-*b*-PAA brushes from different samples.

Sample	Polymer layer thickness (±0.1nm)[a]	M_n of free polymer (kg/mol)[b]	σ (chains/nm^2)[c]	s (nm)	R_G of a collapsed coil (nm)
PS layer					
1	1.7	1.8	0.6	1.3	0.7
2	3.1	4.1	0.5	1.5	0.8
3	4.3	6.9	0.4	1.6	1.0
4	9.5	18.5	0.3	1.8	1.4
5	10.1	13.5	0.5	1.1	1.2
P*t*BA layer					
1	41.1	64.5	0.4	1.6	2.0
2	33.2	73.0	0.3	1.9	2.0
3	24.9	63.2	0.3	2.0	2.0
4	21.7	57.8	0.2	2.1	2.0
5	15.7	51.0	0.2	2.2	2.0

[a] measured in air using ellipsometry; [b] measured by GPC relative to polystyrene standards; [c] calculated from eq. 2

4.4.2 Ellipsometry: Optical properties of PS-*b*-PAA film

In order to accurately determine the thickness of the polymer layer by ellipsometry, the polymer must be optically contrasted from the substrate. This is the case with the PS and PAA whose refractive index is different from the SiO_2 substrate (Figure 4-5). The experimentally measured refractive indices at 589.3 nm (sodium spectral line) for both the PS and PAA blocks were consistent with the literature

values (Table 4-2). However, no difference in refractive index was found between the silica wafer and the initiator layer. This is because the initiator was only 0.2 nm, which exceeds the resolution of the ellipsometer.

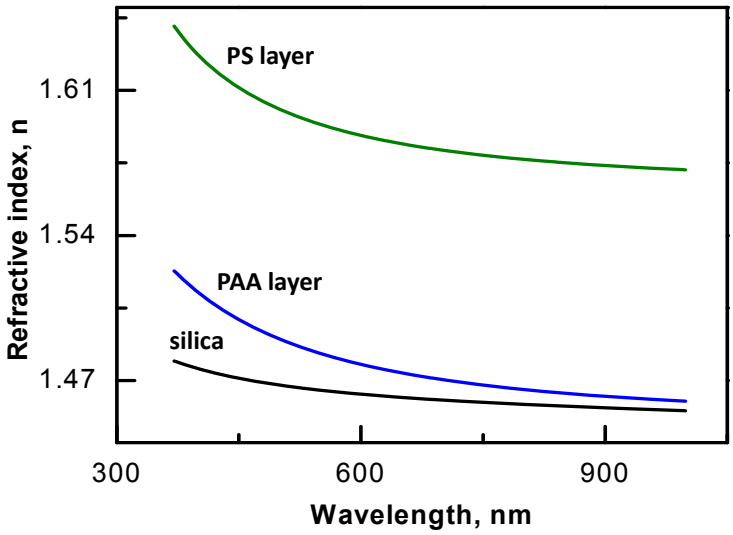

Figure 4-5. Refractive index vs. wavelength for the different layers used in the model illustrated in Figure 4-2.

Table 4-2. Refractive indices obtained by ellipsometry at 589.3 nm.

Polymer	Refractive index	Refractive index from literature[55]	Model
PS	1.5893	1.590-1.592	Polystyrene_g.mat
PAA	1.4788	1.527	Cauchy.mat

4.4.3 pH-dependent swelling studies

The brush swelling in water as a function of pH was investigated using the liquid ellipsometer cell (Figure 4-1). The brushes were equilibrated for 2 h in a given pH before the measurement and the swelling behavior of the PAA layer was

quantified using a swelling ratio (Q), defined as a ratio between swollen film thickness (H) and dry film thickness (h) (eq. 4-3).

$$Q = \frac{H}{h} \qquad \text{(Equation 4-3)}$$

Since only the PAA block is expected to swell with pH in water, the PS layer thickness was subtracted from the total measured thickness and the reported thickness refers to the PAA layer only.

Figure 4-6 shows the swelling behavior measured using ellipsometry for two different PS-*b*-PAA samples (Samples 2 and 3 in Table 4-1 and Table 4-S1). In pure water (pH 5.5), Q = 2.3 and 3.0 for Sample 2 and 3, respectively. Similar swelling ratios were also obtained by AFM step height measurements on a different sample (Sample 5 in Table 4-1 and Table 4-S1). The total thickness of the dry PS-*b*-PAA layer measured by AFM was 12 ± 1 nm and the total thickness measured in MilliQ water at pH 5.5 was 15.5 ± 2 nm, corresponding to PAA swelling ratio $Q \sim 3$. Theoretical studies of polyelectrolyte brushes predict a complex variation in swelling depending on the degree of dissociation of the chain, grafting density, and salt concentration.[17, 60-63] The scaling relationship describing the behavior of weakly charged polymer brushes in good solvents predicts that the degree of dissociation (α) decreases with increasing grafting density (σ) according to $\alpha \propto \sigma^{-1/3}$.[63] Therefore, the pH transition between neutral and charged brushes at high grafting density is expected to be higher than the acid dissociation constant of the acrylic acid monomer (pKa = 4.25)[64] and of PAA in dilute solution (pKa ~ 4.2-5.5)[25,65] . However, our results showing a significant swelling (Q>1) of the PAA brushes in MilliQ water at pH 5.5 and they suggest a partial dissociation of the COOH groups. This behavior differs from recently published data that showed no swelling of PAA brushes under similar conditions (pH 5.5).[26,29] This discrepancy might be assigned to differences in the initial polymer conformation associated with different dry thicknesses together with the assumed molecular weight of the grafted chains. As previously discussed,

the molecular weight of the free polymers in solution used to determine the grafting density is most probably not representative of the grafted chains. Different initial conformations of the chains are therefore expected, which strongly affect the degree of dissociation for given pH.

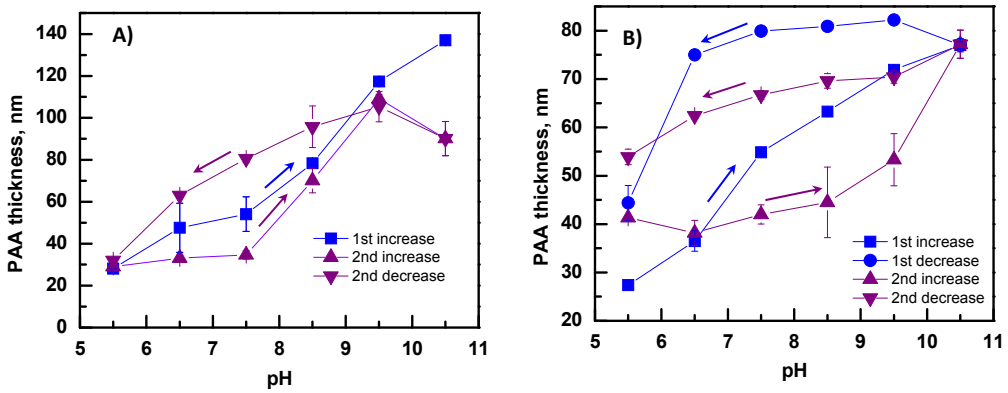

Figure 4-6. PAA thickness, *H*, measured by ellipsometry during first pH increase from 5.5 to 10.5 (squares) and decrease from 10.5 to 5.5 (circles), second pH increase from 5.5 to 10.5 (triangles) and decrease from 5.5 to 10.5 (inverted triangles). A) PS-*b*-PAA brushes with dry PS = 3.1 and PAA = 12.2 nm (Sample 2 in Table 4-1); B) PS-*b*-PAA brushes with dry PS = 4.3 and PAA = 9.2 nm (Sample 3 in Table 4-1). Error bars are average values of three measurements on different areas of the substrate.

Hysteresis effects were observed with brush swelling as a function of pH. An example of this is seen in Figures 4-6 A and B that show the swelling response with pH for two different samples. A progressive swelling ratio, increasing up to a maximum Q = 11.4 for Sample 2 and 8.4 for Sample 3, was observed for the first pH increase. The same maximum Q could not be attained with the second pH increase for sample 2 and a different Q was observed when decreasing the pH for both samples. This hysteresis-like swelling behavior was also previously observed.[66] It was proposed that as the pH gradually increases, the dissociation of the PAA's

carboxylic acid occurs gradually from the outer segments (at water/brush interface) towards those found close to the substrate.[66] Therefore, the maximum degree of dissociation within the brush layer is expected to occur at pH ≈ 10.5. On decreasing the pH, the outer segments are first protonated, causing an increase in the hydrophobicity of the exposed brush. As a result, water cannot penetrate the brush and the inner charged segments cannot be reprotonated, giving rise to a brush swelling hysteresis.

4.4.4 Stability studies

The stability and reversible swelling of the PS-*b*-PAA brushes under extreme pH and added salt were also investigated. Figure 4-7 shows the change in PAA thickness with time when alternately immersing the sample in pH 10.5 and water.

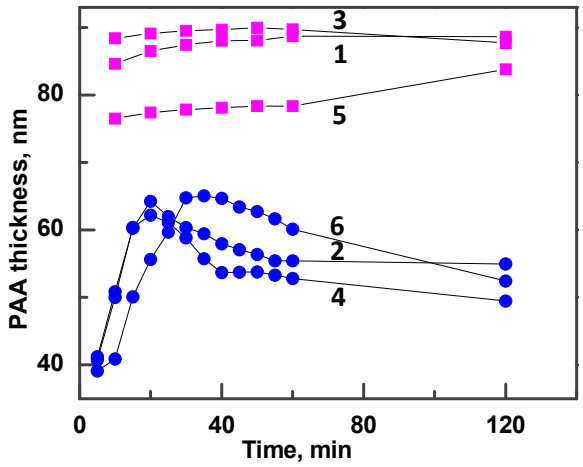

Figure 4-7. Variation of PAA thickness with time when alternately immersing the sample in pH 10.5 (squares) and water (circles).
The numbering of the curves corresponds to the immersion sequence. PS-*b*-PAA brushes with dry PS = 1.7 and PAA = 18.1 nm (Sample 1 in Table 4-1).

At pH 10.5, the brush thickness equilibrated relatively fast and it remained stable for 2 hr. Conversely, the brush thickness equilibration time was much longer (20-30 minutes) when immersed into MilliQ water, owing to the gradual carboxylate protonation that prevents the inner groups from being reprotonated at low pH (vide supra). The slight thickness decrease that observed after 60 min indicates the continuous reprotonation process.

The variation of PAA thickness with pH was relatively constant over 3 cycles when the samples were immersed for 2 hr as reported in Figures 4-7 and 4-8 A, confirming the robustness of the brush and no degrafting occurs. The stability of the PAA brushes was also confirmed over 13 cycles of pH switching with 10 min equilibration per cycle (Figure 4-8 B) where no significant variation in the swelling ratio (9.3±0.9) was observed.

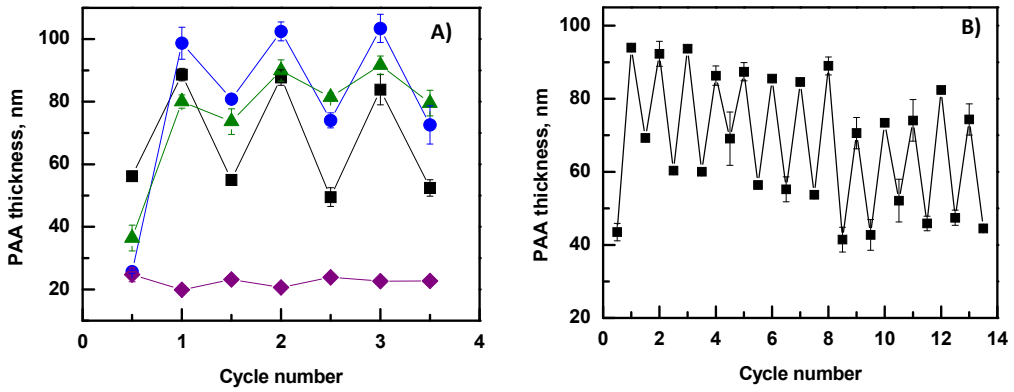

Figure 4-8. Variation in PAA brush thickness (H) with pH without salt (squares) or with different added salts: NaCl (circles), CsCl (triangles), $CaCl_2$ (diamonds) and equilibration times of 2 hours (A), 10 min (B). The integer and fractional cycle numbers correspond to the buffer at pH 10.5 and water immersions, respectively. Layer thickness: PS=1.7 nm, PAA =18.1 nm (Sample 1, Table 4-1) (A) PS=9.5 nm and PAA=9.0 nm (Sample 4, Table 4-1) (B). Three different regions were analyzed for thickness measurements and the error bar represent the standard deviation.

These results confirm the extreme robustness of the PS-*b*-PAA layer and its relatively fast response to variation of environmental conditions. This is based on the significant thickness change that was observed within 10 min after switching the pH. Thickness response measurements shorter than 10 min equilibration time were not possible owing to the lengthy experimental preparation for switching between water and buffered water.

4.4.5 Effect of salt

To the best of our knowledge, the brush stability and swelling/collapsing properties in presence of various salt ions have not been previously reported. Buffered solutions of 10 mM NaCl, CsCl and $CaCl_2$ were used. This concentration was chosen as a critical value, as it was reported previously that PAA brushes can be cleaved at high pH and with salt at greater than10 mM.[28]

Figure 4-8 A shows constant thickness response to pH variation for different salt counterions. This demonstrates that no brush degrafting over 3 swelling/collapsing cycles under these conditions. A PS thickness of 1.7 nm is therefore a sufficient minimum amount of hydrophobic barrier to protect against substrate-initiator hydrolysis for swelling/collapsing switching studies.

Also from Figure 4-8 A, information about swelling properties of PS-*b*-PAA system as a function of counterion radii was extracted. We demonstrated the PAA brush is thicker with sodium salt than without salt (98 vs. 88 nm with and without salt, respectively). The increase in brush thickness with added salt agrees well with Zhulina's theory[63] and with similar experimental work of Wu et al.[54] This swelling is associated with an increase in the degree of dissociation of weak polyelectrolyte brushes with increasing of salt concentration. However, Lego et al,[26] reported no change in PAA brush thickness with salt concentration at pH 6. Conformational differences of the grafted PAA chains in the salt-free solution can explain the

observed discrepancy. In Lego's work, the PAA brushes were undissociated and collapsed when exposed to water at pH < 7. Therefore, added ions could not penetrate the collapsed hydrophobic brush at this pH to swell the brush. In our study, the brushes are already swollen in water (pH 5.5) and therefore they are more permeable to added ions.

For comparable ionic strength, the swelling with Cs^+ was smaller than with Na^+. The maximum swollen thickness with CsCl was 91 nm compared to 103 nm with NaCl (Figure 4-8 A). The difference in swelling response is a result of cesium's lower charge density. The effective (hydrated) size of the cesium ion is smaller than sodium and it can bind fewer water molecules.[67] Sodium ions are also known to favor the dissociation of weak polyelectrolyte brushes by replacing the protons of the COOH groups.[25, 54, 63] This increases the osmotic pressure within the brushes and favors brush swelling.[68] However, it has been proposed that the Cs^+COO^- ion pair is more easily dissociated than Na^+COO^-[67], so Cs^+ ions can more readily leave the brush, and the total concentration of Cs^+ within the brush will be lower, resulting in lower osmotic pressure compared to Na^+.

In contrast to monovalent ions of sodium and cesium, the brush collapsed after exposure to 10 mM $CaCl_2$ at pH 10.5 (19 nm compared to 24 nm in pure water) (Figure 8A). A weak response to pH was observed over a few pH-change cycles (Figure 8A). The same trend with PMAA brushes and calcium salt at comparable concentrations was observed by Konradi et al.[68] However, once the PMAA brushes were immersed in salted solution, they could not be re-swollen in dionized water. Theoretical studies suggest that interactions between the carboxylic groups and calcium ions are ionic (i.e. columbic),[69, 70] whereas experimental studies claim that the binding between polyelectrolyte brush and divalent alkaline-earth ions is a specific interaction.[68] These previously reported experimental studies suggest that divalent ions can associate with either one carboxylic acid group or cross-link two neighboring COO^- groups from different polymer chains.[68] The latter results in less

flexible and rigid polymer networks that have limited swelling behavior. Our results corroborate well with these observations.[68]

4.5 Conclusion

Our study reports for the first time the robustness of a charged polymer brushes and its capacity to undergo reversible conformational changes under extreme conditions of pH. SI ATRP was used to prepare polystyrene-*b*-polyacrylic acid (PS-*b*-PAA) brushes covalently attached to silica via the PS block in a well-controlled manner. The stability was evaluated over pH-change cycles, confirming the extreme robustness of the PS-*b*-PAA layer and its responsiveness to pH and ionic strength. The hydrophobic PS layer was an effective barrier for protecting the surface-initiator bond against hydrolysis, which usually occurs at high pH and ionic strength. A wider operating window of environmental conditions could therefore be used for examining the responsive behavior studies with the PS-*b*-PAA copolymer brushes. The PS-*b*-PAA brushes exhibited pH responsiveness with hysteresis effects, which are presumably associated with a progressive change in the hydrophobicity of the PAA chains upon gradual pH changes. The effect of salt of different chemical nature on the copolymer brush stability and responsiveness was also investigated. Monovalent ions of sodium or cesium cause constant brush swelling/collapsing over repetitive pH cycles. In the presence of divalent calcium ions, the brushes collapsed and they could not be re-swollen in pure water. This contradicts theoretical models,[69] but confirms previous experimental results,[68] suggesting that specific interactions between charged polymer segments and divalent cations lead to cross-linking within the polymer layer. Nonetheless, friction, adhesion, permeability (diffusion or flow), and wetting can potentially be modulated via conformational changes with the stimuli responsive diblock that is a promising new smart material for rapid responsive switching.

4.6 Acknowledgements

Financial support from the Fondation Québécoise pour la Recherche en Nature et Technologies and Natural Sciences and Engineering Research Council of Canada is acknowledged for Discovery and Research Tools and Instrument grants. Canadian Foundation for Innovation is also acknowledged for additional equipment and infrastructures. The Center for Self-Assembled Chemical Structures is also acknowledged.

4.7 Supporting Information

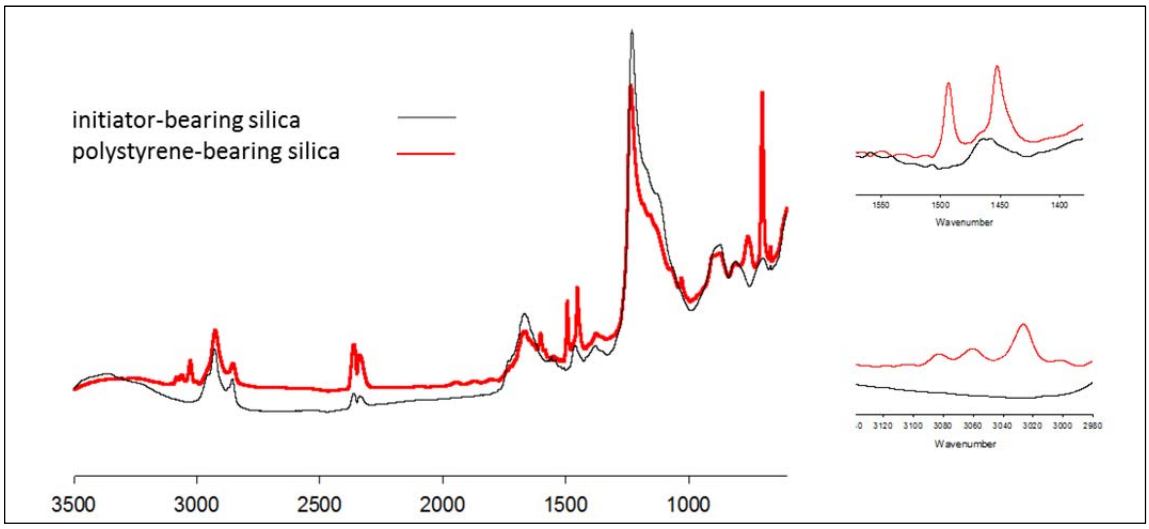

Figure 4-S1. ATR-FTIR spectra of 10nm thick polystyrene brushes grafted from silica wafer.

	PtBA layer			PAA layer	
Sample	**Degree of Polymerization (*N*) [a]**	**R_G of swollen coil (nm)[b]**	**Fully extended length, nm[c]**	**Thickness, nm[d]**	**PS/PAA thickness ratio**
1	503	10	126	18.1	**0.1**
2	570	11	143	12.2	**0.3**
3	493	10	123	9.2	**0.5**
4	451	10	113	9.0	**1.1**
5	398	9	100	1.8	**5.6**

Table 4-S1. Some parameters of PtBA and PAA layers.

[c] calculated using formula: $N=Mn(polymer)/Mn(monomer)$; [b] calculated using equation $R_f \approx aN^{0.6}$, where $a=0.25$ is a characteristic dimension of each repeating unit; [c] calculated from equation $H=aN$; [d] measured in air using ellipsometry;

4.8. References

(1) Feng, W.; Zhu, S.; Ishihara, K.; Brash, J. L. *Langmuir* **2005**, 21, 5980.

(2) Roosjen, A.; Busscher, H. J.; Norde, W.; van der Mei, H. C. *Microbiology* **2006**, 152, 2673.

(3) Schon, P.; Kutnyanszky, E.; Ten Donkelaar, B.; Santonicola, M. G.; Tecim, T.; Aldred, N.; Clare, A. S.; Vancso, G. *J. Colloids Surf., B* **2013**, 102, 923.

(4) Zhu, B.; Eurell, T.; Gunawan, R.; Leckband, D. *J. Biomed. Mater. Res.* **2001**, 56, 406.

(5) Akkahat, P.; Kiatkamjornwong, S.; Yusa, S.; Hoven, V. P.; Iwasaki, Y. *Langmuir* **2012**, 28, 5872.

(6) Akkahat, P.; Mekboonsonglarp, W.; Kiatkamjornwong, S.; Hoven, V. P. *Langmuir* **2012**, 28, 5302.

(7) Welch, M.; Rastogi, A.; Ober, C. *Soft Matter* **2011**, 7, 297.

(8) Chen, K.; Susner, M. A.; Vyazovkin, S. *Macromol. Rapid Comm.* **2005**, 26, 690.

(9) Mallik, A. K.; Rahman, M. M.; Czaun, M.; Takafuji, M.; Ihara, H. *Chem. Lett.* **2007**, 36, 1460.

(10) Mallik, A. K.; Rahman, M. M.; Czaun, M.; Takafuji, M.; Ihara, H. *J. Chromatogr. A* **2008**, 1187, 119.

(11) Miller, M. D.; Baker, G. L.; Bruening, M. L. *J. Chromatogr. A* **2004**, 1044, 323.

(12) Costantini, F.; Benetti, E. M.; Reinhoudt, D. N.; Huskens, J.; Vancso, G. J.; Verboom, W. *Lab Chip* **2010**, 10, 3407.

(13) Costantini, F.; Benetti, E. M.; Tiggelaar, R. M.; Gardeniers, H. J. G. E.; Reinhoudt, D. N.; Huskens, J.; Vancso, G. J.; Verboom, W. *Chem. Eur. J.* **2010**, 16, 12406.

(14) Costantini, F.; Bula, W. P.; Salvio, R.; Huskens, J.; Gardeniers, H. J. G. E.; Reinhoudt, D. N.; Verboom, W. *J. Am. Chem. Soc.* **2009**, 131, 1650.

(15) Comrie, J. E.; Huck, W. T. S. *Macromol. Rapid Commun.* **2008**, 29, 539.

(16) Howse, J. R.; Topham, P.; Crook, C. J.; Gleeson, A. J.; Bras, W.; Jones, R. A. L.; Ryan, A. J. *Nano Lett.* **2006**, 6, 73.

(17) Zhulina, E. B.; Wolterink, J. K.; Borisov, O. V. *Macromolecules* **2000**, 33, 4945.

(18) Sugnaux, C.; Lavanant, L.; Klok, H. A. *Langmuir* **2013**, 29, 7325-7333.

(19) de Groot, G. W.; Santonicola, M. G.; Sugihara, K.; Zambelli, T.; Reimhult, E.; Voros, J.; Vancso, G. J. *ACS Appl. Mater. Interfaces* **2013**, 5, 1400.

(20) Contreras-Caceres, R.; Dawson, C.; Formanek, P.; Fischer, D.; Simon, F.; Janke, A.; Uhlmann, P.; Stamm, M. *Chem. Mater.* **2013**, 25, 158.

(21) Azzaroni, O. J. *Polym. Sci., Part A: Polym. Chem.* **2012**, 50, 3225.

(22) Ross, R. S.; Pincus, P. *Macromolecules* **1992**, 25, 2177.

(23) Bousquet, A.; Ibarboure, E.; Teran, F. J.; Ruiz, L.; Garay, M. T.; Laza, J. M.; Vilas, J. L.; Papon, E.; Rodriguez-Hernandez, J. *J. Polym. Sci., Part A: Pol. Chem.* **2010**, 48, 2982.

(24) Currie, E. P. K.; Sieval, A. B.; Avena, M.; Zuilhof, H.; Sudholter, E. J. R.; Stuart, M. A. C. *Langmuir* **1999**, 15, 7116.

(25) Currie, E. P. K.; Sieval, A. B.; Fleer, G. J.; Stuart, M. A. C. *Langmuir* **2000**, 16, 8324.

(26) Lego, B.; Skene, W. G.; Giasson, S. *Macromolecules* **2010**, 43, 4384.

(27) Tugulu, S.; Barbey, R.; Harms, M.; Fricke, M.; Volkmer, D.; Rossi, A.; Klok, H.-A. *Macromolecules*, **2006**, 40 (2), 168.

(28) Borozenko, O.; Godin, R.; Lau, K. L.; Mah, W.; Cosa, G.; Skene, W. G.; Giasson, S. *Macromolecules* **2011**, 44, 8177.

(29) Liberelle, B.; Giasson, S. *Langmuir* **2008**, 24, 1550.

(30) Lego, B.; Skene, W. G.; Giasson, S. *Langmuir* **2008**, 24, 379.

(31) Lego, B.; François, M.; Skene, W. G.; Giasson, S. *Langmuir* **2009**, 25, 5313.

(32) Gilchrist, V. A.; Lu, J. R.; Keddie, J. L.; Staples, E.; Garrett, P. *Langmuir* **2000**, 16, 740.

(33) Ogieglo, W.; Wormeester, H.; Wessling, M.; Benes, N. E. *ACS Appl. Mater. Interfaces* **2012**, 4, 935.

(34) Xie, H.; Wei, J.; Zhang, X. *J. Phys. Conf. Ser.* **2006**, 28, 95.

(35) Fadeev, A. Y.; McCarthy, T. J. *Langmuir* **2000**, 16, 7268.

(36) Tripp, C. P.; Hair, M. L. *J. Phys. Chem.* **1993**, 97, 5693.

(37) Israelachvili, J. N.; Gee, M. L. *Langmuir* **1989**, 5, 288.

(38) Matyjaszewski, K.; Miller, P. J.; Shukla, N.; Immaraporn, B.; Gelman, A.; Luokala, B. B.; Siclovan, T. M.; Kickelbick, G.; Vallant, T.; Hoffmann, H.; Pakula, T. *Macromolecules* **1999**, 32, 8716.

(39) Audouin, F.; Larragy, R.; Fox, M.; O'Connor, B.; Heise, A. *Biomacromolecules* **2012**, 13, 3787.

(40) Hui, C. M.; Pietrasik, J.; Schmitt, M.; Mahoney, C.; Choi, J.; Bockstaller, M. R.; Matyjaszewski, K. *Chem. Mater.* **2013**.

(41) Gorman, C. B.; Petrie, R. J.; Genzer, J. *Macromolecules* **2008**, 41, 4856.

(42) Huang, C. L.; Tassone, T.; Woodberry, K.; Sunday, D.; Green, D. L. *Langmuir* **2009**, 25, 13351.

(43) Pasetto, P.; Blas, H.; Audouin, F.; Boissiere, C.; Sanchez, C.; Save, M.; Charleux, B. *Macromolecules* **2009**, 42, 5983.

(44) Tsujii, Y.; Ohno, K.; Yamamoto, S.; Goto, A.; Fukuda, T. *Adv. Polym. Sci.* **2006**, 197, 1.

(45) Behling, R. E., Williams, B. A., Staade, B. L., Wolf, L. M., Cochran, E. W. *Macromolecules*, 2009, 42, 1867–1872.

(46) Koylu, D.; Carter, K. R. *Macromolecules* **2009**, 42, 8655.

(47) Jeyaprakash, J. D.; Samuel, S.; Dhamodharan, R.; Ruhe, J. *Macromol. Rapid Commun.* **2002**, 23, 277.

(48) Liu, Y., Klep, V., Zdyrko, B. and Luzinov, I. *Langmuir*, 2004, 20, 6710-6718.

(49) Samadi, A.; Husson, S. M.; Liu, Y.; Luzinov, I.; Kilbey, S. M. *Macromol. Rapid Commun.* **2005**, 26, 1829.

(50) Boyes, S. G.; Akgun, B.; Brittain, W. J.; Foster, M. D. *Macromolecules* **2003**, 36, 9539.

(51) Constable, A.; Brittain, W. *Colloids Surf., A* **2007**, 308, 123.

(52) Rowe, M. A.; Hammer, B. A. G.; Boyes, S. G. *Macromolecules* **2008**, 41, 4147.

(53) Tran, Y.; Auroy, P.; Lee, L. T. *Macromolecules* **1999**, 32, 8952.

(54) Wu, T.; Gong, P.; Szleifer, I.; Vlcek, P.; Subr, V.; Genzer, J. *Macromolecules* **2007**, 40, 8756.

(55) Brandrup, J., Immergut, E. H., Grulke, E. A., Abe, Akihiro, Bloch, Daniel R, Eds Polymer Handbook, 4th ed; Wiley: New York, **1999**.

(56) Kobayashi, M.; Terayama, Y.; Ishikawa, T.; Terada, M.; Soejima, H.; Murakami, D.; Takahara, A. *ACS Sym. Ser.* **2012**, 1101, 183.

(57) Mori, H.; Boker, A.; Krausch, G.; Muller, A. H. E. *Macromolecules* **2001**, 34, 6871.

(58) Degennes, P. G. *Macromolecules* **1980**, 13, 1069.

(59) Milner, S. T.; Witten, T. A.; Cates, M. E. *Macromolecules* **1988**, 21, 2610.

(60) Israels, R.; Leermakers, F. A. M.; Fleer, G. J. *Macromolecules* **1994**, 27, 3087.

(61) Israels, R.; Leermakers, F. A. M.; Fleer, G. J.; Zhulina, E. B. *Macromolecules* **1994**, 27, 3249.

(62) Pincus, P. *Macromolecules* **1991**, 24, 2912.

(63) Zhulina, E. B.; Birshtein, T. M.; Borisov, O. V. *Macromolecules* **1995**, 28, 1491.

(64) Matthew, J. A. D. *Nature* **1988**, 331, 127.

(65) Chen, K. M.; Jiang, X. P.; Kimerling, L. C.; Hammond, P. T. *Langmuir* **2000**, 16, 7825.

(66) Aulich, D.; Hoy, O.; Luzinov, I.; Brucher, M.; Hergenroder, R.; Bittrich, E.; Eichhorn, K. J.; Uhlmann, P.; Stamm, M.; Esser, N.; Hinrichs, K. *Langmuir* **2010**, 26, 12926.

(67) Masiak, M.; Hyk, W.; Stojek, Z.; Ciszkowska, M. *J. Phys. Chem. B* **2007**, 111, 11194.

(68) Konradi, R.; Ruhe, J. *Macromolecules* **2005**, 38, 4345.

(69) Zhulina, E. B.; Borisov, O. V.; Birshtein, T. M. *Macromolecules* **1999**, 32, 8189.

(70) Birshtein, T. M.; Zhulina, E. B. *Ber. Bunsen-Ges. Phys. Chem.,* **1996**, 100, 929–935.

Chapter 5

Organophosphonic acids as viable linkers for the covalent attachment of polyelectrolyte brushes on silica and mica surfaces ‡‡

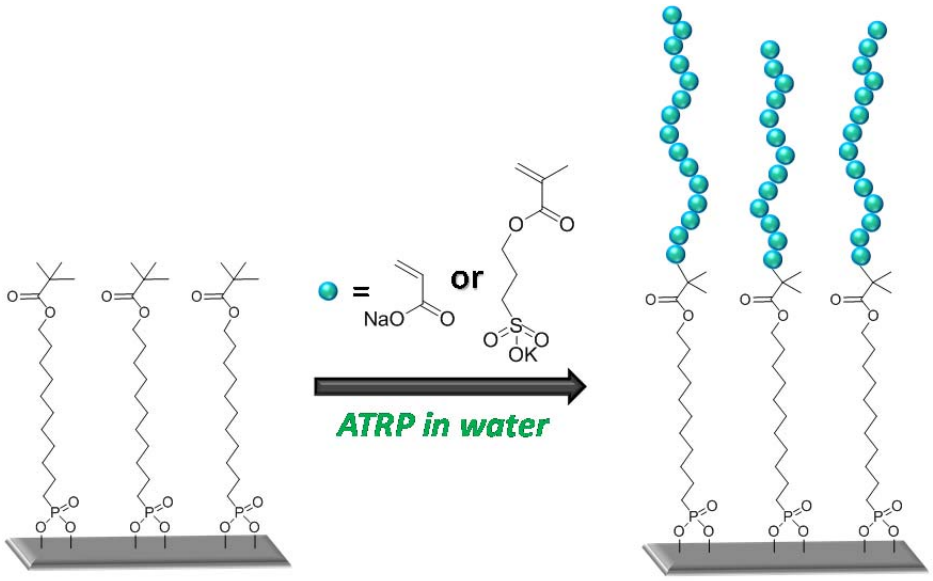

‡‡ ‡‡ This chapter is a verbatim copy of the paper submitted in the *Polymer Chemistry* (**2014**). It is co-authored by Vivian Machado, W. G. Skene and Suzanne Giasson.

5.1 Abstract

We report the first successful preparation of polyelectrolyte brushes using an ATRP initiator that was covalently grafted to silica and mica substrates via an organophosphonic acid. Covalent attachment of the initiator to silica and mica and its subsequent synthesis of polyacrylic acid (PAA) and poly(sulfopropyl methacrylic acid) brushes by water mediated-ATRP was confirmed by ATR-FTIR, ellipsometry, AFM, and contact angle measurements. The initiator–substrate bond was robust and could resist a large range of pH in the absence of salt. Interactions between PAA brushes anchored to mica via the organophosphonic acid initiator were investigated using the Surface Forces Apparatus. The results confirmed the robustness of the initiator–mica bond as the brushes could resist shearing and compression under relatively high applied loads.

5.2 Introduction

Grafting of polymer brushes is a particularly versatile way of tailoring the surface properties of materials such as wettability, lubrication, and biocompatibility.[1-3] Polymer brushes are monolayers of polymer chains with one chain end tethered to a surface. Polymer brushes are generally observed for large surface density of grafted chains for which the limited space forces the chains to stretch. The polymer chain conformation depends on the grafting density, molecular weight and chemical composition of the grafted chains.[4] In addition, end-tethered polymer brushes can change their conformation in response to the external trigger such as solvent quality, pH and/or ionic strength.[5] This dynamic behavior is widely exploited for developing smart materials, having tunable surface properties.[3, 6-8] One of the most suitable methods for preparing polymer brushes having a controlled grafting density and thickness is the *grafting-from* approach. This relies on synthesizing polymers directly from an initiator-modified surface in a well-defined manner.[9] By controlling the

initiator surface coverage and the polymer molecular weight, a wide range of polymer grafting densities and chain conformations are possible.[4]

Silicon oxide derivatives are widely used as substrates for synthesizing and characterizing polymer brushes.[10] Silica surfaces have a significant number of silanol groups that can undergo silanization reactions with organosiloxanes.[11] Surface polymerization takes advantage of an organosiloxane initiator monolayer that is covalently anchored to the surface via a Si–O–Si bond.[12, 13] However, the labile siloxane bond between the surface and the initiator is susceptible to hydrolysis, leading to polymer cleavage from silica substrates in aqueous media under extreme pH and ionic strengths.[14, 15] Organophosphonic acids are attractive alternatives to organosiloxanes for anchoring polymers to substrates. This is in part owing to the multiple bonds occurring between organophosphonic acids and various substrates.[16-18] These are expected to give rise to robustly grafted uniform monolayers. Indeed, grafted organophosphonic acids have shown higher stability than siloxanes on metallic surfaces even at pH 7.5 for 7 days.[19] For this reason, organophosphonic acids have also been grafted onto silica surfaces for various purposes such as immobilizing biological molecules,[20, 21] biosensor applications,[22] and organic thin-film transistors.[23-26] Despite their widespread use, only a limited number of studies have investigated the controlled surface polymerization from organophosphonic acid initiators and these exclusively focused on metal surfaces.[27-31] We therefore report the first controlled ATRP of polyelectrolytes using an organophosphonic acid initiator covalently attached to silica and mica substrates. Polyacrylic acid and poly(sulfopropyl methacrylic acid) brushes were examined owing to their known responsiveness to pH and ionic strength. They were additionally targeted to elucidate the role of brush conformation and electrostatic interactions in controlling adhesion and friction forces between surfaces in an aqueous environment. This is important because the use of dense end-grafted polyelectrolyte brushes has often been proposed for their remarkable lubricating properties. However, the role of the polymer's conformation and its degree of ionization in controlling friction remains unclear.[2, 32-

[34] Water-mediated ATRP was chosen because it is fast, straightforward, and compatible with the targeted hydrophilic monomers.[35] In addition, the desired polyelectrolytes can be prepared without additional experimental conditions and organic solvents that otherwise are incompatible with accurate surface measurements using a Surface Forces Apparatus (SFA). Herein, we demonstrate as a proof-of-concept that the organophosphonic acid (**5**, Scheme 1) is a viable alternative to its siloxane derivative for the ATRP of polyelectrolytes that are covalently grafted on both silica and mica substrates.

5.3 Experimental section

5.3.1 Materials and chemicals

Silicon wafers were obtained from University Wafer Co (100-mm diameter, boron-doped, (100) orientation, one side polished). All chemicals were used as received from Aldrich unless specified. Copper bromide (CuBr) was purified according to the previous report.[35] MilliQ water was obtained from Millipore A10 purification system with a resistivity of 18.2 MΩ·cm at 25° C. All surface manipulations were performed under an air flow cabinet and all glassware was carefully cleaned and oven-dried at 120^{o} C overnight.

5.3.2 5 synthesis

11-(2-Bromoisobutyrate)-undecyl-1-phosphonic acid was synthetized in five steps similarly to previously reported method (see Figure 5-S1 for synthetic scheme).[26]

11-Bromo-1-(tetrahydropyranyloxy)undecane (1). In a 100 mL round-bottom flask equipped with a stir bar, 11-bromoundecanol (3.3 g, 13.1 mmol) and a catalytic amount of *p*-toluenesulfonic acid (15 mg, 0.09 mmol) were mixed in

dichloromethane (15 mL) at room temperature. The flask was then immersed in an ice bath at 0°C and an excess of 3,4-dihydro-2H-pyrane (6 mL, 65.7 mmol) was added drop-wise. After stirring the reaction mixture at room temperature for 73 h, diethyl ether (20 mL) was added. The ethereal layer was washed 3 times with a saturated sodium chloride aqueous solution. It was then dried over $MgSO_4$, filtered, and concentrated under reduced pressure. The crude product was purified by column chromatography (silica gel, eluent – hexane:ether=10:1, stained by vanillin or PMA). The title compound was isolated as a yellowish liquid (3.6 g, 81 %). ^{1}H-NMR (400 MHz, $CDCl_3$): δ 1.28‑1.42 (m, 18H), 1.54-1.59 (m, 6H), 3.41 (m, 2H), 3.5 (m, 2H), 3.72 (m, 1H), 3.87 (m, 1H), 4.57 (dd, 1H). MS (ESI) m/z calculated 359 ($[M+Na+H]^+$); found 359.

11-(Diethylphosphoryl)-1-(2-tetrahydropyranyloxy)-undecane (2). In a 100 mL double-neck round-bottom flask fitted with reflux condenser was loaded with **1** (3.6 g, 10.7 mmol). It was then closed with a septum and triethyl phosphite (30 mL, 175 mmol) was added. The reaction mixture was stirred at 165° C for 48 h. Afterwards, the triethyl phosphite excess was removed by vacuum distillation at 40° C at 4 x 10^{-2} mm Hg. The title compound was obtained as a yellowish liquid (1.46 g, 35 %). ^{1}H NMR (400 MHz, $CDCl_3$): δ 1.25‑1.30 (m, 24H), 1.57 (m,2H), 1.70 (m, 6H), 3.35-3.37 (m, 1H), 3.85 (m, 1H), 4.08 (m, 4H), 4.56 (dd, 1H). ^{13}C-NMR (100 MHz, $CDCl_3$): δ 98.8, 77.4, 77.1, 76.7, 67.7, 62.4, 61.4, 61.3, 30.8, 30.7, 30.5, 29.8, 29.6, 29.5, 29.4, 29.1, 26.3, 25.5, 25.0, 19.7, 16.5. MS (ESI) m/z calculated 415 ([M+Na]+); found 415.

11-(Diethylphosphonyl)-undecanol (3). **2** (1.46 g, 3.7 mmol) and pyridinium-*p*-toluene-sulfonate (PPTS; 50 mg, 0.2 mmol) were combined in a 50 mL two-necked flask along with In methanol (15 mL) . The reaction mixture was refluxed at 60° C for 48 h. Afterwards, the mixture was cooled to room temperature and dichloromethane (20 mL) was added. The organic layer was washed 3 times with a saturated sodium chloride aqueous solution. It was then then dried over $MgSO_4$,

filtered, and concentrated under reduced pressure. The title compound was isolated as a yellowish liquid (1.1 g, 96 %). ^{1}H NMR (400 MHz, $CDCl_3$): δ 1.26‑1.30 (m, 24H), 1.54 (m, 2H), 3.62 (t, 2H), 4.08 (m, 4H). ^{13}C-NMR (100 MHz, $CDCl_3$): δ 77.4, 77.1, 76.7, 63.0, 61.4, 32.8, 30.7, 30.5, 29.5, 29.4, 29.3, 26.4, 25.7, 25.0, 22.4, 16.5. MS (ESI) m/z calculated 309 ($[M+H]_+$); found 309.

11-(2-Bromoisobutyrate)-undecyl-1-diethylphosphonate (4). In a 100 mL round bottom flask was loaded **3** (1.1 g, 3.6 mmol), anhydrous THF (10 mL), and an aqueous pyridine solution (99.5%; 1 mL, 12.4 mmol). 2-Bromoisobutyryl-bromide (1.2 mL, 9.7 mmol) was dissolved in THF (5 mL) and then it was added dropwise to the reaction mixture over 5 min. The reaction mixture was then stirred overnight at room temperature. Afterwards, petroleum ether (20 mL) was added and the organic layer was washed 3 times with 2 M HCl aq, twice with water, and twicet with a saturated sodium chloride aqueous solution. The organic layer was extracted, dried over $MgSO_4$, and filtered. The solvent was removed under reduced pressure and the resulting oil was purified by column chromatography (silica; hexane:ethyl acetate=1:9; stained with $KMnO_4$). The title compound was isolated as a yellow oil (0.6 g, 38 %). ^{1}H NMR (400 MHz, $CDCl_3$): δ 1.31 (24H), 1.67 (m, 2H), 1.92 (s, 6H), 4.08 (m, 4H), 4.16 (t, 2H). ^{13}C-NMR (100 MHz, $CDCl_3$): δ 171.8, 66.2, 61.5, 56.0, 30.8, 29.4, 29.1, 28.4, 26.4, 25.8, 24.9, 22.4, 16.5. MS (ESI) m/z calculated 459 ([M+2H]+); found 459.

11-(2-Bromoisobutyrate)-undecyl-1-phosphonic acid (5). A 50 mL round-bottom flask was loaded **4** (0.6 g, 1.3 mmol), afterwards bromotrimethylsilane (0.1 ml, 0.76 mmol) was added dropwise. The reaction mixture was stirred overnight at room temperature and then it was quenched with acetone/water (4/1) mixture. The excess acetone was removed under reduced pressure and the final product was isolated as a yellow powder (475 mg, 1.18 mmol, 90 %). ^{1}H NMR (400 MHz, $CDCl_3$): δ 1.3 (m, 18H), 1.7 (m, 2H), 1.95 (s, 6H), 4.19 (t, 2H). ^{13}C-NMR (100 MHz, $CDCl_3$): δ 171.9, 77.4, 77.0, 76.7, 66.2, 57.7, 56.0, 30.8, 29.5, 28.4, 25.8, 25.7, 21.6.

MS (ESI) m/z calculated 403 ([M+2H]+); found 403. HR-MS (ESI) m/z calculated 403 ([M+2H]+); found 403.

5.3.3 Substrate preparation and initiator immobilization

Silicon wafers

Silicon wafers were cut into 1x2 cm^2 pieces using a diamond pencil, sonicated in acetone for 20 min and then dried under nitrogen. The substrates were activated using a Piranha solution (H_2SO_4(conc.):H_2O_2=70:30 v:v) for 20 min at room temperature. (Caution: Piranha solution is extremely corrosive and should be used with absolute carefulness!) Afterwards, the substrates were removed from the Piranha solution and they were washed with copious amounts of MilliQ water, absolute ethanol, and finally dried thoroughly under nitrogen. The ATRP initiator (**5**) was solubilized in anhydrous dichloromethane (vide infra) at a concentration of 10^{-2} M. The clean substrates were immersed into the initiator solution overnight at room temperature under argon. They were then removed from the solution, washed with dichloromethane, and sonicated for 15 min in a triethylamine solution (2 mM) in dichloromethane. Afterwards, the surfaces were rinsed with dichloromethane, dried under nitrogen, and finally annealed at 140^oC for 3 h in the oven. The phosphonic acid initiator (**5**) modified surfaces were subsequently either used for ATRP polymer grafting or stored in at desiccator under an inert atmosphere.

SFA samples

Back-silvered mica pieces were glued silver side down to SFA silica discs using an optical adhesive (Norland Products Inc., USA). The prepared surfaces were treated with a H_2O/Ar plasma to generate an active mica silanol surface.[36] The partial pressure of Ar_2 was 80mTorr resulting in total pressure of Ar_2 and water of

300 mTorr. After plasma activation, the disks were immediately transferred into a compartmentalized flask filled with the phosphonic acid initiator solution in anhydrous THF at a concentration of 10^{-2} M. The substrates were then removed from the solution, soaked in 2 mM triethylamine solution in THF for 30 min, rinsed with THF, dried under a steam of nitrogen, and finally annealed at 140^{o}C for 3 h. Afterwards, the **5**-modified SFA samples were used for surface initiated (SI) ATRP of sodium acrylate (NaA).

5.3.4 5 recycling

The excess of **5** used in the grafting solutions was isolated and reused several times without any detrimental effect either on the grafting or polymerization. A 50 mL round- bottom flask containing the **5** solution was closed with a septum and the solvent was evaporated under a stream of argon until dry. The product was stored in the same flask under argon. The product stability and structural integrity were was confirmed by HR-MS (Figure 5-S17).

5.3.5 Synthesis of conventional ATRP initiator and its grafting to silica

The ATRP initiator, 3-(chlorodimethylsilyl)propyl-2-bromoisobutyrate (**6**) was synthesized according to previous reports.[35] Piranha-treated silicon substrates were exposed to a 10^{-3} M initiator solution in toluene for overnight at room temperature under nitrogen.[35] Afterwards, the initiator-covered surfaces were washed with toluene, absolute ethanol, and finally dried under a steam of nitrogen. The freshly prepared initiator-functionalized silica substrates were either used for surface-initiated polymerization or stored in a desiccator until used.

5.3.6 Synthesis of polyacrylic acid (PAA) and poly(3-sulfopropyl methacrylate) (PSPMAA) brushes via ATRP from initiator-functionalized silica and mica surface

A typical polymerization from the initiator-modified substrate (silica or mica) was as follows: bipyridine (129 mg, 0.83 mmol) and CuBr (48 mg, 0.33 mmol) were mixed in 100 mL double-necked round bottomed flask and the mixture was deoxygenated under vacuum and backfilled with argon three times. $CuBr_2$ (15 mg, 0.07 mmol) was added to the mixture and three vacuum-argon cycles were performed. Sodium acrylate (NaA) (9 g, 95.7 mmol) or 3-sulfopropyl methacrylate potassium salt (KSPMA) (23.5 g, 95.7 mmol) was solubilized in milliQ water (15 mL) along with methanol (3 mL) at room temperature. The resulting solution was degased for 30 min by purging it with argon. The monomer was transferred to the catalyst mixture and the mixture was stirred at 50^o until a homogeneous brown solution was obtained. The initiator-bearing substrates (maximum 4) were placed into an oven-dried compartmentalized flask, which was deoxygenated under vacuum and backfilled with argon three times. The monomer/catalyst solution was then transferred to the compartmentalize flask by cannula. Polymerization was done for 1 h at room temperature. The reaction was stopped by opening the flask and exposing the catalyst to air. The substrates were removed, soaked in milliQ water for overnight (> 8 h), and then soaked in ethanol for 1 h followed by drying under nitrogen. Under these conditions, the salt is converted to the corresponding acid.

5.3.7 PAA degrafting/swelling studies

Trizma base buffer solutions (0.1 M) were prepared with MilliQ water and the pH was adjusted to 7.5, 9.0, 9.5, 10.0 and 10.5 with different volumes of HCl (0.1 M). The pH was measured with a Symphony SB20 pH meter with Ag/AgCl

electrode. The ionic strength was adjusted by adding NaCl (10 mM) to the Trizma buffer solution.

5.3.8 Surface characterization

Contact angle measurements

The water wettability of initiator- and polymer-covered substrates was measured with a FTA200 dynamic contact angle analyzer (First Ten Angstrom) in the equilibrium static mode using MilliQ water as the probe liquid. Fta32 Video software was employed for data analyses. At least three separate measurements were done for each substrate and the average contact angle value was determined within an error of $\pm 3^{o}$.

AFM measurements

All surface topographical studies in air (unless specified) were performed using a MultiMode microscope equipped with a NanoScope V extended controller (Digital Instruments, Santa Barbara, CA) at room temperature with a constant humidity $\leq$ 40%. The surfaces were imaged in a tapping-mode using an ACTA silicon probe tip from AppNano with a resonance frequency of ~300 kHz and a spring constant of 40 N/m. All dry images were obtained at 1 kHz scan rate, medium oscillation damping (15–20%) and resolution of 512 x 512 pixels. NanoScope 7.30 software was used to treat the images. At least three different areas were analyzed for each surface.

All AFM images in liquid were recorded using a Dimension 3100 MultiMode Scanning Probe Microscope equipped with Veeco NanoScope V extended controller (Digital Instruments, Santa Barbara, CA) by using HYDRA-All-G silicon nitride

probes tip A or B. Triangular tip A with a resonance frequency of ~66 kHz and a spring constant of 0.29 N/m was used for imaging the polymer-coated surfaces at pH 9.5 and 10.5. Tip B with a resonance frequency of ~17 kHz and a spring constant of 0.045 N/m was used at low pH (5.5-8.5). A sample was fixed inside a custom-made Teflon liquid cell, filled with buffer solution, and left to equilibrate for at least 2 h before scanning**.** All images were done in the tapping mode at 1 kHz scan rate with an image resolution of 512 x 512 pixels and weak oscillation damping (10-15%). NanoScope 7.30 software was used to treat the images. A scratch on the polymer layer was made by using a scalpel and the height difference between bare substrate and an outer layer of the polymer film was measured by step-height analysis at three different regions for each sample.

Spectroscopic ellipsometry

The thickness of the initiator- and polymer-coated silica substrates was measured using an Ellipsometer M2000V from J.A.Woollam Co at a 75° angle of incidence at room temperature in air. The wavelength range from 370 to 1000 nm was used. Three different spots were analyzed for each sample. The modeling and data fitting were performed using the WVASE32 software (J. A. Woollam Co, version 3.768). A 2 nm (±0.03 nm) thick silicon oxide layer was measured prior to surface modification and it was considered as a constant when modeling the initiator and polymer layers using the Cauchy layer, assuming transparent and homogeneous polymer films.

Fourier Transform Attenuated Total Reflection Infrared Spectroscopy (ATR-IR)

ATR infrared spectra of the initiator- and polymer-modified silicon wafers were recorded with a Tensor 27 Bruker Optics spectrometer equipped with a Harrick Seagull accessory. A germanium ATR crystal was used with p-polarized light at an incidence angle of 60^{o}. The spectra were compile from 1024 scans at a resolution of 4 cm^{-1}.

Forces measurements with SFA

The surface forces technique (SFA) and detailed experimental procedures for measuring the normal and friction forces are described elsewhere.[38, 39] In brief, two back-silvered molecularly smooth mica surfaces are glued to cylindrically curved silica lenses of radius R=2 cm. The force−distance profile between the surfaces is obtained by changing the position of the lower surface using a nanopositioner and measuring the actual variation in the separation distance between the surfaces with an interferometry technique using Fringes of Equal Chromatic Orders (FECO) with subnanometric resolution. The interaction force is then determined from the deflection of the spring by using Hooke's law.[38, 39] The upper surface is mounted on a motor-driven sliding device allowing lateral motion. Shearing cycles are carried out by moving the upper surface at constant velocity over a certain distance after which the driving direction is reversed. The upper surface is connected to a vertical cantilever spring whose lateral deflection, allowing the friction force to be determined, is measured using strain gauges with an accuracy of ±10-3 mN.

5.4 Results and discussion

5.4.1 Initiator grafting to silica and mica

The rationale for pursuing an organophosphonic acid (**5**) as an ATRP initiator immobilized on silica substrates was to demonstrate that functional groups other than siloxyl derivatives could be used for controlled surface polymerization of polyelectrolytes. This is of importance given the limited number of examples demonstrating the viability of alternate functional groups for the covalent immobilization of *grafted from* polymers on silica substrates. Organophosphonic acids are advantageous over commonly used trialkoxy silyl counterparts because they consistently form monolayers without stringent deposition protocols. The organophosphonic acid derivative (**5**) was prepared as a proof-of-concept to demonstrate that it could sustain ATRP while being covalently attached to silica substrates. The targeted **5** was prepared by expanding upon known methods, starting from commercially available 11-bromoundecanol.[27] The hydroxyl of 11-bromoundecanol was protected by attaching 2-tetrahydropyranyl group with the presence of catalytic amount of *p*-toluenesulfonic acid. The yield of the protected product **1** was 81%. Nucleophilic displacement of the bromide of **1** by diethyl phosphonate was done in 35% yield. The obtained **2** was deprotected to afford **3** in 96% yield. Next, 2-bromoisobutyryl was introduced to **3** in 38% yield. For the last step, the diethyl groups were removed to afford the final product **5** in 90% yield and 9% overall yield for the five steps.

Owing to the reduced reactivity of silica surfaces towards organophosphonic acids compared to metal oxides, a modified aggregation and growth ("T-BAG") method was used for grafting the initiator to the substrate.[41] This was used as an initial grafting protocol because of the limited number of studies of organophosphonic acid grafted to silica and mica substrates.[21, 42] The given surfaces were immersed into either a 10^{-3} M dichloromethane or THF solution of **5** overnight (Scheme 5-1). The substrates were then cleaned in triethylamine solutions of DCM

and THF by sonication. This was done to ensure the formation of only a monolayer. The substrates were finally annealed thermally at 120-140^{o} C for 3 h to ensure covalent bonding of the targeted **5** to the substrate.[41]

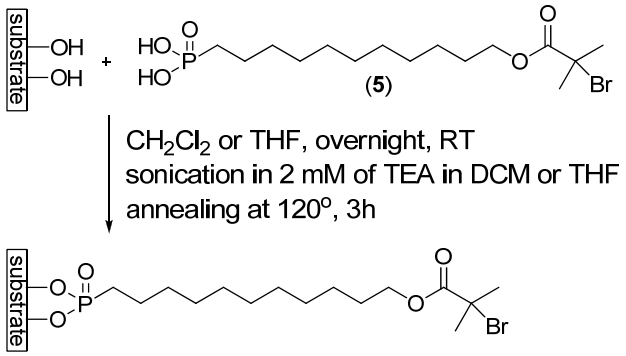

Scheme 5-1. Schematic representation of **5** coupling to silica or mica surfaces.

The resulting **5**-modified surfaces were characterized by water contact angle, ellipsometry, ATR-FTIR, AFM measurements. Water contact angles of 65^{o} and 62^{o} were observed for the initiator-modified silica and mica, respectively (Table 5-1). Meanwhile, an initiator film thickness of 0.9 nm (Table 5-1) was measured by ellipsometry.

Table 5-1. Thickness and contact angle of water on **5**-modified silica and polymer brushes

Substrate	Thickness, nm[a]	Contact angle, degrees [o a]
5-modified silica	0.9±0.2[b]	65±3
5-modified mica	-	62±3
PAA brushes on **5**-modified silica	17±4	25±3
PSPMAA brushes on **5**-modified silica	13±4	30±3

Concentration of the grafting solution of **5** is 10^{-2} M.

[a] The thickness was measured by ellipsometry in air after sonication step.

[b] The error is a standard deviation from three different measurements.

The measured contact angles were similar to previously reported values for alkylsilane initiator-modified substrates bearing an identical initiating group. The large contact angles measured confirm the increased hydrophobicity of the surface upon grafting of **5**. This suggests that the initiator is coupled to the substrate, especially when comparing the contact angle to Piranha treated native glass slides whose θ=0.[14]

While water contact angle measurements only provide qualitative evidence for **5** deposited on the substrate, unequivocal evidence of chemical bonding of **5** to the SiO_2 substrate was provided by ATR-FTIR. Measurements were done after sonicating the initiator-coated substrate in triethylamine solutions in DCM. This step was to remove any physisorbed initiator. Immobilization of **5** on silica was confirmed by comparing its spectra to an authentic powder sample of **5** that was not attached to a surface. Clear evidence of covalent attachment of the initiator to the substrate is had by examining the 800-1300 cm^{-1} spectral region (Figure 5-1).[43]

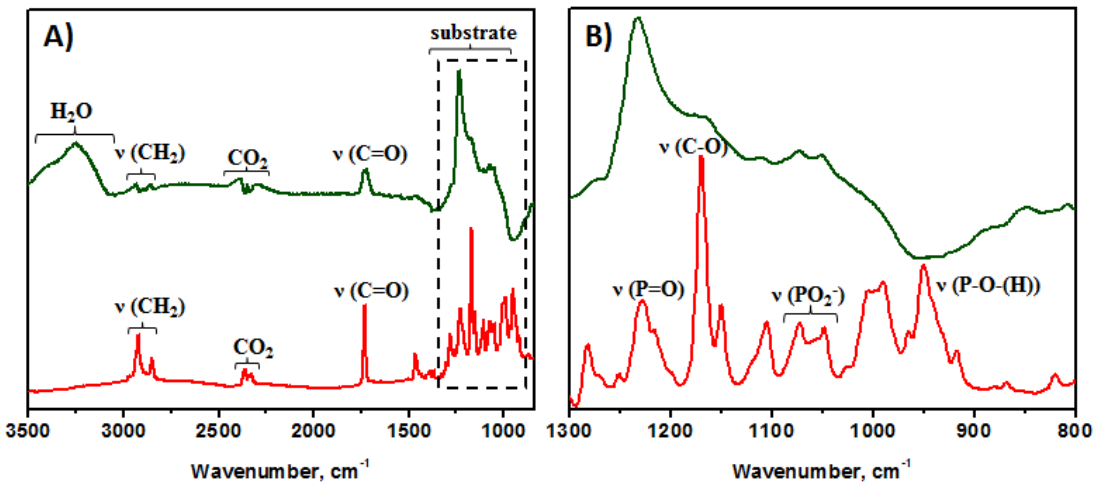

Figure 5-1. A) ATR-FTIR spectra of **5** as a powder (red line) and immobilized on silica (dark green line). The ATR-FTIR spectrum of bare silica was subtracted from the spectrum of the immobilized **5**. B) Expanded region corresponding to the dashed line from (A).

The loss of the P–O–H signal between 930 and 955 cm^{-1} confirms covalent attachment of **5** to the silica substrate. This is further supported by the vibrations from PO_2^- group at 1072-1048 cm^{-1} observed in the spectrum of **5**-modified silica.

ATR-FTIR was further beneficial for providing information about the surface packing. It is well known that the position of the methylene peak correlates with the degree of ordering of the alkyl chains in the film.[44-46] The asymmetric CH_2 stretching of disordered chains usually occurs at higher wavenumbers (~2925 cm^{-1}) than that of well-ordered chains (~2915 cm^{-1}). Figure 5-1A shows the different relative intensity of the two characteristics CH_2 peaks for **5** in powder and immobilized **5**. After immobilizing the initiator on silica, the CH_2 stretching dominates at higher wavenumbers, suggesting a weak organization and alignment of the alkyl chains on the surface. This can be attributed to the bulky 2-bromo-2-methylpropionyloxy groups that prevent the layer from forming a close packed arrangement.[27]

Figure 5-2 illustrates the surface topography of the **5**-modified silica (A2, A3) and mica (B2, B3) surfaces. Randomly-distributed particles-like structures having a relative height of ca. 3 nm can be observed on both substrates. Since the length of a fully extended **5** is 2.05 nm (Figure 5-S18), the observed particle-like structures most probably correspond to initiator aggregates on the surface. However, the overall low surface roughness measured by AFM (rms of 0.4 for silica and 0.2 nm for mica) suggests a relative homogeneous grafted initiator layer.

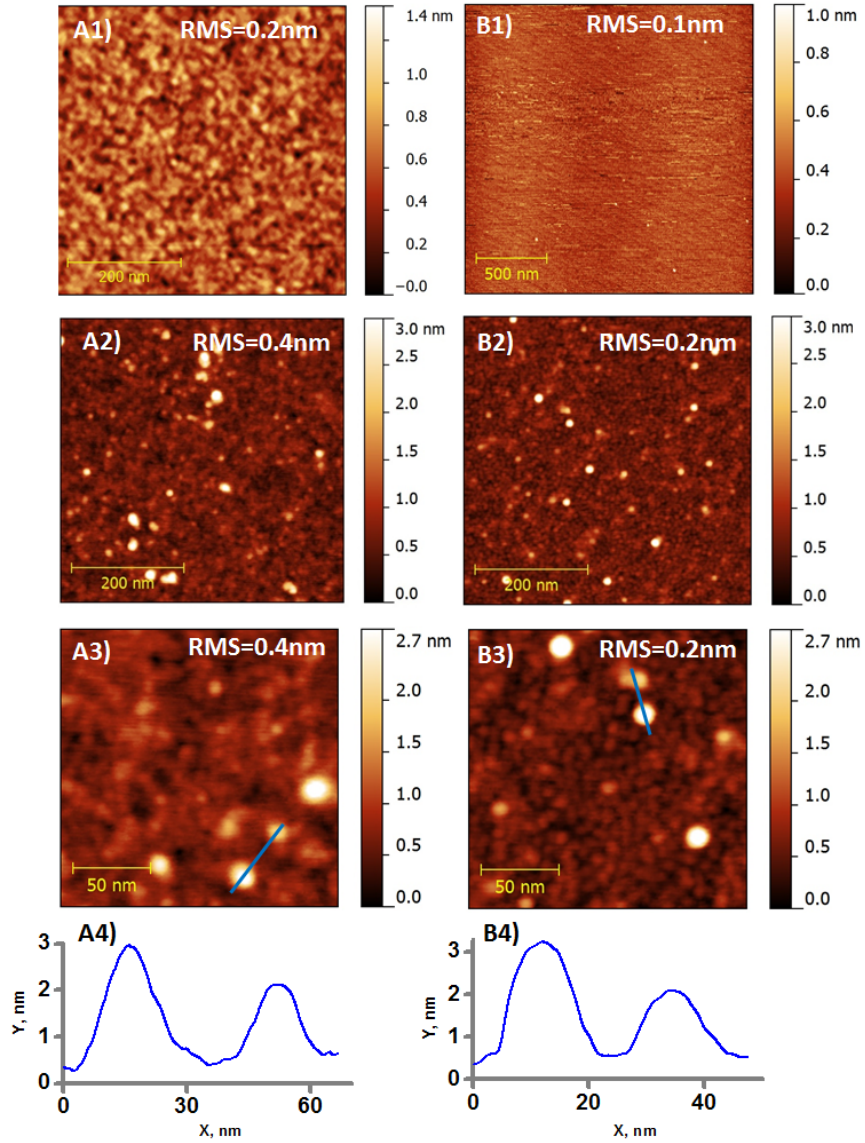

Figure 5-2. AFM images of native silica (A1 (0.5x0.5 um)) and native mica (B1 (2x2 um)), **5**-modified silica (A2 (0.5x0.5 um), A3 (1.75x1.75 um)), and **5**-modified mica (B2 (0.5x0.5 um), B3 (1.75x1.75 um)). AFM images (A2, A3, B2, B3) were obtained with SmartSPM (AIST-NT Inc, Novato) in the semicontact mode and Hi-Res C - 14/Cr-Au probes (Mikromasch). All images were done in air.

5.4.2 ATRP of immobilized organophosphonic acid initiator

The capacity of **5**-immobilized on silica to initiate the polymerization of different monomers was confirmed by synthesizing polyacrylic acid sodium salt (NaPAA) and poly(3-sulfopropyl methacrylic acid) potassium salt (KPSPMAA) polyelectrolyte brushes (Scheme 5-2). The ATRP of NaA and KSPMA using the **5**-modified silica wafer was done in water at room temperature using a CuBr/Bipyridine catalyst. A $CuBr_2$ to CuBr ratio of 1:5 was used to moderate the polymerization. This ratio was found to be optimal for fast polymerization and for forming films of sufficient thickness for accurate swelling studies. They were characterized by ellipsometry, ATR-FTIR, AFM and contact angle measurements. After polymerization, the water contact angle of the coated substrates decreased and the grafted layer thickness increased, compared to the original **5**-immobilized substrates (Table 5-1).

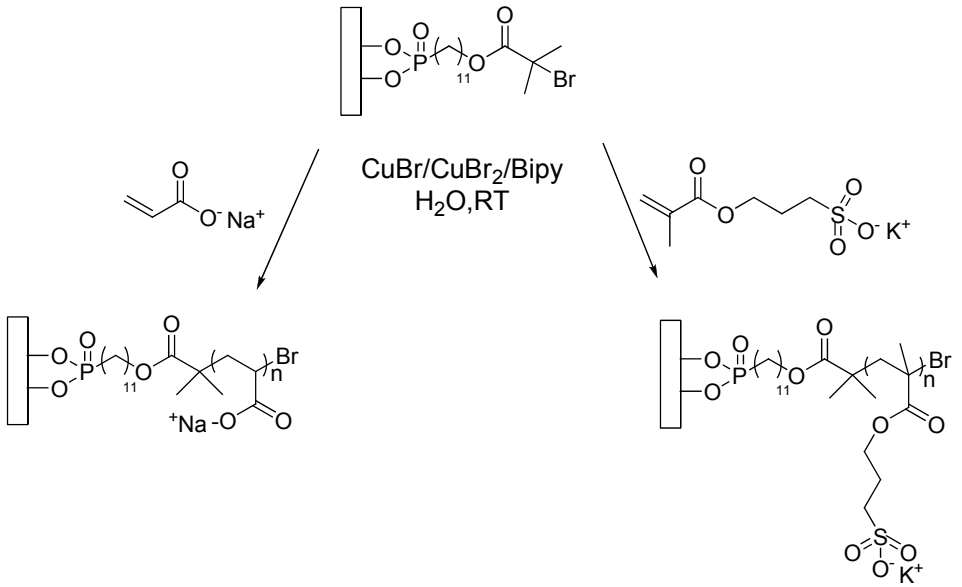

Scheme 5-2. Synthetic scheme for the preparation of PAA and PSPMAA brushes from surface immobilized **5**.

The resulting polyelectrolyte brushes were converted to their corresponding acid (COOH) by washing the surfaces with MilliQ water (vide supra) as confirmed by ATR-FTIR. The ATR-FTIR spectra of the PAA showed a strong signal at 1575 cm^{-1}, corresponding to COO^- (Figure 5-3). Also, the broad peak at 1730 cm^{-1} indicates the presence of hydrogen-bonded carboxylic acids, consistent with previous reports for similar PAA brushes.[47] The presence of both COO- and COOH bands confirms the partial ionization of the carboxylic acid groups. Similarly, the FTIR spectrum of the PSPMAA brushes clearly showed a narrow band at 1730 cm^{-1}, corresponding to the carbonyl. Meanwhile, the sulfonate was confirmed by the two strong peaks at 1195 and 1050 cm^{-1}. These correspond to the asymmetric and symmetric sulfonate stretches.[48]

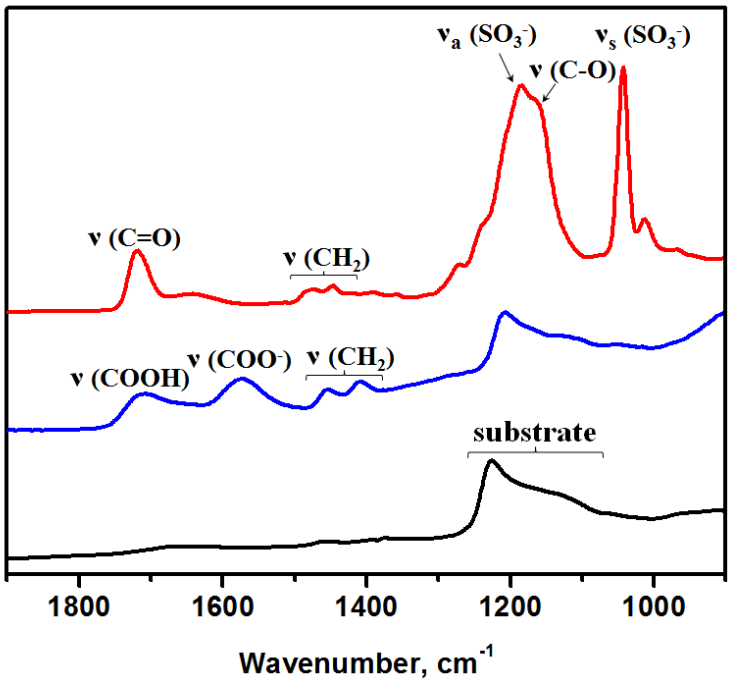

Figure 5-3. ATR FTIR spectra of PSPMAA (red) and PAA (blue) layers immobilized on silica (black) substrates. PAA and PSPMAA layer thickness is 20 and 13 nm, respectively.

The thickness of the polymerized films was quantitatively determined by ellipsometry. An average dry polymer layer thickness of 17 nm for PAA and 13 nm for PSPMAA was measured after 1 h of polymerization (Table 5-1). Both the PAA and PSPMAA layers were smooth with a rms of 0.4 nm (Figure 5-4 A1-A3) and 0.9 nm, respectively (Figure 5-4 B1-B3).

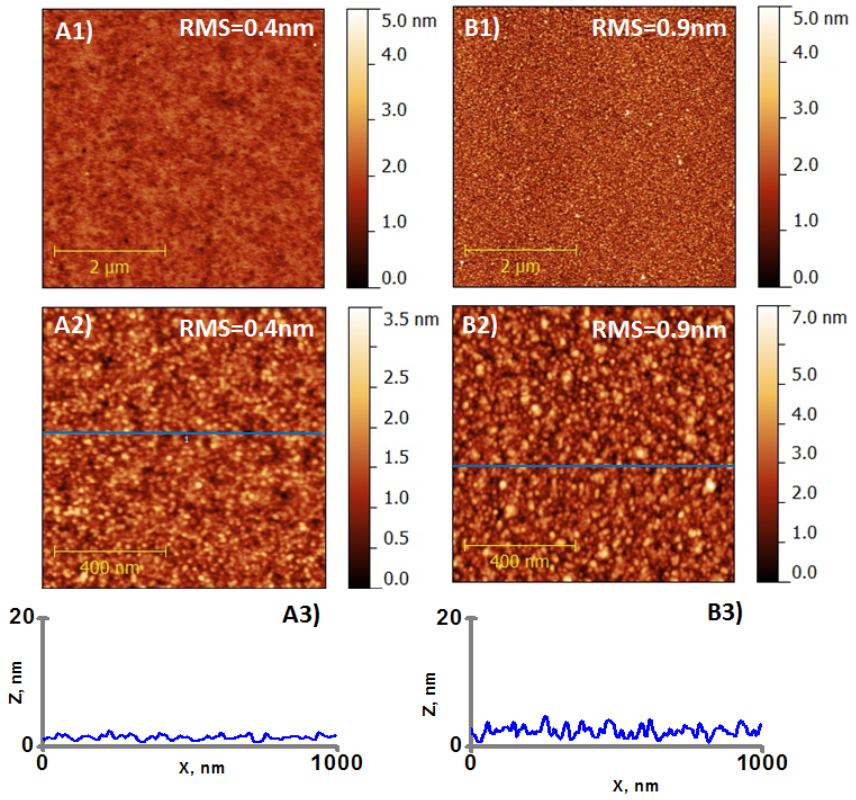

Figure 5-4. AFM images (A1 (5x5um), A2 (2x2 um)) and surface topographical profile (A3) of PAA brushes grafted from **5**-functionalized silica. PAA film thickness=15 nm. AFM images (B1 (5x5um), B2 (2x2um)) and surface topographical profile (B3) of PSPMAA brushes grafted from PI-functionalized silica. PSPMAA film thickness=14 nm. All images were done in air.

It should be noted that significant differences in the polymer layer thickness were obtained when polymerizing the same monomer with identical polymerization

conditions with immobilized **5** and **6**. While both have the same initiator (bromoisobutyrate), the aliphatic chain separating the surface-bound and polymerizable ends of **5** is longer than **6**. Using similar polymerization conditions and an initiator concentration of 10^{-3} M for the surface functionalization, a dry PAA thickness of 2 nm and 120 nm (Figure 5-S12, A) was measured for silica surfaces coated with **5** and **6**, respectively. The different thickness can be attributed to the different initiator surface coverage (Figure 5-5). Since **6** has a shorter aliphatic segment than **5**, it is expected to form a denser monolayer, resulting in a higher amount of initiating sites on the surface. We previously showed that an increase in initiator coverage is associated with an increase in water contact angle.[14, 15] An increase in concentration of the grafting solution of **5** (from 10^{-3} to 10^{-2} M) also resulted in an increase in the contact angle (from ca 60 to ca 65 ^{o}) as well as an increase in brush thickness (from 2 to 19 nm). Therefore, the smaller contact angle measured for the **5** –covered silica (60±3^{o}) compared to **6**-covered silica (72±3^{o}) for the same initiator concentration (10^{-3} M) suggests a difference in the initiator surface coverage. This can explain the difference in the resulting brush thickness.

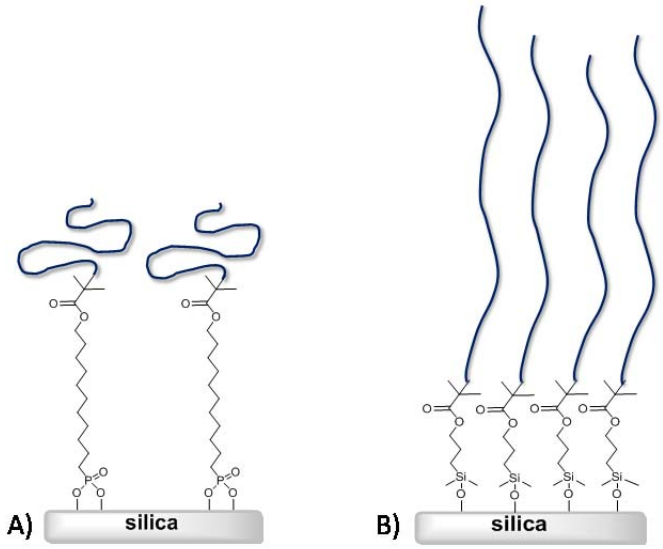

Figure 5-5. Schematic representation of polymer brushes grafted from **6** (A) and **5** (B) immobilized on a silica substrate.

5.4.3 Hydrolytic stability of PAA brushes grafted from a silica immobilized 5 and 6

The stability of the substrate–initiator bond was investigated with PAA brushes polymerized with the silica immobilized **5** and **6** under similar polymerization conditions. The brush swelling and grafting robustness were assessed by measuring the brush thickness at different pH and ionic strength using the AFM step-height method. The thickness of the PAA layer grafted from **6** progressively decreased with increasing pH from 7.5 to 10.0 in the absence of salt (Figure 6). The PAA thickness decrease can arise from either polymer collapse or polymer detachment from the surface. Polymer collapse can be dismissed because the PAA brush was previously demonstrated to swell with increasing pH for this process.[15] This swelling behavior is also confirmed experimentally[15, 49, 50] and predicted by theory[51] for weakly charged polyelectrolyte brushes. Therefore, the decrease in PAA thickness is most probably due to polymer degrafting. This is in contrast to previous studies that reported no PAA degrafting from silica immobilized derivatives of **6** in salt-free solutions at pH between 5.5 and 10.5.[14, 47] Different PAA degrees of ionization and initiator coverage resulting from different experimental conditions can account for the observed discrepancy. The polymerization conditions used for water-mediated ATRP (pH 8.5) favor the ionization of the carboxylic acid to its carboxylate, whereas the PAA brushes obtained in non-aqueous-mediated ATRP are expected to be neutral.[14, 47] Indeed, a previous report confirmed no PAA brush swelling at pH < 7.5, regardless of the initiator surface coverage, when the brush was prepared in organic solvents using siloxane initiator-covered silica.[47] This behavior was explained by the initial hydrophobicity of the PAA brushes prepared in organic solvents that block water and ions from penetrating the brush that would otherwise cleave the substrate–initiator bond. On the other hand, PAA brushes prepared in aqueous-media are significantly swollen at pH 7.5 (Figure 5-6A). They are therefore

more permeable to water and ions and favor hydrolysis of the substrate–initiator bond.

The behavior of the PAA brush prepared from the immobilized-**5** is different from that of the immobilized-**6** (Figure 5-6). In contrast to **6**, the brush thickness for the immobilized-**5** significantly increased from pH 9.0 to 10.0, regardless of the ionic strength. This suggests a more stable substrate–**5** bond compared to its substrate–**6** counterpart under similar polymerization conditions. The thickness increase with pH is the result of the increasing number of deprotonated carboxylic acid groups along PAA chains. This causes the electrostatic repulsion between the chains and brush swelling. At higher pH (10.5), the PAA layer thickness slightly increased in salt-free solutions, whereas it drastically decreased in the presence of 10 mM NaCl (Figure 5-6B, S13). Polymer cleavage was reported for PAA prepared from immobilized-**6** at similar pH and with added salt.[14, 47] It was shown, theoretically and experimentally, that salt can promote the dissociation of the carboxylic acids.[49, 51] This leads to highly stretched chains that are hydrated, making the substrate–initiator more susceptible to hydrolysis by hydroxyl ions, and ultimately, polymer detachment.[14, 47] Even though numerous stimuli-sensitive polyelectrolyte brushes studies have been reported, the exact swelling responses of PAA brushes and the conditions leading to their cleavage from the surface remain unclear. This is in part owing to the lack of systematic control of the initiator grafting density and molecular weight of the brushes between different analyzed samples. Nevertheless, our comparative study (Figure 5-6) clearly shows the resistivity of the substrate–**5** bond towards hydrolysis over a large range of pH, especially in the absence of salt, compared to the substrate–**6** bond. The stability of the substrate–initiator bond was theoretically evaluated using Density Function Theory. This was done by calculating the bond dissociation enthalpy (BDE) of the substrate–initiator bond, using the heats of formation (ΔH_f) of the corresponding compounds. The BDE was calculated according to: [ΔH_f (substrate–initiator) + ΔH_f $(H_2O)_n$] - [ΔH_f (substrate) + ΔH_f (initiator)], where n= 1 for **6** and n=2 for the bidentate bonding for **5** to the surfaces. $Si(OH)_4$ was used as a representative model

for the silica substrate to significantly reduce the computational times. This simplification is valid given only the relative BDE of the substrate-initiator are targeted and not the absolute values. Gas phase geometric optimization was done using the 6-31g* basis set. Single point energies and the corresponding ΔH_f of the optimized geometries were calculated by applying a given solvent continuum. While the absolute ΔH_f cannot be accurately calculated for a given compound, the relative values, and hence the BDE, are highly representative of the actual bond strengths. Therefore, the relative BDE of the different substrate–initiator bonds can accurately be calculated according to: ΔBDE=[BDE(substrate–**5**)] - [BDE(substrate–**6**)]. The calculated ΔBDE was 14 kJ/mol (gas phase), 46 kJ/mol (dichloromethane), and 120 kJ/ mol (water). The theoretical calculations confirmed the substrate–**5** bond is indeed stronger than the corresponding substrate–**6** bond, especially in water.

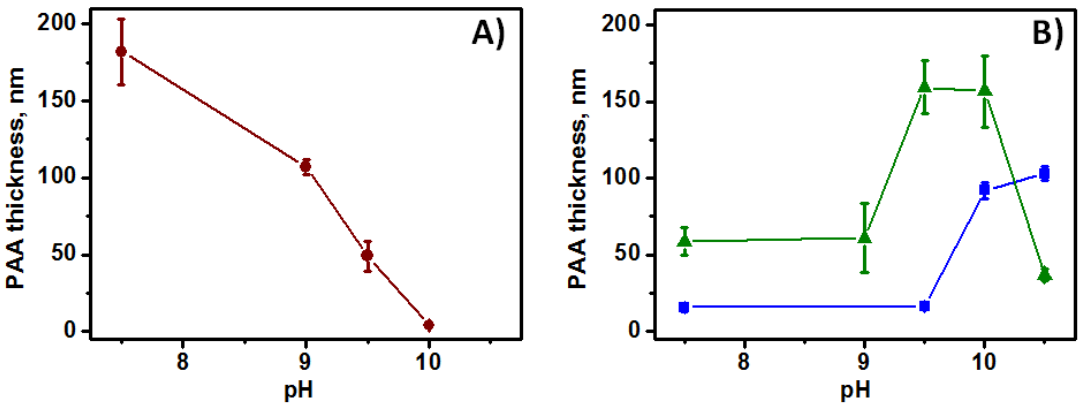

Figure 5-6. A) Variation of the PAA layer thickness grafted from initiator **6** at different pH without added salt. pH was increased from 7.5 to 10.0. Original dry PAA thickness=120 nm. B) Variation of PAA layer thickness prepared from immobilized 5 at different pH without (squares) and with added (triangles) NaCl. Original dry PAA thickness=20 nm. The sample was exposed to non-salty buffer solution with pH increased from 7.5 to 10.5. Sample was soaked in milliQ water for overnight and then exposed to buffer solutions with pH ranged from 7.5 to 10.5 with added salt. All thickness measurements were done in situ using AFM.

5.4.4 Surface forces characterization

Normal and friction forces between two PAA layers of mica immobilized-**5** were measured using SFA under different pH and ionic strength. This was to assess the adhesion, friction and resistance to compression and shear of the polyelectrolyte brushes. The force profiles were measured step-wise during both approach and separation and each separation distance was measured at equilibrium. This was taken at a distance variation of less than 0.5 nm/min. Measurements were done on five different pairs of PAA coated mica surfaces and they were reproduced on different contact positions with the same pair of surfaces. A wait time of 2 hours was set between each approach-separation cycle. The friction forces were measured at different separation distances ranging from large distances (corresponding to a negligible applied normal load) to smaller distances, corresponding to pressure of ca 40 atm for all pairs of surfaces. As for the force profiles, the lateral motion was initiated once the variation in the separation distance was less than 0.5 nm/min. The reported friction forces, F_s, are the average kinetic forces measured in the steady-state conditions (i.e., constant driving velocity and friction forces). The reported measurements were done at a sliding velocity of 1 μm/s for comparison with previously reported results. All reported friction forces were measured in the absence of surface damage, confirmed by the direct visualization of the contact region with the optical interferometry technique used for force measurements.

Figure 5-7 shows the measured normal force profiles in water at 25 °C for different pH (5.5 and 9.5) and salt concentrations (0 and 10 mM NaCl) between two PAA layers on mica prepared from immobilized-**5**. For given pH and salt concentration, the forces profiles were not systematically reproducible and they exhibited hysteresis. These results suggest significant surface heterogeneity and thickness variability between the pairs analyzed. This most likely is from slight variances in the different degrees of polymerization[52, 53] and polydispersities[54] of the brushes between different samples, even when polymerized in the same reactor using

identical polymerization conditions.[9, 55] The variable polydispersity of the polymer brushes are confirmed by AFM surface roughness measurements. The film roughness (rms) of PAA polymerized from mica immobilized-**5** ranged from 1.3 to 2.3 nm (Table 5-S1). This is much rougher than previously reported *grafted to* PAA brushes whose surface roughness was 0.5 nm.[49] The rough film polymerized from the immobilized-**5** suggests that the polymer molecular weight and/or grafting density are not well controlled with *grafted from*. Therefore, the polymer's structural changes in response to its surroundings cannot be accurately quantified. Nevertheless, the on-approach and separation force profiles measured are typical of those for polymer brushes. Only the on-approach measured surface profiles are illustrated for clarity. It should be noted that the force profiles do not clearly exhibit the long-rang exponential decay that is characteristic of double-layer electrostatic interactions. This would suggest that onset of the repulsion corresponds to the initial compression of the two apposing brush layers (i.e. twice the non-perturbed brush thickness). Half the onset distances for the mica immobilized PAA range between 50 and 225 nm is significantly larger than the measured AFM step-heights for the corresponding silica immobilized PAA of ca 20-160 nm (Fig. 5-7). This can be explained by the two different approaches used to determine thickness with both instruments, AFM and SFA. The AFM thickness (or step-height) was determined using a semi-contact mode, which does not exclude the compression of the brushes. With SFA, the thickness was inferred from the range of the repulsive forces which is sensitive to the non-compressed outer most segments of the brushes. In addition, the long-ranged repulsive forces may also include some non-contact electrostatic effects. Therefore, it is expected to measure a larger thickness by the non-compressed SFA compared to AFM.

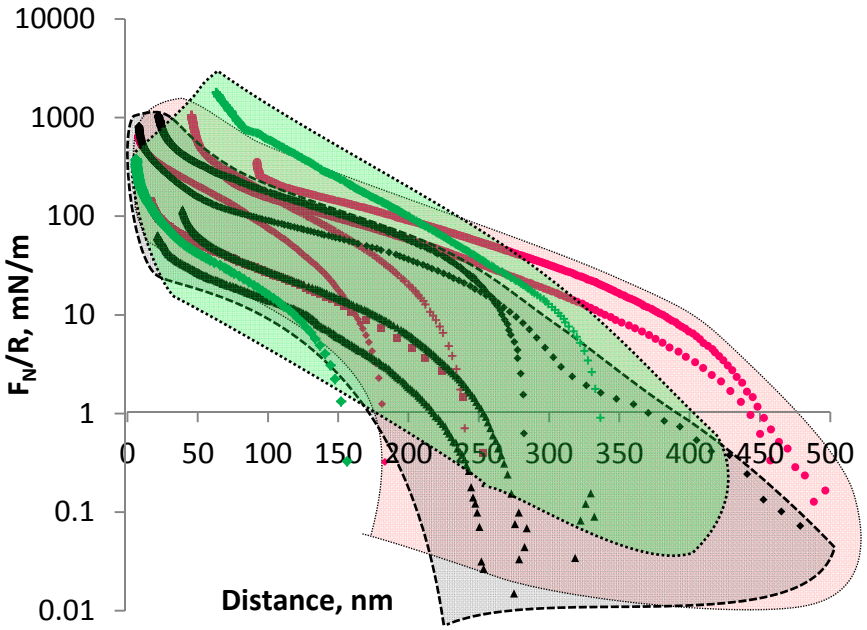

Figure 5-7. Normalized force profiles measured on approaching two opposing PAA brushes across (pink) water, (green) buffer solution pH 9.5 without salt and (gray) buffer solution pH 9.5 with salt. The shade areas represent the variability in the measured force profiles and the most representative profiles are illustrated. The PAA brushes were prepared on five mica pairs obtained from three independents experiments. (■) sample 1, (●) sample 2, (▲) sample 3 (◆) sample 4 and (+) sample 5.

The relationships between the friction force (F_S) and the normal load (F_N) for three different experimental conditions with and without added salt are depicted in Figure 5-8. As can be seen from the normal forces profiles, the responsiveness of the brush to changes in pH and ionic strength cannot be unequivocally identified from the F_S measurements (Figure 5-8). The F_S versus F_N curves are delimited by two linear regimes, which set the limiting values of the friction coefficient. The friction coefficients measured with the different samples range from ca 0.4 to 1.1 in salt-free water and increase to a maximum value of 3.9 with added salt. The values are

relatively high compared to those previously measured between two *grafted to* PAA brushes under similar experimental conditions.[49] The measured friction coefficients are more consistent with those measured by AFM for poly(2-(dimethylamino)ethyl methacrylate) brushes *grafted-from* gold.[50]

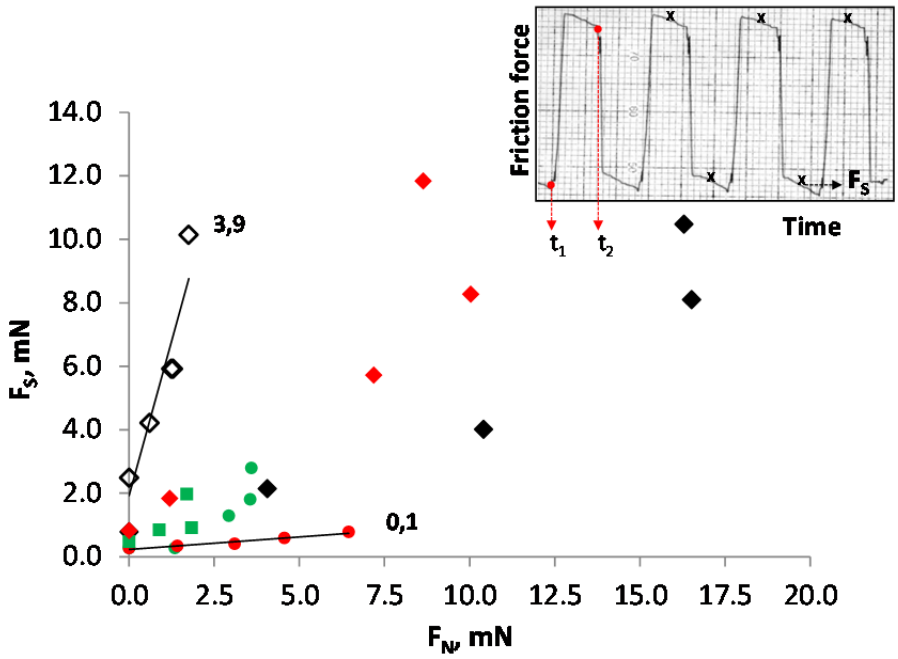

Figure 5-8. Friction force, F_S, as a function of the normal force, F_N, between two opposing PAA brushes measured in water (red symbols), buffer solution pH 9.5 without salt (green symbols) and buffer solution pH 9.5 with 10 mM salt (black symbols). Sample 1 (■), sample 2 (●), and sample 4 different spots (◆, ◇). All measurements were done at a sliding velocity of 1μm/s. Inset: typical friction traces. t_1 and t_2 illustrate times where sliding direction was reversed.

The different friction coefficients for the *grafted-to* and *grafted-from* PAA brushes are most probably due to variations in the surface roughness, where the rms of *grafted*-from PAA in water was 1.3 as opposed to 0.4 for the *grafted-to* PAA. This is based on the well-known fact that the surface roughness has a significant effect on the friction coefficient, where it increases with surface roughness.[56,57] It is worthy to

note that although high friction coefficients were obtained, the surfaces were not damaged during the force analyses. No surface damage was observed even under applied loads up to 20 mN/m, corresponding to pressures of ca 40 atm. This confirms the strong covalent attachment of the organophosphonic acid to the mica substrate and illustrates the suitability of this anchoring group as a robust alternative to siloxanes.

5.5 Conclusions

An organophosphonic acid (**5**) was investigated as an alternative to commonly used organosiloxanes for robustly immobilizing an ATRP initiator to silica and mica. Covalent attachment of a monolayer of **5** to both mica and silica substrates was possible. We demonstrated for the first time that the covalently grafted **5** to silica underwent surface polymerization of NaPAA and KPSPMAA via water-mediated ATRP to afford polyelectrolyte brushes. The swelling behavior of the resulting grafted PAA brushes and their resistance to cleavage from the substrate at pH<10.5 demonstrated the robustness of the **5**–substrate bond. The robustness of the **5**–mica bond was further illustrated by surface force measurements, where PAA brushes resisted shearing and compression upwards of several atmospheres. It was successfully proven that organophosphonic acids are viable alternatives to siloxanes derivatives for the robust covalent attachment of ATRP initiators to silica surfaces. **5** is an attractive anchor for preparing covalently immobilized responsive smart materials that can sustain a wide range of environmental conditions. Meanwhile, SFA measurements demonstrated the complexity of controlling the thickness and surface homogeneity of PAA brushes prepared from water-mediated ATRP. The polydispersity and molecular weight of the polyelectrolytes *grafted-from* **5**-substrates are important parameters that need to be examined in more detail because they affect the surface roughness of the polymer film and the brush surface properties.

5.6 Acknowledgements

Financial support from the Natural Sciences and Engineering Research Council of Canada and Fondation Québécoise pour la Recherche en Nature et Technologies are acknowledged. Canadian Foundation for Innovation is also acknowledged for additional equipment and infrastructures. The Center for Self-Assembled Chemical Structures is also acknowledged. The authors thank Prof. C. Pellerin and Ms. M. Richard-Lacroix for access to the ATR-FTIR instrument and measurements, respectively. AIST NT and Mr. A. Kayev are also acknowledged for high resolution AFM images of the **5**-modified substrates.

5.7 Supporting information

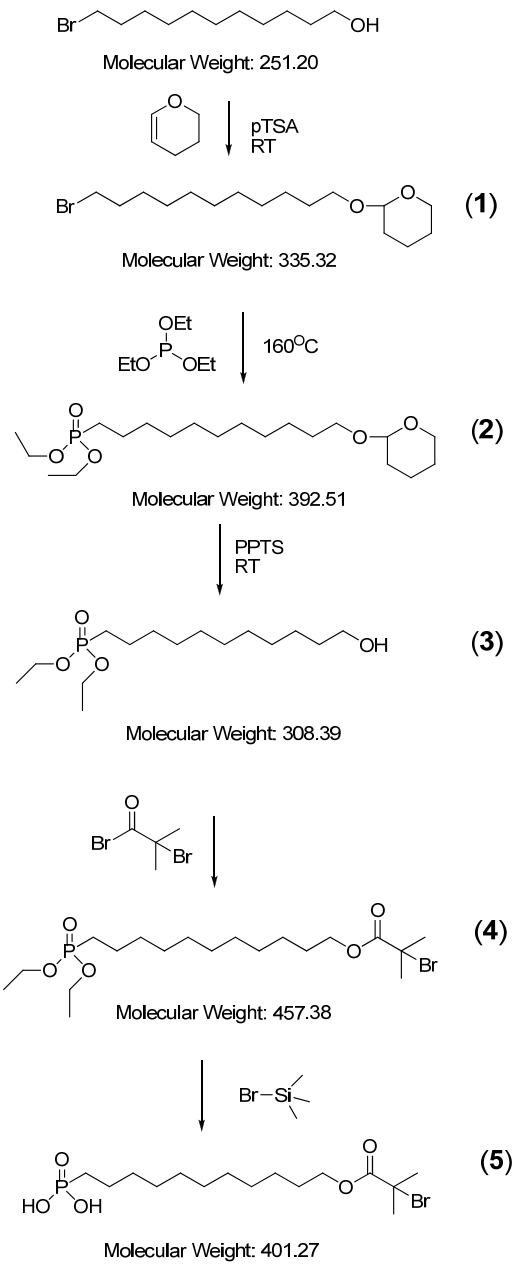

Figure 5-S1. Synthetic scheme for the preparation of phosphonic initiator (**5**).

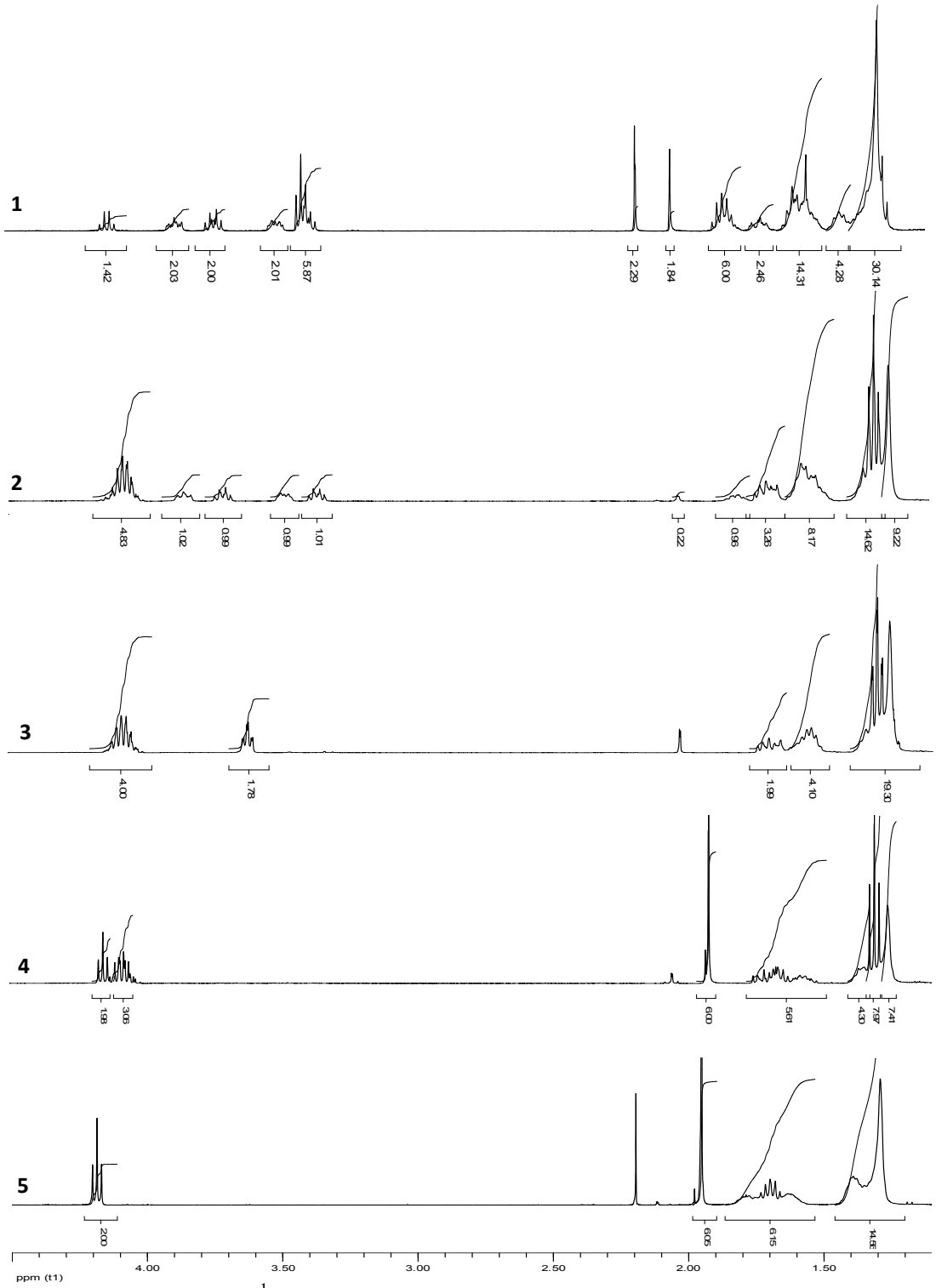

Figure 5-S2. ^{1}H NMR spectrum of **1**, **2**, **3**, **4** and **5** in chloroform.

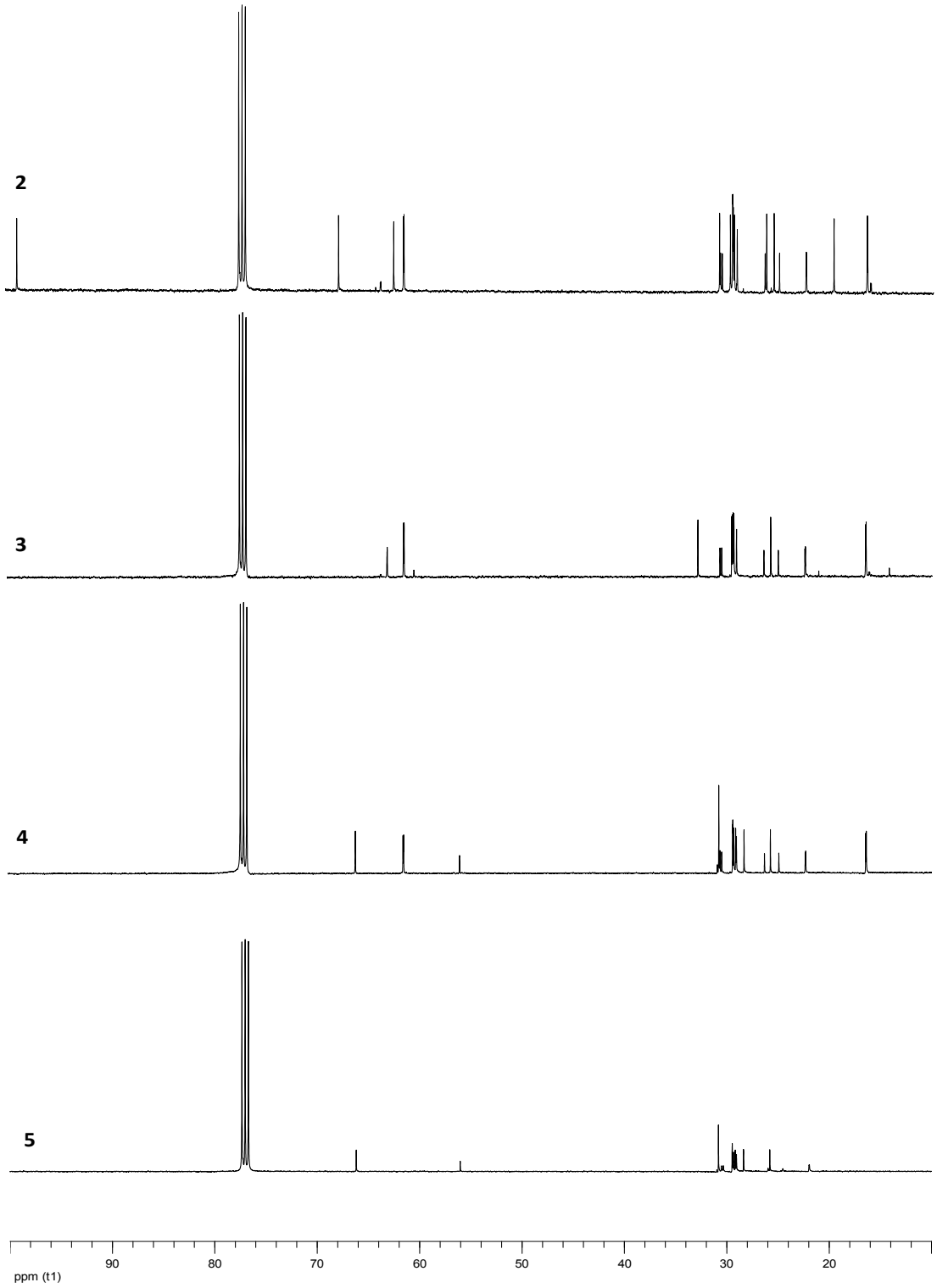

Figure 5-S3. ^{13}C NMR spectrum of **2**, **3**, **4** and **5** in chloroform.

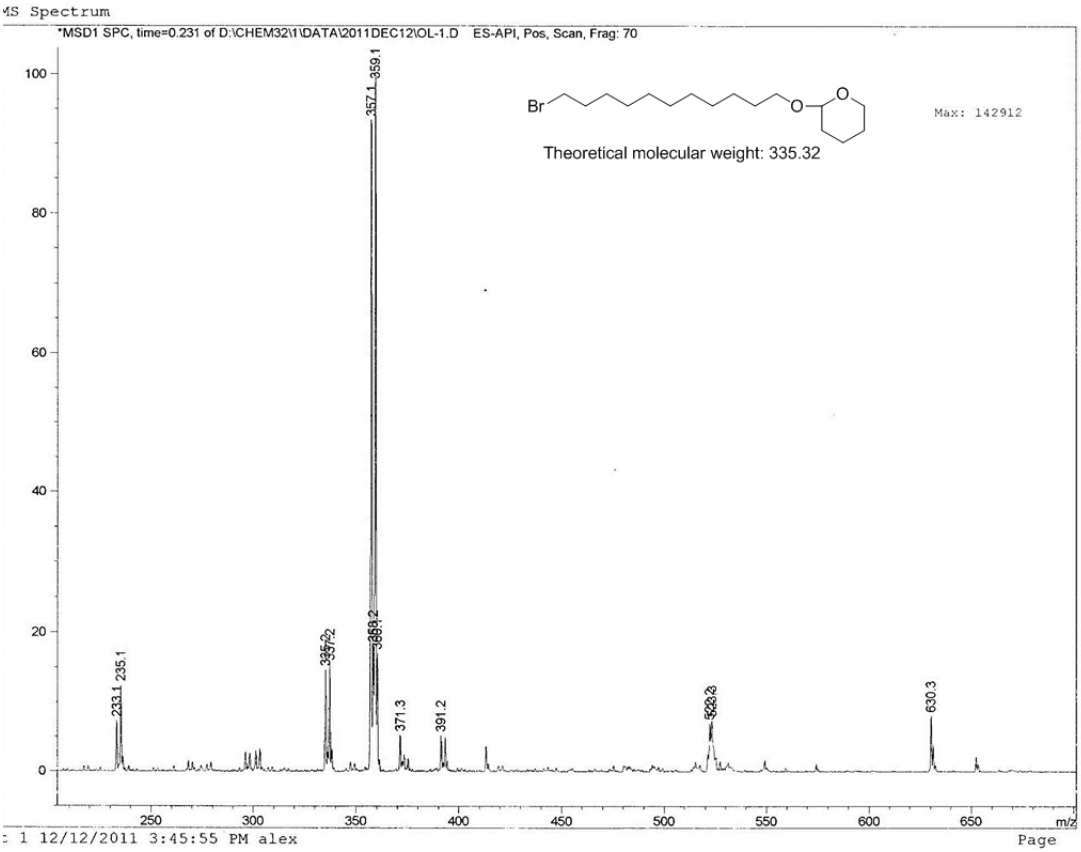

Figure 5-S4. Mass spectrum of **1**.

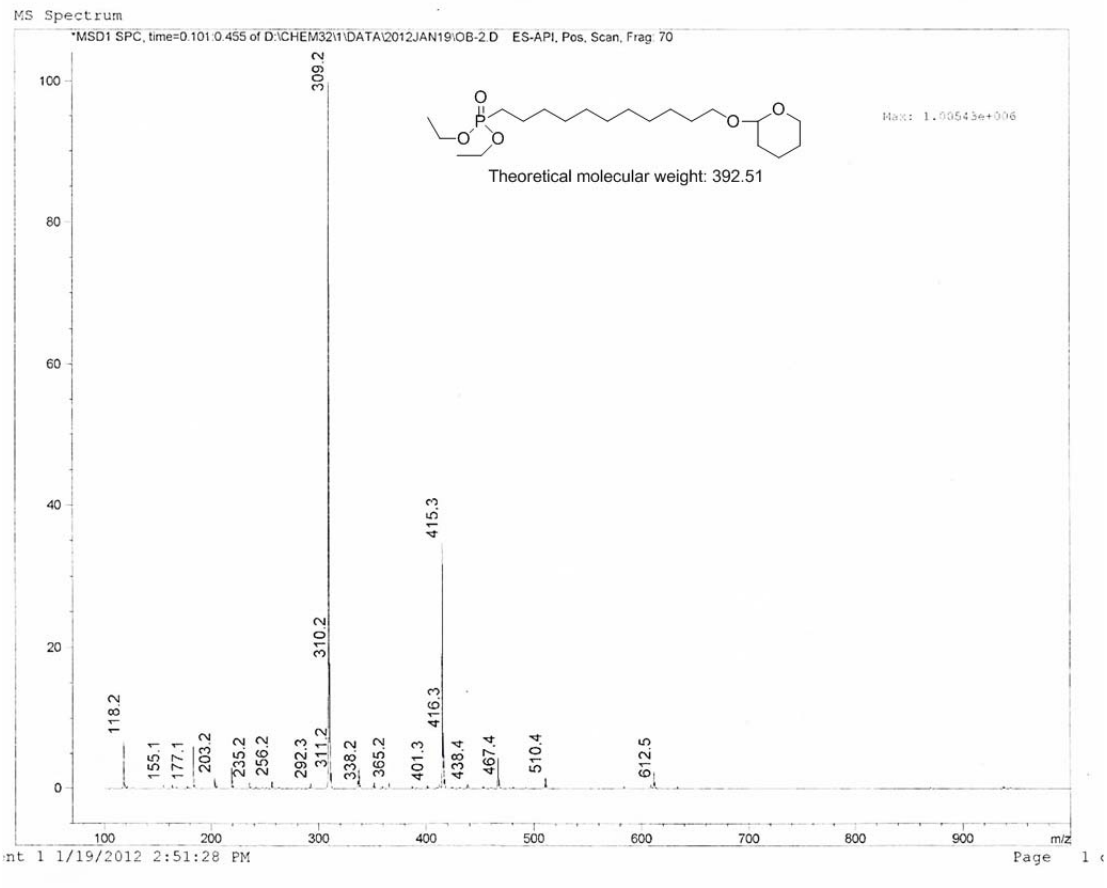

Figure 5-S5. Mass spectrum of **2**.

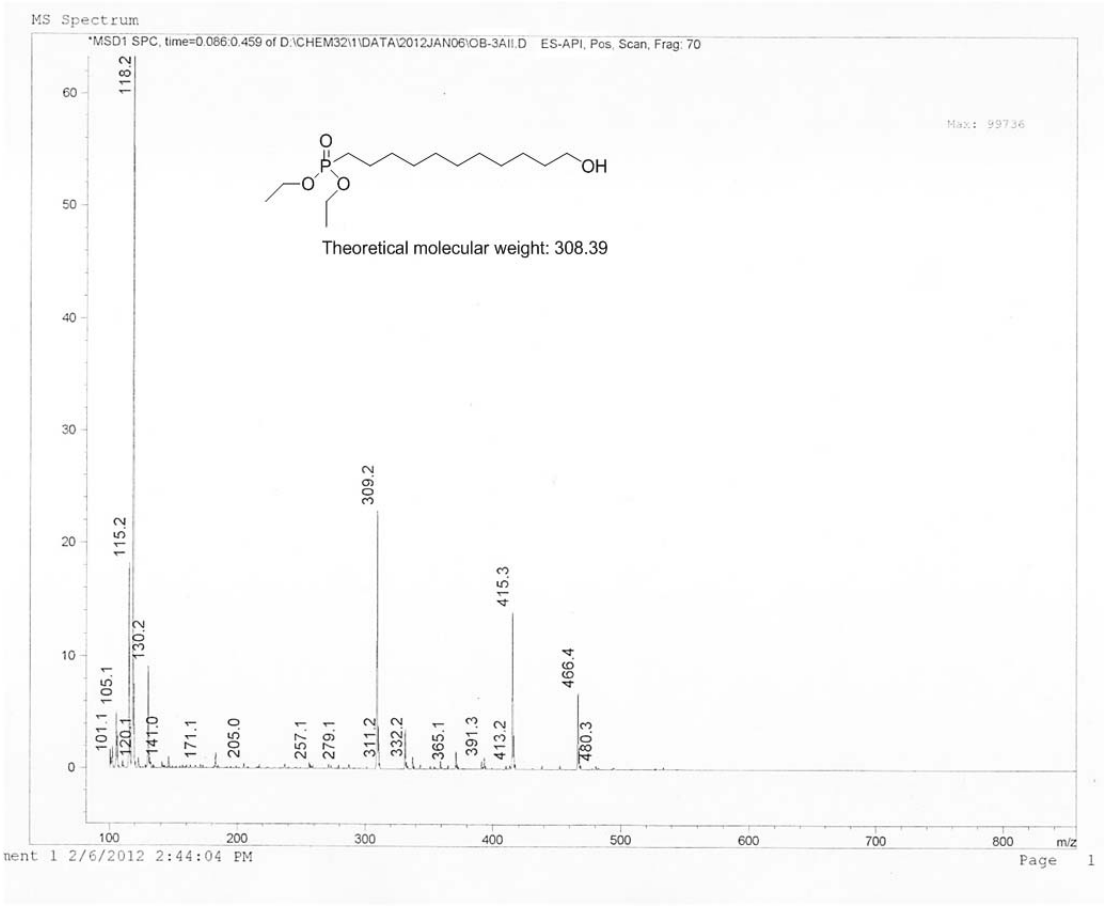

Figure 5-S6. Mass spectrum of **3.**

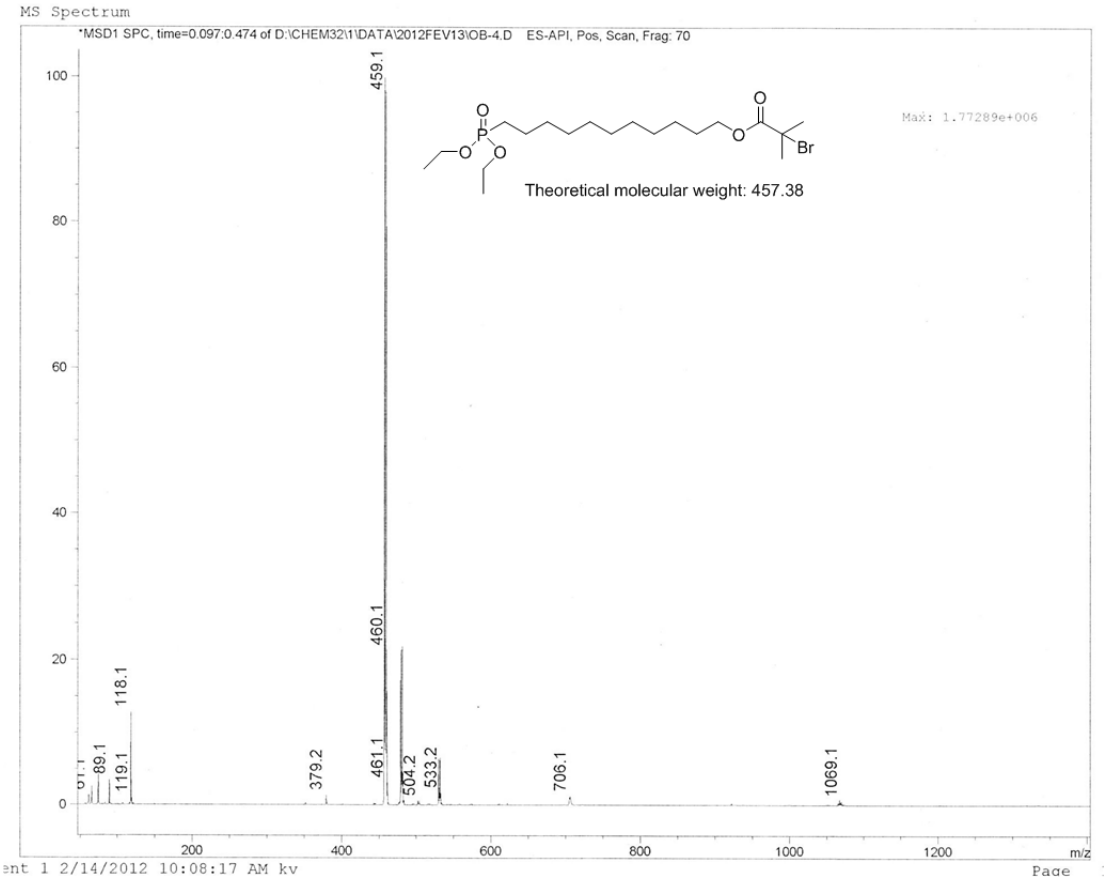

Figure 5-S7. Mass spectrum of **4**.

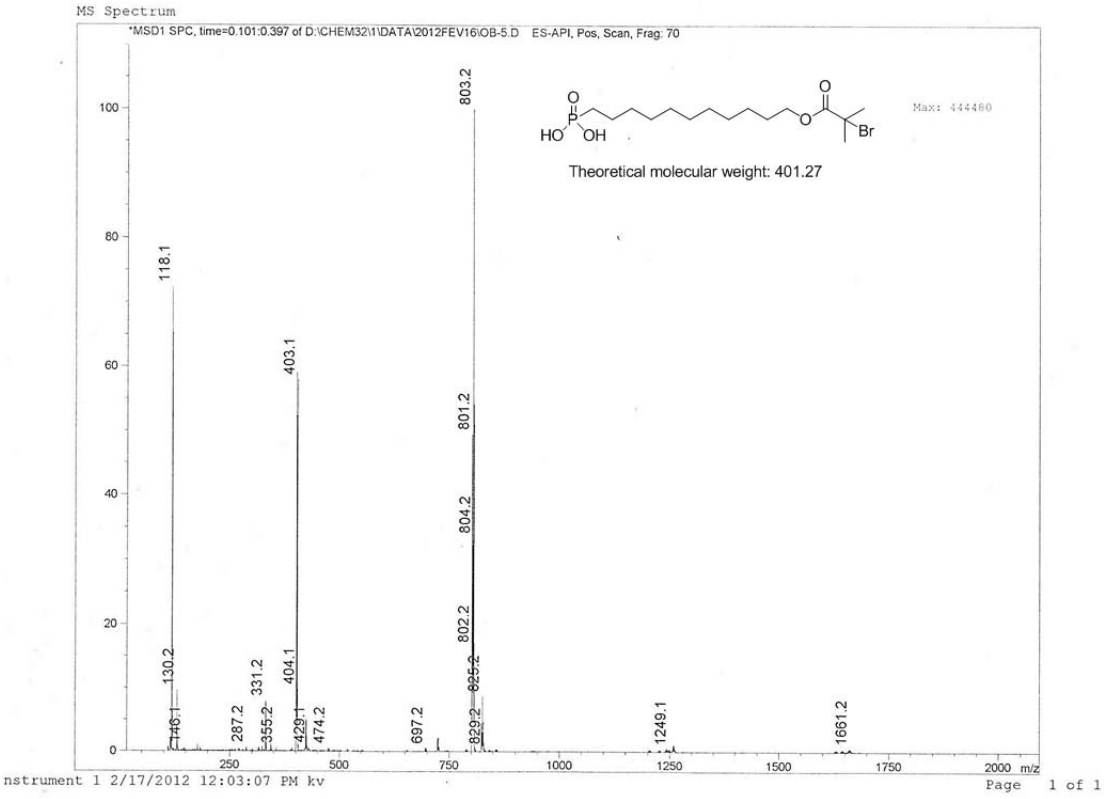

Figure 5-S8. Mass spectrum of **5.**

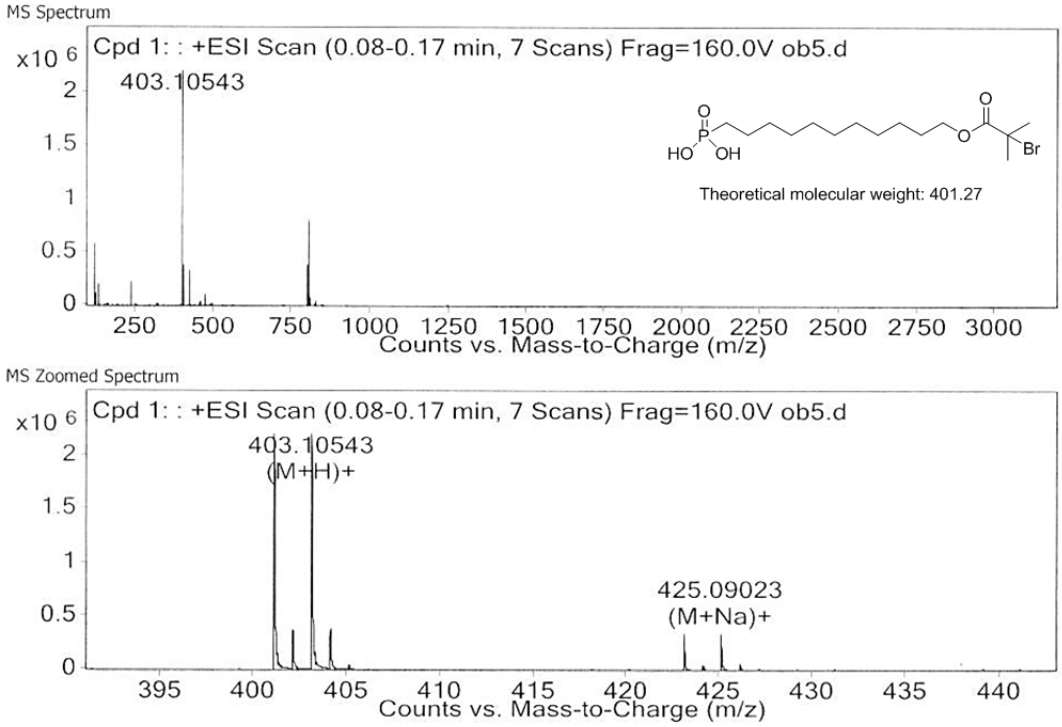

MS Spectrum Peak List

Ion	Ion Formula	Abund	*Expe. m/z*	*Calc. m/z*	Diff(ppm)
(M+H)+	C15H31BrO5P	2244287.5	401.10728	401.1087	-3.53
(M+Na)+	C15H30BrNaO5P	349695.1	423.09209	423.09064	3.41

Figure 5-S9. High resolution mass spectrum of **5**.

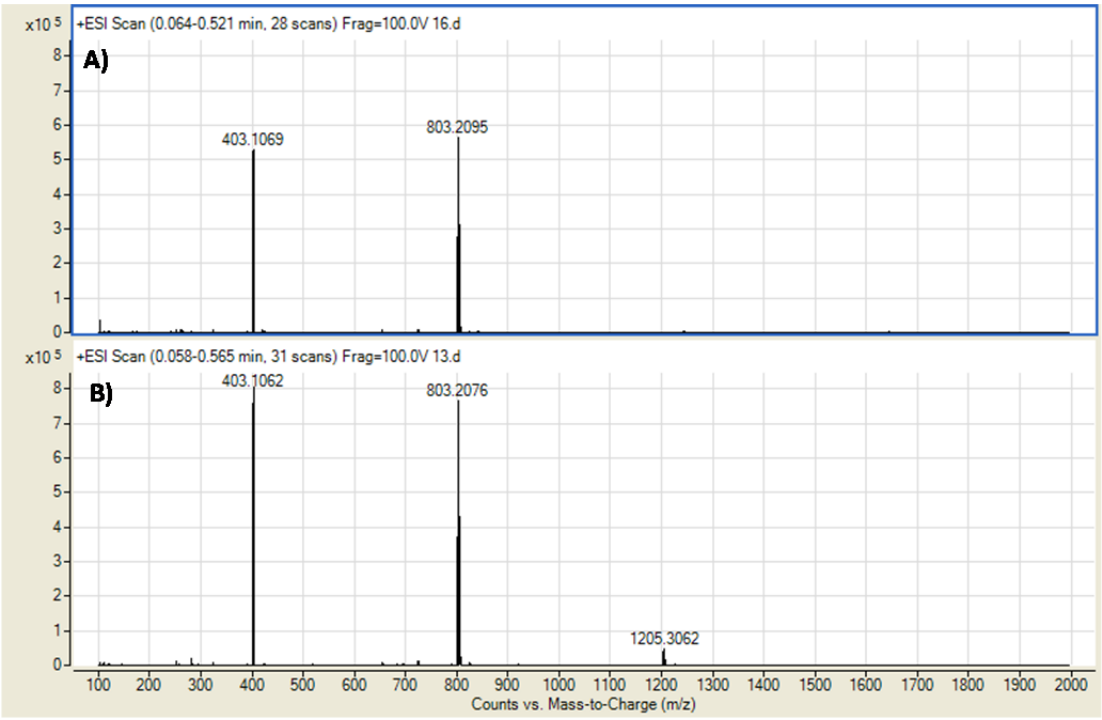

Figure 5-S10. High resolution mass spectra of freshly synthesized **5** (B) after 5 recycling cycles.

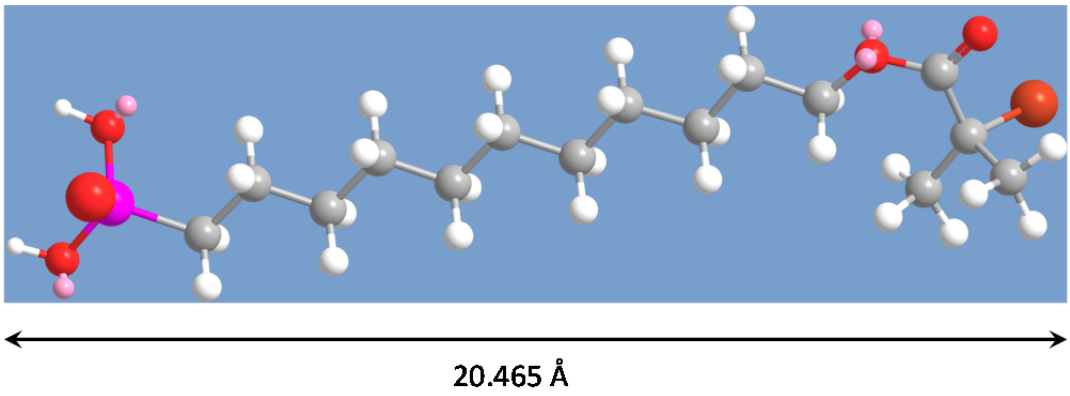

Figure 5-S11. Theoretically calculated length of **5** after energy minimization. Chem3D software was used in option MM2, with a RMS gradient of 0.100.

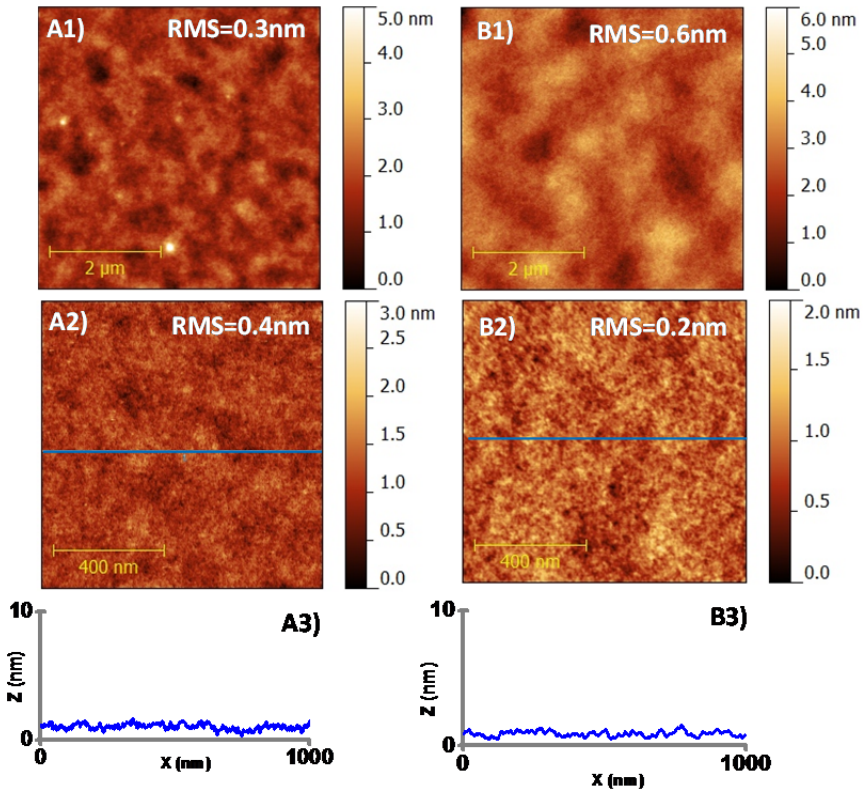

Figure 5-S12. PAA (A) and PSPMAA (B) brushes on silica. Polymer grafting reaction was performed with the conventional (siloxane) initiator. Thickness of PAA layer = 120 nm and PSPMA layer =156 nm.

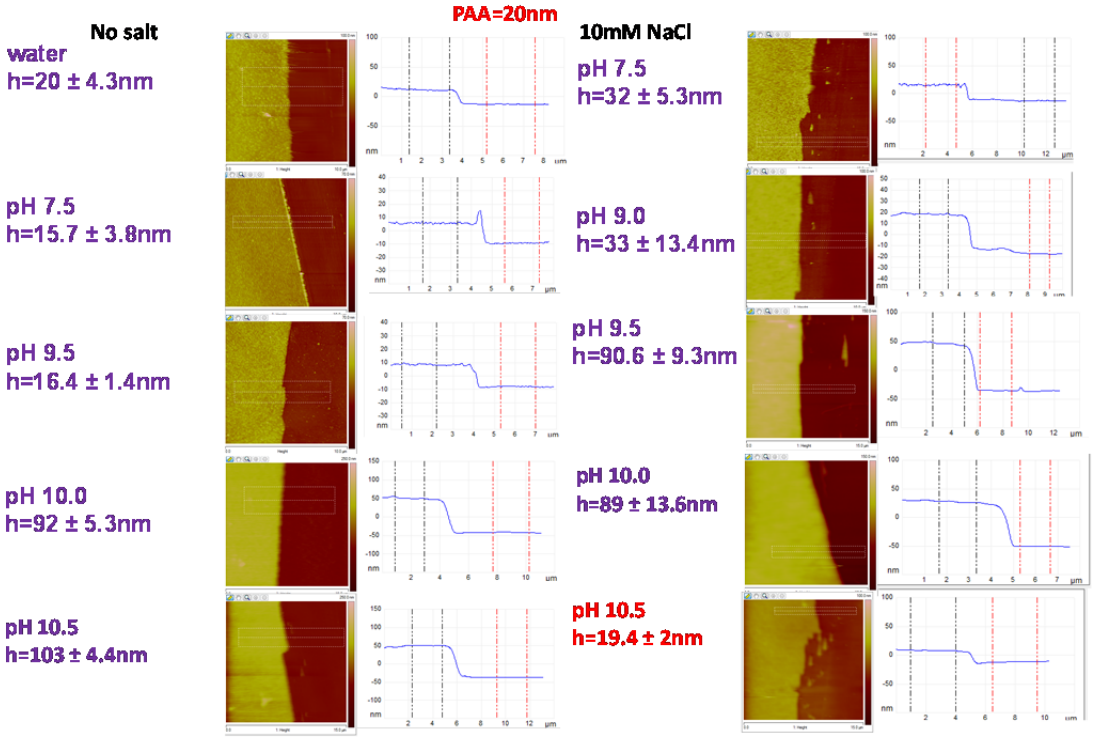

Figure 5-S13. Degrafting studies of PAA brushes synthesized from **5**-modified silica wafer. Thickness of PAA layer in air = 20nm.

Table 5-S1. PAA layer roughness measured under different conditions. The size of analyzed area is 4x4um. Polymer grafting reaction was performed with **5**.

Conditions	Roughness, ±0.2nm
water	1.3
pH 9.5 no salt	1.5
pH 9.5 with added 10mM NaCl	2.3

5.8 References

(1) Minko, S. *Polym. Rev.* **2006**, *46*, 397.

(2) Rühe, J.; Ballauff, M.; Biesalski, M.; Dziezok, P.; Gröhn, F.; Johannsmann, D.; Houbenov, N.; Hugenberg, N.; Konradi, R.; Minko, S.; Motornov, M.; Netz, R.; Schmidt, M.; Seidel, C.; Stamm, M.; Stephan, T.; Usov, D.; Zhang, H. In *Polyelectrolytes with Defined Molecular Architecture I*; Schmidt, M., Ed.; Springer Berlin Heidelberg: 2004; Vol. 165, p 79.

(3) Azzaroni, O. *J. Polym. Sci. Pol. Chem.* **2012**, *50*, 3225.

(4) Barbey, R.; Lavanant, L.; Paripovic, D.; Schuwer, N.; Sugnaux, C.; Tugulu, S.; Klok, H. A. *Chem. Rev.* **2009**, *109*, 5437.

(5) Hui, C. M.; Pietrasik, J.; Schmitt, M.; Mahoney, C.; Choi, J.; Bockstaller, M. R.; Matyjaszewski, K. *Chem. Mater.* **2013**.

(6) Tokarev, I.; Motornov, M.; Minko, S. *J. Mater. Chem.* **2009**, *19*, 6932.

(7) Degennes, P. G. *Macromolecules* **1980**, *13*, 1069.

(8) Tsujii, Y.; Ohno, K.; Yamamoto, S.; Goto, A.; Fukuda, T. *Adv. Polym. Sci.* **2006**, *197*, 1.

(9) Tripp, C. P.; Hair, M. L. *J. Phys. Chem.* **1993**, *97*, 5693.

(10) Schwartz, D. K. *Annu. Rev. Phys. Chem.* **2001**, *52*, 107.

(11) Zhao, X. L.; Kopelman, R. *J. Phys. Chem.* **1996**, *100*, 11014.

(12) Onclin, S.; Ravoo, B. J.; Reinhoudt, D. N. *Angew. Chem. Int. Edit.* **2005**, *44*, 6282.

(13) Wasserman, S. R.; Tao, Y.-T.; Whitesides, G. M. *Langmuir* **1989**, *5*, 1074.

(14) Borozenko, O.; Godin, R.; Lau, K. L.; Mah, W.; Cosa, G.; Skene, W. G.; Giasson, S. *Macromolecules* **2011**, *44*, 8177.

(15) Lego, B.; Skene, W. G.; Giasson, S. *Macromolecules* **2010**, *43*, 4384.

(16) Tugulu, S.; Barbey, R.; Harms, M.; Fricke, M.; Volkmer, D.; Rossi, A.; Klok, H.-A. *Macromolecules,* **2006**, *40 (2)*, 168.

(17) Hotchkiss, P. J.; Jones, S. C.; Paniagua, S. A.; Sharma, A.; Kippelen, B.; Armstrong, N. R.; Marder, S. R. *Acc. Chem. Res.* **2012**, *45*, 337.

(18) Queffelec, C.; Petit, M.; Janvier, P.; Knight, D. A.; Bujoli, B. *Chem. Rev.* **2012**, *112*, 3777.

(19) Cattani-Scholz, A.; Pedone, D.; Dubey, M.; Neppl, S.; Nickel, B.; Feulner, P.; Schwartz, J.; Abstreiter, G.; Tornow, M. *ACS Nano* **2008**, *2*, 1653.

(20) Midwood, K. S.; Carolus, M. D.; Danahy, M. P.; Schwarzbauer, J. E.; Schwartz, J. *Langmuir* **2004**, *20*, 5501.

(21) Cattani-Scholz, A.; Pedone, D.; Blobner, F.; Abstreiter, G.; Schwartz, J.; Tornow, M.; Andruzzi, L. *Biomacromolecules* **2009**, *10*, 489.

(22) Liao, K. C.; Ismail, A. G.; Kreplak, L.; Schwartz, J.; Hill, I. G. *Adv. Mater.* **2010**, *22*, 3081.

(23) McDermott, J. E.; McDowell, M.; Hill, I. G.; Hwang, J.; Kahn, A.; Bernasek, S. L.; Schwartz, J. *J. Phys. Chem. A* **2007**, *111*, 12333.

(24) McDowell, M.; Hill, I. G.; McDermott, J. E.; Bernasek, S. L.; Schwartz, J. *Appl. Phys. Lett.* **2006**, *88*.

(25) Bora, A.; Pathak, A.; Liao, K. C.; Vexler, M. I.; Kuligk, A.; Cattani-Scholz, A.; Meinerzhagen, B.; Abstreiter, G.; Schwartz, J.; Tornow, M. *Appl. Phys. Lett.* **2013**, *102*.

(26) Minet, I.; Delhalle, J.; Hevesi, L.; Mekhalif, Z. *J. Colloid. Interf. Sci.* **2009**, *332*, 317.

(27) Barthelemy, B.; Devillers, S.; Minet, I.; Delhalle, J.; Mekhalif, Z. *J Colloid. Interf. Sci.* **2011**, *354*, 873.

(28) Babu, K.; Dhamodharan, R. *Nanoscale Res. Lett.* **2008**, *3*, 109.

(29) Devillers, S.; Barthelemy, B.; Delhalle, J.; Mekhalif, Z. *Appl. Mater. Inter.* **2011**, *3*, 4059.

(30) Barthelemy, B.; Devillers, S.; Minet, I.; Delhalle, J.; Mekhalif, Z. *Appl. Surf. Sci.* **2011**, *258*, 466.

(31) Chen, M.; Briscoe, W. H.; Armes, S. P.; Cohen, H.; Klein, J. *ChemPhysChem* **2007**, *8*, 1303.

(32) Raviv, U.; Frey, J.; Sak, R.; Laurat, P.; Tadmor, R.; Klein, J. *Langmuir* **2002**, *18*, 7482.

(33) Raviv, U.; Giasson, S.; Kampf, N.; Gohy, J.-F.; Jérôme, R.; Klein, J. *Nature* **2003**, *425*, 163.

(34) Schorr, P. A.; Kwan, T. C. B.; Kilbey, S. M.; Shaqfeh, E. S. G.; Tirrell, M. *Macromolecules* **2002**, *36*, 389.

(35) Lego, B.; Skene, W. G.; Giasson, S. *Langmuir* **2008**, *24*, 379.

(36) Liberelle, B.; Banquy, X.; Giasson, S. *Langmuir* **2008**, *24*, 3280.

(37) Israelachvili, J. *J Colloid. Interf. Sci.* **1973**, *44*, 259.

(38) Israelachvili, J. N.; Adams, G. E. *J. Chem. Soc. Faraday Trans. I* **1978**, *74*, 975.

(39) Israelachvili, J. N.; Mcguiggan, P. M.; Homola, A. M. *Science* **1988**, *240*, 189.

(40) Paniagua, S. A.; Hotchkiss, P. J.; Jones, S. C.; Marder, S. R.; Mudalige, A.; Marrikar, F. S.; Pemberton, J. E.; Armstrong, N. R. *J. Phys. Chem. C* **2008**, *112*, 7809.

(41) Silverman, B. M.; Wieghaus, K. A.; Schwartz, J. *Langmuir* **2005**, *21*, 225.

(42) Hanson, E. L.; Schwartz, J.; Nickel, B.; Koch, N.; Danisman, M. F. *J. Am. Chem. Soc.* **2003**, *125*, 16074.

(43) Woodward, J. T.; Ulman, A.; Schwartz, D. K. *Langmuir* **1996**, *12*, 3626.

(44) Quinones, R.; Raman, A.; Gawalt, E. S. *Thin Solid Films* **2008**, *516*, 8774.

(45) Allara, D. L.; Nuzzo, R. G. *Langmuir* **1985**, *1*, 45.

(46) Allara, D. L.; Nuzzo, R. G. *Langmuir* **1985**, *1*, 52.

(47) Tsarevsky, N. V.; Matyjaszewski, K. *Chem. Rev.* **2007**, *107*, 2270.

(48) Anderson, H. H. *Inorg. Chem.* **1964**, *3*, 108.

(49) Borozenko, O.; Ou, C.; Skene, W. G.; Giasson, S. *Polym. Chem.* **2013**.

(50) Liberelle, B.; Giasson, S. *Langmuir* **2008**, *24*, 1550.

(51) Zhulina, E. B.; Birshtein, T. M.; Borisov, O. V. *Macromolecules* **1995**, *28*, 1491.

(52) Nordgren, N.; Rutland, M. W. *Nano Lett.* **2009**, *9*, 2984.

(53) Matyjaszewski, K. *Prog. Polym. Sci.* **2005**, *30*, 858.

(54) Stiernstedt, J.; Nordgren, N.; Wågberg, L.; Brumer Iii, H.; Gray, D. G.; Rutland, M. W. *J. Colloid. Interf. Sci.* **2006**, *303*, 117.

(55) Tsarevsky, N. V.; Braunecker, W. A.; Brooks, S. J.; Matyjaszewski, K. *Macromolecules* **2006**, *39*, 6817

Chapter 6

Conclusions and future work

6.1. Conclusions

The main goals of the present work were to prepare well-defined weakly charged polymer brushes, study their responsiveness with variation of pH and ionic strength, and correlate the brush conformation with the surface properties. Weakly charged brushes are of particular interest because they adopt a large variety of conformations when an external stimulus is applied. To prepare well-defined polymer brushes, SI-ATRP was chosen as an ideal method because it allows control over the polymer brush layer thickness, composition, and macromolecular architecture. For accurate conformation-properties studies, a robust substrate-polymer connection is required. For silica substrates, the ATRP with a siloxane initiator is typically used, because it provides a Si_{silica}-O-$Si_{initiator}$ connection that is robust, and can resist the polymerization and characterization conditions. However, it was shown in the literature that this bond can hydrolyze resulting in polymer degrafting. The exact degrafting conditions were unknown. Thus, we aimed to determine the conditions that triggered undesired polymer detachment and to design a robust polymer brush system that would be stable under a wide range of environmental conditions. Changes in conformation of end-grafted polymers generally lead to changes in surface properties such as friction and adhesion. As it was shown previously by Raviv et al., polyelectrolyte brushes in aqueous environments have extremely low friction coefficients.[§§] However, the exact mechanism of effective brush lubrication is still unclear. Correlating the surface properties of covalently attached brushes with different environmental conditions (pH and ionic strength) would help to elucidate the lubrication mechanism and reveal the role of polymer conformation.

We are interested in polyacrylic acid brushes because its conformations can be finely tuned by varying the pH and ionic strength. The conventional PAA brush synthesis is usually done with an acrylate polyester, which can be converted to PAA

[§§]Raviv, U.; Giasson, S.; Kampf, N.; Gohy, J.-F.; Jérôme, R.; Klein, J. *Nature* **2003**, *425*, 163.

by removing the protecting ester groups. This approach has several drawbacks. First of all, harsh deprotection conditions are required that could detach the polymer leading to changes of polymer grafting density. Moreover, a washing step is required to remove the hydrolyzing solution. Direct PAA synthesis in water avoids the deprotection step and leads to a well-defined polyelectrolyte in one step. **Chapter 2** is the first report of successful direct polymerization of sodium acrylate (NaA) from initiator-functionalized mica surface using water-mediated ATRP. Despite mica being commonly used as a substrate for force measurements, there are few reports showing the covalent attachment of polymers on mica because of its inertness toward chemical modification. Developed by Lego et al., the protocol of covalent immobilization of an ATRP initiator on mica involves activating the surface with water-argon plasma, and grafting the chlorosilane-based ATRP initiator via siloxane bond.[***] In **Chapter 2** we used this approach to activate mica and we showed the initiator monolayer could successfully initiate the polymerization of NaA in water, resulting in thick and smooth PAA layer of 95 nm within 70 min. We grafted PAA from both mica and silica surfaces under the same reaction conditions. The thickness of the layers for these two substrates was different. The PAA thickness on silica was 57 nm while, for the mica substrate, the layer was about 95 nm. This difference could be due to the polymer brush cleavage as a result of substrate-initiator bond hydrolysis in alkaline conditions, which are required for water ATRP. As it was shown before in the literature, after activation, silica has more stable surface hydroxyl groups than mica. This should lead to denser polymer brushes on silica than on mica. At high polymer layer thickness, brush degrafting can be facilitated because of the stretched polymer conformation that, in turn, facilitates the penetration of hydroxyl ions close to the surface resulting in substrate-initiator bond rupture.

Absolute evidence of polymer brush degrafting and the conditions under which it occurs were demonstrated in **Chapter 3.** We grafted PAA brushes from their

[***]Lego, B.; Skene, W. G.; Giasson, S. *Langmuir* **2008**, 24, 379.

precursor (P*t*BA) from silica (glass slide) using SI-ATRP. To dynamically monitor polymer degrafting under different pH and salt conditions, we attached a fluorescence probe (PMOH) to the PAA chains and used TIRF microscopy. We observed strong fluorescence decrease at pH≥9.5 in the presence of salt indicating the brush detachment. Moreover, we performed complex studies to assure the decrease of fluorescent intensity was a result of polymer detachment rather than detachment of the fluorophore. We suggested that at low pH, the substrate-initiator bond was shielded by undissociated polymer units situated close to the substrate. Salt ions in combination with high pH caused full ionization of the attached polymer, resulting in the substrate-initiator bond being exposed to hydroxyl ions. The latter caused the substrate-initiator bond hydrolysis and resulted in polymer detachment. In **Chapter 3** we unambiguously proved for the first time that the substrate-initiator bond could be hydrolyzed, and the observed polymer thickness decrease was a result of this process. Obtained results are of importance for polymer brush conformational studies where a wide range of pH and ionic strength are required, and knowing the substrate-initiator bond hydrolyzing conditions could help avoid polymer detachment.

In the subsequent chapter we developed a strategy to prevent polymer cleavage. This approach relied on introducing a polystyrene buffer layer between the siloxane initiator and PAA block (**Chapter 4)**. This was done by SI-ATRP that allows grafting the first PS block, and then, extending it with PAA block by using bromide end groups. Acting as a hydrophobic barrier, the PS layer prevents water from penetrating close to the substrate and, thus, prevents substrate-initiator bond hydrolysis. In **Chapter 4**, we demonstrated the protective properties of the PS block as a function of its thickness. We showed that even the smallest PS thickness of 1.7 nm can effectively protect the $Si_{substrate}$-O-$Si_{initiator}$ bond from hydrolysis under the extreme alkaline conditions with the presence of different salt ions. Multiple cycles of pH-change confirmed the robustness of PS-*b*-PAA brushes as well as its responsiveness to the variation of pH and ionic strength. The PAA thickness change was used to measure the brush responsiveness. Relatively fast constant response

(within 10 minutes) was observed upon pH switching from 10.5 to 5.5. This can be potentially used in engineering of smart stimuli-responsive materials. Moreover, pH-induced swelling of PS-*b*-PAA brushes was studied, where we observed pronounced hysteresis of swollen brush thickness upon step-wise pH changes. We attributed this hysteresis-like behaviour to changes in brush hydrophobicity. pH increase caused the dissociation of the carboxylic acid groups of the outer brush regions, resulting in hydrophilicity increase and allowing the buffer solution to penetrate inside the brush and dissociate the rest of COOH groups. pH decrease, in contrast, resulted in an increase of hydrophobicity of the outer brush regions and decelerated the protonation COO^- groups because of the restricted penetration of buffer solution through the brush. Additionally, we studied the role of salt ions of different valencies on brush swelling. Either sodium or cesium monovalent ions resulted in constant brush swelling/collapsing ratios upon several cycles, while the addition of calcium ions caused brush collapse and the brush could not be re-swollen. Thus, these results should attract considerable attention from those interested in synthesis and characterization of well-defined responsive polymer layers, brush conformational studies upon applying external stimulus, and design of smart switching materials.

As an alternative to commonly used siloxane ATRP initiators, we proposed to use organophosphonic acid initiator (**5**) to graft to silica-based substrates. In **Chapter 5**, we described the first example of **5** grafting to silica and mica. The covalent attachment of **5** to silica was confirmed by ATR-FTIR. AFM studies revealed the formation of homogeneous initiator layer on both substrates. We showed that the grafted phosphonate layer could effectively initiate the polymerization of sodium acrylate and 3-sulfopropyl methacrylate in water. The constant thickness of prepared PAA and PSPMA brushes confirmed the stability of silica-initiator interface in alkaline conditions, which are required by water-mediated ATRP. Moreover, we evaluated the stability of $Si_{substrate}$-O-$P_{initiator}$ bond with respect to pH and ionic strength by monitoring changes in thickness of grafted PAA layer. We revealed that PAA brushes were stable in a wide range of pH (from pH 7.5 to 10.5), and brush

degrafting occurred at pH 10.5 with added salt only. These results confirm that used organophosphonic acid is a suitable ATRP initiator for silica because it is attached to the substrate through covalent bond, capable of initiating the polymerization, and assures stable substrate-polymer connection in a wide range of pH. These findings can be adopted to create stable silica-polymer interface. Usage of phosphonate linkage to graft polymer from silica could be beneficial for many applications such as biosensors, chromatographical and catalytical platforms, where the extended range of applied environmental conditions is required.

Confirmed hydrolytic stability of PAA brushes grafted from phosphonate-modified silica allowed pH- and ionic strength-induced changes of PAA's surface properties to be investigated with Surface Forces Apparatus. The force profiles showed no changes in the range and amplitude of interactions regardless of pH and ionic strength, suggesting non-significant differences in polymer conformations. This was attributed to the sample thickness variability, which, in turn, related to the polymer preparation technique (water-mediated SI-ATRP). With this technique the relatively large polymer molecular weight distribution is possible. The friction was varied with sample and did not show significant difference between conditions. This was explained by the initial surface roughness as well as a roughness increase upon swelling. Thus, the large variability between samples prevented clear correlation of degree of ionization with friction to be observed.

To conclude, these results present a significant contribution to the *polymers on surface* field. We showed for the first time that the $Si_{substrate}$-O-$Si_{initiator}$ bond can be hydrolysed resulting in polymer brush detachment. We determined the exact pH and ionic strength conditions that resulted in the siloxane linkage hydrolysis. We suggested a strategy to prevent polymer degrafting: by using hydrophobic PS layer as a protector for substrate-initiator bond. This approach resulted in stable and responsive PS-*b*-PAA brushes that allowed studying of pH-induced brush swelling over a wide range of environmental conditions, including the extreme conditions of

pH and ionic strength. Additionally, we used phosphonic acid ATRP initiator as an alternative to commonly used organosilanes to functionalize silica. We showed that the phosphonic acid initiator could be successfully grafted to silica and mica surfaces, and initiate the polymerization of PAA and PSPMA brushes in water. We confirmed the stability of $Si_{substrate}$-O-$P_{initiator}$ bond under polymerization conditions and demonstrated its resistivity towards hydrolysis in a wide range of pH. Thus, the choice of the "protector" for the siloxane substrate-initiator bond, either PS layer or organophosphonic acid, depends on two main factors: what conditions (pH and salt concentration) the brushes will be exposed to, and what polymerization medium (organic solvent or water) will be used.

6.2. Future perspectives

While substantial work of synthesis, characterization and studying pH- and ionic strength responsiveness of polyelectrolyte brushes were done, there is still space for future work. Here, we propose several ideas that can be pursued in order to complete the current project and explore PE brushes more extensively.

PS-*b*-PAA brushes: stability studies. In **Chapter 4**, we presented PS layer of 1.7 nm as a good protector for the substrate-initiator bond against hydrolysis. Prepared PS-*b*-PAA brushes were stable at pH 10.5 with added 10 mM NaCl during 2 h. However, the brush stability at higher salt concentration was not studied. Thus, we propose to verify the stability of PS layer at concentration of NaCl >>10 mM. The extreme salt concentrations might require a thicker than 1.7 nm PS layer.

PS-*b*-PAA brushes: studying of surface properties. We showed that PS-*b*-PAA brushes are exceptionally stable under a wide range of environmental including extreme conditions. This makes PS-*b*-PAA brushes ideal candidates for brush conformational studies via monitoring their surface properties (adhesion and friction)

with one of the forces measuring techniques. Lateral force microscopy with colloidal probe can be used to evaluate the interactions between polymer layers. After performing appropriate calibration procedures, it will be possible to measure an absolute value of friction force and correlate it with pH and ionic strength. PS-*b*-PAA brushes can be grown from both microsized silica beads and flat silica substrates under the same polymerization conditions. This will assure identical brushes thickness on both substrates. Interaction forces can be measured with AFM, equipped with liquid cell that will allow varying the pH and ionic strength of solutions. This approach does not have limitations in sample preparation as SFA. The grafting of PS-*b*-PAA brushes from SFA samples is restricted because the adhesive used to glue mica on SFA discs can be dissolved by multiple organic solvents (acetone with heating, DCM, etc.) that are used for brush synthesis. This will lead to sample destruction. Thus, the colloidal probe approach is advantageous. PS-*b*-PAA brushes will be prepared using solvent-mediated ATRP as described in **Chapter 4**. Therefore, the variability in polymer thickness mentioned in **Chapter 5** will be minimized. This is because of the absence of side reactions that are usually present in water-mediated ATRP, and, which can influence the polymerization kinetics and molecular weight distribution.

Control over PI surface coverage. For polymer brushes prepared using SI-ATRP the control over initiator surface coverage is necessary because it determines the grafting density of attached chains. In **Chapter 5,** we showed the successful PI attachment to silica and mica, but the PI grafting kinetics was not explored. Also, the PI reactivity towards polymerization at different surface coverage must be examined. The initiator surface coverage could be investigated as a function of coupling time and concentration of initiator solution. The changes of surface coverage can be monitored by measuring the water contact angle. The increase in initiator surface density will lead to an increase of hydrophobicity and, consequently, to increased water contact angle. In **Chapter 5**, we used one concentration of initiator solution (10^{-3} M). Other concentrations (10^{-1} and 10^{-2} M) can be investigated and obtained

initiator monolayers can be studied in terms of polymerization reactivity. So, our next step will be to investigate the PI adsorption kinetics and prepare initiator-functionalized surfaces with different PI surface coverages. Different initiator surface coverages will result in polymer brushes with varied grafting density, i.e. with different polymer chain conformations. This will allow studying the role of brush conformation in controlling surface properties such as adhesion and friction.

Studying PAA brush surface properties. Following the previous idea, we propose to investigate the surface properties of PAA brushes as a function of polymer grafting density. In **Chapter 5,** we studied PAA brushes of similar polymer grafting density because we assumed identical initiator surface coverage. To understand the role of main brush parameters such as polymer layer thickness, grafting density, and degree of ionization in polymer-polymer interactions, brushes of significantly different thicknesses and grafting densities should be studied as a function of pH and ionic strength. Thus, the goal for future work would be to prepare brushes of different thicknesses and grafting densities, and correlate the surface properties (friction, adhesion, distance dependant inter-surface forces) with layer thickness, polymer degree of ionization and environmental conditions.

Studying of PSPMAA brush surface properties. With water-mediated ATRP, we were able to prepare PSPMAA brushes from phosphonate-modified silica. PSPMAA is a polymer that can tune its conformation in response to ionic strength. Studying surface properties of PSPMAA brushes as a function of ionic strength would be beneficial for understanding the role of salt ions in effective lubrication, and correlating changes in friction and adhesion with polymer conformation.

Si_{silica}-O-$P_{initiator}$ bond hydrolytic stability. The grafting of PI to silica was done through Si_{silica}-O-$P_{initiator}$ bond. We studied the hydrolytic stability of substrate-initiator linkage by monitoring changes in the thickness of the grafted polymer layer under different environmental conditions. It was shown before that polymer degrafting, because of the rupture of substrate-initiator bond, can be facilitated for

thick polymer layers. Thus, to perform accurate stability studies, we propose to graft the phosphonate initiator to the glass slide, modify its end groups with fluorescent tags, and apply TIRF microscopy to visualize the layer. Then the solutions of different pH and ionic strength can be flowed, and the same methodology to analyse the changes of fluorescent intensity as described in **Chapter 3** can be used.

Brush sensing applications. PS-*b*-PAA brushes are sufficiently robust to sustain a wide range of pH without degrafting and at the same time stay responsive. So, this property can be potentially used in sensor engineering. Tokareva et al. showed an example of a nanosensor based on poly(2-vinylpyridine) (P2VP) brushes that change their conformation in acidic conditions.[†††] Brush thickness was reversibly altered by changing pH from 5.0 to 2.0. The gold nanoparticles were deposited to the brush surface and enhanced transmission surface plasmon resonance spectroscopy was applied. Similar methodology can be used to build PS-*b*-PAA-based sensor that will be operated in alkaline conditions. Such sensor will work in a wide pH range and will be able to sustain extreme conditions of pH and ionic strength.

[†††] Tokareva, I., Minko, S., Fendler, J. H., Hutter, E. *J. Am. Chem. Soc.* **2004**, 126, 15950.